University of Bath

UNIVERSITY OF BATH

PHD

Physicomechanical properties of bacterial P(HB - HV) polyesters and their uses in drug delivery

Akhtar, Saghir

Award date:
1990

Awarding institution:
University of Bath

Link to publication

PHYSICOMECHANICAL PROPERTIES OF

BACTERIAL P(HB-HV) POLYESTERS AND

THEIR USES IN DRUG DELIVERY

submitted by

Saghir Akhtar BSc, MRPharmS.

for the degree of Doctor of Philosophy

of the University of Bath

January 1990

This research has been carried out at the School of Pharmacy and pharmacology of the University of Bath under the joint supervision of Dr C.W. Pouton and Dr L.J Notarianni.

UMI Number: U020771

Dissertation Publishing

UMI U020771

"I hope that my Lord will guide me
forever closer to the right road"

Al – Koran 18:24.

ACKNOWLEDGMENTS

To my parents,

for all your love and encouragement

and my family,

for your unfailing support.

SUMMARY

Biodegradable polymers have important uses in drug delivery systems. Bacterially produced poly-D(-)-3-hydroxybutyrate (PHB) and its copolymers with poly-3-hydroxyvalerate (P(HB-HV)) have emerged as new candidates for use in drug delivery devices.

Current literature available on the synthesis and physical properties of these polyesters is reviewed. Experimental studies of the physicomechanical properties of bacterial P(HB-HV) polyesters and their potential use in drug delivery are reported.

Mechanical, thermal, ageing and crystalline properties have been investigated in detail. These properties were generally dependent on both polymer molecular weight and copolymer composition. Static tensile testing of solvent cast films showed that PHB was relatively hard and brittle whereas copolymerization with HV produced tougher, less brittle and more pliable copolymers. Mechanical properties of polymer films were modified on incorporation of a particulate drug (Sodium Fluorescein). Differential Scanning calorimetry (DSC) and Thermogravimetric analysis were used to assess thermal properties. Melting points, glass transition temperatures, and thermal degradation temperatures were determined. Mechanical and thermal properties of solvent cast films changed with time following manufacture. The ageing effect was related to copolymer composition.

Spherulitic crystallization kinetics and morphology were assessed using polarized light microscopy, DSC and X-ray diffraction. Crystallization rate and morphology were influenced by crystallization temperature, copolymer composition, presence and concentration of a model drug (Methyl Red) and to some extent polymer molecular weight.

Spray drying was investigated for producing injectable polymer microparticles for drug delivery. Successful use of the process was limited to low molecular weights of PHB. Drug release (Methyl Red) from implantable solvent cast and melt-pressed films was also investigated. Release was dependent on polymer molecular weight, copolymer composition, drug loading and fabrication technique. Release of Methyl Red was predominantly

controlled by diffusion rather than polymer erosion.

Bulk properties of P(HB – HV) polymers and drug release kinetics from melt pressed discs were thought to be related to the underlying crystalline morphology within films. This hypothesis is discussed in detail and indications for future work in this area are suggested.

LIST OF CONTENTS

ORIGINS AND SCOPE

Poly – D(–) – 3 – hydroxybutyrate (PHB) and its copolymers with poly – D(–) – 3 – hydroxyvalerate (P(HB – HV)) are optically active, crystalline polyesters produced by a wide variety of bacteria and a number of other microorganisms [137]. These polymers are the most common in the more general class of polyhydroxyalkanoates (PHA) which are produced by microorganisms as energy reserve materials. As a consequence of recent advances in biotechnology, P(HB – HV) polymers can be produced in multikilogram batches from the bacterial fermentation of a glucose utilizing mutant of *Alcaligenes eutrophus.*

The major advantage of these 'biopolymers' is that they can be extracted from bacteria in a very pure form. This is in contrast to conventional synthetic thermoplastics, such as polylactide/polyglycolide (P(LA – GA)) systems, which can contain inorganic catalyst residues even after extensive purification.

Preliminary reports suggested that P(HB – HV) polymers were both biodegradable and biocompatible [149]. The homopolymer, PHB, degrades to the monomer, D(–) – 3 – hydroxybutyric acid, which is a normal constituent of blood and therefore likely to be tolerated well *in vivo.* Further studies at Bath showed that these polymers degraded by surface hydrolysis [286 – 287]. The surface confined (heterogeneous) degradation of these polymers offers the potential advantage of predictable drug release kinetics. This is in contrast to the situation with P(LA – GA) systems (widely used for drug delivery purposes) which undergo homogeneous degradation (bulk hydrolysis). This degradation method results in unpredictable permeability changes within the bulk polymer and consequently leads to unpredictable drug release kinetics from P(LA – GA) systems. On the basis of these preliminary studies indicating potential advantages of P(HB – HV) biopolymers over existing biodegradable polymers, these materials were chosen as potential candidates for drug delivery systems.

At the onset of this research, although much information was available on the biosynthesis of P(HB – HV) polymers, little was known of their physicomechanical

properties or of their potential for use in drug delivery applications.

It was the aim of this research to study the fundamental physicomechanical properties of P(HB–HV) polymers and to examine their possible use in delivering both macromolecular and low molecular weight drugs. Chapters 2, 3, 4 and 5 report on the mechanical, thermal, ageing and crystalline properties of P(HB–HV) polyesters. Wherever possible the influence of model drugs on the fundamental properties of these polymers has been examined. In particular, the influence of a model drug, Methyl Red, on the crystalline morphology and subsequent drug release kinetics from these polymers has been investigated.

In terms of drug delivery, both spray–dried microparticles and thin film matrices (solvent cast and melt–pressed) have been examined as drug carriers. The study was limited to the use of model drugs and did not extend to therapeutic actives. Methyl Red was used as a model for low molecular weight drugs and preliminary studies on macromolecular drugs were carried out using Azocasein.

Microparticles have traditionally been prepared by batch processes involving organic solvent evaporation. Such processes are likely to encounter scale up problems and thus, may be economically unviable. It was, therefore, that in this study, spray drying was investigated as a continuous process for producing injectable microparticles and is discussed in Chapter 6. For comparative purposes, melt–pressed and solvent cast films were also examined as drug carriers for implantation (chapter 7).

CHAPTER 1

INTRODUCTION

1.1 Rationale for controlled drug delivery

Conventional methods (oral and parenteral) of administering low molecular weight drugs suffer from several disadvantages [1 – 7]. One of the major disadvantages is that they involve frequent and repeated doses which not only leads to compliance problems but also results in peak and trough fluctuations in the plasma drug concentrations. Such variations in plasma drug concentrations are particularly undesirable when aiming to maintain plasma drug levels within a narrow therapeutic range (i.e when differences between therapeutic and toxic concentrations of drug in plasma are small) [7]. If plasma drug levels rise above the toxic limit then, as a consequence of the non – targetted nature of conventional drug delivery, systemic side effects will occur.

A number of approaches have been examined for targetting drugs to specific sites in order to avoid systemic side effects. These include the use of soluble polymers [8 – 10], monoclonal antibodies [11 – 13] and particulates such as polymer microspheres [14 – 20], emulsions [21] and liposomes [22 – 30]. However, the injection of particulate systems into the circulation results in rapid uptake by cells of the reticuloendothelial system (RES) and therefore targetting using particulate systems is largely limited to the RES [31 – 34]. Although modification of particle surfaces with certain coatings has allowed some control in targetting to specific sites within the RES [17 – 19], targetting to extravascular sites is problematic and for it to realize its full potential must overcome vascular endothelial and cellular barriers [32].

The limitations of conventional drug delivery systems are further highlighted in the delivery of polypeptide drugs. Recent advances in bioengineering and cell biology have led to the development of many pharmacological active peptides such as tissue plasminogen activator (for treatment of thrombi), erythropoietin (for treating anaemia in renal failure), atrial natriuretic factor (treatment of hypertension) and interferons (indicated in certain cancers) [35 – 38]. The routine use of such peptides in medicine is unlikely to be feasible using traditional methods of drug administration. Macromolecular peptides are usually ineffective by the oral route as they are rapidly

degraded and deactivated in the gastrointestinal tract by proteolytic enzymes [39]. Those which are stable under such conditions may still not pass through biological barriers because of their chemical polarity and large molecular weights [40]. Consequently, at present they are administered parenterally. However, parenteral administration is often complicated by their very short half-lives [41]. Frequent injections are required to maintain effective or therapeutic plasma concentrations of peptides but peak and trough effects remain. This problem may be overcome by using biodegradable polymers as matrices for sustained or controlled delivery of peptides (and low molecular weight drugs) for implantation or parenteral administration.

Polymer matrix (monolithic) devices are essentially of two types. One in which the drug is physically dispersed as discrete solid particles within the polymer matrix and the other in which the drug is dissolved in the polymer matrix at concentrations below its saturation solubility [42].

The aim of such devices is to allow for the controlled release of drugs into the body over long periods of time (weeks or even months), thereby constantly maintaining a therapeutic plasma drug concentration that is above the minimum effective level but below the toxic level. The formulation should ideally be biodegradable for two reasons. Firstly, so that the device can disappear from the site of administration obviating the need for surgical removal of the drug-depleted device. Secondly, the degradation of the polymer can potentially be used to precisely control the rate of drug release from the matrix. Biodegradable polymers also offer opportunities for the protection of labile macromolecules as an additional property, coupled to the advantages of controlled release [43]. The breakdown products of such a formulation should be non-toxic and biocompatible [40].

It should, however, be noted that although much work in the past has been carried out using polymer devices in the aim of achieving a zero-order drug release profile [44-45], this may not always be the ideal release pattern. The optimum delivery of

endogenous peptides may require release rates and profiles which mirror those observed during their normal physiological release and may be of a pulsatile nature [46]. The mode of delivery is clinically important since, for example in the case of luteinizing hormone – releasing hormone (LHRH) analogues, opposing pharmacological effects have been observed depending on whether they are delivered in a pulsatile or continuous manner [38]. Pulsatile administration of LHRH, which mimicks the natural secretory pattern, causes a sustained secretion of gonadotropins [47 – 48]. However, administration of long acting synthetic analogues of LHRH as a single daily subcutaneous injection has been shown to desensitize (down – regulate) the receptors in the pituitary gland and thus inhibit the release of gonadotropins [66 – 68]. In the case of LHRH, continuous release and subsequent down regulation of receptors in the pituitary gland is clinically more useful than pulsatile release. This fact is now being exploited clinically for female contraception [38] and Zoladex, a preparation allowing continuous release of a LHRH analog is currently available for the treatment of prostate carcinoma.

Recent evidence suggests that the biological response to a given drug may also vary according to the body's circadian rhythms [49 – 50] and hence the drugs chronopharmacology will influence the required release profile for optimum delivery of the agent [50]. It should also be emphasized that for devices which do not deliver direct to the circulation, the rate at which drug is delivered to the implant site does not necessarily reflect its rate of delivery to the circulation. A constant rate of release of a drug into tissues (other than directly into blood by intravenous administration) will not necessarily produce a constant concentration in blood plasma [51]. The latter depends on factors such as the oil – in – water partition coefficients of lipid soluble drugs, molecular size of lipid soluble drugs and local blood flow [51].

1.2 Biodegradable matrices for drug delivery.

Biodegradable, bioerodible and bioresorbable are terms which are often used interchangeably in the literature to refer to simple hydrolysis and/or enzymatically induced hydrolytic degradation of polymers. However the precise definition for each term

has varied from author to author and has led to some confusion in their meaning. This problem has been highlighted in a recent review by Holland *et al* [52]. For example Williams [53] defines biodegradation as the biological breakdown of the polymeric material, as opposed to simple hydrolytic breakdown, whereas Gilding [54] reports that the phrase 'biodegradable polymer' refers to any polymer that undergoes *in vivo* degradation. The term bioerodible has been used by Heller [53 – 57] who defined it as the conversion of an initially water insoluble material to a water soluble material which may or may not involve major chemical degradation. In this thesis, biodegradation is taken to refer to hydrolytic, enzymatic and microbial degradation processes occurring in a polymer which do not necessarily proceed to a stage where the physical form of the polymer is altered.

Heller [53 – 57] has proposed three different mechanisms for the erosion of biodegradable polymers, however in practise erosion usually occurs by a combination of these mechanisms. Type I erosion occurs when water – soluble polymers that have been insolubilized by covalent crosslinking undergo hydrolysis at either the cross – links (Type IA) or at the water – soluble backbone (Type IB). Type II erosion occurs when water – insoluble polymers become water – soluble as a result of either hydrolysis, ionization or protonation of pendent groups. Type III erosion occurs by random cleavage of an insoluble polymer backbone producing aqueous – soluble oligomers. In the case of hydrophobic biodegradable polymers, erosion can be further classified as either homogeneous (bulk erosion) or heterogeneous (surface erosion) [53 – 57]. The former involves water uptake into the bulk of the matrix to cause random hydrolytic breakdown of polymer chains and therefore, random changes in the permeabilty of the matrix. In contrast, surface erosion involves controlled hydrolysis at the outer surface such that the bulk of the matrix remains essentially unchanged. Surface eroding devices potentially offer more predictable release kinetics than matrices undergoing bulk erosion and provided surface eroding devices maintain a constant surface geometry, constant drug release rates can be obtained [57].

Historically, the pioneering studies on implantable controlled drug delivery focused on non-biodegradable systems [58-60] such as polyethylene [58], silicone [59] and more recently ethylene vinyl acetate copolymers [63-80]. The first reports of non-biodegradable polymers for sustained release of peptides appeared in the early 1970's [61-62]. It was shown that prolonged release of immunoglobulin, luteinizing hormone, bovine serum albumin (BSA), insulin and prostaglandin could be achieved using cross-linked polyacrylamide and polyvinylpyrrolidine gels [61-62]. Subsequent studies by Langer and Folkman [63] using polyhydroxyethylmethacrylate and ethylene-vinyl acetate copolymers demonstrated that large molecules with molecular weights up to 2×10^6 Da can be released steadily from the implanted polymeric device over periods longer than 3 months. However, the reproducibility of the drug release was poor in these studies and was later improved upon, firstly using a low temperature solvent casting method [64-65] and later by using a sintering technique [69-70] for incorporating macromolecules into polymer matrices.

The studies of Langer and coworkers [71-74] showed that the release of proteins (using BSA as model) from biocompatible ethylene-vinyl acetate copolymers (EVAC) was dependent on particle-size and drug loading. The release mechanism involved diffusion of the protein through interconnecting channels in the matrix which were initially formed by the insolubilized polypeptide particles during matrix casting. The geometry of the device also influenced release rate [75]. Release rate was inversely proportional to the polymer molecular weight [76]. Release rates approaching zero order could be achieved by utilizing a hemisphere device with an impermeable coat, but which contained a small hole at the centre of the flat face [74]. Release durations of several months were reported. Additional controls on release rates of BSA could be obtained using magnetism [77-78] and ultrasound [79]. Although Langer and coworkers [80] have demonstrated the *in vivo* efficacy of continuous insulin release from EVAC copolymers for more than 100 days in diabetic rats, the ultimate utility of controlled release devices for insulin therapy may best be achieved by regulated pulsatile release in response to blood glucose levels.

In early studies, biodegradation of the polymer was not considered and was thought to represent a less well defined and unnecessary experimental variable [81,]. Subsequently, interest in biodegradable polymers developed for two reasons. Firstly, as the field expanded from research to application, it was recognized that surgical removal of a drug depleted delivery system was difficult, yet leaving non-degradable foreign materials in the body for an indefinite time period constituted an undesirable toxicological hazard [82]. Secondly, delivery of macromolecules and drugs with poor solubility could not be facilitated by diffusion through the polymers [73,81] and controlled erosion of polymer was thought to offer greater potential for controlling release of such drugs.

It was not until the advent of resorbable surgical sutures in the early 1970's [83] that research into biodegradable delivery systems gained momentum. A number of different classes of biodegradable polymers have been investigated for potential in controlled drug delivery applications. These include polyesters [84-85], polyamides [86], polyurethanes [87], polyacrylonitriles [88-89] and polyphosphazenes [90]. Because of their development as surgical sutures, polyglycolide (PGA), poly-DL-lactide (PLA) and their copolymers (P(LA-GA), have been the most extensively studied biodegradable systems for drug delivery.

1.2.1 P(LA-GA) polymers for drug delivery

A number of excellent reviews exist on the use of P(LA-GA) polymers for use in drug delivery and surgical applications [43,52,82,84,91-94]. These synthetic polymers are biocompatible [91-96] and hydrolytically degrade to the monomeric acids L-lactic acid, D-lactic acid, and glycolic acids. L-Lactic acid and glycolic acids are metabolized by the Krebs cycle whilst D-lactic acid is excreted intact [38]. The degradation rate is dependent on copolymer composition and related to the crystallinity of the polymers [91-93]. Poly-DL-lactide is amorphous but Poly-L-lactide (37%) and polyglycolide (up to 50%) are crystalline [93,97]. Copolymers comprising of 25-75 mole% GA are thought to be amorphous [97]. Consequently these copolymers degrade more rapidly than the crystalline

homopolymers. Careful choice of monomer composition can produce devices which can degrade completely over a desirable timescale of months to years [91,93].

The P(LA – GA) polymer systems have been used as matrix implants and as microparticles for the delivery of many therapeutic agents including local anaesthetics [98 – 99], vaccines [43], cytotoxic agents [100], steroids [101], narcotic antagonists [102 – 103], nucleic acids [104] and more recently, peptide drugs [40,41,105 – 111]. Drug release from these polymers usually occurs by a combination of diffusion and polymer degradation. In the case of P(LA – GA) microspheres containing a LHRH analog, triphasic release of the peptide has been reported [109 – 111]. In the initial phase the peptide is released from the surface layers and channels within the polymer matrix connected to the outside layers. This initial phase is followed by a "dormant" period in which the remaining peptide is trapped within the bulk matrix and is eventually released in the third phase when bulk erosion of the device occurs [109 – 111].

The major commercial success of P(LA – GA) systems to date results from their use as matrices for the continuous delivery of LHRH analogs in the treatment of prostate cancers. In one formulation, the peptide hormone (goserelin) is dispersed within a P(LA – GA) copolymer matrix (Zoladex; ICI) which degrades slowly to release the peptide over a 28 day period when inserted parenterally as a small cylindrical implant into the abdominal wall [40,41,112]. In another parenteral formulation, P(LA – GA) copolymer microcapsules deliver another LHRH analog (Decapeptyl; Ipsen Biogen) at therapeutic levels for over a month [495]. Furthermore, poly – L – lactide microspheres containing bromocriptine (Parlodel; Sandoz) have also been marketed [495] and P(LA – GA) microspheres containing norethisterone have been undergoing clinical trials and are likely to be marketed for long term contraception [113,495].

The major disadvantage of P(LA – GA) systems is that they undergo bulk hydrolysis (homogeneous degradation) as opposed to surface erosion (heterogeneous degradation) [114]. Because changes in permeability during bulk hydrolysis of P(LA – GA) matrices cannot be predicted with time, the resultant drug release kinetics are also somewhat

unpredictable. In addition, the matrix can disintegrate before drug release is complete [57] and the resultant burst in the rate of drug delivery could in some cases be fatal. Such bursts have been reported [115]. In view of these drawbacks, delivery systems having more desirable release kinetics have been examined. Hydrophobic polymers that undergo surface erosion, such as polyorthoesters and polyanhydrides, have been investigated as alternatives.

1.2.2 Polyorthoesters

Polyorthoesters can be sub-divided into the commercially developed Chronomer (Alza) series [116] and those developed by Heller and colleagues [117, 119-126] at SRI International. It is the latter series of polyorthoesters which are discussed below.

Heller *et al* [119] have synthesised surface eroding polyorthoesters by the condensation of diols and diketene acetals. Linear and cross linked aliphatic polyorthoesters have been prepared which can degrade in time frames of a few hours to many months by the addition of various basic or acidic excipients [121]. Polyorthoesters are stable in basic environments, hydrolyse slowly at physiological pH and become progressively more labile as the pH to which they are exposed is lowered [121]. Taking advantage of the pH dependence of the rate of orthoester cleavage, Heller and colleagues [117-126] have been able to achieve preferential hydrolysis at the surface by either adding basic substances (e.g. $Mg(OH)_2$) to suppress degradation in the bulk or by incorporating acidic catalysts (e.g. acid anhydrides) to promote degradation on the surface. Polyorthoesters are amorphous and by varying the ratio of the diol used, polymers with glass transitions between 20°C and 115°C can be prepared [119]. Drug loaded polyorthoester devices can be fabricated by blending both drug and excipient into the heat-softened polymer [119] or by physical mixing of drug and excipient into the viscous prepolymer and subsequent curing of the cross-linked polyorthoester at 76°C [124-126]. Although initial studies with methylene blue suggested that drug release could be predominantly controlled by polymer erosion [117-118], this has not always been the case with therapeutic drugs

[122 – 126]. Release of norethindrone from circular polyorthoester devices containing

sodium carbonate as the basic excipient, in fact, was not mediated by polymer erosion

but rather by the formation of a swollen hydrophilic layer at the surface of the

device allowing release of the drug by diffusion through the swollen polymer [122 – 123].

Although polymer erosion was thought to control both *in vitro* and *in vivo* (rabbit)

release of levonorgestrol from cross linked polyorthoester devices containing Mg(OH)$_2$

[124], incorporation of 5 – fluorouracil and a LHRH analog into the same polymer resulted

in predominantly diffusion controlled release [125]. However, as the release of the two

drugs was modified on changing the diol or the amount of copolymerized 9,10 –

dihydroxystearic acid used in the synthesis, polymer erosion was thought to be

involved, albeit to a lesser extent because changes in the drug release rates reflected

the expected changes in polymer erosion rates [125].

As a result of the variable drug release patterns obtained with cross linked

polyorthoesters, Heller and coworkers [126] have recently examined the cure behaviour of

polyorthoester implants in order to improve reaction conditions such that devices having

reproducible erosion and drug release behaviour routinely can be prepared. Clearly, the

non – reproducible release behaviour and the inclusion of additives (up to 10%w/w), which

in some cases [119] can be greater than the loading of the therapeutic agent, makes

polyorthoesters less than ideal materials for drug delivery. Furthermore, the long – term

biocompatibility of polyorthoesters and their hydrolysis products is yet to be reported

even though preliminary studies indicate absence of any adverse tissue reaction during

in vivo release experiments [117].

1.2.3 Polyanhydrides

In designing a biodegradable system that would degrade by surface erosion without the

use of additives, Langer and coworkers [129 – 134] have developed polyanhydrides based on

a variety of aliphatic and aromatic dicarboxylic acids. The aliphatic polyanhydrides

were initially proposed by Hill and Carothers in the 1930's [127,128] to be substitutes

for polyesters in the textile industry. The idea was later rejected because of their

hydrolytic instability. However by combining aliphatic segments with the more hydrolytically stable aromatic anhydrides, Langer and colleagues [130] have been able to achieve a service life in the range 2 weeks to several years for 1mm-thick polyanhydride devices. For example in the series poly[bis(p-carboxyphenoxy) alkane anhydrides] by changing the alkane from a methyl to a hexyl group, degradation rates in the range 10^{-1} to 10^{-4} mg/hr/cm^2 were obtained [130]. Degradation of polyanhydrides was pH dependent, being enhanced at high pH and slower in acidic conditions [130]. However, polyanhydrides can undergo hydrolysis under atmospheric conditions and therefore need to be stored in an anhydrous environment [134]. A recent report suggested that the materials were stable when properly packaged into aluminium foil under anhydrous conditions and the shelf life can be further extended when stored at subambient (-20°C) temperatures. However, no formal stability data were presented for the polymers [134].

The polyanhydrides are thought to be crystalline [133] and have been reported to have good biocompatibility [131]. The *In vitro* growth of mammalian cells was unaffected as measured by cell morphology and cell growth rate [131]. No inflammatory responses were observed when the polymers were implanted either into the corneas of rabbits for 6 weeks or subcutaneously into rats for 6 months. The degradation products of the polymers were thought to be nonmutagenic, noncytotoxic and were reported as having low teratogenic potential [131]. However, biocompatibility studies were only carried out on poly[bis(p-carboxyphenoxy) propane anhydride] (PCPP), poly(terepthalic acid anhydride) (PTA) and their copolymers with sebacic acid [131] and consequently, the biocompatible nature of other polyanhydrides cannot be inferred.

Drug release studies from injection-moulded devices of PCPP containing p-nitroaniline, as a model drug, showed that predominantly erosion controlled release could be obtained for up to 8 months [130]. As a result of this and a previous study with cholic acid as a model drug [129], Langer and coworkers have investigated release of a peptide (insulin) from polyanhydrides [132,133]. In the initial study, incorporation of insulin into polyanhydride microspheres (PCPP:sebacic acid, 21:79) was achieved by use of a "hot-

melt" technique since water could not be present during the encapsulation process due to the hydrolytic instability of the polymer bonds [132]. The hot–melt technique involved incorporation of peptide at temperatures above the melting of the polymer. Although the melting temperature of this polymer (76°C) was significantly lower than of the pure PCPP (225°C), the temperature employed (~80°C) can be expected to have deleterious effects on a peptide hormone. At least some of the insulin incorporated was biologically active as evidenced by *in vivo* reduction in blood glucose levels in diabetic rats for 3 to 4 days, which paralleled the rate of polymer erosion [132]. Clearly this technique of peptide incorporation was limited to polyanhydrides with low melting temperatures. In order to utilize the higher melting polymers, insulin has subsequently been incorporated into polyanhydride microspheres using a modified organic phase precipitation method involving only organic solvents [133]. However, insulin release was much faster than polymer erosion and 10% insulin loaded microspheres (50–300um) gave 4–5 days glucose control in diabetic rats [133].

The polyanhydrides, clearly, have advantages over polyorthoesters and P(LA–GA) polymers as potential drug delivery systems and on the basis of the above studies and further biocompatibility studies of polymer implants in the brains of a number of mammals, FDA has approved their experimental use in humans to treat glioblastoma multiforme, a universally fatal form of brain cancer [134].

Nevertheless, because of their highly reactive polymer bonds, polyanhydrides are susceptible to hydrolysis on storage and can also lead to drug–polymer interactions especially at high fabrication temperatures [133]. Furthermore, the inability to use water during fabrication may prevent intimate mixing of water–soluble drugs into the polyanhydride matrix. The use of high temperatures and purely organic solvents may significantly affect the stability of some peptides which may preclude their use in polyanhydride systems.

1.3 Area of Research

As a consequence of recent advances in biotechnology, poly−D(−)3−hydroxybutyrate (PHB) and its copolymers with D(−)−3−hydroxyvalerate (P(HB−HV)) have emerged as a new set of candidates for use in drug delivery. These polymers are the most common in the more general class of polyhydroxyalkanoates (PHA) which are produced by a number of microorganisms as energy reserve materials.

The major advantage of these 'biopolymers' is that they can be extracted from bacteria in a very pure form. This is in contrast to conventional synthetic thermoplastics, such as P(LA−GA) systems, which can contain inorganic catalyst residues even after extensive purification.

This study is concerned with determining the physico−mechanical properties of P(HB−HV) copolymers and investigating their potential for drug delivery.

The current literature available on P(HB−HV) biopolymers is reviewed in detail below. The subject of crystallinity and crystalline properties is also introduced briefly and remains a major theme throughout this thesis.

1.4 P(HB−HV) Polyesters

P(HB−HV) biopolymers are optically active, stereoregular polyesters which are members of the general class of compounds known as polyhydroxyalkanoates (PHA). The structure of P(HB−HV) polyesters is compared with that of the P(LA−GA) copolymers in Figure 1.1 and some examples of other polymers within the PHA series of biopolymers are given in figure 1.2.

1.4.1 Biosynthesis

The homopolymer PHB was first discovered in bacteria (*Bacillus megatarium*) by Lemoigne in the 1920 s [135−136]. It has subsequently been found in a number of different microorganisms including soil bacteria [137], estuarine microflora [138], blue green

a) Poly(hydroxybutyrate-co-hydroxyvalerate)

$$\left[\begin{array}{c} CH_3 \\ | \\ CH-CH_2-\overset{\overset{\displaystyle O}{||}}{C}-O \end{array}\right]_x \left[\begin{array}{c} CH_3 \\ | \\ CH_2 \\ | \\ CH-CH_2-\overset{\overset{\displaystyle O}{||}}{C}-O \end{array}\right]_y$$

HB   HV

b) Poly(lactide-co-glycolide)

$$\left[\begin{array}{c} CH_3 \ \ O \\ | \ \ \ || \\ CH-C-O \end{array}\right]_x \left[\begin{array}{c} O \\ || \\ CH_2-C-O \end{array}\right]_y$$
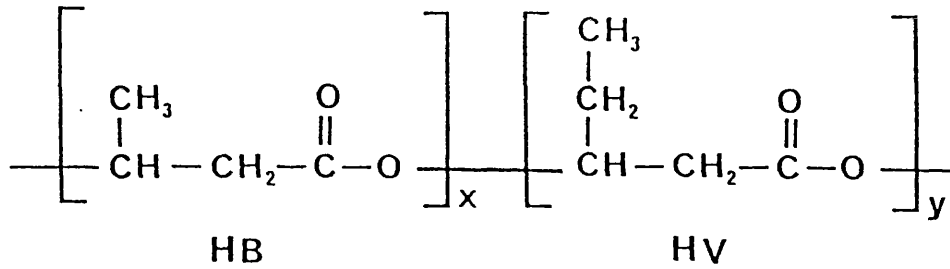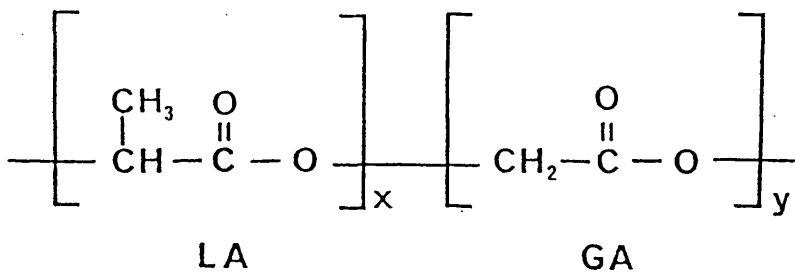
LA   GA

Figure 1.1. Structure of biodegradable P(HB – HV) and P(LA – GA) polyesters.

$$\left[O - \underset{\underset{\displaystyle R}{|}}{CH} - CH_2 - \underset{\overset{\displaystyle O}{\parallel}}{C} \right]$$
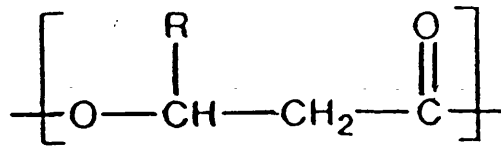
R = propyl, β-hydroxycaproate
R = butyl , β-hydroxyheptanoate
R = pentyl, β-hydroxyoctanoate
R = hexyl , β-hydroxynonanoate
R = heptyl, β-hydroxydecanoate
R = octyl , β-hydroxyundecanoate
R = nonyl , β-hydroxydodecanoate

Figure 1.2. The general structure and some examples from the PHA class of biopolymers.

algae [139] and microbially treated sewage [140]. Indeed its presence in bacteria has been used to taxonomically characterize the *Pseudomonad* species [141]. The major function of PHB in microorganisms is to serve as an intracellular energy and carbon storage product in much the same way as glycogen in mammalian tissue [137]. PHB is also thought to have minor roles in cellular functions such as sporulation [142], encystment [143] and gene expression [144]. The polymer accumulates in discrete, membrane bound granules in the bacterial cell [145-146] from which it can be extracted directly with organic solvents such as chloroform [147], or by membrane rupturing techniques such as mechanical, chemical and enzymatic disruption of cell walls [148]. Figure 1.3 shows PHB polymer molecules coming out of a bacterial cell. The percentage of PHB in bacterial cells is normally low, from 1% to 30%, but under controlled fermentation conditions of carbon excess and nitrogen limitation, overproduction of polymer can be encouraged to yields of up to 80% of dry cell weight [137,140]. This fact has been commercially exploited by Marlborough Biopolymers Ltd (a subsidary of ICI Plc) who currently produce multikilogram batches of P(HB-HV) polymers (Biopol) from a glucose-utilizing mutant of *Alcaligenes eutrophus*. The biodegradable polymers were largely developed by ICI as novel commodity plastics not dependent on the supply of petroleum [149-153].

The exact mechanism of biosynthesis and the elucidation of biochemical pathways involved in polymer accumulation/utilization in microorganisms has attracted much research interest over the years. The biosynthesis of PHB and other PHA s has been reviewed by Senior and Dawes [137,154], Oeding and Schlegel [155] and more recently by Lafferty *et al* [148]. However, because the biosynthetic pathway is still not fully understood, strong research interests remain in this area. Consequently, the majority of the literature available on PHB concerns its biosynthesis.

The exact nature of the enzymes involved in the synthesis and subsequent utilization of the energy reserve polymers are known to vary between microorganisms [137,148, 156]. The general pathway involved in the biosynthesis and degradation of PHB in *Alcaligenes eutrophus* in simplified form is represented in Figure 1.4. Essentially this scheme

Figure 1.3. An electron micrograph showing the spilling out of polymer from a bacterial cell.

(Photograph courtesy of A. Webb, ICI, UK).
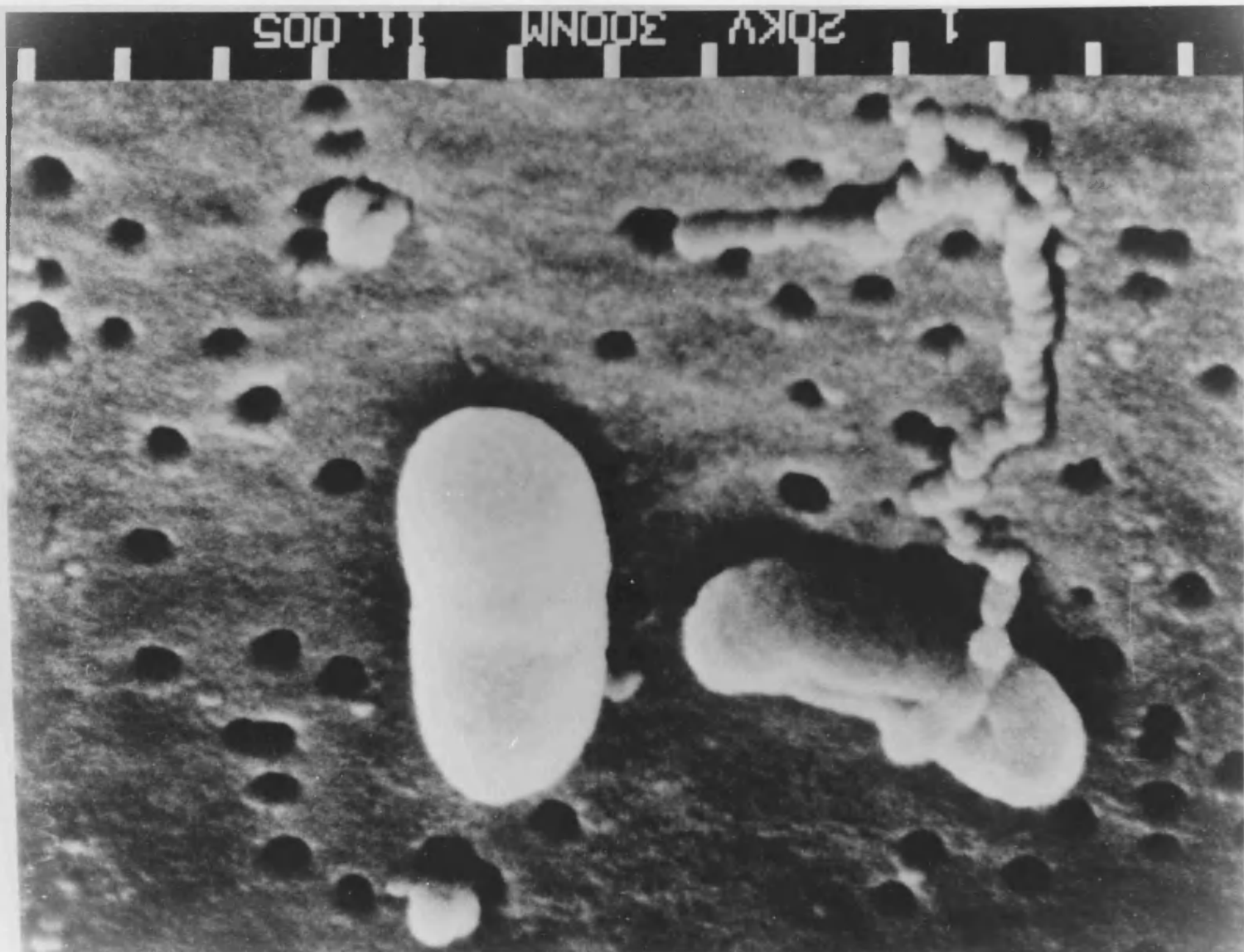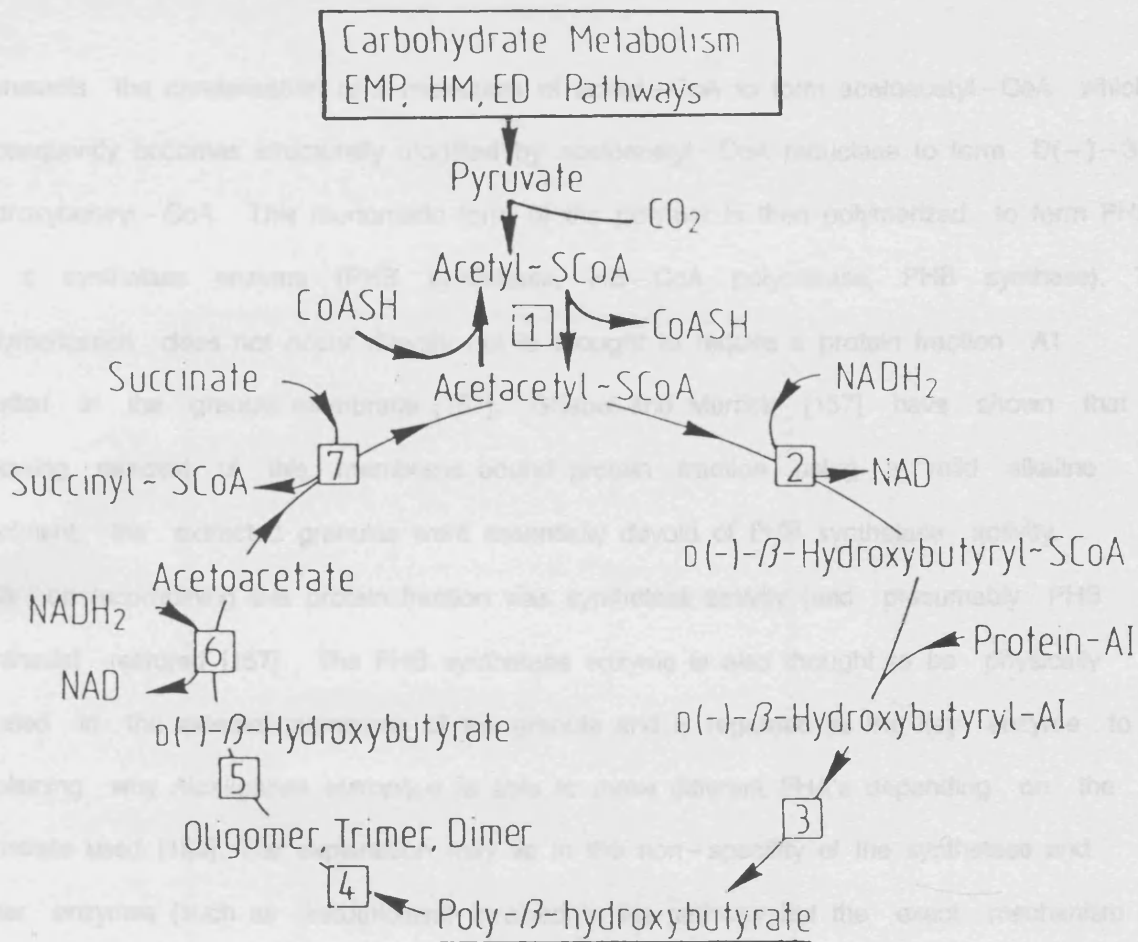
General pathway and enzymes involved in the biosynthesis and degradation of poly-β-hydroxybutyrate by microorganisms (*Alcaligenes eutrophus, Azotobacter beijerinckii*).
(1) β-Ketothiolase (β-ketoacylthiolase, acetacetyl-CoA thiolase)
(2) Acetacetyl-CoA reductase
(3) Poly-HB polymerase (Poly-HB synthetase)
(4) Poly-HB hydrolase
(5) Dimer hydrolase
(6) β-Hydroxybutyrate dehydrogenase
(7) Thiophorase (acetacetyl-SCoA thiokinase; Acetoacetate-succinyl-CoA transferase)

EMP Embden-Meyerhof-Parnas pathway
HM Hexose-Monophosphate pathway
ED Entner-Doudoroff pathway.

Figure 1.4. A simplified biosynthesis and degradation pathway of poly – D(–) – 3 – hydroxybutyrate in *Alcaligenes eutrophus*. (After ref. 137 and 148).

represents the condensation of 2 molecules of acetyl–CoA to form acetoacetyl–CoA which subsequently becomes structurally modified by acetoacetyl–CoA reductase to form D(–)–3–hydroxybutyryl–CoA. This monomeric form of the polymer is then polymerized to form PHB by a synthetase enzyme (PHB synthetase, HB–CoA polymerase, PHB synthase). This polymerization does not occur directly but is thought to require a protein fraction A1 located in the granule membrane [157]. Griebel and Merrick [157] have shown that following removal of this membrane bound protein fraction using a mild alkaline treatment, the extracted granules were essentially devoid of PHB synthetase activity. Only on recombining this protein fraction was synthetase activity (and presumably PHB synthesis) restored [157]. The PHB synthetase enzyme is also thought to be physically located in the external membrane of the granule and is regarded as the key enzyme to explaining why Alcaligenes eutrophus is able to make different PHA's depending on the substrate used [158]. The explanation may lie in the non–specifity of the synthetase and other enzymes (such as ketothiolase) involved in the pathway but the exact mechanism has yet to be demonstrated. This may not be possible until the structure of the synthetase enzyme is elucidated.

The synthesis half of the pathway in Figure 1.4 occurs during conditions of carbon excess whereas during balanced growth of the bacteria, the acetyl–CoA would normally be involved in other biochemical pathways (e.g. TCA or Krebs cycle) to produce energy and other cellular materials [137,148]. Consequently, PHB synthesis is regulated by all biochemical pathways producing or utilizing acetyl–CoA, the initial component in prokaryotic synthesis of PHB. PHB synthesis is also thought to be stimulated by conditions of oxygen, nitrogen and phosphorous limitation [137,148] (see Figure 1.5).

The reutilization of PHB proceeds within Alcaligenes eutrophus by hydrolase enzymes which depolymerize the polymer to initially its oligomeric and eventually, monomeric fractions. The monomer is converted to acetoacetate by 3–hydroxybutyrate dehydrogenase and the intracellular depolymerization is completed when acetyl–CoA is formed from acetoacetate by the action of a thiokinase enzyme. Thus acetoacetyl–CoA is made

Substrate

Balanced
growth

Carbon excess

Acetyl CoA

Energy

oxygen
phosphorus   }—— limitation   PHB
sulphur

Cell materials
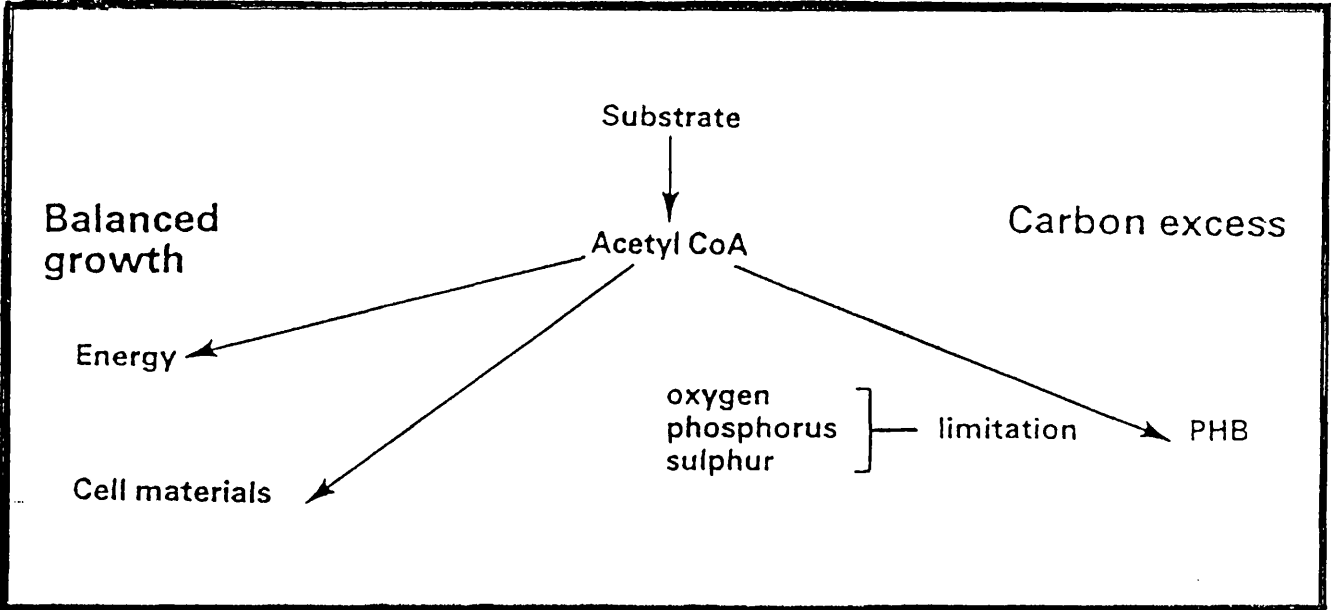
Figure 1.5. An overview of cellular conditions necessary for PHB
synthesis.   (After ref. 152).

available for incorpoation into energy producing biochemical pathways [137,148].

In *Alcaligenes eutrophus*, glucose has been found to the most efficient substrate for the commercial production of the homopolymer, PHB [151 – 152]. Other substrates such as methanol, sucrose, hydrogen, ethanol and acetic acid can also be used to produce the homopolymer [159 – 161]. Using various intracellular pathways such as the Hexose – Monophosphate pathway (HM), the organism is able to convert these substrates to the required acetyl – CoA. However, by modifying the substrate (carbon source) of *A.eutrophus*, other PHA's can be produced. P(HB – HV) copolymers are produced using a combination of glucose and propionate [151 – 153]. By adjusting the composition of the carbon sources, copolymers with up to 47 mole% HV content have been produced [149 – 153]. P(HB – HV) copolymers containing up to 30 mole% HV content are available commercially. There had been suggestions that HV contents in excess of 50 mole% could not be produced because of a relatively fast metabolic pathway from propionyl – CoA to acetyl – CoA, but recently Doi *et al* [162] have been able to synthesise copolymers with up to 95 mole% HV from *A. eutrophus* fed on pentanoic and butyric acid substrates. Doi and colleagues, who have carried out much work on PHA biosynthesis [162 – 173], have also shown that novel copolyesters of 3 – hydroxybutyrate (3 – HB) and 4 – hydroxybutyrate (4 – HB) can be produced from *A. eutrophus* when fed on nitrogen – free cultures of either butyrolactone and butyric acid [172] or 4 – HB and 4 – chlorobutyric acid [169]. Doi *et al* [167] also found that by growing the organism on pentanoic and 4 – HB acids, a novel terpolyester of 3 – HB, 3 – HV and 4 – HB could be produced.

The majority of biosynthetic P(HB – HV) and P(3 – HB – 4 – HB) copolymers have been shown by ^{13}C – NMR to be statistically random [165,169,171,176,177], this suggests that enzymes responsible for P(HB – HV) synthesis are non – specific and can polymerize related monomers with equal efficiency. However, a recent report by Doi and colleagues [173] has shown that some of the polymers extracted from *A. eutrophus* (ATCC17699, NCIB11599) were actually mixtures of two or three random copolymers. Using a variety of substrates the organism was able to synthesise some P(HB – HV) copolymers whose sequence distributions,

as determined by ^{13}C-NMR, followed neither Bernoulian nor first-order Markovian conditions, Indicating that they were neither random nor block copolymers. With the aid of thermal analysis showing displaced melting endotherms, the authors were able to interpret the sequence distributions on the basis of a model of a mixture of two random copolymers [173]. It is now thought that because NMR can hardly discern beyond the triad level, the characterization of more complex sequences arrangements (such as partial blocks or higher order regularities) cannot easily be achieved without using complimentary techniques [174]. As a result alternative techniques such as Fast Atom Bombardment-Mass Spectrometry (FAB-MS) [174] and Pyrolysis-MS [175] have been investigated for sequence determination.

One of the first reports pertaining to the natural existence of other PHA's was that of Wallen and Rohwedder [178]. The authors reported that physical blends of PHB and PHV (1:5) were accompanied by small quantities of C_6 and C_7 PHA s. Findlay and White [179] have reported the presence of at least 11 different PHA's in the microbial mass of marine sediments. Witholt and coworkers [180] found that *Pseudomonas oleovorons* growing on octane as substrate were able to produce polyhydroxyoctanoate. Using the same organism Lenz and coworkers [181-182] have recently been able to use the sodium salt of a range of n-alkanoic acids as substrates to produce PHA s containing up to 12 carbon atoms. Although all the recovered polyesters were heteropolymers, containing up to 6 different monomers, GC-MS analysis showed that the major monomer unit always had the same number of C atoms as the n-alkanoate substrate used. The authors also observed that when fed on C_9 and C_{10} substrates, the next most abundant monomer contained 2 carbons less than the n-alkanoate used for growth [182]. This finding suggested that the PHA synthesising enzymes in *P.oleovorons* had higher specifity for certain long chain substrates. This is in sharp contrast to observations with those organisms preferentially synthesising P(HB-HV) even with long chain substrates.

The non-specifity of the biosynthetic enzymes in polymer accumulating organisms has proved to be an advantage for it offers the potential of synthesizing unusual polymers

not readily synthesized chemically. The potential for making biodegradable materials with specific and preselected properties has increased commercial interests in PHA research over the last decade. This fact, coupled with advances in genetic engineering has led to studies which aim to manipulate the bacterial genes responsible for PHA synthesis in order to obtain increasingly more efficient synthesis and extraction. Indeed Peoples and Sinksey [183-184] have suggested that PHB synthesis could be used as a model system for bioengineering purposes.

Peoples and Sinskey [183] have been able to isolate the genes encoding for the first two enzymes in the biosynthetic pathway for both *Zoogloea ramigera* and *A. eutrophus*. The authors have been able to characterize the genes and report to have developed enzyme overproduction systems [183-184]. Sinskey *et al* [185] are currently investigating the location of the PHB polymerase structural gene(s) by subcloning experiments. Overproduction of PHB during the exponential growth of *Azotobacter vinelandii* UWD, a novel strain formed by transformation of the UW and 113DNA strains of *A. vinelandii*, has been reported by Page and Knosp [186].

Recently Friehs and Lafferty [187] have used genetic engineering methods to enhance the substrate spectrum of *A. eutrophus* H16. By using parts of the vector pMMB33 and a DNA fragment of the *Bacillus subtilis* chromosome, a plasmid was constructed bearing the gene for levanase, an enzyme able to hydrolyse various saccharides (cheap substrates). Transfer of this gene into *A. eutrophus* enabled the strain to hydrolyse sucrose but not to the desired efficiency. The limited growth on sucrose was attributed to inefficient transport of sucrose into the cell and/or poor secretion of levanase into the medium [187].

The genes for the first two enzymes of the PHB biosynthetic pathway in *A.eutrophus* have also been cloned and expressed in *Escherichia coli* by Slater *et al* [188] and by Schubert *et al* [189]. The *E.coli*, which does not normally synthesise the polymer, has been reported to accumulate PHB to levels approaching 80% of the dry cell weight [188]. The biosynthetic pathway in *E. coli* is thought to be controlled in a manner similar to that

found in *A. eutrophus.* The major significance of synthesising PHB in *E. coli* is that all the genetic engineering principles that apply to this organism can now be utilized in optimising the production of PHB and other PHA's. There has been a recent report that a PHB synthesizing mutant of *E. coli* has been developed from which the polymer can be extracted by mild heat treatment rather than by expensive solvent extraction techniques currently employed [190]. This strain is thought to release the accumulated polymer by thermally induced cell lysis at a low temperature of only 42°C [190]. Clearly this is an area of great commercial interest and will undoubtedly attract much further research interest.

1.4.1.1 Morphology of PHB granules

PHB and other PHA's accumulate in discrete spherical granules in the cell cytoplasm. Granules have a diameter in the range between 100 and 800nm [137,191] and are enclosed in a unit membrane approximately 2–4nm thick [191–192]. The granules are typically composed of 98% polymer and 2% protein.

The granule was originally thought to consist of a solid, central polymer core, surrounded by a intermediate zone consisting of fibrils, lamellae and chains of PHB [137,191]. The polymer was thought to be in a crystalline state and led to the hypothesis that simultaneous biosynthesis and crystallization occurred [191]. The view that PHB is solid *in vivo*, was based on studies with freeze–dried granules and prevailed despite the fact that it leads to numerous difficulties in understanding the enzymology of PHB. The most obvious of these is the problem of how it is possible for the synthase and depolymerase enzymes to operate so efficiently on a close packed solid. Recent studies by Barnard and Sanders [193–194], using high resolution ^{13}C–NMR on live cells, have suggested that PHB is predominantly in a mobile state (but not in solution) within the storage granules of *A. eutrophus* and other organisms. The authors demonstrated that water was an integral part of the granule and acts as a plasticizer for the polymer [194]. The authors propose that the enzymes involved in the PHA biosynthetic pathway

operate only on a mobile hydrated material and that the solid granules characteristic of dried cells are partially artifactual [194]. This work suggests that *in vivo* PHB is much more flexible and has an effective glass transition which is much lower than that of the solid state but the mechanism by which water plasticizes the polymer is not entirely clear. Interestingly, recent NMR studies of the analogous storage compound in humans have suggested that liver glycogen is also more mobile than previously thought [195]

1.4.2 Chemosynthesis

The chemical synthesis of PHB and similar polyesters has been reported by a number of authors [196–209]. From the early studies it was apparent that polycondensation of 3-hydroxybutyric acid does not lead to high molecular weight polymers, since the acid readily dehydrates to crotonic acid [196]. Further studies on the synthesis of PHB from racemic β-butyrolactone (BL) using various catalysts led to low molecular weight polymers with properties very different to those of bacterial PHB [197–199]. Agostini *et al* [201] were the first to report the synthesis of partially stereoregular PHB using a triethylammonium/water catalyst system. They found that by using racemic BL, a partially crystalline but optically inactive PHB (i.e. DL–PHB) could be obtained [200,202]. However, by using optically active BL (i.e. D(+)–BL) of 73% optical purity they were able to synthesize an optically active analog of the naturally occurring polymer [201]. Tani *et al* [203–204] also reported the synthesis of higher molecular weight PHB from racemic BL and were able to achieve increased crystallinity by means of solvent extraction. Both groups found that the X–ray diffraction patterns of synthetic PHB derived from racemic or partially active monomer were identical with that of bacterial PHB [200,209].

Racemic PHV (i.e DL–PHV) has also been chemically synthesized from racemic β-valerolactone (VL) by Tani and coworkers [204] when using the same experimental conditions as those for PHB synthesis. More recently Bloembergen *et al* [206] have used racemic BL and VL to prepare partially stereoregular PHB and PHV homopolymers. However by adjusting the mole ratio of the $AlET_3/H_2O$ catalyst system they were able to produce a

high molecular weight polymer fraction with a high level of stereoregularity. This fraction was reported to be highly crystalline and ^1H-NMR analysis showed that the fraction contained 85% to 87% isotactic diads [206]. The properties (melting temperature, heats of fusion and X-ray structure) of the synthetic homopolymers were reported as being similar to those of naturally occurring homopolymers [206].

In an earlier study, Bloembergen et al [207] were able to chemically synthesize statistically random P(HB-HV) copolymers from racemic BL and VL. The major significance of this was that copolymers containing the full composition range of up to 100% HV could be synthesized including those which are, as yet, commercially unavailable by biosynthesis. However, although the synthetic copolyesters were reported to be highly crystalline, they were not optically active and the low yield of stereoregular material (<25% w/w of total polymer) was considered to be a drawback. In a more recent study, the authors [208] were able to remove the atactic fractions by extraction with ethanol or acetone, to leave behind a high molecular weight polymer fraction with enhanced stereoregularity and sharp melting points.

Although the above synthetic studies were aimed at producing polymers identical to those found in bacteria, the less crystalline fractions may be preferable for some drug delivery applications providing they could be obtained in a pure form.

1.4.3 Crystalline properties

P(HB-HV) polyesters are semicrystalline polymers which have been reported to have very high degrees of crystallinity (60-80%) [149, 210-211]. The degree of crystallinity is one of the most important basic parameters characterizing semicrystalline polymers [212]. It affects virtually all other bulk properties of the polymer including mechanical, physical, thermodynamic and optical [213]. Pharmaceutically, crystallinity will influence polymer properties such as rate and mechanism of degradation, drug compatibility and drug diffusion and therefore drug release. The way in which these polymers crystallize from solution and from the melt has received great attention over

the last few years [210 – 211,214 – 218]. The exceptional purity and chemical regularity of

PHB (due to its biological origin) make it an ideal model substance for fundamental

studies of polymer morphology, crystallization and nucleation [214]. The crystallization

of P(HB – HV) polyesters from the melt is a subject of this study and will be discussed in

more detail in chapter 5. The basic concepts involved in polymer crystallization are

given below.

1.4.3.1 Crystallization in polymers

Unlike conventional "small molecule" crystals, where crystallinity generally results

from regular packing of ions or atoms, crystallinity in polymers results from regular

packing of molecular chains. The pre – requisites for crystallization include that the

polymer chains exhibit chemical and stereo – regularity [219]. The isotactic nature of the

side appendages on a linear backbone of P(HB – HV) polymer chains naturally lend

themselves to ordering by satisfying some of the structural requirements for

crystallization. Further details on structural requirements for polymer crystallization

can be found in more general books and reviews [219 – 220].

1.4.3.2 Models of crystallinity

Although polymers were known to crystallize, failure to produce crystals of a

macroscopic size for the majority of polymers suggested that they were not completely

crystalline [219]. Indeed all macroscopic properties indicated that bulk polymers

consisted of either microcrystals with large degrees of imperfection, or of an intimate

mixture of microscopic crystalline and amorphous phases.

In fact, for many years, the latter was the accepted view of polymer crystallinity. The

state of the bulk polymer was regarded as that of crystals of the order of several

hundred Angstroms in size imbedded in an amorphous matrix. The polymer chains (which in

a typical polymer are 0.1 – 10um in length) were viewed as threading their way through

more than one crystallite (in which they were ordered) via amorphous regions (in which

they were less ordered). This concept of polymer crystallinity is known as the 'fringed

micelle' model and is depicted in Figure 1.6 [221 – 222]. The relative abundance of the two phases, crystalline and amorphous, is termed the degree of crystallinity.

The validity of the fringed micelle model of polymer crystallinity came into serious question in the mid 1940 s, when it could not be successfully used to explain the structure of the then newly discovered spherulites [223]. Spherulites are spherically symmetric collections of crystallites which commonly result when polymers are crystallized from the melt and are discussed in more detail in chapter 5.

Then in 1957 [224 – 226] it was discovered that single crystals of polymers (polyethylene) could be grown from dilute solution. The type of structures observed in these early investigations can be represented by Figure 1.7 which shows single crystals of PHB. The crystals are sheet – like and often termed lamellae. Lamellae form because of the kinetics of nucleation and growth [220]: they can develop faster than crystals with alternative molecular conformations [227]. The discovery of lamellae was to radically change the concept of polymer morphology and its consequences. Keller [224] proposed that this discovery necessitated that a single molecule thread many times through the same crystal, which it does by folding in the crystal surface. This marked the advent of the chain – folded concept of polymer crystallinity. The evidence from which Keller drew his conclusions on chain – folding was supported by similar, independent observations of Fischer [225] and Till [226].

Knowing the crystal structure of polyethylene from the work of Bunn [226], Keller's electron diffraction experiments proved that the polymer chains were arranged perpendicular to the large, flat faces of the lamellar crystals. The thickness of the lamellar crystals was in the vicinity of 11 – 14nm (depending on temperature of crystallization) and this was far less than the contour length of polymer molecules (approximately 200nm). On the basis of this information, Keller concluded that the upper and lower surfaces of the single crystals consisted of chain folds.

Density measurements of polymer single crystals were somewhat lower than their
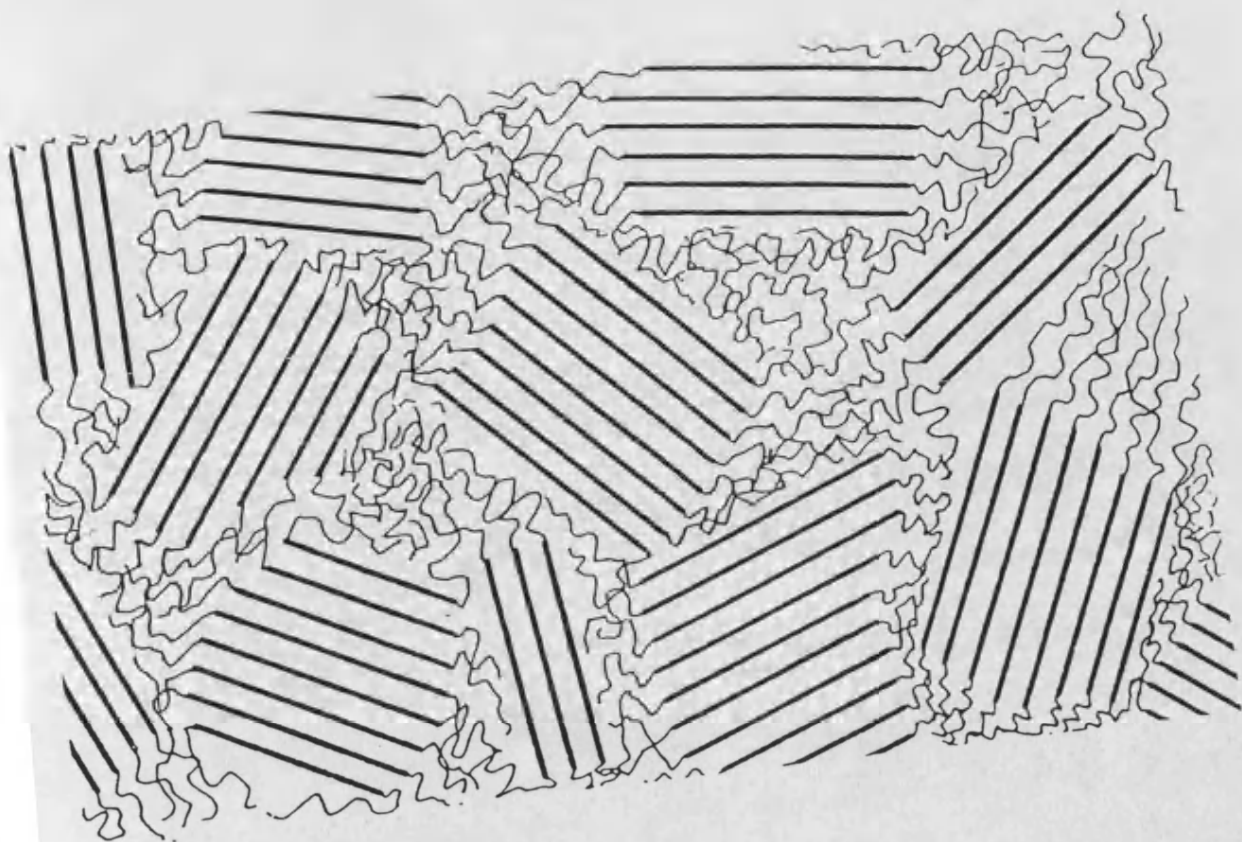
Figure 1.6. The Fringed Micelle model of polymer crystallinity. (From ref.230).

Figure 1.7. Solution grown single crystals of PHB.

(Photograph courtesy of Lyn Welland, University of Bristol, UK).

Scale bar = 2nm.   ├─────────────────┤
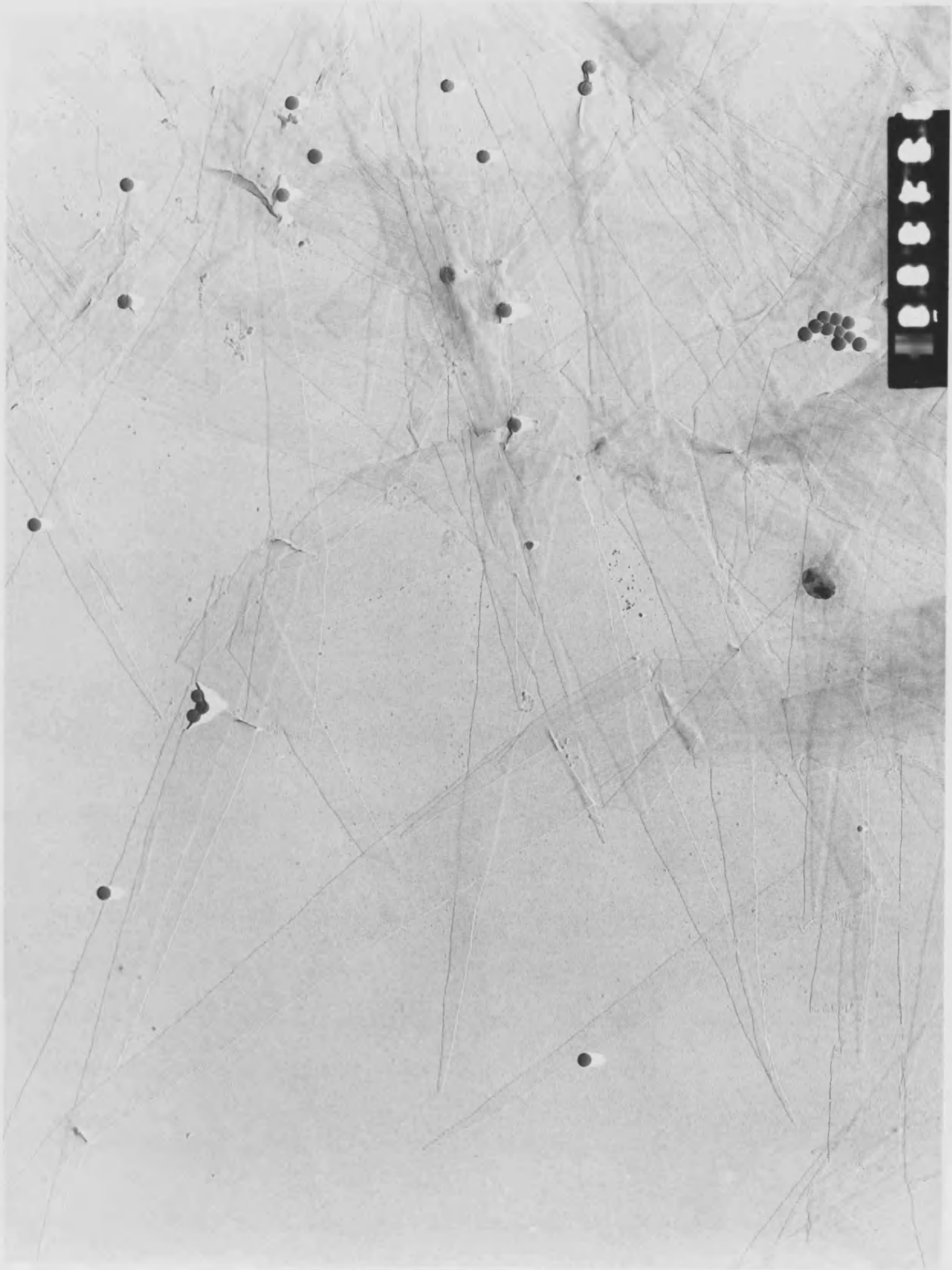
theoretical crystal densities (PHB is no exception) calculated from the dimensions of the unit subcell [219]. This density defect suggested that polymer single crystals were not 100% crystalline but contained amorphous regions which made them polycrystalline in nature. It is thought that the amorphous component causing the density defect results from the irregularity of the chain folded surface [229]. The chain folded model of crystallinity depicting varying amounts of irregularity in the folding of chains is given in Figure 1.8. Even when folding is regular (adjacent re-entry) there remains a density defect and for that reason the folds, themselves, have been regarded as the amorphous regions [229-230]. Although the chain-folded model of crystallinity is regarded as basically correct, there still remains some confusion over the exact reasons for the density defect and hence, the nature of the amorphous component. Some investigators attribute practically the entire density defect in single crystals to surface roughness in the form of long loose folds, while others attribute it an an amorphous surface zone arising mostly from non-adjacent re-entry on a large scale. Furthermore, Hoffman et al [220] suggested that the amorphous zone may actually consist of independent polymer chains that are physically adsorbed on the fold surface.

Chain folding is not unique to traditional synthetic polymers but has also been reported to occur in a number of biological polymers including sonically degraded salmon sperm DNA [231] and synthetic peptides as exemplified by the calcium and barium salts of poly (L-glutamic acid) [232]. There is also a suggestion that DNA of viruses may crystallize by chain folding when packed into the intact head of the virus [233]. Clearly, the phenomenon of crystallization with chain folding is a very common one.

1.4.3.3 Crystal structure of PHB and P(HB-HV) copolymers.

Historically, Marchessault and coworkers [234] made the first solid state investigation of PHB and to date Marchessault's group has continued to study the crystalline properties of this polymer. In 1963 [234] they were the first to produce single crystals of PHB and were able to deduce, from x-ray diffraction data, that PHB had a fibre repeat
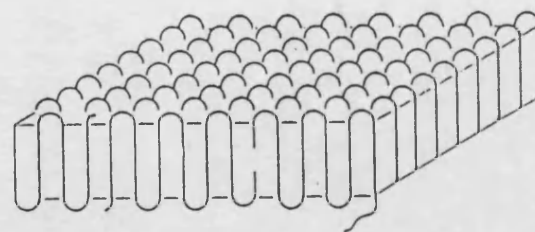
A Regular, adjacent re-entry folds similar to those postulated as present in pyramidal crystals that have been grown from solution
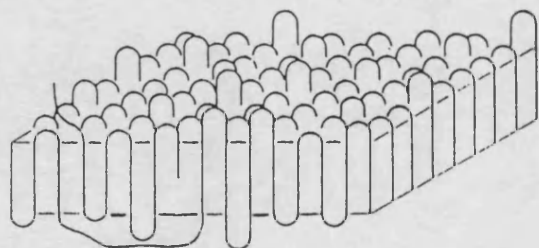
B Irregular, adjacent re-entry folds in which the extent or thickness of the irregular layer is suggested to be proportional to the temperature

C Switchboard, or nonadjacent re-entry model in which an even more nonordered amorphous layer is present on both sides of the lamellae than in the irregular model

Figure 1.8. The Chain Folded models of polymer crystallinity (from ref. 230).

of 0.59nm. Although Lundgren et al [147] found that PHB from different bacterial genera gave identical X-ray diffraction patterns irrespective of source, the crystal structure remained unknown.

The detailed crystal structure of the homopolymer, PHB, was first identified by Okamura and Marchessault in 1967 [235-236]. Using X-ray diffraction the unit cell (more accurately sub-cell) was identified as orthorhombic with the lattice parameters a= 0.576nm, b= 1.320nm and c= 0.596nm (fibre axis) and is represented in Figure 5.3 (chapter 5). They proposed that PHB existed as a right handed helix with a two fold screw axis and that two anti-parallel chain molecules pass through the sub-cell. The latter finding was in accord with the proven occurrence of chain folding in single crystals of PHB [234]. On the basis of the above findings, Okamura and Marchessault proposed that the space group for PHB was $P2_12_12_1$ and that the theoretical crystal density was 1.262 g/cm^3. The amorphous density was later proposed to be 1.171 g/cm^3 [214]. Further structural studies on PHB using electron or x-ray diffraction by Marchessault and coworkers [237-239], Yokouchi et al [209] and recently by Bruckner et al [240] have generally confirmed the original findings of Okamura and Marchessault [235].

The crystal structure of PHV is similar to PHB and was first reported by Yokouchi et al [205]. X-ray diffraction studies on melt-drawn samples of synthetic racemic PHV showed that the unit cell was also orthorhombic with the lattice parameters: a= 0.932nm, b= 1.002nm and c= 0.556nm (fibre axis) and had the same space group as PHB [17]. The lattice parameters for the subcell of synthetic PHV were latter confirmed by Pundsack and Bluhm [241] using a specimen tilting technique to obtain 3-dimensional electron diffraction data of PHV single crystals.

Marchessault et al [242] showed that naturally occurring PHV had similar sub-cell dimensions to the synthetic racemic PHV except that the lattice parameter "a" was significantly higher at 0.952nm. The study was carried out on a polymer sample extracted from activated sludge [242] which was thought to a physical blend of PHB and PHV.

However there was some uncertainty about the nature of the polymer sample and therefore the reported pure PHV crystals may well have been those of a heteropolymer.

It is thought that due to the similar crystal structures (and dimensions of the monomeric units) of PHB and PHV, in statistically random P(HB-HV) copolymers (synthetic and naturally occurring), the HB and HV units can co-crystallize within either sub-cell [208,210]. This is termed isodimorphism and the sub-cell chosen for crystallization depends on HV content. The PHB sub-cell is found at HV contents below about 30 mole%, above which the PHV sub-cell is used for co-crystallization [210]. However, there had been earlier, a suggestion by Mitomo et al [243-244] that HV units were incapable of crystallizing and remained amorphous but this work has been subsequently reported to be inaccurate by the co-authors [245].

1.4.3.4. The degree of crystallinity of P(HB-HV) polymers.

Early workers reported that the homopolymer was about 60-90% crystalline [149]. This has been confirmed by more recent work [211,214] and is essentially correct. However, the early reports of copolymers being less crystalline [149,246,247] are now thought to be misleading. On the basis of their heats of fusion, Holmes and colleagues [149,247] reported that the crystallinity of P(HB-HV) copolymers decreased with increasing HV content and Owen [248] using wide-angle X-ray diffraction studies on melt-crystallized samples came to the same conclusion. However, because the heats of fusion for the 100% crystalline copolymers are not yet known and because of the unknown contribution of HV to the amorphous phase, a matter currently under investigation [249-250], the use of copolymer heats of fusion and their comparison with the heat of fusion of the homopolymer to determine the degree of crystallinity is not valid. It is now known that the rate of crystallization in the copolymers is slower than the homopolymer (chapters 4 and 5) [211,251] and therefore after relatively short periods of time following fabrication the copolymers are known to be less crystalline than the homopolymer. It is thought that Owen did not allow samples to attain equilibrium crystallinity before

assessing their degrees of crystallinity [250].

The present view is that the P(HB–HV) copolymers have similar degrees of crystallinity to PHB [211]. These results concurred with the opinion that P(HB–HV) copolymers are isodimorphic [210]. However, a recent report showing that density of the copolymers decreases with increasing HV content [249], is incompatible with the previous suggestions that crystallinity remains constant independent of HV content and that there is equal concentration of HV in the crystal and amorphous phases [210–211]. It is therefore likely that some exclusion of HV units from the P(HB–HV) lattice occurs during crystallization of copolymers and this may explain the fall in density with increasing HV content. The overall degree of crystallinity may still remain essentially independent of HV content, but will be influenced by the degree of HV inclusion for each P(HB–HV) copolymer.

Crystallinity of the unusual copolyesters of 3–HB and 4–HB has been reported to decrease with increasing 4–HB content when determined by thermal methods [169]. Furthermore, PHA s containing long side appendages (n–pentyl or greater), as produced by Lenz and coworkers [182] by growing *P.oleovorons* on long chain substrates, are also crystalline (melting range 45–61°C; heat of fusion up to 8.3 cal/g).

1.4.4 Solubility and Conformation of PHB In solution.

P(HB–HV) polymers are soluble in a number of organic solvents [252–253]. The solubility of the homopolymer, PHB, in various solvents is summarized in Table 1.1. The solubilities are naturally dependent on temperature and polymer molecular weight. Chloroform has been the most common solvent used for P(HB–HV) polymers. To achieve complete solubilization at even modest concentrations (2%w/v polymer), the crystalline polymer can require refluxing in chloroform (~62°C) for up to 24 hours. No reports on the solution conformation of P(HB–HV) copolymers exist in the literature, but initial studies by Marchessault *et al* [254–255] suggested that the homopolymer, PHB, actually retained its solid–state helical conformation in solution following their studies with

chloroform, trifluoroethanol (TFE) and ethylene dichloride. The authors based their conclusions on optical rotatary dispersion (ORD) experiments which showed a helix – coil transition for PHB when the temperature or the solvent composition was varied. However, they ignored their results from viscosity experiments which suggested a random coil conformation of PHB in chloroform [254]. Akita *et al* [256] using both viscosity and light scattering data concluded that the molecular conformation of PHB in what Marchessault *et al* [254–255] called helicogenic solvents was essentially random coil and the molecule was expanded by an unusually large volume exclusion. These authors used PHB samples with narrow molecular weight distributions in contrast to the studies of Marchessault *et al* [254] where samples used had polydispersities ranging up to 6. Further work on PHB by Fujita and coworkers [257–259] confirmed that an unusually large volume exclusion occurs in TFE. The more recent work of Doi *et al* [176], who used ^{13}C–NMR to show that the PHB molecule in chloroform was not rigid but rather flexible, supports the random coil hypothesis.

Table 1.1. Solubility Properties of PHB (After refs. 148 and 252)

Highly soluble in:

Chloroform	Ethylene carbonate	Dimethylformamide
Dichloromethane	Propylene carbonate	Ethylacetoacetate
Di –, tri –, and	Trifluoroethanol	Triolein
tetra – chloroethane	Acetic anhydride	Acetic acid
Dichloroacetate	1N Sodium hydroxide	Alcohols (with more than 3 Carbon atoms)

Fairly soluble in:

Dioxane	Toluene
Octanol	Pyridine

Insoluble in:

Water	Dilute mineral acids	Ethyl acetate
Methanol	Alkaline hypochlorite	Ethylmethylketone
Ethanol	Diethylether	Tetrahydrofuran
Propan – 1 – ol	Hexane	Ethylformiate
Propan – 2 – ol	Benzene	Butyl acetate
Cyclohexanol	Cyclohexanone	Valeric acid
Carbontetrachloride		Tributyl citrate

1.4.5 Physicomechanical properties

When extracted from different bacterial sources, the homopolymer, PHB, has essentially similar properties [260]. Furthermore, the properties of PHB extracted from *Alcaligenes eutrophus* are thought not to vary with the nutrients used for fermentation [150]. Molecular weights of the polymer obtained have been reported to change with the bacterial source but there have been suggestions that the variation in molecular weight may due to the extraction process used [159]. The different extraction processes are thought to lower the polymer molecular weight to varying extent [159]. A recent report by Scandola *et al* [261] showed that PHB extracted from *Rhizobium* sp. using HCl (0.1M) had a molecular weight of 60K but when extracted with acetone PHB samples had molecular weights of the order 10^6.

PHB is a crystalline thermoplastic with melting range of $160-180°C$ depending on the molecular weight and thermal history of the sample [149,211,214,262-263]. It can be melt or solution processed into films, sheets and fibres [149,246]. P(HB-HV) copolymers are also semicrystalline thermoplastics but generally have lower (as low as $80°C$ [262]) melting points than the homopolymer depending on the HV content [262-263]. There appears to be a eutectic minimum in their melting points at about 30 mole% HV [210]. The eutectic minimum is a rare occurrence in normal copolymer systems where melting points usually continue to fall with increasing comonomer content [262]. Based on this eutectic minimum coupled with the facts that the degree of crystallinity appeared to be high (60-80%) and independent of HV composition and that NMR analysis showed comonomer sequence distributions to be Bernoulian, Marchessault and colleagues [210,262] concluded that the P(HB-HV) polymers were isodimorphic. The crystal structures and dimensions of the unit cell, as mentioned above and according to Marchessault et al [210], further satisfy the criterion necessary for isodimorphism. However there remains some doubt as to the extent of HV inclusion within crystals and hence the relative distribution of HV into amorphous and crystalline domains [249-250].

The glass transition temperatures of PHB and P(HB-HV) copolymers have been reported by

Akhtar and Pouton [263] to lie in the range −5 to +20°C (as determined by differential scanning calorimetry) and appeared to be independent of copolymer composition but dependent on the thermal history of the polymer. This suggests that the amorphous regions of the polymers will exist in the rubbery state at physiological temperatures.

Baptist and Werber [260] were the first to report empirical data on the mechanical properties of the homopolymer. In a general paper outlining the isolation and characterization of PHB from *Rhizobium* sp., they noted the relatively brittle nature of the crystalline homopolymer and suggested that its properties may be improved by plasticization with a variety of esters, chlorinated hydrocarbons, polyglycols and some nitriles [260]. These compatible plasticizers were thought to lower the tensile modulus by suppressing or slowing down crystallization. However, no supporting evidence was given to confirm this statement.

Akhtar *et al* [264] have shown, using static tensile tests on chloroform cast thin films (30 − 50um), that although the homopolymer PHB is relatively hard and brittle, copolymerization with HV produces tougher, less brittle and more pliable polymers. It was suggested that in some cases, the copolymers may be preferable for manufacture and implantation of biomedical devices [264]. These authors further noticed that the inclusion of a particulate drug (Sodium Fluorescein) modified (lowered tensile strength and elongation) the mechanical properties of these polymers [264]. The use of hydroxyapatite and other fillers in PHB has been used to modify the mechanical properties of the polymer for certain surgical applications [265 − 268].

Dynamic mechanical properties of P(HB − HV) polymers have been studied by several groups [248,261,269,275]. Using isotropic copolymer films cast from both chloroform and methylene chloride, Owen [248] showed that the modulus decreased with increasing HV content. Owen [248] used two P(HB − HV) copolymers, one containing 17 mole% HV but the other was quoted as having 25 − 30 mole% HV. The latter sample is now thought to have contained only 20 mole% HV [270]. There have also been suggestions that mechanical

properties change with time on storage [269]. The morphological changes on storage (ageing) have been examined in this study and are further discussed in chapter 4. The homopolymer, PHB, is thought to be thermally unstable at temperatures marginally above the melting point [247]. Barham *et al* [214] have reported that a PHB sample stored at 190°C for 1 hour had degraded to half its original molecular weight. It is well known that the major pyrolysis product of PHB is crotonic acid [247,260,271] and that this was produced by the β-elimination reaction [247,273]. Grassie *et al* [272], using Thermal Volatilisation Analysis (TVA) and subambient TVA (SATVA), showed that significant quantities of PHB oligomers and small quantities of isocrotonic acid were also evolved on heating the polymer to around 300°C. In addition, small amounts of carbon dioxide, propene, ketene, acetaldehyde and 3-butyrolactone were also reported to be evolved but the authors showed that these were secondary products formed by further decomposition of the primary products [272].

Billingham *et al* [247] have recently studied ways of improving the melt stability of synthetic and bacterial PHB. The degradation properties of the synthetic and naturally occurring polymers were similar once the catalyst residues were removed [247]. The authors found that PHB was, in practical terms, on the limit of melt processability but could be moulded and extruded satisfactorily within a small processing window of short residence times. They found that conventional stabilizers had little effect in preventing degradation of PHB. They were able to increase the thermal processing window of PHB by incorporating plasticizers. However, the amount of plasticizer that could be included into PHB was limited because of its high crystallinity and therefore this method was not as effective as in other polymer systems [247].   Although much information is available on the thermal processing of PHB, little is known, as yet, about P(HB-HV) copolymers. Several reports have suggested that the copolymers are more stable and can be processed without significant degradation [247,262].

P(HB-HV) polymers are known to exhibit piezoelectricity [274-277]. The orthorhombic subcell of the crystalline polymers lacks symmetry and therefore mechanical deformation

of the crystal in directions other than tension results in surface polarization or charging. Since electrical stimulation is thought to promote bone healing and repair [278], P(HB – HV) polymers have been suggested for use as bone pins and plates [149].

1.4.6 Biodegradation

1.4.6.1 Microbial degradation

The potential use of PHB and related polyesters as commodity plastics relies on their biodegradation in natural environments. Extracellular enzymes of a number of microorganisms have been reported to cause degradation of PHB [137]. Figure 1.9 shows the extracellular degradation of PHB by a mycelial fungus. Many soil bacteria are known to completely degrade PHB and utilize the polymer as a carbon source [137,148,279]. Merrick et al [280] showed that extracellular degradation of PHB by Pseudomonas sp. yields the dimeric 3 – hydroxybutyrate, which was then later reported as being actively taken into the bacterial cell and hydrolysed to the monomer by the intracellular hydrolase [281,282]. The monomer can then participate in intracellular biochemical pathways providing energy for the bacterium. The exoenzyme is thought to be released during the growth phase of the organism but mainly at its cessation [281]. Further work by Lusty and Doudoroff [282] showed that the extracellular depolymerase of P. lemoignei actually consisted of two fractions, A and B. Fraction A converted the polymer to the monomer and dimer whereas fraction B of the depolymerase yielded the trimer. The extracellular depolymerase enzyme from Alcaligenes faecalis has been isolated and fully characterized by Tanio et al [283 – 285]. This organism was able to utilize PHB as the sole carbon source. The extracellular depolymerize when purified by Tanio et al [283 – 284] had a molecular weight of 48K (gel filtration) or 50K (polyacrylamide gel electrophoresis) and was optimally functional at a pH of 7.5. The depolymerase converted the PHB to predominantly the dimer but small amounts of the monomer were also detected [283 – 284]. The enzyme activity of this depolymerase was found to decrease when treated with trypsin [285]. This loss of activity was attributed to the removal of the hydrophobic site on the depolymerase by trypsin [285]. It is now evident that a broad

Figure 1.9. A scanning electron micrograph showing extracellular degradation of a PHB film by a mycelial fungus. Note the etching of the polymer film adjacent to the fungus.

(Photograph courtesy of A. Webb, ICI, UK)
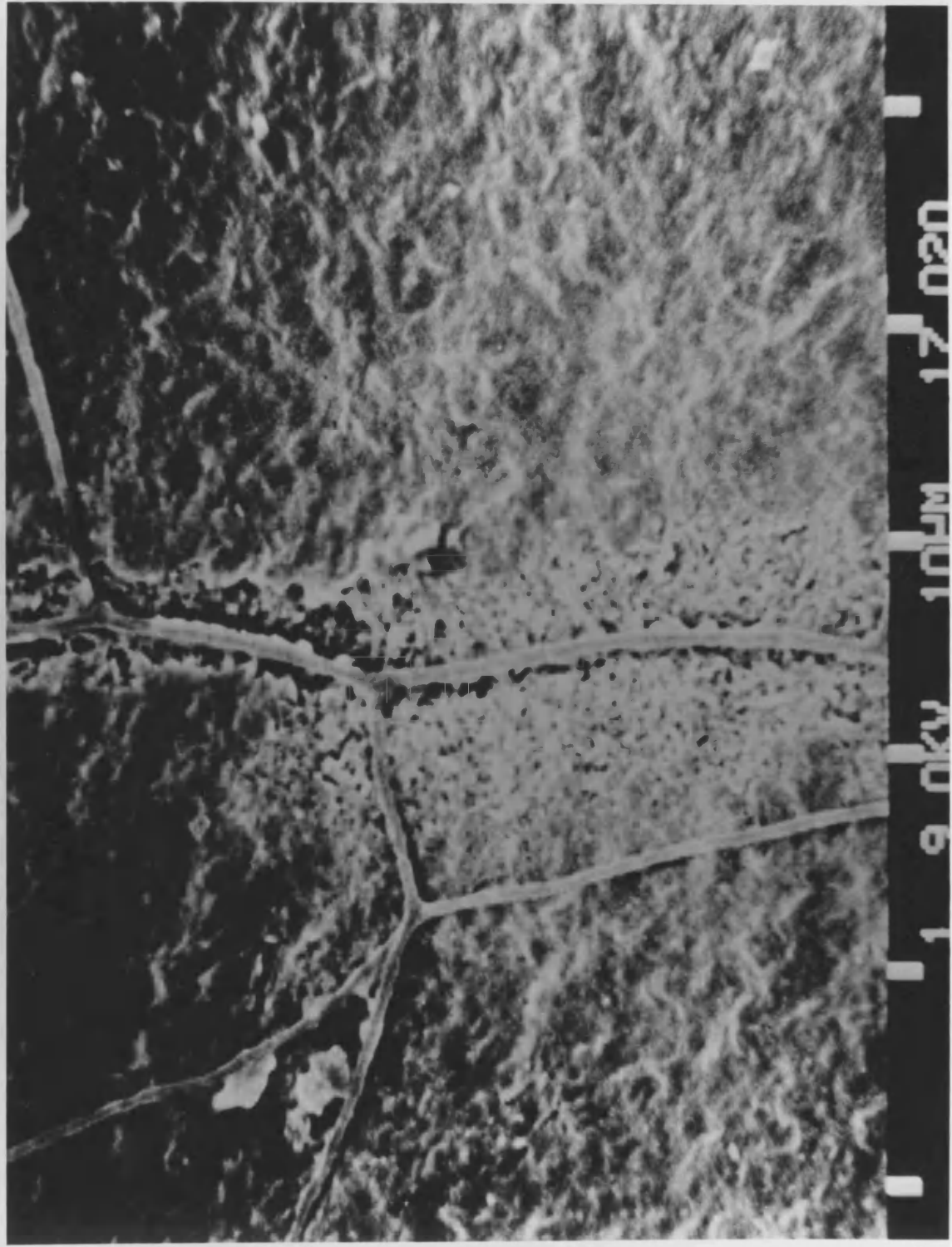
spectrum of bacteria can depolymerize PHB and presumably other PHA's. Table 1.2

summarizes the biodegradation of PHB in soil and various other environments.

Table 1.2 Biodegradation of PHB in Various Environments (After refs. 148 and 246).

Environment	Period for Dissolution of 1mm thick-section (weeks)	Average rate of surface erosion (um/week)	Period for 100% weight loss of 50um thick packaging film (weeks)
Anaerobic Sewage	6	100	0.5
Estuarine sediment	40	10	5
Aerobic sewage	60	7	7
Soil at 25°C	75	5	10
Sea water at 15°C	350	1	50

Doi *et al* [172] have recently reported that the P(3-HB-4-HB) copolymer containing 17mole% 4-HB degraded more rapidly in soil than pure PHB. However, no comparison was made with P(HB-HV) copolymers. Although few (if any) reports are currently available on the degradation of other PHA s it is likely they too are degraded by microorganisms but possibly at different rates. Furthermore it remains to be seen whether mammalian enzymes can influence the degradation of P(HB-HV) and other PHA polymers.

1.4.6.2 *In vitro* and *in vivo* degradation of P(HB-HV) polymers.

In a manner similar to the microbial degradation, *in vitro* degradation of PHB is thought to proceed to the monomer, D(-)-3-hydroxybutyric acid. The acid is a normal constituent of blood and along with acetoacetate and acetone represents one of the three ketone bodies which are produced endogenously as a result of ketogenesis. It is therefore thought that PHB will be well tolerated *in vivo*. However, limited information is available, at present, on the hydrolytic degradation of P(HB-HV) polymers and even less (if any) on other PHA s.

Majid *et al* [286-287] have reported that the *in vitro* degradation of PHB proceeded relatively slowly when compared to P(LA-GA) polymer systems. Their studies on the

degradation of thin solvent cast films (85um) at 37°C and pH 7.4 suggested that the half life of these PHB films was about 152 weeks [287]. They found that the degradation rate of P(HB – HV) copolymers appeared to be more rapid but the relationship was not linear (Figure 1.10). The rate of hydrolysis (mass loss over a 50 week period) in these polymers was reported to follow zero – order kinetics but the authors expressed some reservation because the degradation data from some copolymers could also be made to fit first – order kinetics [286]. Because water uptake into the polymers was too low to be measured precisely (less than 0.01%), the above results led the authors to conclude that in vitro degradation of P(HB – HV) polymers proceeded by a surface erosion mechanism. This was also confirmed by molecular weight analysis of degraded polymer samples. The molecular weight of PHB remained unchanged throughout the 50 week degradation period in which the polymer films incurred a 15% mass loss. Similar results were found for the copolymers under accelerated degradation conditions (0.1N NaOH, 75°C) where mass losses of up to 87% for the copolymer containing 12 mole% HV, resulted in little or no molecular weight loss [286 – 287]. This was in contrast to the bulk hydrolysing P(LA – GA) polymers in which mass loss during the degradation process was accompanied by large decreases in molecular weight [286 – 287]. A brief report by Gilding [54] also confirmed that no molecular weight loss of PHB samples was detected after 6 months of in vitro hydrolysis.

Tighe and coworkers [288 – 289] have also carried out extensive in vitro degradation studies with P(HB – HV) polymers. In their first study [288] they examined the effect of copolymer composition, molecular weight, fabrication technique, pH and temperature of the media together with effects of plasma on the hydrolytic degradation of P(HB – HV) copolymers. Using a combination of techniques to assess bulk and surface erosion, such as gravimetric and goniophotometric analysis, the authors found that degradation was enhanced when using alkaline media conditions, elevated temperature or low molecular weight polymer [288]. Also increasing HV contents of P(HB – HV) polymers up to 20 mole%, progressively increased degradation rates [288] which in principle was slightly different to the findings of Majid et al [286 – 287] who reported a maximum for 12mole%
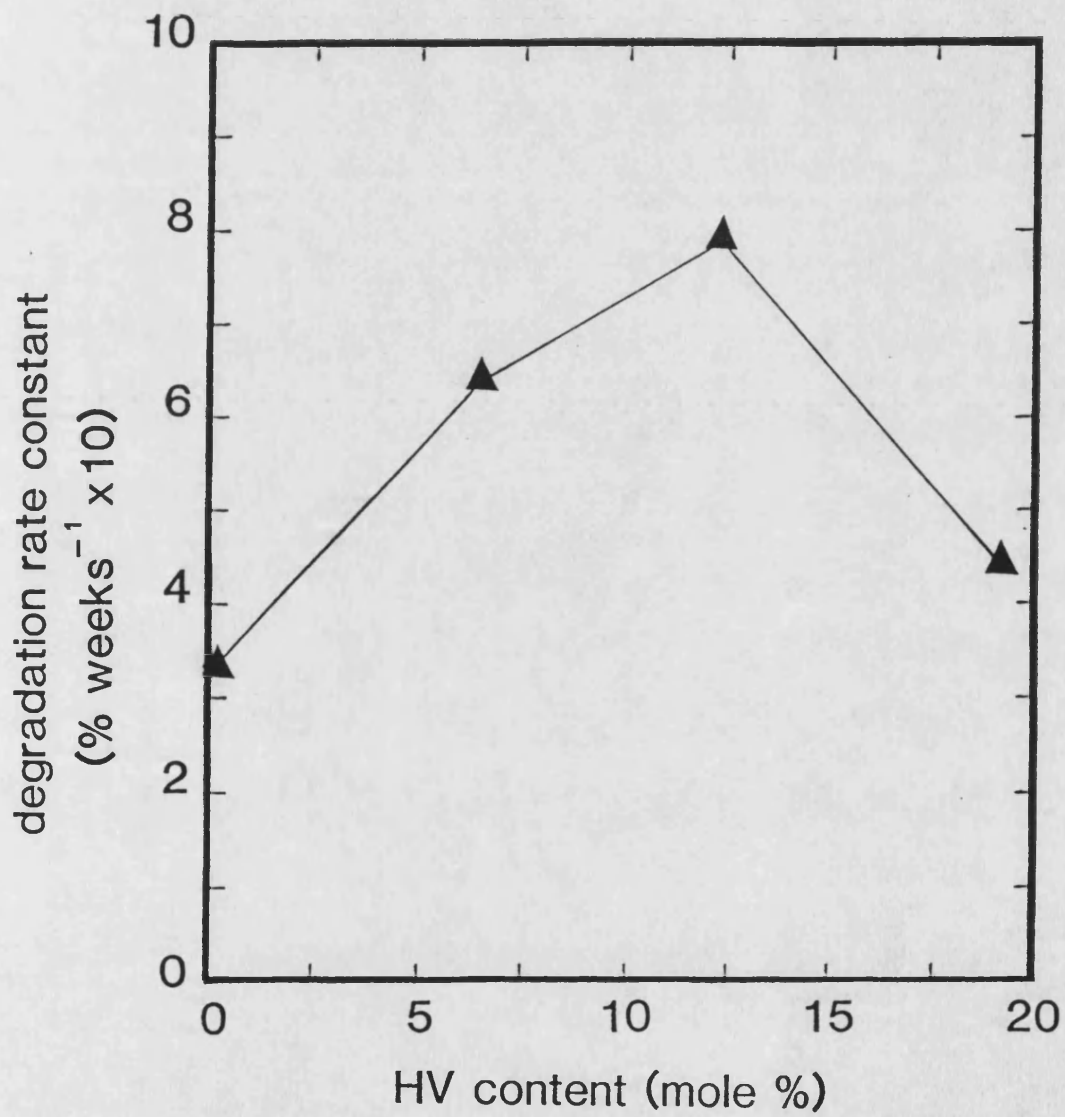
Figure 1.10. The *in vitro* degradation rates of P(HB – HV) polyesters. (After ref. 286).

HV. Tighe and colleagues [288] also found that fabrication technique had a profound effect on the degradation rate of the polymer. In using four different fabrication techniques, the authors reported increasing stability to hydrolytic attack in the order cold compressed discs, solvent cast films, melt pressed discs and injection moulded devices [288]. The trend reflected changes in porosity (compaction) and crystallinity which appeared to be the main determinants of polymer degradation.

The gravimetric data of P(HB – HV) polymers obtained by Tighe and coworkers [288] is at variance with that reported by Majid et al [286 – 287]. Tighe and coworkers [288] found that although surface erosion does occur over the initial stages of the degradation, this is eventually superceded by the underlying bulk hydrolysis in the latter stages of degradation as indicated by rapid weight loss and increased porosity of the matrix. These results have been supported in a recent report by Knowles and Hastings [265]. The differences reported, both in the rate and mechanism of P(HB – HV) polymer degradation, may be explained by reference to the sterility of the release media used in the different studies. In the case of Majid et al [286 – 287] the media used for degradation studies was steam sterilized prior to use, thereby eliminating possible contamination with microorganisms. However, no sterilization of media in the other studies was reported. A preliminary study [290] in this laboratory has shown that by using non – sterilized distilled water as the hydrolysing medium, degradation of P(HB – HV) polymer films (30 – 50um thick) occurred within 2 – 3 weeks, during which time all mechanical integrity of films was lost. The effect was more pronounced with copolymers. Subsequent microbiological analysis of the medium suggested the presence of *pseudomonas* sp., amongst others, as the contaminating agents [290]. Clearly much further work is necessary to to establish the role of both bacteria and mammalian enzymes on the degradation of P(HB – HV) polymers.

In contrast to the above studies, Miller and Williams [291 – 292] using mechanical property changes to monitor the *in vitro* and *in vivo* degradation of P(HB – HV) polymers, reported little or no degradation of PHB monofilaments. Although their failure to

measure cross-sectional areas of some monofilaments before tensile testing, made interpretation of some their results difficult, they concluded that the homopolymer biodegrades *in vivo* (sub-cutaneous implant in rats) only after pre-degradation with 10Mrad gamma-irradiation where the rate of degradation was much faster *in vivo* than *in vitro*. They found that increasing the HV content of P(HB-HV) copolymers (8-17 mole%) did not enhance degradation but at elevated temperature conditions (phosphate buffered saline pH7.2 at 60°C or 70°C) increasing HV content actually retarded the degradation rate [291].

Doyle and Bonfield [268], using PHB (initial Mw range 0.5-1.5 x 10^6) alone and in combination with hydroxyapatite found that injection moulded samples that had been sterilised by gamma-irradiation (2.5Mrad dose) showed significant hydrolytic degradation during a four month study period. Degradation was monitored by mechanical property changes of specimens immersed in sterile phosphate buffered saline pH 7.4 at 37°C. However, the authors did not measure the molecular weight of the polymer after melt processing or after irradiation sterilization and therefore the molecular weight of PHB samples used in the degradation were not known [268]. Furthermore, a recent report by Gerlach and Pesch [293] suggested that a P(HB-HV) copolymer containing 17mole% did biodegrade when specimens (25x3x2 mm), of an unknown physical form, were implanted subcutaneously into rats. The implanted copolymer specimens exhibited a progressive decrease in both flexural strength and Youngs modulus during implantation (2.2% after 1 month, 13.5% after 2 months and 18.5% after 3 months).

Other reports on *in vivo* degradation of PHB have included those of Kronenthal [294], who suggested that onset of degradation occurred within 8 weeks in an unspecified species, and Korsatko *et al* [1989] who suggested that *in vivo* degradation of PHB follows zero-order kinetics. However, in both these reports little data were presented to support their conclusions on *in vivo* degradation of PHB.

Clearly the physical form of the polymer is a major determinant of the degradation rate.

Although it was not entirely clear as to how the monofilament fibres of Miller and Williams [291] were processed , it is thought that they were most likely orientated fibres produced either by melt spinning or extrusion and consequently exhibited high crystallinity and low porosity which resulted in their relatively slow rates of degradation. Such devices which exhibit good stability to hydrolytic attack have advantages for use in surgical devices such as bone pins and plates. To this end, P(HB-HV) polymers are thought to be good candidates to fill the existing gap in the degradable polymer spectrum at the long term stability end [265].

In order to accelerate the degradation of P(HB-HV) polymers and thereby increase their applicability, Tighe and coworkers [289] have recently blended the polymers with a range of polysaccharides such as amylose, dextran, dextrin and sodium alginate. Using P(HB-HV) copolymers containing 12 and 20 mole% HV, they found that the degradation rate of these copolymers could be dramatically increased by varying the ratio and type of polysaccharide included [289]. The enhanced degradation with additives was attributed to the more rapid solvent uptake into the bulk of the matrix as the additive dissolved or leached out eventually causing matrix disintegration [289].

The use of additives (albeit biodegradable) has frequently been regarded as undesirable in biomedical polymers. Their use in implants will undoubtedly require toxicological and biocompatibility studies over and above those required for the virgin polymer. However, their use in drug delivery applications especially via the oral route may be more acceptable and undoubtedly offers greater control over degradation rate and possibly drug release.

1.4.7 Biocompatibility

The suitability of PHB and P(HB-HV) copolymers for inclusion in drug delivery or other biomedical applications will not only depend on the biodegradation properties but also on their biocompatibility. The term biocompatibility refers to the mutual acceptability of the polymer and its surrounding physiological environment. Williams [295] has

described biocompatibility as a two component phenomenon: the effects of the physiological environment on the polymer and the effects of the polymer on that same environment. The former will influence polymer degradation and the second, the tissue response to the implanted polymers.

Early work by Korsatko et al [296] indicated the toxicological acceptability and biocompatibility of the homopolymer, PHB, as a compressed tablet implanted subcutaneously into the neck folds of mice. Further work by the same group [148] suggested that after an implantation period of 5 weeks, a connective tissue capsule containing many cells is formed around the PHB tablet. They did report a slight inflammation in the capsule zone during the implantation period in which the cell population of the capsule changed from mostly neutrophile granulocytes after 5 weeks to mostly lymphocytes after 20 weeks [148]. This reflected a change from an acute to a chronic inflammatory response by the mice to the PHB tablet and the authors suggested that this response was typical of any host reaction to a foreign implant. No necrotic tissue was formed near the implant [148]. A recent report by Gerlach and Pesch [293] on the biocompatibility of a P(HB – HV) copolymer containing 17 mole% HV also suggested the formation of a connective tissue capsule but only after 2 weeks implantation into rats (implant site not mentioned). They found that all specimens (25x3x2 mm) produced an inflammatory response within the first week in that the reactive zone was limited to only a thin layer of polymorphonuclear leucocytes and occasional lymphocytes [293].

In vitro biocompatibility studies by Lafferty et al [148] showed that PHB did not affect cell growth or cell metabolism, measured as glucose consumption and lactate production, when compressed PHB tablets were exposed to mouse fibroblast cells in culture.

The in vivo and in vitro biocompatibility of PHB and P(HB – HV) copolymers has also been carried out by Kennedy et al [297 – 299]. The in vivo biocompatibility was assessed by monitoring inflammation in male Wistar rats. Following intramuscular injection of polymer microspheres (20 – 40um) into the rat thigh muscle, enzyme assays, using alkaline

and acid phosphatase, were employed to monitor acute and chronic inflammation, respectively. Although an acute inflammatory response was noticed which was attributed to the initial trauma of injection, no chronic inflammation was observed [297]. The biocompatibility of the polymers was also evaluated using cell culture techniques. The effects of P(HB–HV) polymers on the growth of CHO–K1 (Chinese Hamster Ovary) cells in culture were monitored over a 60–hour period. The polymers, used as solvent cast films, did not inhibit growth of cells during this period, thereby suggesting good biocompatibility [298–299].

Juni and Nakano [300] have also studied the in vivo biocompatibility of PHB by injecting microspheres (100um) into the rat thigh muscle. The results were similar to the study of Kennedy et al [297] in that a transient acute inflammation was observed which terminated after 7 days post–injection [300]. The microspheres were further reported as being encapsulated by connective tissue during a 4 week post–injection study period [300]. Doyle and Bonfield [268,301], who have been investigating PHB for use in hip replacement, have carried out preliminary implantation studies in rabbits which showed good integration between PHB and bone with no evidence of a chronic inflammatory response. They further reported that in vitro studies (unspecified conditions) with PHB and PHB–hydroxyapatite composites suggested that the polymers were non cytotoxic [268].

Despite the initial acute inflammation observed in the various in vivo studies with P(HB–HV) polymers, which is probably in response to the trauma of implantation or injection, P(HB–HV) polymers show good in vitro and in vivo biocompatibility.

1.4.8 Biomedical applications

Although the potential of PHB for use in biomedical applictions (surgical sutures) was originally proposed in the early 1960 s [302], the commercial development by ICI in the 1970 s was not primarily for these reasons. ICI had originally intended to use the bacterially produced thermoplastics as commodity plastics [149–152]. The principle of producing plastics from bacteria feeding on renewable resources such as sugar (glucose),

first occurred to ICI during the energy crisis of the early 1970 s. However the subsequent oversupply of oil and gas feedstocks in the 1980 s, made ICI's original proposal economically unviable. It was then that the research interests into other applications of PHB and related polymers gained momentum.

1.4.8.1 Drug Delivery Applications

A number of authors have investigated the potential use of P(HB – HV) polymers for controlled or sustained drug delivery. Korsatko et al [148,303,304] have studied the in vitro and in vivo release of 7 – hydroxyethyltheophylline (HET) in the form of a compressed tablet made from PHB (Mw 260K). They found that in vitro release was dependent on drug loading; with drug loadings of 60 – 80% HET release was complete within 24 hours but with lower drug loadings of 5 – 30% release of drug was extended for up to 50 days [303]. The authors reported that PHB has good compaction properties but varying compaction pressure between 196.2 – 981 N/tablet did not influence release of 7 – HET. Drug release from tablets implanted subcutaneously into the neck folds of female mice was slower than in vitro release [148,304]. This was probably related to the smaller volume of release medium available during in vivo release.

Gould et al [305] have studied drug release from matrices produced by direct compression of P(HB – HV) polymers for oral administration. The rationale of these matrices was that not only do they have the benefit of simplified processing but, unlike polyvinylchloride, if they are retained inadvertently in the gut they will slowly erode by hydrolytic and enzymatic routes preventing retention and potential strictures on chronic dosing [305]. The authors using two copolymers containing 12 mole% (Mw 350K) and 20 mole% HV (Mw 300K) found that release was dependent on matrix porosity, copolymer composition and on the molecular weight of the drug used. It was also concluded that drug release was independent of polymer molecular weight. However, because of the similarity of the molecular weights used (300 and 350K) and the fact that molecular weight effects were compared across two different copolymer compositions such an

interpretation becomes difficult. The authors also found that increasing the copolymer composition decreased the rate of fluorescein (model drug) release from the compressed matrices. On the introduction of porosigens (such as microcrystalline cellulose and lactose) to increase matrix porosity , the authors found that drug release could be enhanced [305].

Brophy and Deasy [306] found that by increasing the polymer molecular weight, increased rates of sulphamethizole release were observed from irregularly shaped PHB microparticles (Mw 140K, 500K and 1000K). The authors were unclear as to the reasons for this finding but attributed it to uneven drug distribution which may have been worst at higher polymer molecular weights. The porous particles (101.5 – 1590um) were prepared by grinding a solvent evaporated polymer matrix containing the suspended drug. The particle size was controlled by the grinding time employed. The authors found that by decreasing particle size from 1590um to 101.5um, substantial increases in drug release were obtained because of the increased surface area of the drug – loaded particles. Particles prepared from P(HB – HV) copolymers (17 and 30 mole% HV) released drug more slowly than the homopolymer. The authors explained this in terms of improved matrix formation with copolymers leading to possibly better drug distribution. Release was biphasic and the burst effect observed in drug loaded P(HB – HV) particles could be eliminated by overcoating with polylactide [306]. However, release of drug was predominantly diffusion controlled and independent of polymer erosion. The *in vivo* absorption of orally administered PHB particles containing 50% sulphamethizole in greyhound dogs was reported to correlate well with the *in vitro* release profiles (0.1N HCl, 37°C) [306].

The *in vitro* and *in vivo* release of an anticancer agent, lomustine (CCNU), from PHB and PLA microspheres has been studied by Bissery *et al* [307 – 309] as potential carriers for drug targetting. They found that ^{14}C – labelled microspheres (1 – 12um) injected intravenously accumulated mainly in the lungs, liver and spleen after 7 days post-injection [307]. The PHB microspheres, prepared by solvent evaporation (emulsion deposition), were a complex mixture of individual particles (1 – 12um) and assorted

aggregates consisting of smaller particles irreversibly fused together [307]. Deviations from sphericity were most noticeable with PHB microspheres and was attributed to the highly crystalline nature of PHB [307]. Although both PLA and PHB microspheres were found not to contain surface pores, release of CCNU from PHB was more rapid (release complete within 24 hours) than from PLA (70% released after 90 hours). No explanation for the difference was offered by the authors [307]. In another report [309] the same authors stated that release of CCNU from PLA microspheres (median size 3um) was complete within 7 days. On the basis of particulate tissue distribution, they evaluated the use of PHB and PLA microspheres in Lewis lung carcinoma bearing mice. They concluded that CCNU loaded PHB microspheres had little effect on Lewis lung carcinoma and only PLA microspheres with the drug could increase the survival of carcinoma bearing mice over controls [309].

Juni et al [300,311 – 312] have studied release of anticancer agents such as aclarubicin, doxorubicin, bleomycin and 5 – fluorouracil from PHB matrices. Contrary to the above results, Juni and colleagues [300,311 – 312] have found that the release of these anticancer agents occurred relatively slowly from PHB. For example, PHB microspheres (170um mean diameter) containing 13% aclarubicin hydrochloride released only 10% of the drug after 5 days in saline solution at 37°C [311]. The slower release may be due to the higher particle size used and/or to the nature of the drug. The authors were able to increase the rate of drug release by incorporating ethyl or butyl esters of fatty acids into the PHB microspheres. Esters of fatty acids with more than 10 or 12 carbon atoms were found to substantially enhance drug release [311]. There appeared not to be any significant change in the crystallinity of drug – loaded PHB microspheres upon inclusion of the additives and therefore, the authors, in a study of the mechanism involved in release enhancement, suggested release was facilitated by drug diffusion through channels formed by the additives in the PHB matrix [312].

Further work on microparticles has been carried out by Koosha et al [312 – 313] who have prepared PHB nanoparticles (170 – 210nm) by a high pressure emulsification technique [312]

and by Akhtar et al [314] who prepared PHB microparticles (20–40um) by spray drying. These authors reported relatively fast release of prednisolone [313] or Methyl Red (a model drug) [314] from PHB microparticles which was essentially complete within 48 hours. Akhtar et al [314] found that release of the model drug from solvent cast films (30–50um thick) occurred more slowly but was predominantly not erosion controlled in both films and spray–dried microparticles of PHB. The mechanism of release was thought to involve a combination of simple diffusion and aqueous channel formation [314] (see chapters 7 and 8).

Recently Deasy et al [315–316] have investigated cold compressed PHB compacts containing physical dispersions of tetracycline and metronidazole for the treatment of peridontal disease in human volunteers. In a study with 12 human volunteers clinically diagnosed as having gingivitis, a compact (7.5mm diameter) containing 50% tetracycline was bonded to an upper molar tooth of each volunteer and was found to produce therapeutic levels of the antibiotic in saliva of patients throughout the 10–day study period [315]. All patients showed clinical improvement but this was not maintained when the compact was removed. Metronidazole was found not to be as effective as tetracycline [316]. In vitro release studies in simulated saliva (pH 6.6; 37°C) showed that release was independent of compaction pressure in the range 106–318 kg/cm^2. Decrease in PHB molecular weight or alteration to PLA tended to decrease drug release and increasing HV content of P(HB–HV) copolymers (17 and 30 mole%) tended to increase the initial drug release [315]. This was thought to be due to easier drug diffusion through the copolymer compacts [315].

There have also been reports of PHB matrices being used to deliver peptides [318–320]. In a veterinary application, Mcleod et al [320] have tested PHB implants for their efficacy to continuously release low levels of LHRH when administered subcutaneously, and thus to stimulate tonic LH secretion, promote preovulatory follicle growth and induce ovulation in acyclic sheep. They found that PHB implants were superior to oil–based depot injections in prolonging release of hormone sufficient (2–4 days) to cause ovulation in ewes. By using two LHRH–PHB (50ug /50mg or 40ug/15mg) implants per animal a

success rate of up to 94% was obtained [320]. This success with PHB implants in veterinary applications will undoubtedly stimulate further research with biodegradable PHA's in drug delivery of macromolecules.

1.4.8.2 Other Medical uses

Although much research interest has been focused on drug delivery applications, P(HB – HV) polymers have also been considered in a number of other biomedical uses.

The fact that P(HB – HV) polymers have a chiral centre has initiated research into controlled degradation of polymers to produce products useful for synthesising enantiomerically pure compounds (EPC) [148 – 149]. Both pyrolysis and chemical degradation have been suggested for depolymerization [321 – 324]. Seebach and colleagues [322 – 324] have been able to produce high yields (75 – 90%) of D(–) – 3 – hydroxybutanoates from PHB depolymerized chemically in the presence of alcohols at 80 – 160°C using a tetraethoxytitanium catalyst [324]. Such optically active compounds cannot always be obtained in high yields from conventional synthetic routes and are thought to be useful starting reagents for the synthesis of EPC.

Webb and Adsetts [325] have suggested that PHB could be used in surgical dressings. A solution of polymer in chloroform could be applied to wounds directly. The polymer would form a transparent film which the authors claim would allow continuous monitoring of the affected area without removal of the dressing. Furthermore, the film would adapt to the contours of the affected area during evaporation of solvent [325].

Other uses of PHB reported have included using it has a medical dusting powder [326], in fabrication of ostomy bags [327], nappy liners [327], and tampon ejectors [328]. However, probably the most exciting application of PHB is in bone replacement therapy [149,266 – 267].

The homopolymer offers potential advantages over the currently used materials in bone replacement therapy in that its mechanical properties closely resemble those of cortical

bone. Mismatch of mechanical properties such as Elastic Modulus has been a major problem with metals currently used in bone replacement [329]. The mechanical compatibility of PHB and PHB – Hydroxyapatite composites has led to their investigation in hip replacement therapy [266 – 268,301]. Furthermore, Doyle and colleagues [268,301] have reported that PHB and its composites have superior integration properties with bone when compared to metals and other polymer systems such as polyethylene and polylactide. The reason for the superior integration properties remains unclear but may be due to the polymers piezoelectric properties.

Evidently P(HB – HV) polymers have considerable potential in both drug delivery and other biomedical applications. However, much further research and development is necessary before these polymers realize their full potential.

CHAPTER 2

MECHANICAL PROPERTIES

2.1 INTRODUCTION

The mechanical properties of a material are concerned with the effects of stress on that material. They provide information as to the behaviour of the material under this stress which can be indicative of the materials suitability for its intended purpose.

In order to assess the desirability of P(HB – HV) systems for biomedical applications, a knowledge of their mechanical properties is essential. Polymers with inadequate mechanical properties are unlikely to be used in biomedical applications such as bone pins or implants for long – term drug delivery. Mechanical failure in such systems could result in potentially fatal consequences. Indeed, Hastings [330] has stated that polymers intended for surgical implantation must satisfy the double requirement of adequate long – term mechanical properties and surface compatibility.

2.1.1 AIMS AND OBJECTIVES

In this study the mechanical properties of a range of P(HB – HV) copolymers have been examined using official static tensile tests. The aims and objectives for this investigation were:

1. To study the effect of polymer molecular weight on the mechanical properties of PHB.

2. To study the influence of composition on the mechanical properties of P(HB – HV) copolymers.

3. To study the influence of incorporating model drugs into polymers on their mechanical properties.

4. To evaluate the suitability of radiation and autoclaving as methods for sterilizing P(HB – HV) biopolymers.

2.1.2 PRINCIPLES OF TENSILE TESTING OF POLYMERS

There are a bewildering number of mechanical tests which can be used to gain both qualitative and quantitative information on the bulk mechanical properties of materials. However, only some are recognised as official tests by either the American Society for Testing and Materials [331] or the British Standard Institute [332]. A list of mechanical tests relevant to polymers and plastics is given by Aulton [333] and an excellent review of published literature relating to both official and unofficial tests applicable to polymers can be found in a book by Lever and Rhys [334].

The tensile test is probably the most important single test [335] and certainly the most widely used of all the mechanical tests [336]. It has been used extensively to characterise polymeric materials for use in biopharmaceutical applications such as tablet film coatings [337 – 341], surgical implants [342 – 343] and surgical sutures [344 – 345]. A typical tensile test requires:

a) a test specimen, usually in a dumb – bell shape with a smooth gauge section between the enlarged ends

and b) a test machine that applies, measures and records various loads.

There are many types of tensile testing machines [346] available but the principle of them all is that the test specimen is held at one end by a fixed clamp or grip and the other end by a movable one. The grips are then drawn apart and the tension in the specimen is measured at various grip separation distances. A load cell usually relays the measured force – displacement profile onto a chart recorder which can be easily converted to the stress – strain profile of the material from a knowledge of testing variables and specimen dimensions.

Figure 2.1 gives a schematic representation of the Instron 1122 tensile testing machine used in the present study and Figure 2.2 shows a typical stress – strain profile that can be obtained from such a machine. Superimposed on this figure are the material properties which can be calculated.
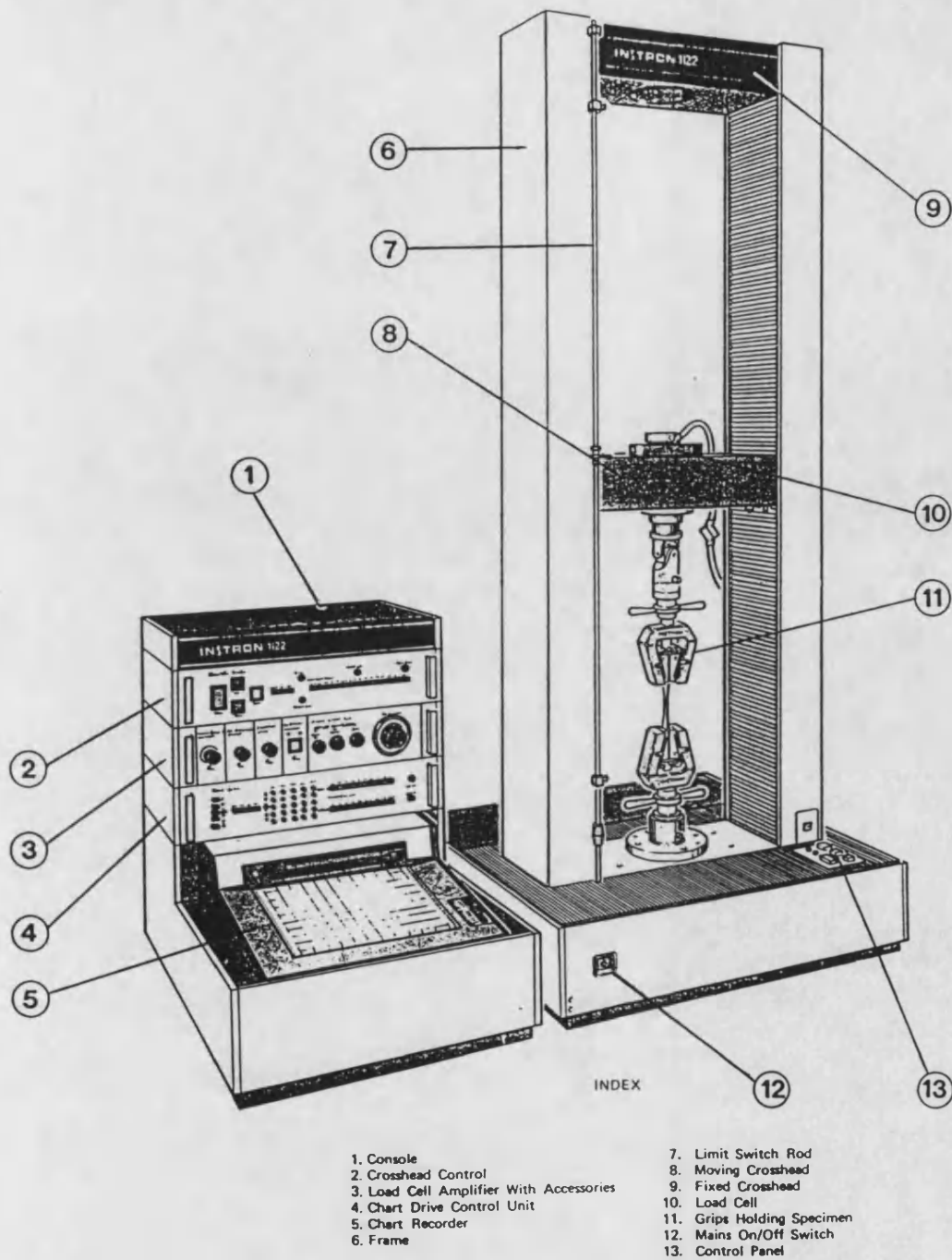
Figure 2.1. A schematic diagram of the Instron 1122 Tensile Testing machine.

INDEX

1. Console
2. Crosshead Control
3. Load Cell Amplifier With Accessories
4. Chart Drive Control Unit
5. Chart Recorder
6. Frame

7. Limit Switch Rod
8. Moving Crosshead
9. Fixed Crosshead
10. Load Cell
11. Grips Holding Specimen
12. Mains On/Off Switch
13. Control Panel
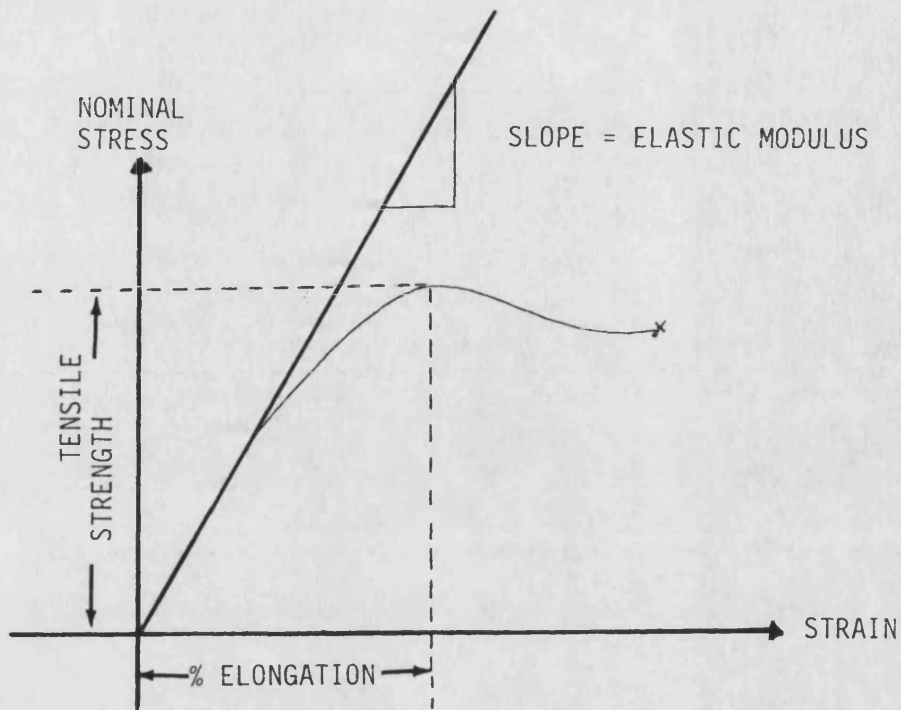
Figure 2.2. A typical stress – strain profile from which mechanical properties of polymers were determined.

A list of definitions for the mechanical properties as used in this study is given below:

Stress is defined as the ratio of the applied force on a specimen to its original cross-sectional area,

i.e. stress $= \dfrac{\text{applied force}}{\text{original cross-sectional area}}$

Tensile strength (TS) is defined here as that stress corresponding to the maximal load experienced by the test specimen during the tensile test. This may correspond to the breaking stress of brittle polymers which undergo little or no plastic deformation or to the yield strength of polymers undergoing considerable plastic deformation. Values of TS give an indication of the overall strength of a polymer but in isolation are not very important in predicting performance.

Percent Elongation (%E) is a measure of polymer ductility. It was taken as that strain corresponding to the maximal load or stress experienced by the specimen and is expressed as a percentage.

$\%E = \dfrac{\text{increase in length}}{\text{original length}} \times 100$

Elastic Modulus (EM) is a measure of polymer stiffness or rigidity. It was calculated as the applied stress divided by the corresponding strain in the region of linear elastic deformation (Hookean behaviour) i.e. slope of the linear portion of a stress-strain profile.

Toughness can be crudely estimated by measuring the area under the curve (AUC) of a stress-strain profile. The AUC is a function of the work done (force x displacement) in deforming a material and as such closely resembles the polymer film toughness. Toughness has not clearly been defined; it is bound up with impact strength but this is

only a guide. It is much more a function of stress, elasticity, and internal damping [333]. Toughness is expressed as Jm^{-3} from the following relationship:

$$\text{Stress} \times \text{Strain} = \frac{N}{m^2} \times \frac{m}{m} = \frac{Nm}{m^3} = \frac{Joules}{m^3} = Jm^{-3}.$$

2.2 MATERIALS

The homopolymer, PHB, and the P(HB−HV) copolymers were produced biosynthetically by the continuous fermentation of a glucose utilising mutant of *Alcaligenes eutrophus* and were purchased from Marlborough Biopolymers Ltd (a subsidary of ICI), Billingham, UK. The biopolymers were characterised as discussed below and their molecular characteristics are summarised in Table 2.1. All polymers purchased were of high purity medical grade.

Polyethylene (PE) of high density was purchased from BDH chemicals, Poole, UK. Batch No.1726200. Mw = 400K.

Para−toluenesulphonic acid (PTSA) was purchased from Fisons, UK. Batch No.T/2500 43

Methyl Red: BDH Chemicals, Poole, UK. Batch No.9898770F

Sodium Fluorescein: BDH chemicals ,Poole, UK. Batch No.5555630A1009

All solvents both HPLC and SLR grades and were purchased from Fisons,UK.

Table 2.1   Molecular Characteristics of P(HB−HV) Biopolymers.

Polymer	Symbol	Batch No.	Nominal (ICI) HV content (mole%)	^{1}H−NMR HV content (mole%)	Mw	Mn	Mw/Mn
PHB	PHB800K	BX GV9	0	0	765K	506K	1.51
P(HB−HV)	PHV6	BX	6.60	7.47	410K	267K	1.53
P(HB−HV)	PHV12	BX PV12	12.60	11.99	1 293K	908K	1.42
P(HB−HV)	PHV20	BX T−37	20.00	19.98	1 665K	770K	2.16
P(HB−HV)	PHV27	BX PV13	27.00	27.79	−	−	−

2.3 METHODS

2.3.1 Characterisation of materials

2.3.1.1 Determination of Copolymer composition

The HV content of P(HB-HV) copolymers was determined by ^{1}H-NMR according to the method described by Bloembergen et al [211]. This method was chosen in preference to the Fourier transform infra-red (FTIR) method proposed by the same authors because of its greater accuracy.

^{1}H-NMR spectra of 1%w/v solutions of P(HB-HV) copolymers in deuterated chloroform were recorded using a JEOL GX-270MHZ spectrometer in the pulse Fourier transform (FT) mode. A 5.5-s pulse repetition was employed with a 3KHz spectral width, 32K data points and 100 accumulations. The HV content (expressed as mole%) was calculated from the relative magnitudes of the integrated areas of the methyl resonances in the side groups of HB and HV monomeric repeating units. Examples of ^{1}H-NMR spectra for some P(HB-HV) copolymers are given in Figures 2.3-2.5.

Recently reports [347-348] have indicated that copolymer composition can also be determined from an optical rotation method. This method is based on a linear relationship between the specific rotation of P(HB-HV) copolymers and HV composition. However, this method is less accurate because it depends on calibration with samples of known HV contents determined by an alternative technique (NMR or FTIR). Furthermore, the optical rotation method has been reported to be less reliable for HV contents below 15 mole% [348].

2.3.1.2 Determination of polymer molecular weight

The molecular weight distributions of the biopolymers were determined by gel permeation chromatography (GPC) according to the method described by Majid [286,349]. A schematic representation of the apparatus used is given in Figure 2.6. Briefly, 20uL polymer samples (1%w/v) in chloroform were injected into a Mixed-PL gel (5um) column, 0.3 x 30cm, (Polymer Labs,UK) previously calibrated with polystyrene (PS) standards (Polymer
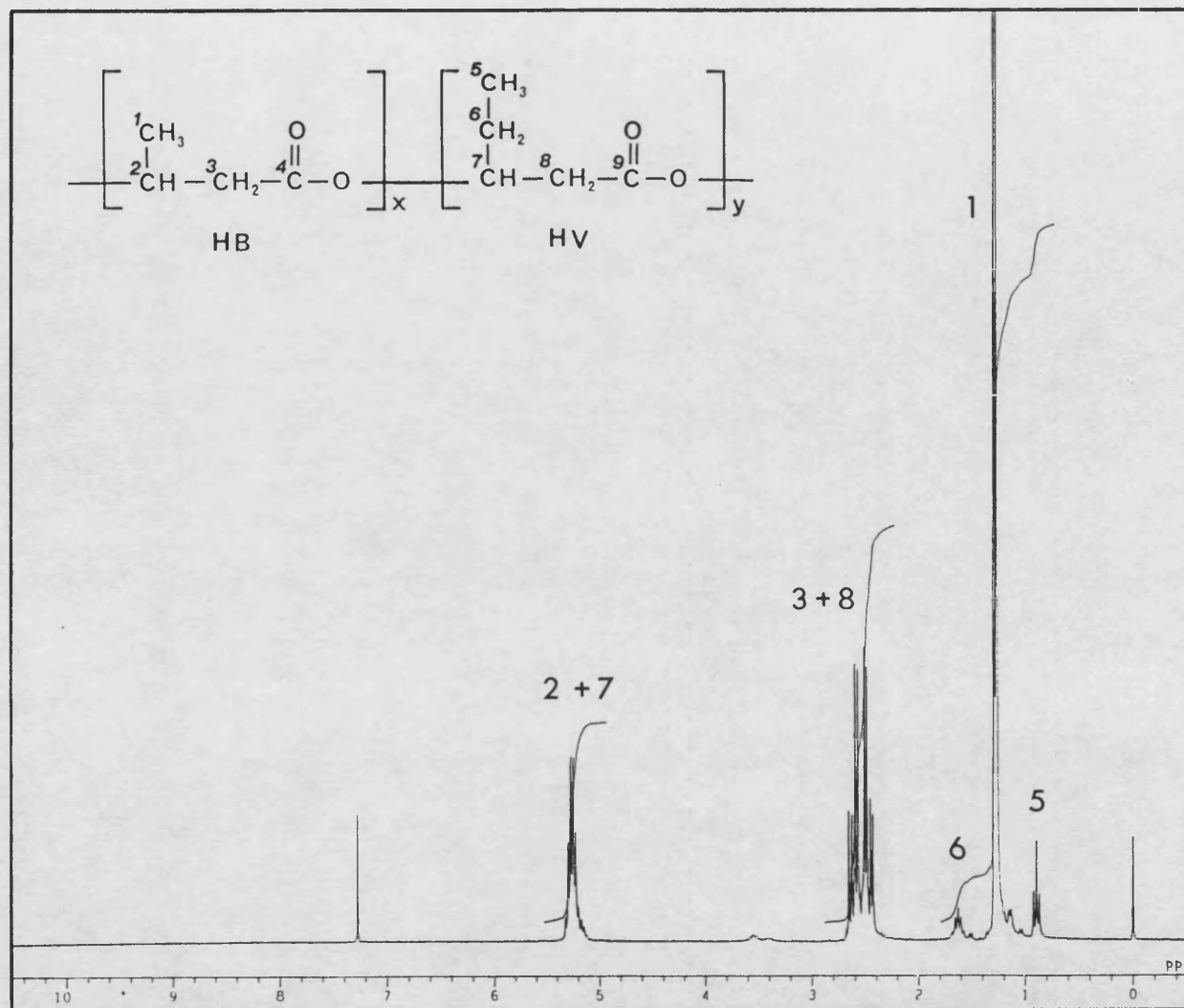
Figure 2.3. ^1H – NMR spectrum of a P(HB – HV) copolymer containing 7.47 mole% HV. Chemical shifts are in ppm downfield from TMS (Me$_4$Si).

Figure 2.4. ^1H-NMR spectrum of a P(HB − HV) copolymer containing 19.98 mole% HV. Chemical shifts are in ppm downfield from TMS (Me$_4$Si).
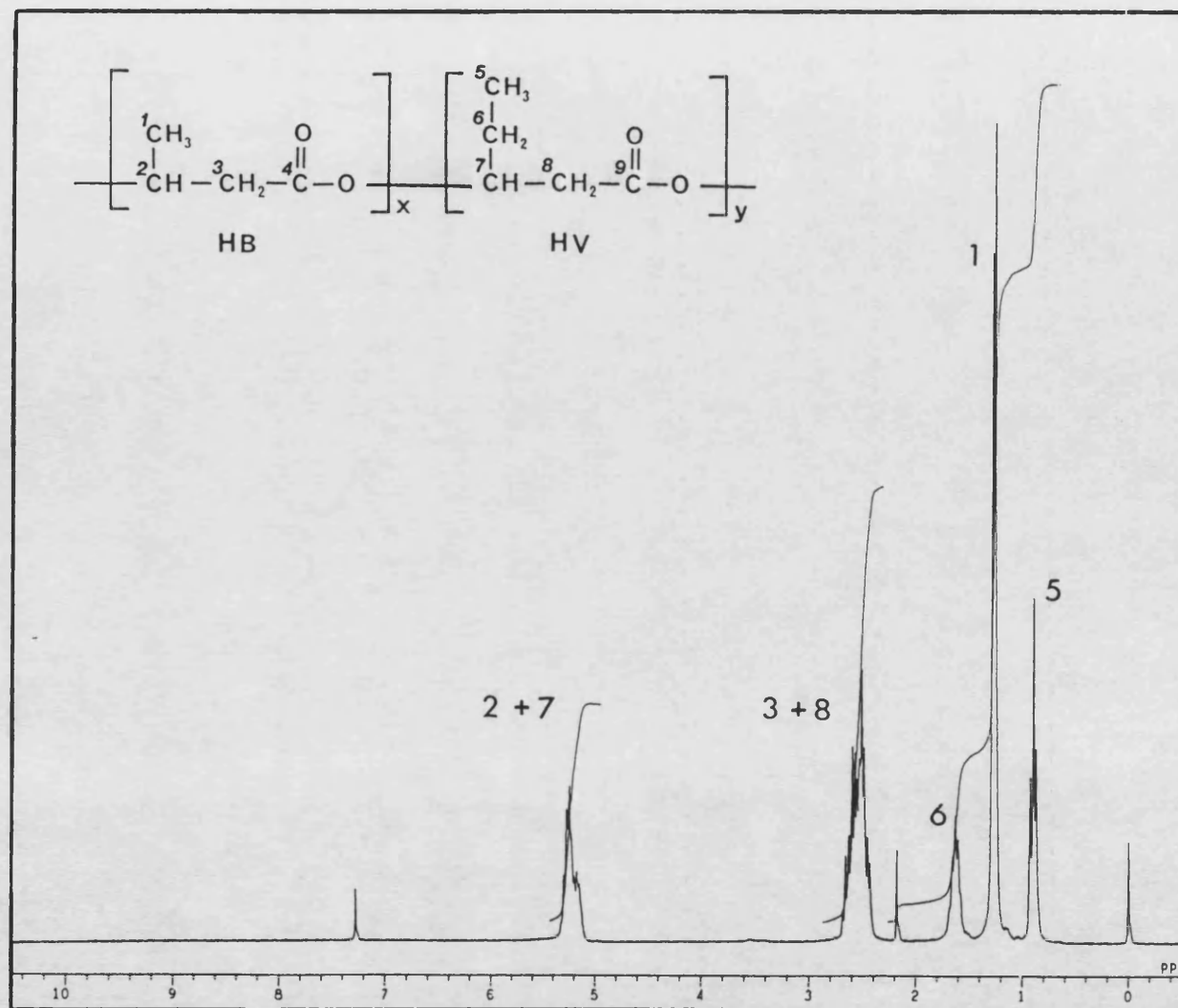
Figure 2.5. ^1H-NMR spectrum of a P(HB–HV) copolymer containing 27.79 mole% HV. Chemical shifts are in ppm downfield from TMS (Me$_4$Si).

Figure 2.6. A schematic representation of the gel permeation chromatography apparatus (after ref. 286).
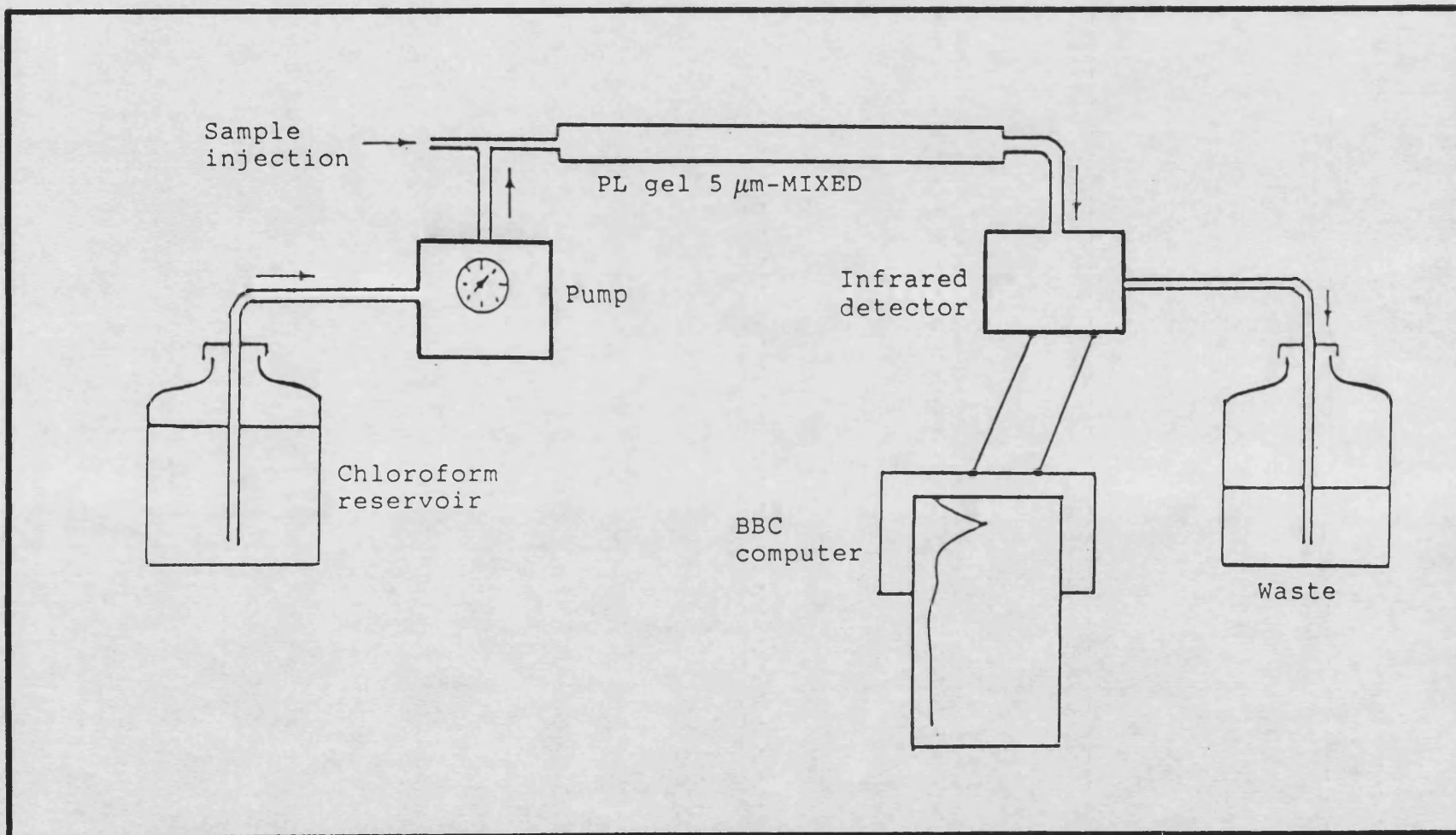
Labs,UK). A mobile phase of HPLC grade chloroform at 25°C was used and eluent detection

was achieved using an infra-red spectrophotometer (Perkin Elmer 782) set at 1760cm^{-1} to

detect the carbonyl (C=O) resonance characteristic of P(HB-HV) biopolymers. PS detection

was based on the C-H stretch occurring at 2730cm^{-1}. Data were stored and analysed using

a BBC Master microprocessor interfaced to the IR detector. Mark-Houwink constants used

were K=1.065 x 10^{-2} ml/g, a=0.728 for PS and K=1.510 x 10^{-2} ml/g, a=0.756 for PHB as

quoted by Majid [286,349].

2.3.2 Preparation of PHB samples with different molecular weights

A series of lower molecular weight polymer samples were prepared from high molecular

weight PHB (PHB800K) by non-aqueous catalytic degradation [286].

PHB800K (2%w/v) was dissolved by refluxing in a methanol:chloroform (1:5) mixture. The

mixture was then cooled to ambient and the catalyst, PTSA (0.2%w/v), was added to the

polymer solution and refluxed at 61°C for timed intervals. The reaction was stopped at

the appropriate time by pouring the refluxed mixture into excess iced water, in which

the PTSA was soluble. The mixture was then continually agitated for 15 mins to effect

removal of the catalyst before precipitating out the degraded polymer by the addition

of excess methanol. The degraded polymer was then filtered through a Whatman No.52

filter paper and the filtrate was washed with water and methanol to remove any traces

of PTSA still remaining. The degraded polymer samples of different chain lengths were

then further purified as described below and their molecular weights determined by GPC.

Table 2.2 gives the molecular weight details of the degraded polymers.

Table 2.2. The molecular weight characteristics of PHB samples prepared by non-aqueous catalytic degradation.

Sample	Reflux time (mins) (0.2%w/v PTSA)	Molecular weight ($\times 10^{-3}$) Mw	Mn	Polydispersity (Mw/Mn)
1	0	765	506	1.51
2	10	513	324	1.58
3	15	384	226	1.70
4	20	250	167	1.50
5	30	236	152	1.56
6	45	204	159	1.28
7	60	193	136	1.42

2.3.3 Purification of biopolymers.

Although the 'as supplied' polymers were of a medical grade, they were further purified as a routine procedure. Purification was achieved by refluxing in chloroform (2%w/v), filtering the polymer solutions (Whatman No.52 filter paper) and recrystallizing with excess methanol. The recrystallized polymers were washed with water and methanol and dried in a vacuum oven at 45°C for 12 hours.

The polymers were then redissolved by refluxing in chloroform to an initial concentration of 2%w/v. To achieve higher concentrations (4%w/v), suitable for casting films of the required thickness, the polymer solutions had to be further concentrated by evaporating chloroform in a rotary evaporator.

2.3.4 Addition of model drugs to polymer solutions

Sodium Fluorescein was used as a model water-soluble drug of low molecular weight. The particulate drug (Feret diameter 30 ± 15um, Mean ± S.D; n=200; Joyce-Loebl Magiscan Image Analyser) was accurately weighed and added to concentrated polymer solutions to achieve a range of drug loadings in the dried polymer films. Drug-polymer suspensions were sonicated in a sonic bath (Deakon FS100 Frequency sweep; Deakon Ultrasonics Ltd,UK) for 30 mins to obtain suitable mixing.

Methyl Red was used as a model chloroform-soluble drug of low molecular weight and

incorporated into polymers in the same way as above. The chemical structures of the model drugs are given in Figure 2.7.

2.3.5 Casting of polymer films from solution

Films were cast onto dry, degreased glass plates using a Thin Layer Chromatography Applicator with an adjustable clearance. A suitable clearance setting was chosen to produce a dry film thickness of 30 – 50 um. A spirit level was used to ensure films were cast onto a flat, level surface.

2.3.6 Drying of films cast from solution

The resultant cast films were dried in two stages: a) initially overnight in a drying cabinet in which the films had been cast and b) in an oven at 45 ± 1°C for 12 – 18 hours to ensure complete dryness.

2.3.7 Preparation of melt processed films

Purified polymer powders were melt pressed in a Moores model C194 (Birmingham, UK) hand melt press. Polymer powders were size reduced using a pestle and mortar and then placed in a mould consisting of two aluminium plates ($20cm^2$) separated by four aluminium spacers of fixed thickness. The plates were lined with Mellinex polyester sheeting (Scott Bader, Bristol) to prevent the polymer from adhering to the mould. The polymers were pressed at 15psi pressure with top and bottom plattens at 165°C for 10 mins. The mould was then removed from the hot press and slowly cooled to ambient before films were peeled and stored.

2.3.8 Storage of polymer films

All film samples were stored at 25°C over silica gel for one week prior to testing.

2.3.9 Cutting of test specimens from polymer films

Test specimens were cut from films (melt processed and solvent cast) using a sharp
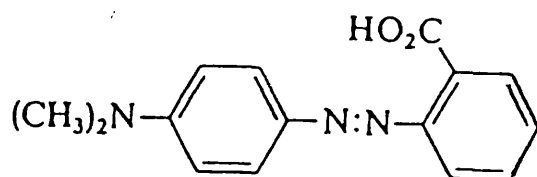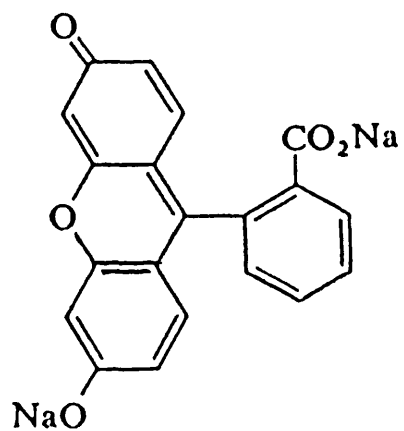
Figure 2.7. Chemical structures of Methyl Red (A) and Sodium
Fluorescein (B).

scalpel and a dumb – bell shaped template of guage length 40mm and width of 6.5mm. All specimens were visually inspected for cutting and film defects with only the best specimens being used for testing. All defective specimens were discarded. The thickness of each specimen was measured in 4 separate places along the gauge length and the mean value used in calculations of cross – sectional area. In the case of solvent cast films a minimum of 5 specimens from each film and two films for each polymer or polymer – drug mixture were taken for testing. For melt – pressed films a minimum of 5 specimens were taken from a combination of different films. **Properties or replicate films were not significantly different from each other (p > 0.05).**

2.3.10 Static Tensile testing of films.

Static tensile tests were carried out using an Instron 1122 testing machine according to the ASTM D 882 – 80a standard test procedure. A strain rate of 5mm/min and ambient test conditions were employed in all cases. A calibration load of 500 grams and a load cell of 2000 grams force were used. Lightweight pneumatic grips were used to minimise local stress concentrations introduced by heavier grips.

2.4 RESULTS AND DISCUSSION

2.4.1 The effect of molecular weight on the mechanical properties of solvent cast films of PHB.

A minimum molecular weight (MW) of approximately 190K – 200K was required to form a thin film specimen of PHB from solution. PHB samples of molecular weights below this threshold value did not form a mechanically intact film from chloroform solutions of concentrations up to 10%w/v. Such samples were found to spread easily onto glass as concentrated solutions and formed 'wet' films on partial drying. However, on further drying these films shattered into small pieces of brittle polymer often leaving behind a mosiac pattern of dried polymer pieces on the glass plate.

The need for a minimum molecular weight to form a film is not peculiar to PHB but is also characteristic of other crystalline polymers with glass transitions close to

ambient temperature [336]. The reason for this threshold MW in crystalline polymers is similar to that given by Gent [350] for brittle amorphous polymers. Gent states that a minimum number of chain entanglements are required before the polymer becomes strong enough to carry a load or form a specimen. Similarly, very low molecular weight samples of crystalline PHB are very brittle and a minimum number of tie-molecules between crystallites are necessary to produce a mechanically intact specimen. Peterlin [351] has defined tie-molecules as those which go from one crystalline domain to another and are responsible for holding these domains together. The threshold number of tie-molecules provide sufficient cohesive energy to overcome the opposing shrinkage forces (solvent evaporation on drying) responsible for shattering the polymer into small pieces of very low strength.

Figures 2.8-2.10 show the effect of MW of PHB on the tensile strength (TS), %elongation (%E) and elastic modulus (EM) of solvent cast films. The TS and EM followed the same trend in that above the minimum MW the properties increased rapidly with increasing MW to reach a limiting value or plateau between MW's of approximately 200K-300K. Although mean values of %E appeared to increase with increasing molecular weight, the %E was not significantly different ($p > 0.05$) for molecular weights above 300K.

The generally higher values of TS, %E and EM for molecular weights above the threshold was indicative of the increased toughness, strength and ductility of PHB at high molecular weights ($>300K$). At low MW's PHB was extremely brittle and this was thought to be largely due to the accumulation of chain ends and low molecular weight fractions reducing the number of tie-molecules between crystallites. However even at high MW PHB was relatively hard and brittle as shown by the very high EM (1500 - 2000 MPa) and very low % E values ($<2\%$). The effects of molecular weight on the mechanical properties of PHB showed similar patterns to those reported for polyethylene [352], polystytrene [353-354] and a range of other polymers [355-357] in polymer science.
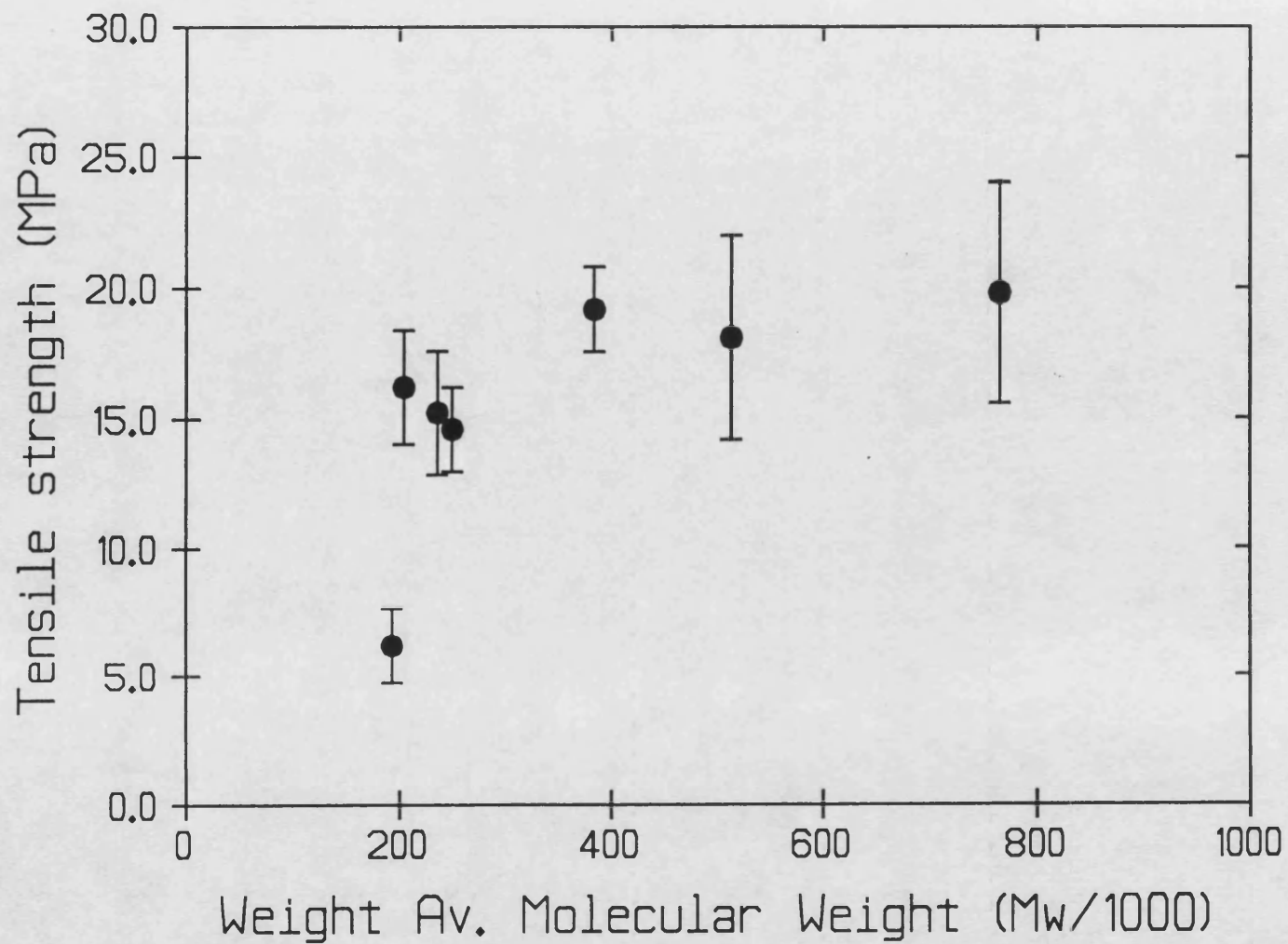
Figure 2.8. The influence of polymer molecular weight on the tensile strength of solvent cast films of PHB (Mean ± S.D; n = 10).
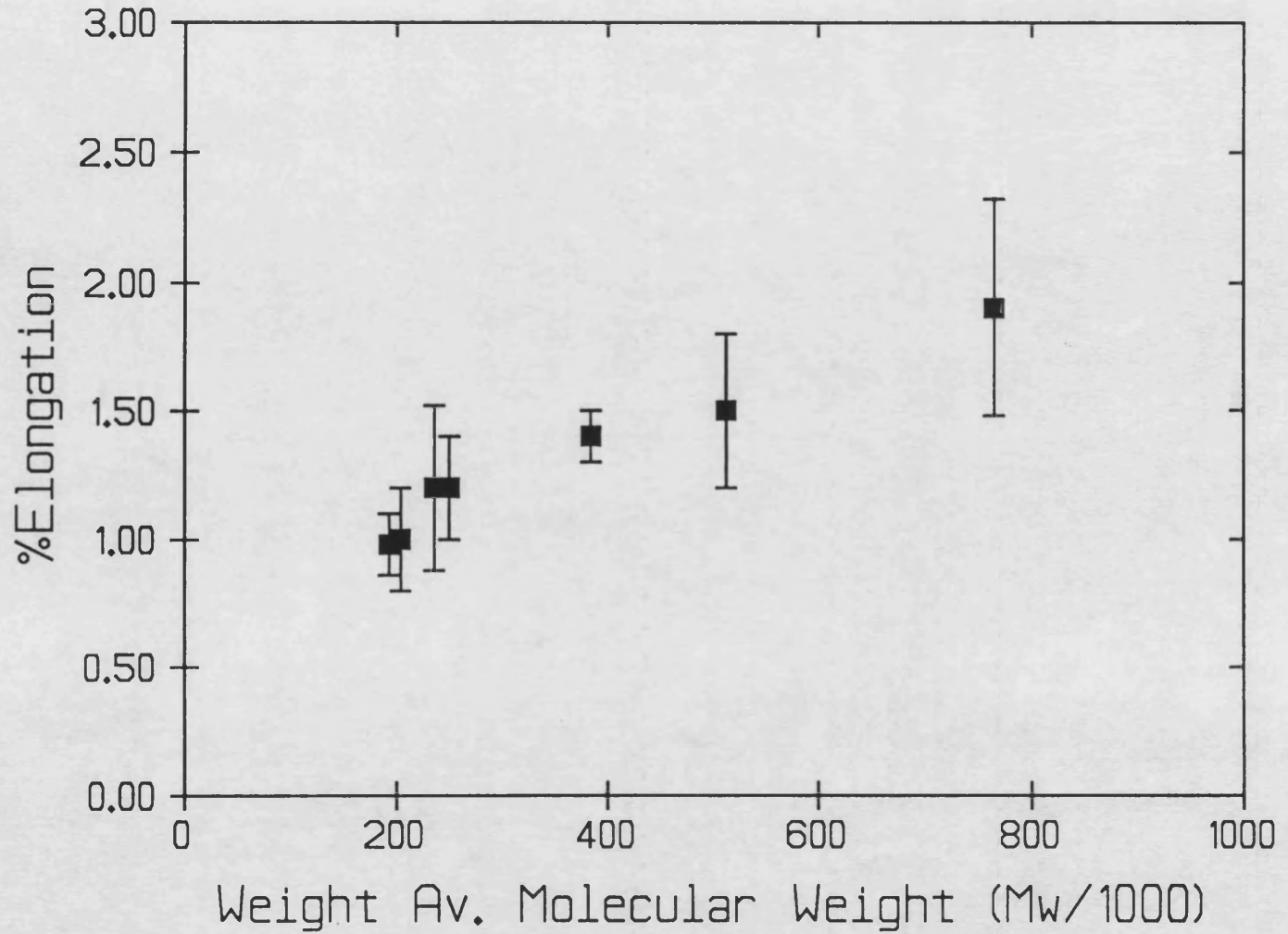
Figure 2.9. The influence of polymer molecular weight on the % elongation of solvent cast films of PHB (Mean ± S.D; n = 10).
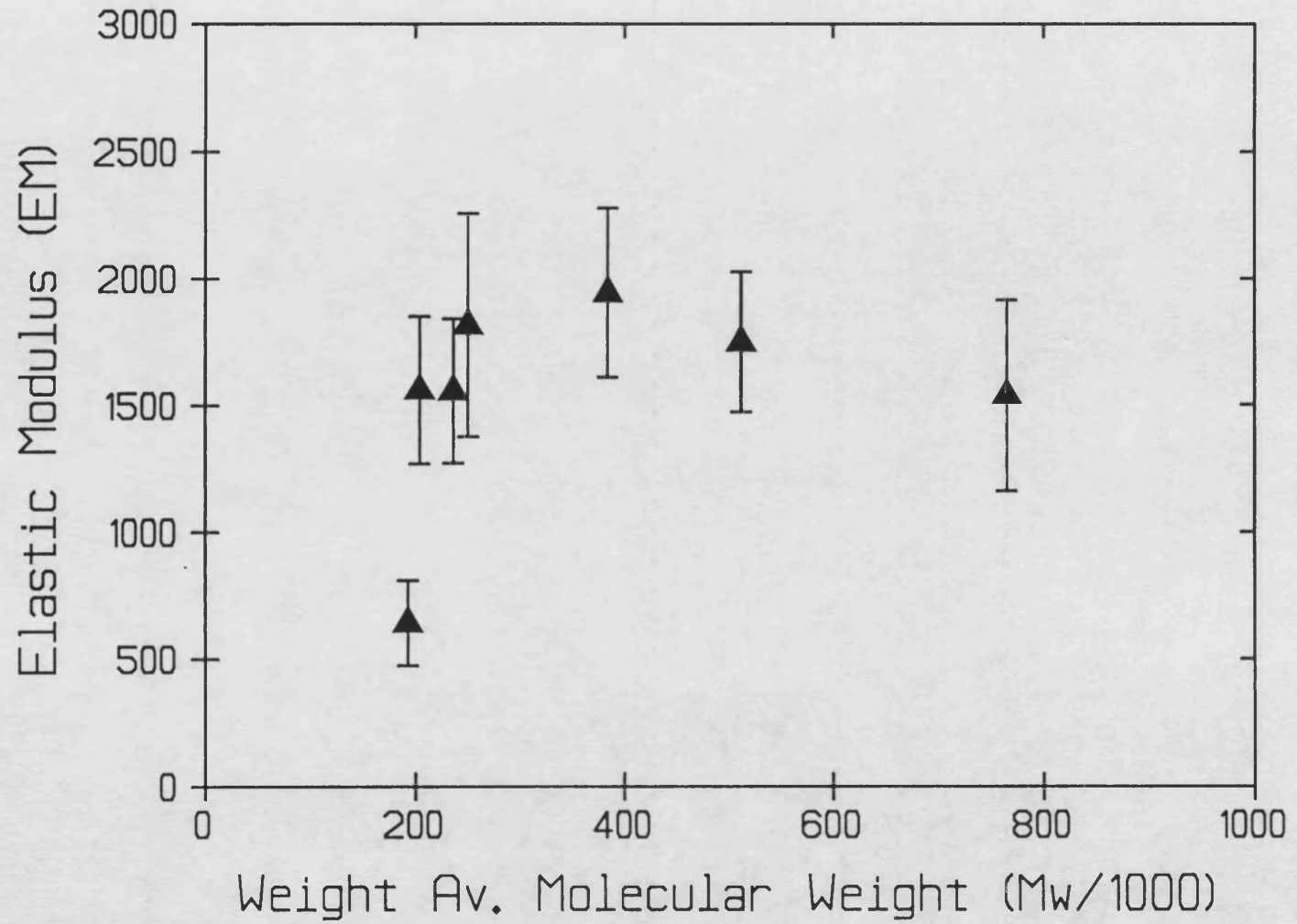
Figure 2.10. The influence of polymer molecular weight on the Elastic Modulus of solvent cast films of PHB (Mean ± S.D; n = 10).

2.4.2 The effect of P(HB−HV) copolymer composition on their mechanical properties.

2.4.2.1 Solvent cast thin films

Figures 2.11−2.13 show the effect of HV content of P(HB−HV) biopolymers on the TS, %E and EM of solvent cast thin films. The TS values in Figure 2.11, with the exception of PHV6, were not significantly different ($p > 0.05$) for the range of copolymer compositions studied. Hence, it was concluded that TS changed little with composition for copolymers containing up to 27 mole% HV.

However, Figures 2.12 and 2.13 show that copolymer composition greatly influenced both the ductility (%E) and rigidity (EM). The %E changed little for small increases in HV content up to 7 mole% when compared to the homopolymer. However, further increases in HV content produced a marked rise in the property culminating in over a 5 fold increase in %E for PHV27 when compared to the homopolymer, PHB. The EM in Figure 2.13 showed a steady, almost linear decline in polymer stiffness with increasing HV content of P(HB−HV) biopolymers. For PHV27 the EM is approximately a third of that for PHB.

Toughness of polymers can be estimated from the areas under the curves of stress−strain profiles [333]. Table 2.3 gives toughness values of P(HB−HV) polymers estimated from stress−strain profiles from solvent cast films.

Table 2.3   Toughness values for P(HB−HV) biopolymer

PHV CONTENT (MOLE%)	TOUGHNESS (MJm^{-3})
0	6.0
6.6	5.0
12.6	21.4
20.0	49.9
27.0	58.6

The toughness of P(HB−HV) copolymers progressively increased with increasing HV content and followed a similar trend to %E. PHV27 was found to be approximately 10 times tougher than PHB.
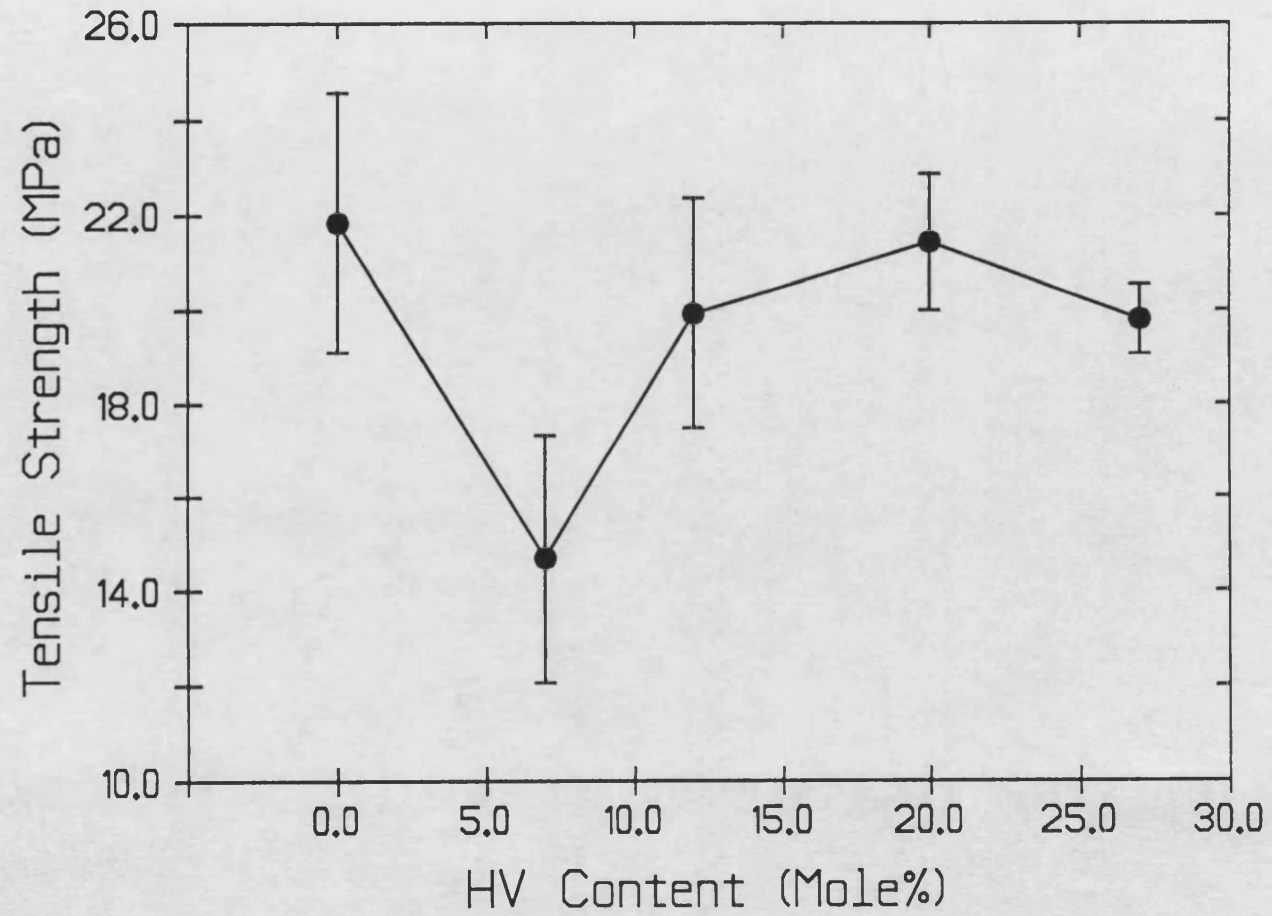
Figure 2.11. The variation in tensile strength with P(HB–HV) copolymer composition (Mean ± S.D; n=10).
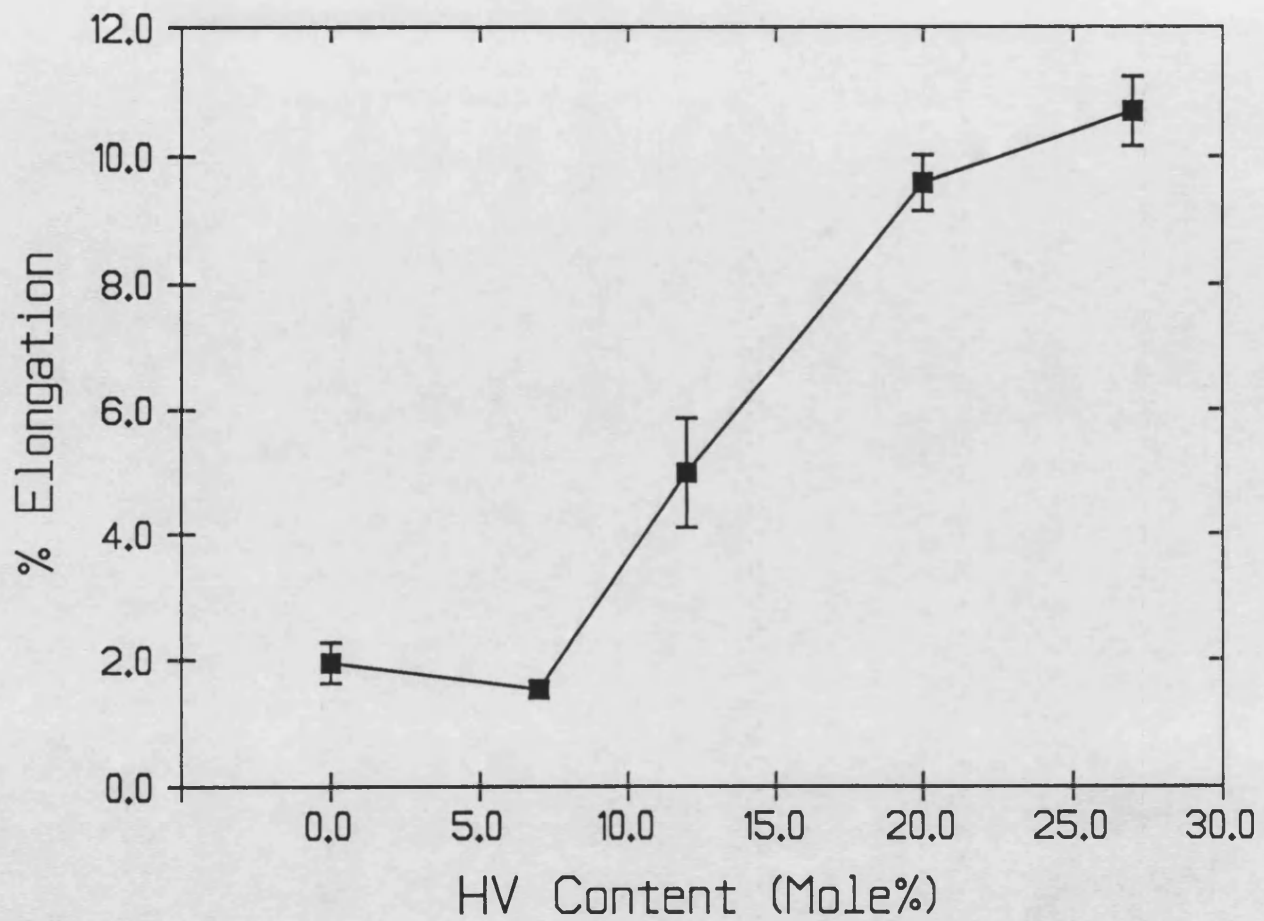
Figure 2.12. The variation in % elongation with P(HB – HV) copolymer composition (Mean ± S.D; n = 10).
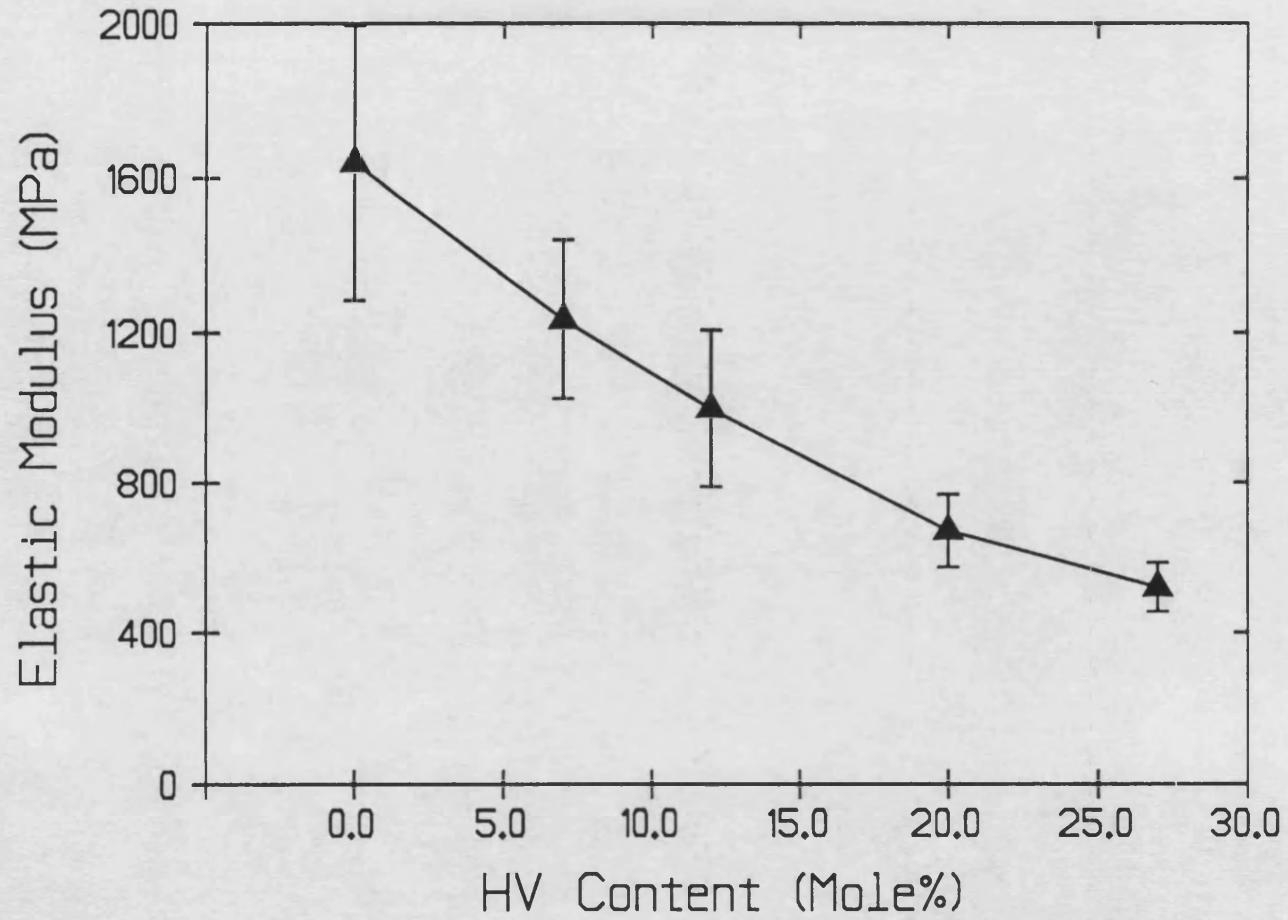
Figure 2.13. The variation in Elastic Modulus with P(HB – HV) copolymer composition (Mean ± S.D; n = 10).

2.4.2.2 Melt − pressed films

PHB is known to be thermally unstable at temperatures marginally above its melting point [247]. However, the P(HB − HV) copolymers are relatively more stable. Although they have lower melting temperatures the copolymers degrade at about the same temperature as PHB and therefore have larger windows for thermal processing (see chapter 3). To minimise thermal degradation of PHB, melt − pressed films (300 − 400um) were fabricated under pressure at 165°C. Because of their relative thermal stability, P(HB − HV) copolymers could also be processed at this temperature without degradation. Although molecular weight of samples was not determined to assess degradation, no colouring of melt − pressed films was observed. In preliminary studies, PHB films processed at 190°C for 10mins became brown or off − white in colour due to thermal degradation and hence, the lower processing temperature was chosen to avoid polymer degradation.

The mechanical properties of melt − pressed P(HB − HV) polymer films followed the same trends as those seen in solvent cast films and are compared with high density polyethylene (HDPE) in Table 2.4.

Table 2.4 Mechanical properties of melt − pressed P(HB − HV) polymer films.

| Polymer | Mechanical Property (Mean ± S.D; n=5) | | |
	TS (MPa)	%E	EM (MPa)
PHB380K	28.7 ±5.1	1.88 ±0.66	2543 ±180
PHV12	17.4 ±1.5	2.41 ±0.41	1154 ±322
PHV20	20.7 ±2.0	2.46 ±0.36	1086 ± 76
PHV27	17.5 ±1.3	7.88 ±0.84	475 ±179
HDPE	25.0 ±2.2	8.70 ±1.13	680 ±115

Although melt − pressed P(HB − HV) polymer films exhibited similar trends to those cast from solution, the values of the mechanical properties were not identical. Melt − pressed PHB380K films had slightly higher TS and EM values. The melt − pressed copolymer films had much lower values for %E when compared to those for solution cast films. This may have

been partly due to the greater thickness of melt-pressed films or possibly due to some thermal degradation.

Of the P(HB-HV) polymers studied, the properties of PHV27 more closely resembled those of HDPE. Although polyethylene had a higher TS than PHV27, the %E and EM were not significantly different (p>0.05). Both polymers exhibited 'necking' with similar elongations at fracture of about 90% in melt-pressed films. The mechanical properties of the homopolymer, PHB, have been reported to be similar to those of polypropylene [149].

According to the general polymer classification of Lever and Rhys [334] or Allcock and Lampe [394] (Figure 2.14), PHB was regarded as being hard and brittle and the copolymers with increasing HV content became progressively tougher, less rigid (softer) and more ductile. Indeed P(HB-HV) copolymer films with HV contents of 12mole% and above exhibited necking and ductile fracture.

The dependence of mechanical properties on P(HB-HV) composition cannot easily be explained by differences in their degrees of crystallinity. Bloembergen et al [211] have reported that equilibrium degrees of crystallinity are similar for copolymers containing up to 47 mole % HV. In this study it is proposed that differences in mechanical properties may be better explained by differences in crystalline morphology and this will be discussed in chapters 5 and 8.

On the basis of their favourable mechanical properties P(HB-HV) copolymers may be preferable for manufacture and implantation of surgical and drug delivery devices [264].

2.4.3 The effect of Sodium Fluorescein (SF) as particulate drug inclusions on the mechanical properties of P(HB-HV) copolymer films.

Studies with model drugs were carried out with the P(HB-HV) copolymer containing 20 mole% HV (PHV20) because of its superior mechanical properties and film forming ability. Drug loaded films had a uniform distribution of SF particles within the PHV20 matrix.
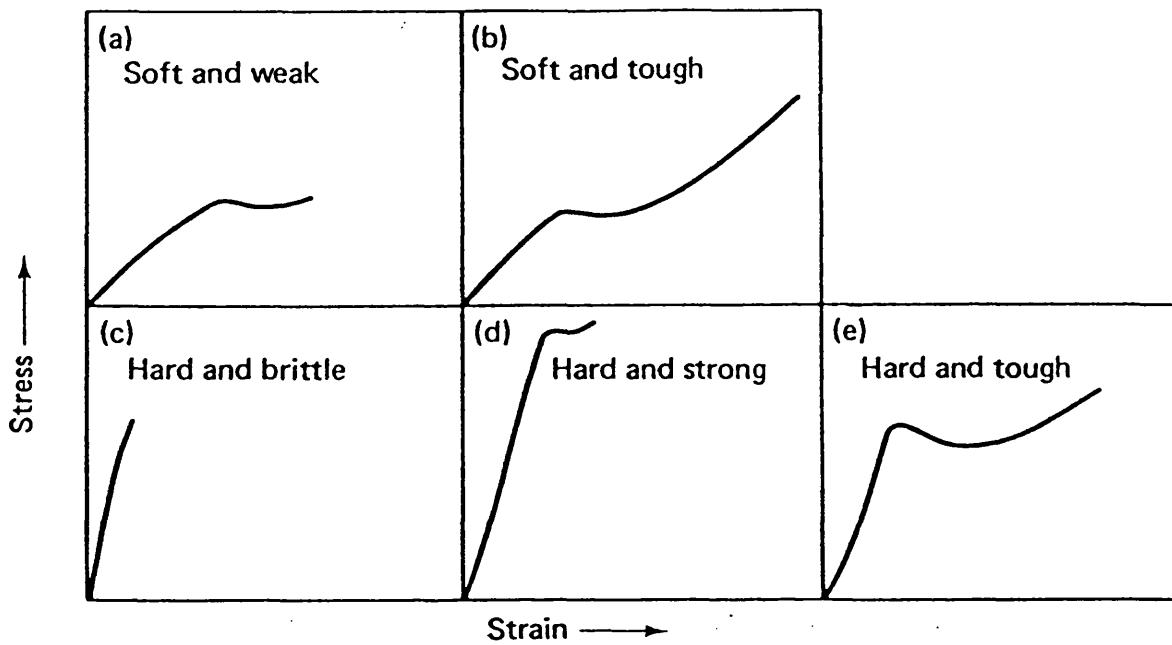
Figure 2.14. Polymer classification on the basis of characteristic stress – strain profiles (after ref. 334 and 394).

Figure 2.15 shows that TS was markedly reduced upon the inclusion of particulate drug in PHV20 films. The addition of only 2%w/w drug gave rise to over 30% reduction in TS. On comparison with the drug-free PHV20 films, drug loadings of 10%w/w lead to over 40% loss in the property. The explanation for the reduction in TS of drug loaded polymer films was thought to be the induction of flaws or microcracks at the particle-polymer interface caused by the presence of SF. Such defects reduce the tensile strength according to Griffiths theory of crack propagation [358].

In Figure 2.16 a similar trend was seen for %E with increasing drug concentrations in PHV20 films. In this case, the incorporation of 2%w/w drug reduced %E by over 40% and over 50% reduction was observed for films containing 10%w/w drug. Nielsen [336] suggested that the main reason for a reduction in %E for polymers filled with rigid particulates is that, although the film is part filler (drug) and part polymer, all the elongation comes from the polymer. Therefore the actual elongation experienced by the polymer is much greater than that measured macroscopically [336,359]. However, Nielsen's theory is complex and incomplete at present and the expected results depend upon the exact fracture mechanism [336].

Figure 2.16 also shows that EM values were not significantly different (p>0.05) for drug loadings up to 10%w/w when compared to drug-free PHV20 films. However, Aulton and Abdul-Razzak [338], working on tablet film coatings, have shown that the inclusion of titanium dioxide particles in hydroxypropylmethylcellulose films produced large increases in modulus. This effect was, however, more pronounced at concentrations greater than 10% and may also occur with the PHV20-SF systems at higher drug concentrations than those employed in this study. It should be noted that increases in modulus are dependant on the nature of the particulate filler or drug (eg rigidity of filler) and the strength of adhesion between filler and polymer [359]. These are variables which need to be addressed when assessing the mechanical properties of drug loaded polymeric implants and surgical devices.

Although the present work has shown that the inclusion of a particulate drug into
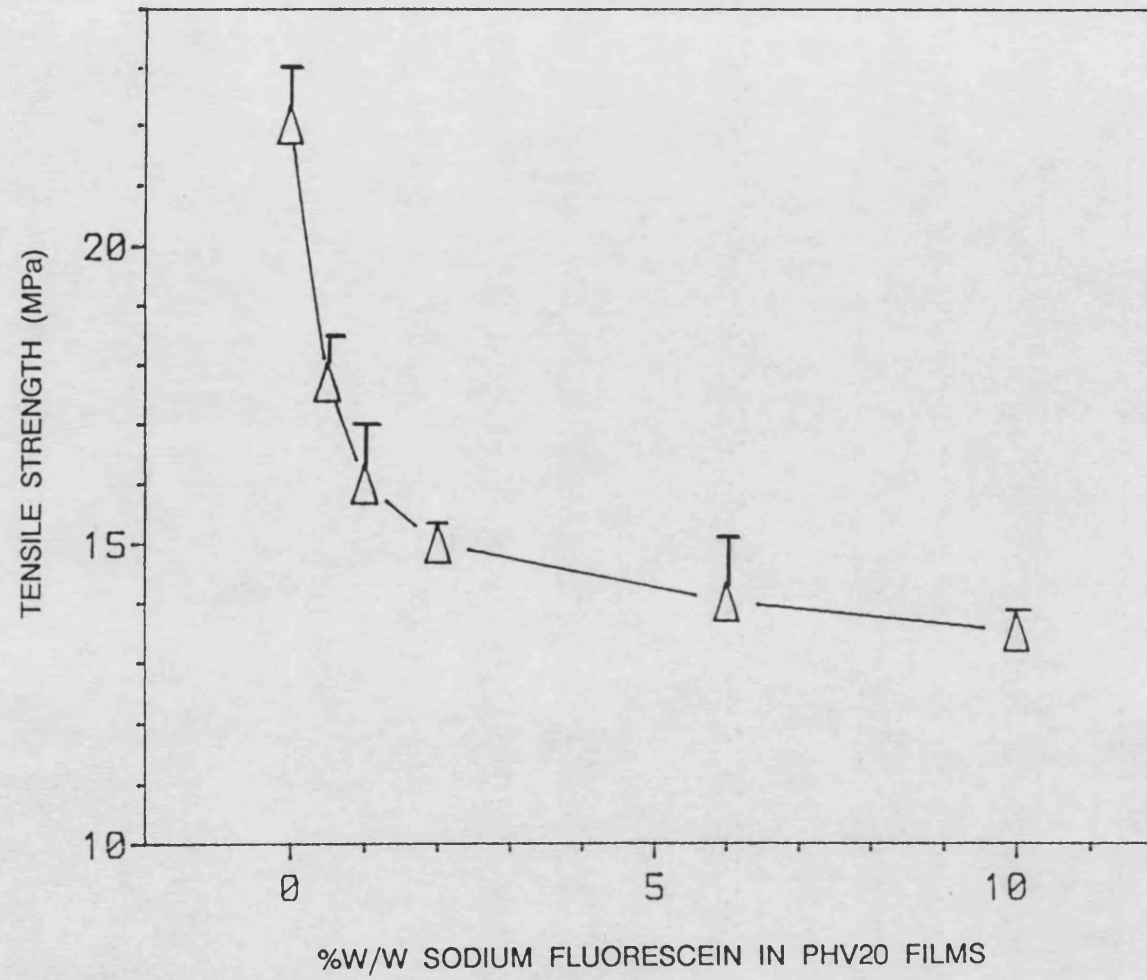
Figure 2.15. The influence of drug concentration on the tensile strength of PHV20 films (Mean ± S.D; n=5).
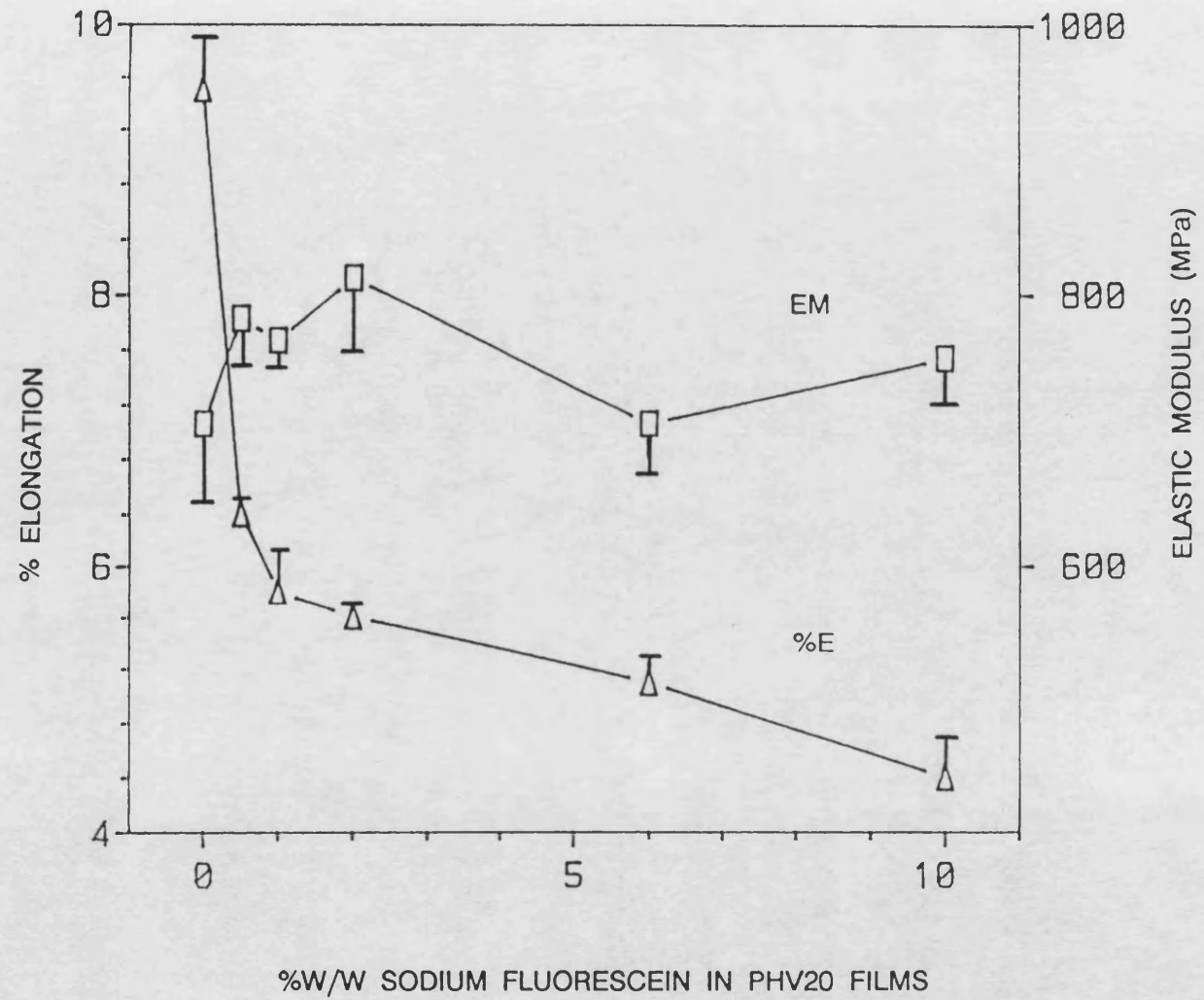
Figure 2.16. The influence of drug concentration on the % Elongation and Elastic Modulus of PHV20 films (Mean ± S.D; n=5).

polymeric matrices reduces TS and %E, exceptions to these trends may occur with other drugs. A number of models have been proposed by Nielsen [336,359] and others [360-361] to predict the changes in properties of polymers on the inclusion of rigid particulate fillers but they must be used with caution as exceptions are not uncommon. One such exception in polymer science is the use of carbon black filler in rubber to actually increase the tensile strength of rubber [336].

2.4.4 The effect of inclusion of Methyl Red, a chloroform-soluble drug, on the mechanical properties of P(HB-HV) copolymers.

Methyl Red was soluble in the polymer solutions and resulted in films in which drug appeared to be homogenously distributed.

Table 2.5 shows that the mechanical properties of PHV20 were little affected by Methyl Red concentrations of up to 10%w/w and is in contrast to the effects seen on inclusion of the particulate drug, SF. The reason for this was thought to be that Methyl Red formed a continuous phase with the polymer and did not induce the type of flaws in the polymer matrix caused by the particulate drug. However, it is thought that even chloroform soluble drugs may greatly modify properties at high concentrations when the drug is a major component of the composite. Indeed, mechanical properties are likely to closely resemble those of the pure drug as the proportion of the drug increases.

Table 2.5   The mechanical properties of Methyl Red loaded PHV20 biopolymer films.
(Mean ±S.D, n=10).

Methyl Red Concentration (%w/w)	Tensile Strength (MPa)	Elongation (%)	Elastic Modulus (MPa)
0	22.44 ±1.13	9.58 ±0.14	671 ± 97
1	19.08 ±1.42*	8.28 ±1.52*	653 ±132
2	21.02 ±0.78	9.25 ±0.30	694 ± 56
5	20.40 ±0.51	9.55 ±0.36	745 ± 64
7	19.30 ±1.02*	8.29 ±0.60*	707 ± 48
10	19.10 ±0.55*	7.92 ±0.56*	689 ± 35

*significantly different to control (p<0.05)

2.4.5 The influence of radiation and steam sterilization on the mechanical properties of biopolymers.

Measurements of mechanical properties can be used to assess changes in bulk properties of materials. The correlation between mechanical properties and bulk properties has been used to indicate polymer-additive interactions [362-364], radiation damage [291] and polymer degradation [268,291-293]. In this section mechanical properties have been determined to assess any changes in bulk properties of polymer treated with either gamma-irradiation (2.6Mrad dose) or steam sterilization (bench autoclave 121°C for 20 mins).

Table 2.6 shows the effect of sterilization treatments on the mechanical properties of PHV20 films. All batches of PHV20 films were prepared and stored under identical conditions. Two batches (n=5 per batch) of PHV20 films were used for irradiation studies and one batch was used for steam sterilization.

At the standard gamma-irradiation dose of 2.6Mrad PHV20 films were unaffected in terms of tensile strength or Elastic modulus. However, %E was significantly lower (p>0.05) than the control value.

The effects of gamma-irradiation on polymers has been extensively investigated in recent years [365-368]. Radiation is known to induce complex changes in polymers including random chain scission and cross-linking [366,377]. The reduced ductility of PHV20 films was presumably due to molecular weight changes induced by chain scission but these were not determined in this study.

Table 2.6 The effect of Sterilization Treatments on the Mechanical Properties of PHV20.

| Sample Treatment | | Mechanical Property (Mean $\pm$S.D, n=5) | | |
		T.S (MPa)	%E	EM (MPa)
Control PHV20		20.47 $\pm$1.56	5.99 $\pm$0.56	840 $\pm$23
Gamma – irradiation (2.6 Mrad dose)	Batch1	18.08 $\pm$1.12	4.73 $\pm$0.18*	798 $\pm$44
	Batch2	19.60 $\pm$4.95	4.95 $\pm$0.14*	881 $\pm$58
Steam Sterilization (autoclave 120°C for 20 mins).		11.41 $\pm$1.75*	7.83 $\pm$1.55*	375 $\pm$61*

* significantly different to control ($p < 0.05$)

Miller and Williams [291] have recently shown that irradiation of P(HB – HV) copolymer monofilaments with doses up to 10Mrad progressively reduced tensile strength and extensibility and that a 20Mrad dose was sufficient to destroy all mechanical integrity of the specimens. The authors assumed that mechanical property changes induced by radiation were due to molecular weight loss but this was not confirmed. The authors neglected to measure cross – sectional area and hence, were unable report values for TS and EM of the unirradiated polymer which made interpretation of some of their results difficult [291].

Table 2.7 The effect of steam sterilization on the mechanical properties of PHB films.

| Sample Treatment | Mechanical Property $\pm$S.D. | | |
	T.S (MPa)	%E	EM (MPa)
Control PHB	21.84 $\pm$2.74	1.95 $\pm$0.32	1537 $\pm$379
Steam Sterilization (autoclave 120°C for 20 mins).	21.41 $\pm$1.75	1.93 $\pm$0.55	1475 $\pm$161

Steam sterilization did not affect the mechanical properties of the homopolymer, PHB, (Table 2.7) but significantly modified those of the PHV20 copolymer. As shown in Table

2.6 the TS and EM of PHV20 were reduced by approx 50% but the %E was increased by approximately 30%. The melting range of PHV20 (see chapter 3) is close to the sterilization temperature and consequently the partial melting of films resulted in gross mechanical property changes. The use of high temperature steam sterilization will only be applicable to the homopolymer or P(HB-HV) copolymers with softening points greater than the temperature of sterilization.

2.5 CONCLUSIONS

A minimum MW of 190-200K was required to form a thin solvent cast film of PHB. Above this threshold MW for mechanical integrity of a specimen, the mechanical properties of PHB improved until a critical MW (approximately 300K) was reached beyond which the properties remained stable.

PHB was relatively hard and brittle and copolymerization with HV produced tougher, less brittle and more pliable polymers. These may be preferable for manufacture and implantation.

The inclusion of drugs may adversely affect polymer properties. The effects may be marked even at low concentrations with particulate drugs.

Steam sterilization may be used for P(HB-HV) biopolymers with melting temperatures well above those employed in autoclaving but may induce gross changes in mechanical properties for those that have lower melting ranges.

Gamma-irradiation at the recommended 2.6Mrad total dose was sufficient to induce changes in mechanical properties of PHV20 films. The loss in properties must be taken into account, if this method is to be employed for sterilizing biomedical devices fabricated from P(HB-HV) biopolymers. However the magnitude of the changes caused by the 2.6Mrad total dose would probably not be great enough to preclude the use of sterilization by gamma-irradiation.

CHAPTER 3

THERMAL PROPERTIES

3.1 INTRODUCTION

3.1.1 PRINCIPLES OF DIFFERENTIAL SCANNING CALORIMETRY (DSC)

Differential Scanning Calorimetry (DSC) and Differential Thermal Analysis (DTA) are related techniques used to monitor enthalpy changes of a sample as a function of temperature. The Nomenclature Committee of the International Confederation for Thermal Analysis have defined DSC as [369]:

"A technique in which the difference in energy input into a substance and a reference material is measured as a function of temperature whilst the the substance and reference material are subjected to a controlled temperature programme".

DTA is essentially the same as DSC but in DTA differences in temperature between reference and substance are measured as a function of temperature [370].

General reviews on DTA and DSC include those by Smothers and Chiang [371], Mackenzie [372], Murphy [373], Wunderlich [374] and Schultze [375]. However more specific reviews on polymer characterization using these techniques include those by Turi [376], Chiu [377], Smith [378] and Barrel and Johnson [379].

DSC is mainly used for studies of physical transitions [380] and is the technique used in this investigation. Polymer features such as moisture interactions, glass transitions, melting temperatures, compatibilty and crystallinity may be determined by this technique [364].

The equipment used in both DTA and DSC is similar. The arrangement of temperature sensors (platinum) in a typical DSC instrument are shown in Figure 3.1. Sample and reference materials are usually held in crimped aluminium pans. In the event of a transition occurring, thermal energy is added or subtracted from the sample or reference in order to maintain isothermal conditions. The energy is precisely equivalent in magnitude to the energy absorbed or evolved in the particular transition and is represented by the peak area on a DSC trace. Figure 3.2 shows an hypothetical DSC trace
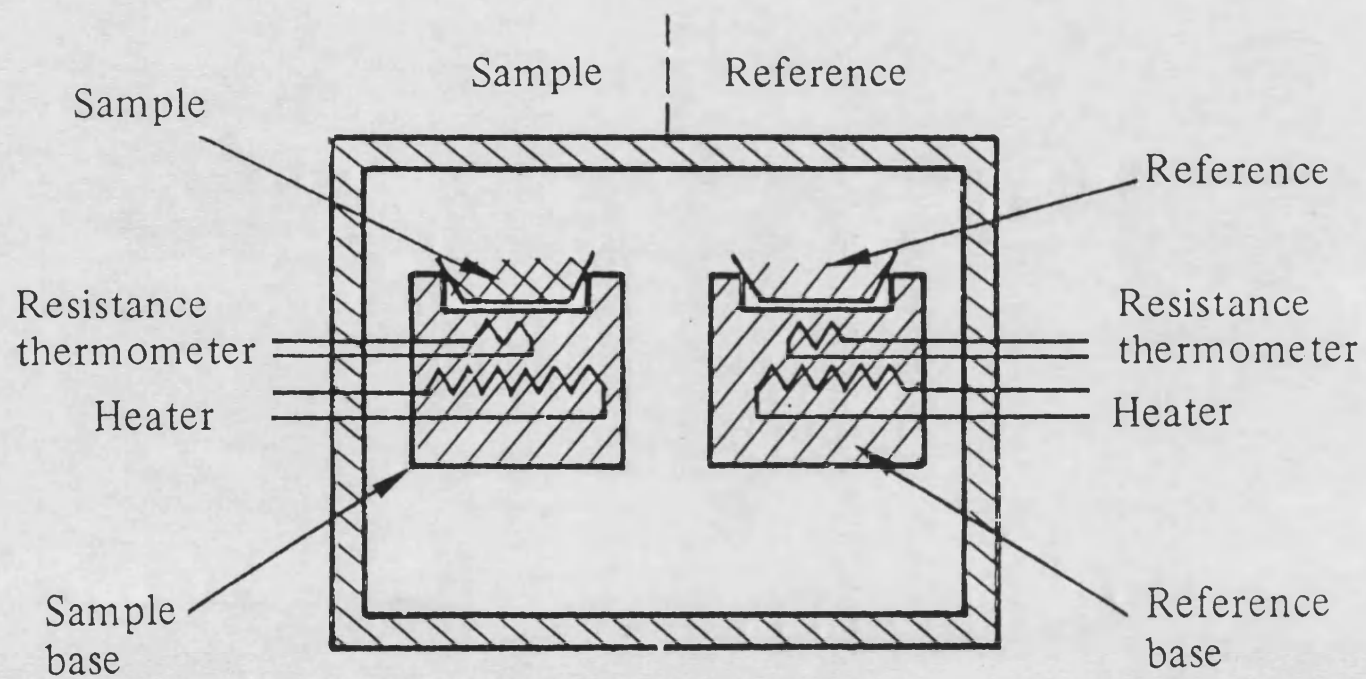
Figure 3.1. The arrangement of temperature sensors in a typical DSC apparatus (after ref. 390).
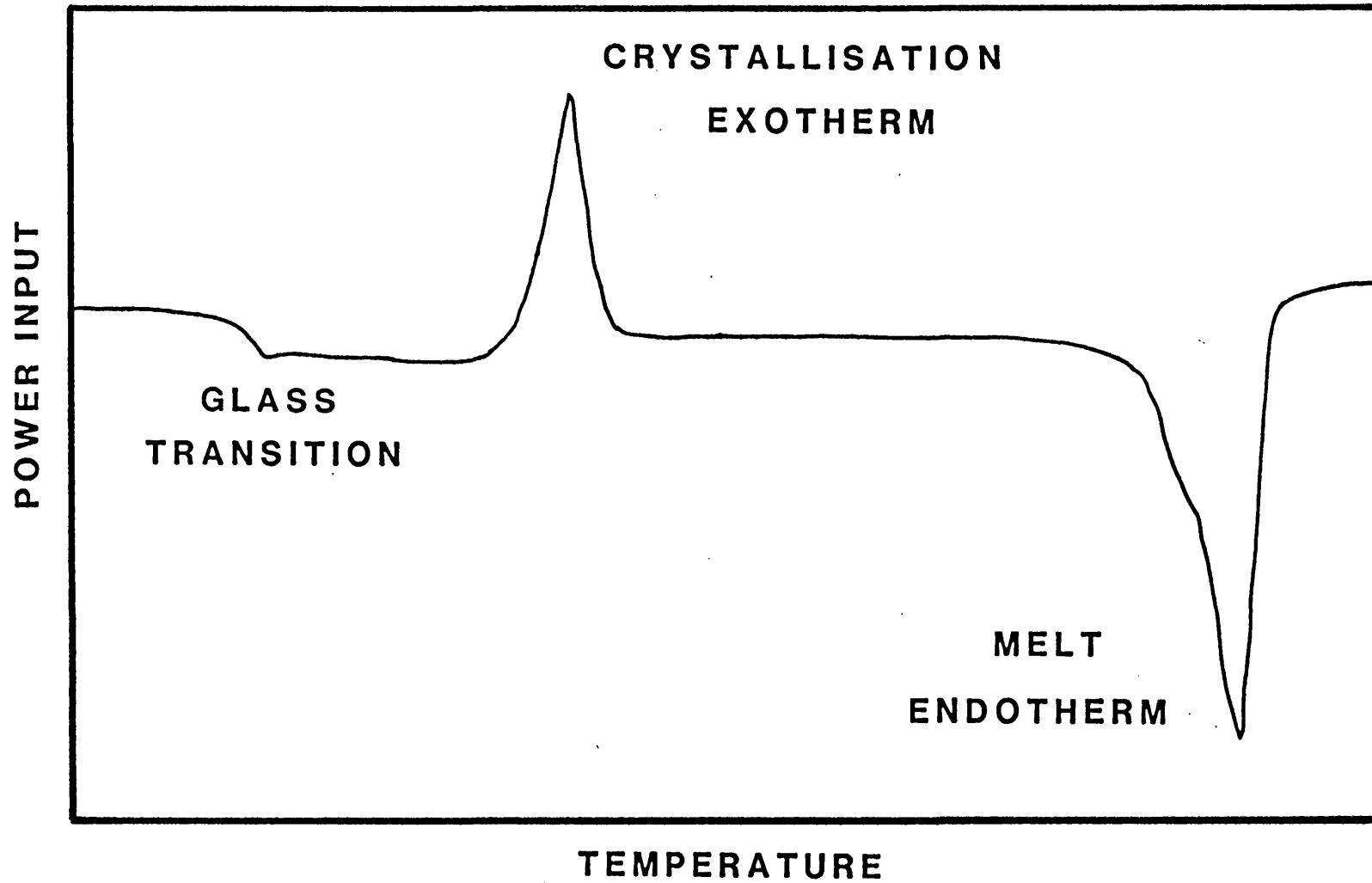
Figure 3.2. A hypothetical DSC trace representing some common transitions observed in polymers.

representing physical transitions commonly seen in polymers. A DSC trace is often termed a 'thermogram' in the pharmaceutical literature and although the former is the most accurate both are used interchangeably in this report.

3.1.2 PRINCIPLES OF THERMOGRAVIMETRIC ANALYSIS (TGA).

Thermogravimetric analysis (TGA) is a dynamic technique which monitors the weight changes in a sample as a function of temperature. The technique is considered to be the most important method for studying polymer stability and degradation [377] but can also be used to provide useful information on moisture interactions and residual solvent [364].

General reviews on TGA of polymers include those by Chiu [380], MacCullum [381], and Thompson [382].

Experimentally a polymer sample is placed in a furnace while being suspended from one arm of an automatic-reading, precision electrobalance. The change in sample weight is recorded as a function of temperature during the programmed heating of the sample. A typical TGA curve is represented in Figure 3.3.

TGA is basically a means for studying polymer behaviour and not an absolute identification tool [380]. Therefore it is often used in combination with DSC to provide information on weight changes occurring during transitions detected by the DSC. It has also been used in combination with other analytical techniques including mass spectrometry (MS) [383-384], gas chromatography (GC) [385] and GC-MS [386].

3.1.3 AIMS AND OBJECTIVES

1. To study the melting behaviour and glass transitions in P(HB-HV) polymers using DSC.

2. To study the thermal degradation of P(HB-HV) polymers using TGA.

3. To compare the properties of P(HB-HV) with those of Poly-L-lactide.
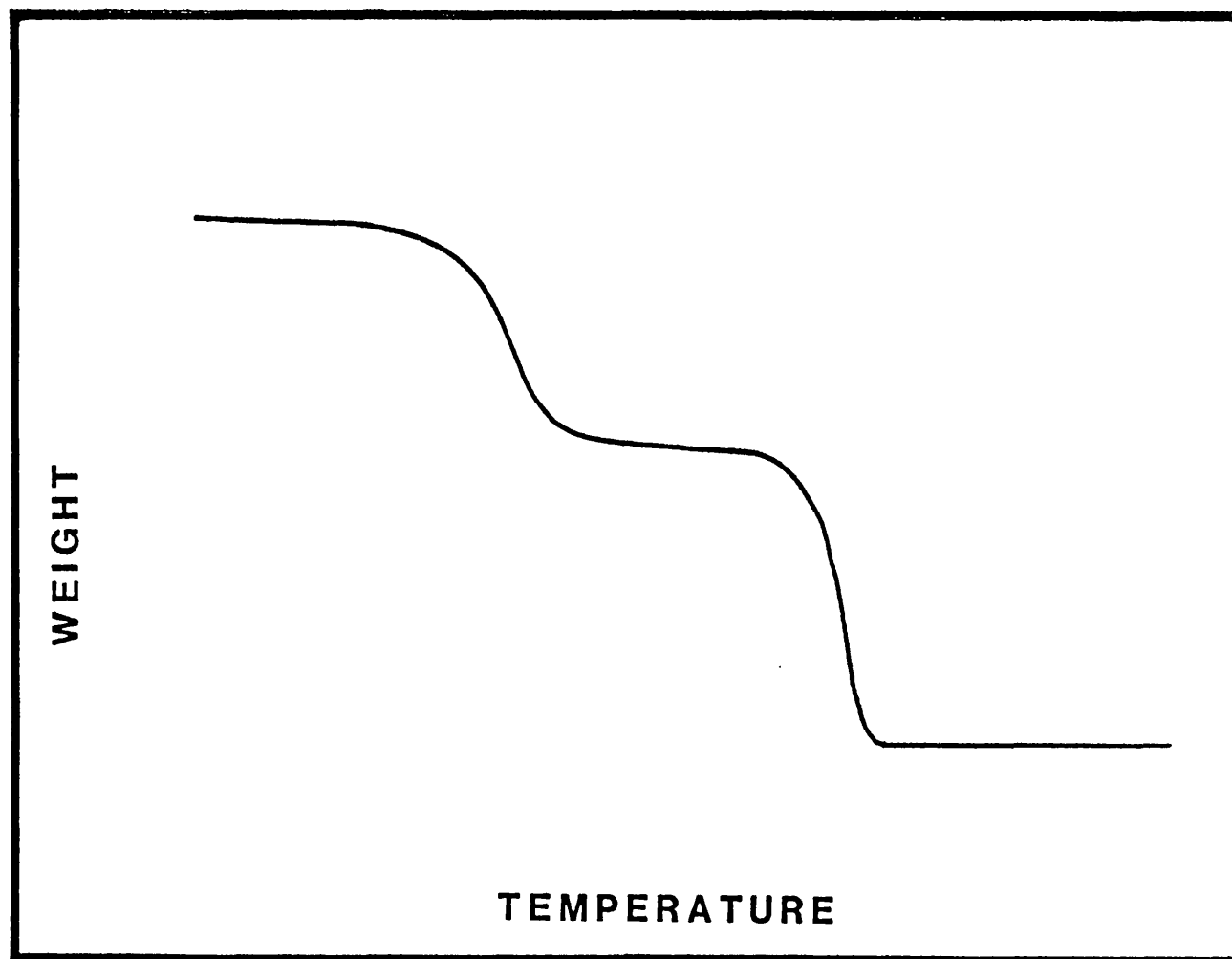
Figure 3.3. A hypothetical TGA trace representing a two stage weight loss.

3.2 MATERIALS

Poly-L-lactide (PLA) of 300,000 Mw was purchased from Polysciences, UK.

Poly L-lactide-co-glycolide), P(LA-GA) 90:10, and 10:90 were gifts from Cyanamid of Great Britain Ltd, Gosport, UK.

PHB43K and PHB380K (the numbers indicate the Mw) were purchased from Marlborough Biopolymers Ltd. Quinine was purchased from Fisons, UK.

All other materials used were identical to those given in Chapter 2.

3.3 METHODS

3.3.1 Differential Scanning Calorimetry (DSC)

Melt-quenched amorphous samples were prepared by cooling molten polymers rapidly in liquid nitrogen. This was carried out to erase previous thermal history of polymer samples before determination of melting and glass transition temperatures.

DSC scans to determine glass transitions (T_g), melting points (T_m) and heats of fusion $(\triangle H_f)$ of polymers were recorded on a Dupont DSC 910/9900 Thermal Analyser. All other DSC scans were obtained using a Perkin Elmer DSC-7/PE 7700 Thermal Analysis System.

Instruments were calibrated with Indium $(T_m = 156.4°C$, $\triangle H_f = 28.47$ KJ/Kg) at the required heating or cooling rates prior to use. Standard heating rate was 20K/min and typical sample mass used was 3-5mg in lightly crimped aluminium pans with inverted lids. Reference in all cases was an empty aluminium pan crimped as above.

3.3.2 Thermogravimetric Analysis (TGA)

Polymer samples (3-5mg) were heated at a programmed heating rate of 20K/min, unless otherwise stated, in a Perkin Elmer TGA-7/PE 7700 Thermal Analysis System.

3.4 RESULTS AND DISCUSSION

3.4.1 Melting behaviour of P(HB-HV) biopolymers.

The melting of polymer crystals is essentially the reverse of crystallization, but is more complicated than the melting of low molecular weight materials. Characteristically, polymers do not have sharp melting points but the melting takes place over a range of temperatures [387-388]. The melting range is further classified by the onset and peak melting temperatures as shown in Figure 3.4.

The onset melting temperature is defined as the intersect on the baseline of a tangent drawn to the leading edge of the main peak [380]. The difference between the onset and peak temperatures provides a measure of the range over which melting occurs. The range and shape of the melting curve contains information on the size and order within crystallites and in general the quality of the crystallinity [389]. However, the onset and peak temperatures are often not distinguished and sometimes used synonymously in the literature.

The melting range is influenced by a number of factors including the programmed heating rate within the DSC. Daniels [390] gives a detailed account on the influence of operating parameters, including sample mass, on DSC traces. The sample mass in this study was kept constant within the range of 3-5mg. Table 3.1 shows the relationship between heating rate and peak melting temperature for PHB380K. Increasing the programmed heating rate from 5K/min to 20K/min produced a corresponding 4°C rise in peak T_m.

Table 3.1. The effect of DSC heating rate on the melting points of PHB380K
(Mean $\pm$ Range; n = 2)

Heating Rate	Melting Temperature (°C)	
Kmin^{-1}	Onset	Peak
5	161.5 $\pm$ 0.1	170.0 $\pm$ 0.1
10	162.0 $\pm$ 0.2	172.3 $\pm$ 0.4
20	163.4 $\pm$ 0.1	174.1 $\pm$ 0.1
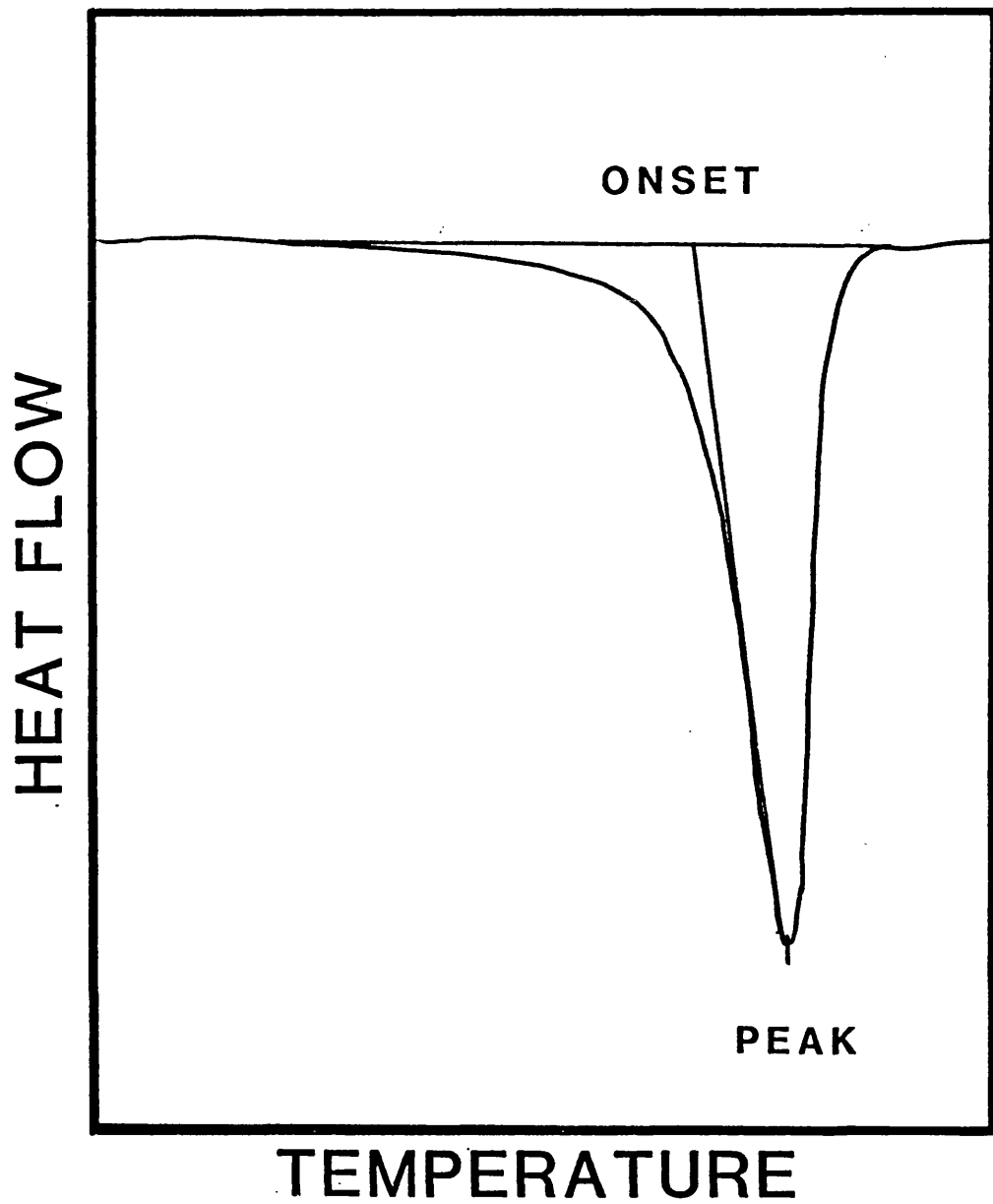
Figure 3.4. A DSC melt endotherm showing the onset and peak melting temperatures of a polymer.

As a result of T_m varying with heating rate, it has been suggested [389] that the definition of Flory [391] for melting points should be used. Flory [391] has defined the melting point as that temperature at which crystallinity just persists. This implies that melting of the most stable crystallites is determined rather than a less precise measure of average melting point [389]. In the DSC this is usually determined by extrapolation to zero mass or zero heating rate. Extrapolation of T_m values for PHB to zero heating rate gave a peak melting point of 169°C. However values obtained in such a manner are thought to be dependent on the heating rates chosen for extrapolation and the concept has been replaced by the determination of equilibrium melting temperature [389]. This is further discussed in chapter 5.

Table 3.2 shows the effect of molecular weight (MW) on the melting behaviour of PHB. Molecular weight fractions were prepared by non-aqueous catalytic degradation as described in chapter 2. In general the peak melting point increased with increasing molecular weight of PHB. The melting temperature of PHB23K was significantly lower ($p < 0.05$) than of PHB molecular weights in the range 250K-800K. This was thought to be due to the higher proportion of chain ends in the low MW polymer which are responsible for introducing crystal defects and lowering T_m. However, the effect of molecular weight on melting temperatures of PHB within the molecular weight (Mw) range of 250K – 800K was weak. This finding is not unusual and the influence of MW on melting point has been reported by Young [392] to be weak when the MW of the polymer is sufficiently high to have useful mechanical properties. For PHB the mechanical properties stabilised at about MW 300K, which is in close agreement with the melting point data. Mechanical properties were thought to stabilize when the cohesive forces within the bulk polymer were strong enough for the polymer to have useful properties (see Chapter 2). The heat of fusion appeared to be variable and no correlation with molecular weight of PHB could be established.

Table 3.2. The melting behaviour of PHB molecular weight fractions prepared by non–aqueous catalytic degradation (Mean ± Range; n = 2)

| Molecular Weight (x 1000) | | Mw/Mn | Melting Temperature (°C) | | Heat of Fusion (J/g) |
Mw	Mn		Onset	Peak	
23	13	1.8	160.1 ±0.3	168.2 ±0.3	87.5 ±2.1
250	167	1.5	164.4 ±0.1	173.8 ±0.2	101.5 ±9.5
384	226	1.7	165.0 ±0.2	174.8 ±0.4	96.1 ±9.3
513	324	1.6	165.9 ±0.1	177.3 ±0.1	86.2 ±3.2
765	506	1.5	166.5 ±0.1	176.8 ±0.1	99.5 ±1.1

Figure 3.5 shows DSC melt endotherms of 'as supplied' P(HB–HV) copolymers to highlight the relationship between copolymer composition and melting temperature. Melt endotherms were recorded at a programmed heating rate of 20K/min. The data on the melting behaviour of P(HB–HV) biopolymers is summarized in Table 3.3

Table 3.3. Data on the melting behaviour of P(HB–HV) polyesters (Mean ± Range; n = 2 Heating rate 20kmin^{-1}).

| Polymer | Melting Temperature (°C) | | Heat of Fusion (J/g) |
	Onset	peak	
PHB380K	163.4 ±0.1	174.1 ±0.1	91.7 ±0.3
PHV6	129.8 ±0.4	150.0 ±0.1	77.2 ±2.9
PHV12	111.4 ±0.5	135.9 ±0.1	66.6 ±0.6
PHV20	79.1 ±2.4	115.0 ±0.4	54.1 ±7.3
PHV27	41.7 ±0.1	83.8 ±0.1	51.3 ±0.3

The melting point or range of P(HB–HV) copolymers was dependent on HV content. PHB380K melts at a peak melting temperature (peak T_m) of 174°C but as the HV content was increased the peak T_m was progressively lowered to a value of 83°C for PHV27. A similar trend was seen for their heats of fusion ($\triangle H_f$). The results are shown graphically in Figures 3.6 and 3.7.

The heats of fusion of a polymer can be indicative of the mass fraction degree of

Figure 3.5. DSC melt endotherms of 'as supplied' P(HB – HV) copolymers.

O MOLE% HV

6

12

20

27

0   100   200
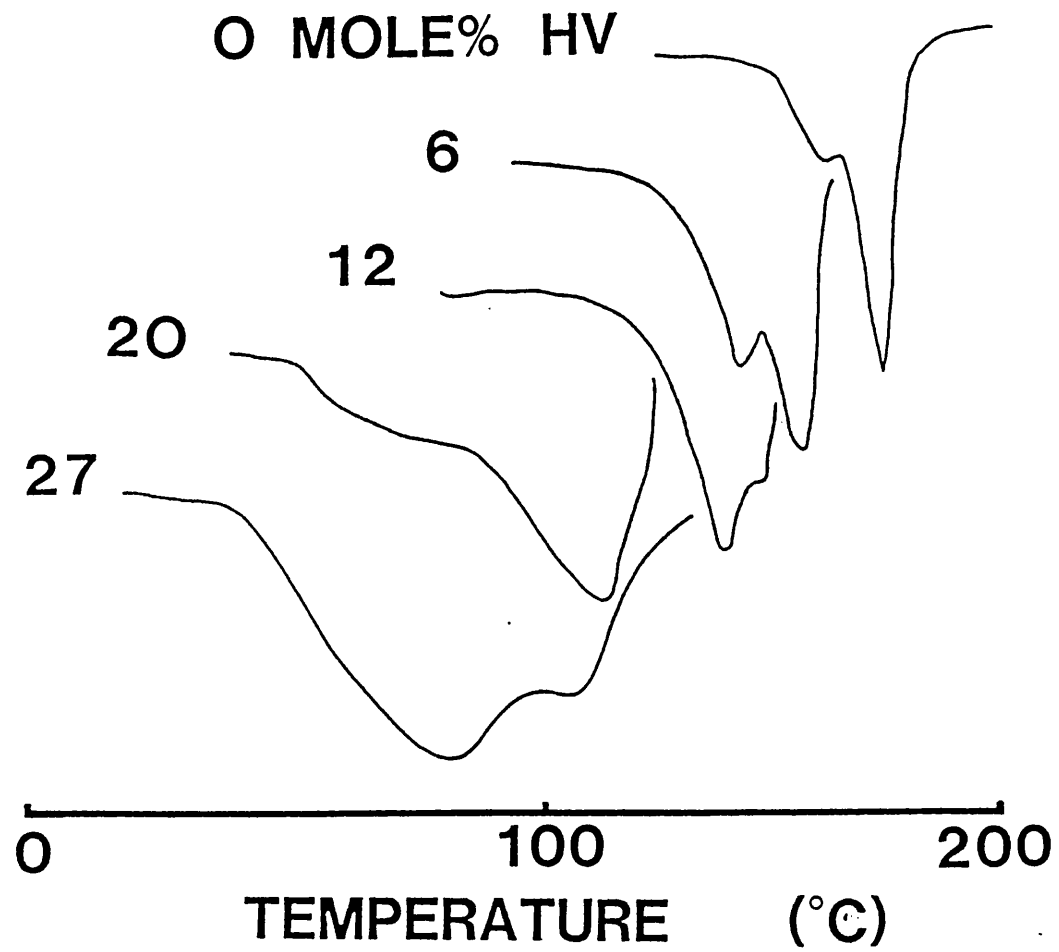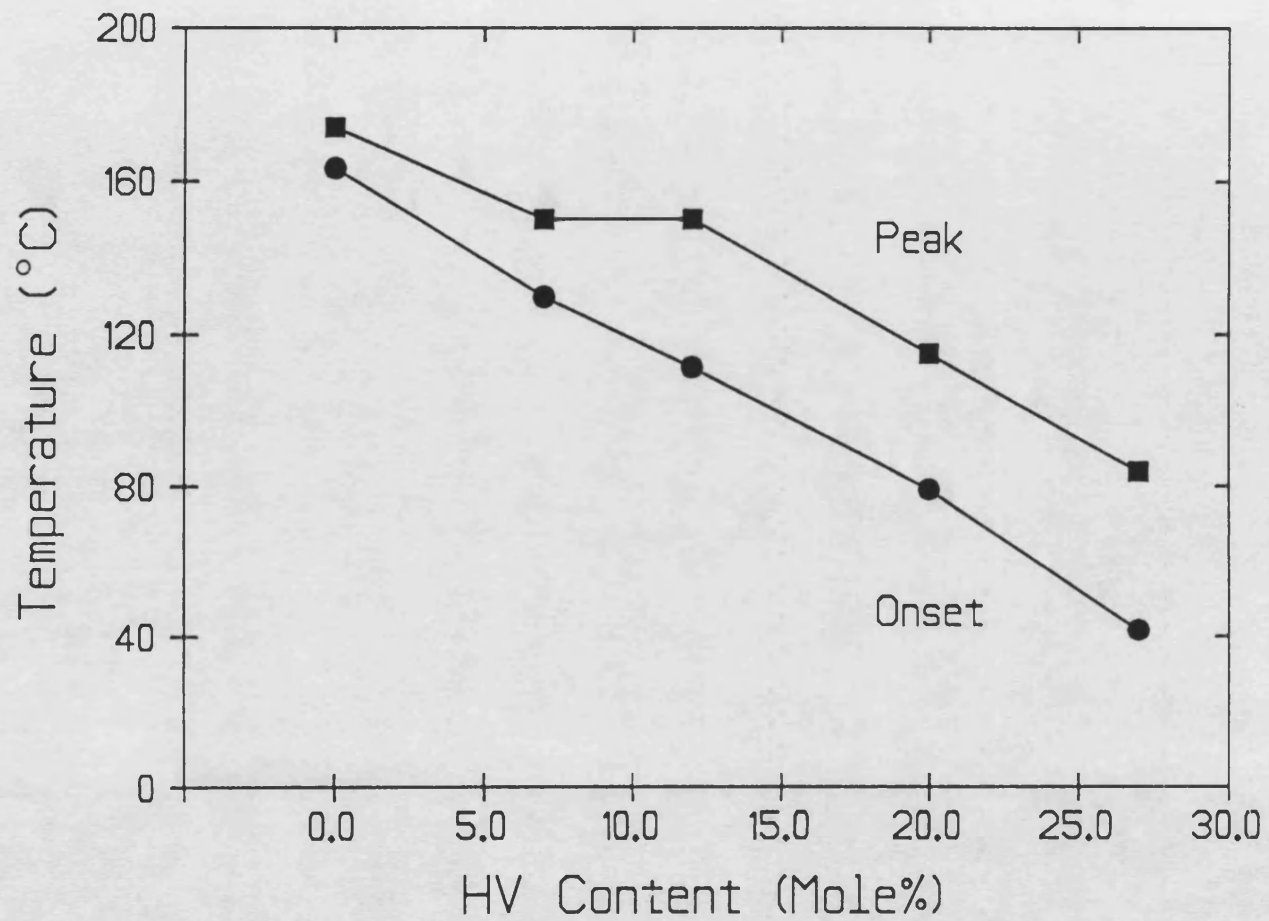
TEMPERATURE   (°C)

Figure 3.6. The variation in onset and peak melting temperatures with P(HB – HV) copolymer composition.

(Mean, n = 2; data from Table 3.3)
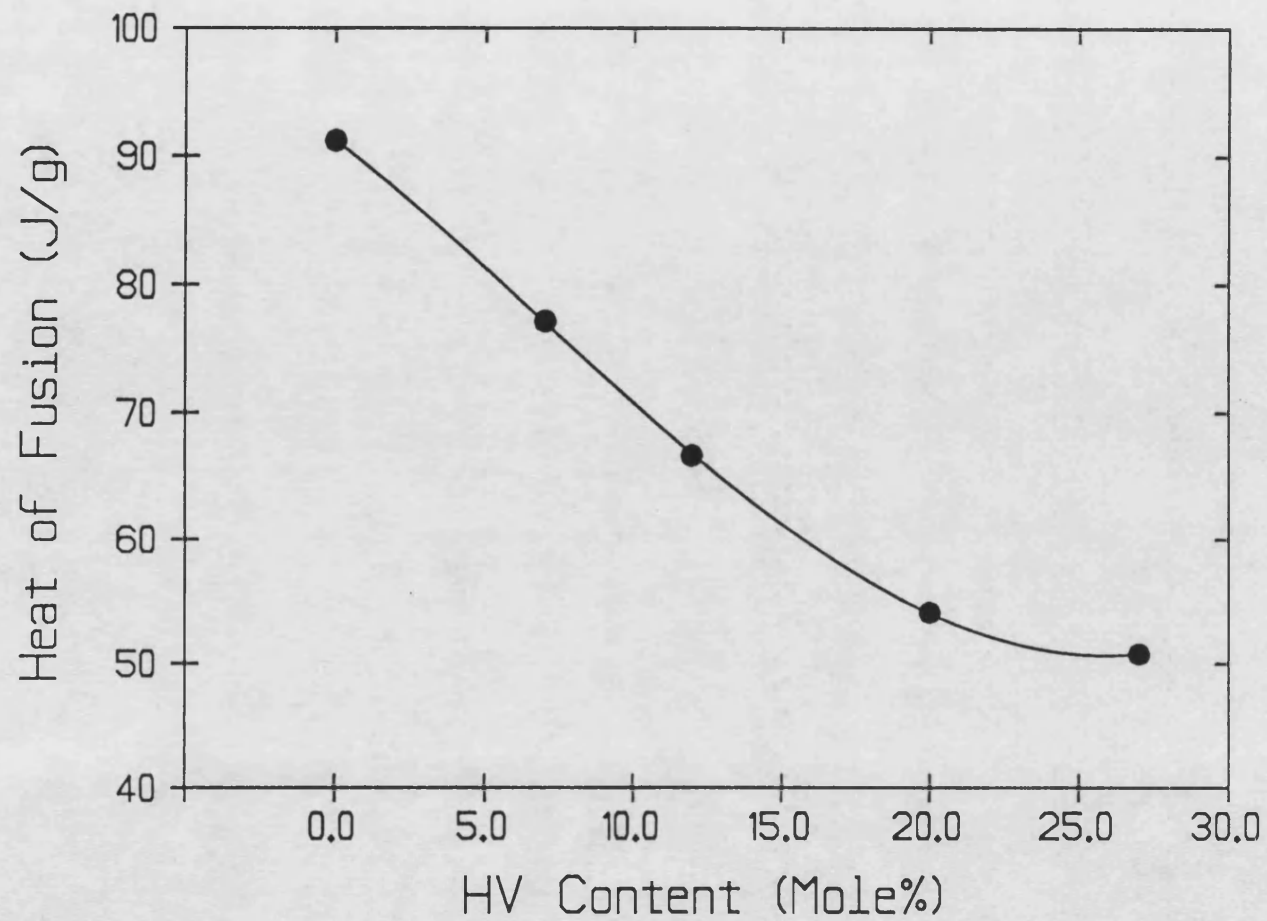
Figure 3.7. The variation in heats of fusion with P(HB – HV) copolymer composition.

(Mean, n = 2; data from Table 3.3)

crystallinity of that polymer if the value for the heat of fusion of the 100% crystalline polymer is known [389]. The heat of fusion estimated for the 100% crystalline PHB has been reported by Barham *et al* [214] to be 146 J/g. The values obtained in this study suggest that the 'as supplied' PHB800K was up to 69% crystalline. However contrary to the assumption of Holmes and colleagues [149,247], the progressive decrease in heats of fusion values for P(HB–HV) copolymers cannot be taken to represent a corresponding decrease in their degrees of crystallinity. This is mainly due to the fact that the values for the 100% crystalline copolymer will be different at each HV content, possibly because of crystal defects. There is also recent evidence [249–250] to suggest that there may be some exclusion of HV units from the common crystal lattice of these polyesters. The exclusion of HV units may explain why density measurements and heats of fusion values do not relate to the crystallinities determined by X–ray diffraction techniques.

The depression in melting points of copolymers with increasing HV content was thought to be due to HV units acting as impurities within the PHB matrix. In addition, the extra methyl group of HV introduced into the side–chain of the PHB polymer may introduce crystal defects in copolymers to lower T_m. The PHB crystalline lattice is thought to accept the ethyl group of HV, but less readily than the PHV lattice accommodates the smaller methyl group of HB [208]. The introduction of the ethyl group of HV within the PHB lattice, therefore, may only occur at the expense of introducing crystal defects and imperfections. This is manifested in a progressive increase in the range or breadth of the melt endotherm with increasing HV content. This can be seen from the melt endotherms of the copolymers in Figure 3.5 and can also be deduced from the progressive increases in the differences between onset and peak temperatures shown in Table 3.3. The melt endotherms for the P(HB–HV) polymers also show double melt endotherms. The existence of multiple peaks in polymer melting is a common but complex phenomenon which may be explained by a distribution of crystallite sizes [393] and is further discussed in chapter 4.

The T_m of copolymers would normally be expected to fall progressively until the melting point of pure PHV is attained. The literature value for the melting point of pure PHV is 105 - 108°C [205]. However, a recent report by Marchessault and coworkers [210] has shown that bacterial P(HB - HV) polyesters from *Alcaligenes eutrophus* exhibit eutectic - like minima in their melting points and heats of fusion at approximately 30 mole% HV content. In a more recent report, Marchessault and coworkers have shown a similar eutectic - like minimum for synthetic P(HB - HV) copolymers [208]. These P(HB - HV) copolymers were chemically synthesized by ring opening polymerization of mixtures of β - butyrolactone and β - valerolactone using a stereoselective alumoxane catalyst. The melting temperatures of synthetic copolymers were found to be similar to those determined by the authors for the biosynthetic copolymers. However, the heats of fusion were consistently lower for the synthetic copolymers and these were attributed to calibration differences between the two separate DSC instruments used in their study [208]. The authors reported that the synthetic P(HB - HV) copolymers exhibited eutectic - like minima in melting points and heats of fusion at approximately 30 mole% [208,210]. However, closer examination of their data over the full composition range, suggests that the minima for the synthetic P(HB - HV) copolymers occurred at about 40mole%. The results of this study on the melting data for bacterial P(HB - HV) polymers containing up to 28 mole% HV correlate well with those reported by Marchessault and coworkers [210].

This phenomenon of a melting point minimum is not normally seen in most copolymer systems [210]. However in the case of P(HB - HV) the eutectic - like minima may be explained by the fact that the statistically random P(HB - HV) copolymers exhibit isodimorphism. Both the HV and HB components of the crystalline P(HB - HV) copolymers are thought to co - crystallize within the same unit cell because of their similar main - chain conformations and molecular dimensions [208,210].

3.4.2 Glass transitions in P(HB - HV) biopolymers.

The glass transition represents the rather sharp change that occurs from the glassy to

the rubbery or flexible thermoplastic states in nearly all linear-type polymers [394].

It is characteristic of a polymer and related to its structure. In fact, the glass transition temperature (T_g) varies with the type of skeletal atoms present, with the types of side groups, and even the spatial disposition of the side groups [394]. A knowledge of the glass transition of a polymer is not only useful for identification but also provides information of the polymers properties and molecular structure [395]. In biomedical applications of polymers, a knowledge of the T_g will indicate whether the polymer exists as a brittle glass or as a flexible thermoplastic with enhanced chain mobility at physiological temperatures. Information on polymer chain mobility will be important in drug diffusion and controlled drug release properties of polymers.

The T_g strongly depends on the thermal history and crystallinity of polymers [393] and for that reason samples were standardised to an amorphous morphology for T_g determinations. Amorphous samples of PHB could only be produced if the quenching (cooling) rate was equal to or greater than 40K/min. Slower cooling rates allowed the PHB to recrystallize. The presence of the amorphous state was confirmed, on a subsequent heating cycle in the DSC, by the presence of an exotherm of crystallization with a heat of crystallization close to the heat of fusion (within 50-70% of the heat of fusion; see section 3.4.3). Completely amorphous polymers were not obtained in this study. This was expected since the presence of some order even in amorphous states has been observed for crystalline polymer systems [396]. The absence of an exotherm of crystallization would suggest that the sample had crystallized and was no longer amorphous. P(HB-HV) copolymers could be quenched to an amorphous state at slower rates of cooling than for PHB (Table 3.4) because the rate of crystallization was slower in copolymers and was dependent on HV content (see chapter 5).

Table 3.4 Minimum rates of cooling required to obtain amorphous morphologies for P(HB−HV) polymers.

Polymer	Cooling Rate
PHB380K	40 K/min
PHV6	20 K/min
PHV20	10 K/min
PHV27	5 K/min

Melt−quenched amorphous P(HB−HV) copolymers were heated from subambient temperatures, usually −15 or −20°C, to melt in a Dupont DSC apparatus at 20K/min. Figure 3.8 shows a typical DSC trace for PHB from which glass transitions were determined using the Dupont DSC data analysis software. The onset temperature was the chosen method for T_g determination. The T_g results are summarized in Table 3.5.

Table 3.5   Glass Transition Temperatures of P(HB−HV) polyesters.

Polymer	T_g range (°C)
PHB380K	−5 to +8
PHV6	0 to +5
PHV12	−5 to +3
PHV20	+10 to +18
PHV27	+15 to +20
PLA	+56 to +59
P(LA−GA)90:10	+55 to +58
P(LA−GA)10:90	+35 to +38

The glass transition temperature varied between −5 to 20°C for the range of P(HB−HV) copolymers containing up to 27mole% HV content but the relationship was not linear. These values were much lower than those determined for P(LA−GA) systems (included in Table 3.5). The experimental values of T_g for P(LA−GA) polymers were in agreement with those cited in the literature [92,97,403]. However the values found in the literature for P(HB−HV) polymers vary considerably and are dependent on the method used for T_g determination. Holmes and colleagues [159] have reported that the homopolymer has a T_g of 10°C when determined by dynamic mechanical testing and was found to decrease with
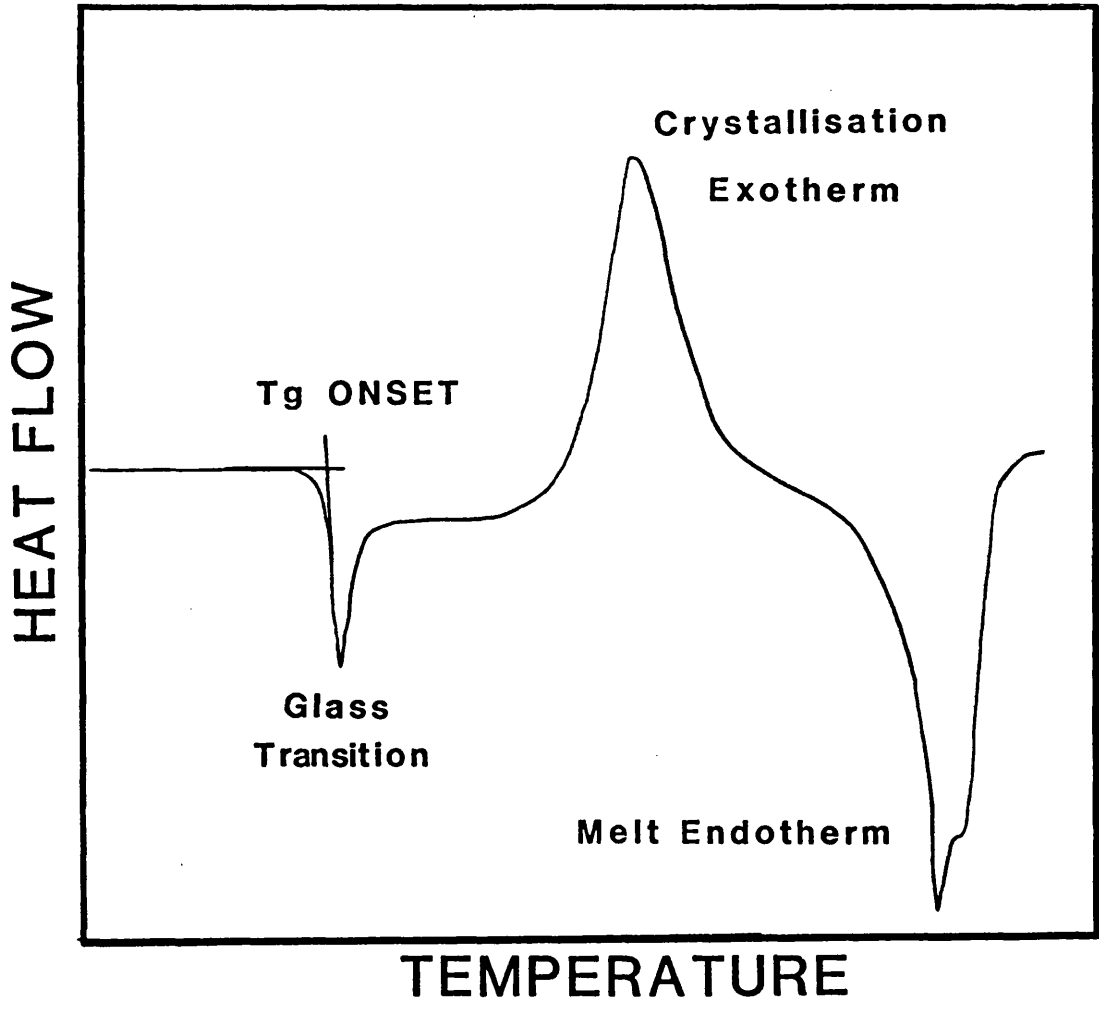
Figure 3.8. A typical DSC trace from which the glass transition onset temperature was calculated.

Increasing HV content to a value of $-6^{\circ}C$ for a copolymer containing 25 mole% HV. Barham *et al* [214] have reported that PHB has a T_g in the range -1 to $+4^{\circ}C$ determined by dilatometry whereas dynamic mechanical analysis by Owen has suggested the homopolymer has a T_g value of $7^{\circ}C$ and a copolymer containing 17 mole% HV has a T_g of $-1^{\circ}C$. The discrepancies are mainly due to the highly crystalline nature of P(HB-HV) biopolymers which makes detection of T_g difficult and imprecise. For the same reason the T_g of polyethylene is a matter of some dispute [392] and values have been quoted between $140^{\circ}K$ and $270^{\circ}K$ $(-133$ to $-3^{\circ}C)$.

The relatively low T_g of the homopolymer, PHB, is due mainly to the flexibility of the polymer backbone allowing easy rotation about the main bonds. Structural considerations suggest that the T_g for P(HB-HV) copolymers should progressively decrease with increasing HV content as is confirmed by the findings of Holmes and colleagues [159]. However, this was not found to be the case in this study but the results may have been complicated by differences in the molecular weights of the copolymers used. The T_g of polymers is found to increase with increasing molecular weight and the behaviour has been approximated by Young [392] to an equation of the form

$$T'_g = T_g + K/M$$

where T'_g is the value of T_g for a polymer sample of infinite molar mass and K is a constant dependent on polymer free volume.

As discussed earlier the T_m of P(HB-HV) polymers is also dependent on similar structural factors as those outlined for T_g because both T_m and T_g are controlled principally by main-chain stiffness. It is not surprising, therefore, that a correlation is found between T_m and T_g for polymers undergoing both transitions. Boyer [397] found that when expressed in Kelvins the value of T_g is between 0.5 and 0.8 T_m. The T_g values of P(HB-HV) polymers as shown in Table 3.5 suggest that the correlation approximates to about 0.6 T_m and falls within the limits predicted by Boyer [397].

The possibility of predicting polymer properties from their chemical structure has been

investigated [398] and reviewed by Askadskii [399]. He illustrates how a number of polymer properties including T_m and T_g can be predicted from information on Van der Waals' volumes of atoms and suggests that this makes synthesis of polymers with accurate predefined properties a practical reality [399].

The onset of the T_g marks a significant change in the physical properties of the polymer. A glassy polymer will lose its stiffness and have a tendency to flow above T_g. The glass transition temperatures of the P(HB – HV) copolymers are close to ambient and suggest that at body temperature the biopolymers will certainly be above their T_g values and in the rubbery state. The added chain mobility at the higher temperatures is likely to modify polymer properties from those at ambient. It is recommended, therefore, that whenever possible polymer properties should be evaluated at the temperature of use. The changes in polymer behaviour above T_g may greatly influence polymer permeability and drug release.

3.4.3 Crystallization exotherms and the influence of drugs.

When a melt – quenched amorphous sample of a crystalline polymer is re – heated to melt in a DSC it first undergoes a glass transition followed by a crystallization exotherm and finally an endotherm for the remelting of crystals. A representative DSC thermogram showing such transitions for PHB43K is given in Figure 3.9. The crystallization exotherm for PHB43K occurred at 63°C at a heating rate of 20K/min. Studies with PHB 380K showed that peak exotherm temperature was dependent on the DSC heating rate (39,43 and 51°C at programmed heating rates of 5, 10 and 20 $Kmin^{-1}$ respectively) [400]. Typical values for the heat of crystallization of PHB on heating melt – quenched samples was in the range $^-48 - ^-62$ J/g (53 – 68% of the heat of fusion). Typically for P(HB – HV) copolymers, the heat of crystallization was also approximately 50 – 70% of the respective heat of fusion. Using the assumption that crystallization is essentially the reverse of melting then the value for the heat of crystallization, for each polymer, should be the same as the value for its heat of fusion providing all the crystallization of the sample

Figure 3.9. A DSC trace for PHB43K showing the glass transition, crystallization exotherm and the melt endotherm.
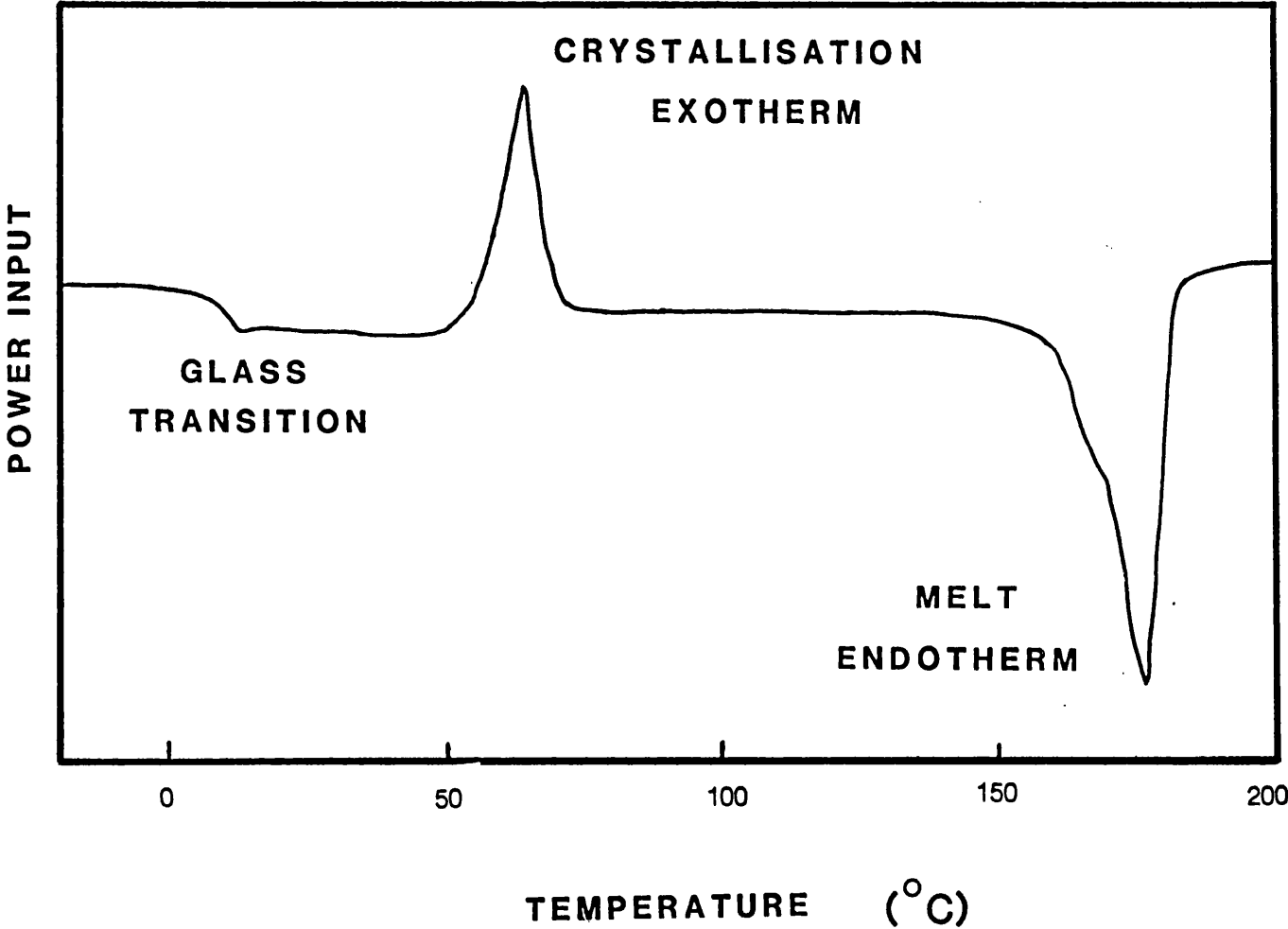
occurs within the DSC heating programme. However, the heat of fusion for PHB and P(HB–HV) copolymers was generally greater than the heat of crystallization suggesting that some order existed within the amorphous PHB and P(HB–HV) polymers prior to the DSC heating cycle. This may have been as a result of rapid crystallization of polymers outside of the DSC cycle or due to intrinsic local order within the amorphous polymer [396].

Recrystallization of polymer also occurred when PHB was cooled from the melt at a temperature below the minimum rate for obtaining an amorphous state. The crystallization exotherm for PHB43K cooled at 20K/min occurred at peak temperature of 82 ± 1°C. Typical values for the heat of crystallization of PHB43K were -50 ± 6 J/g and a representative DSC thermogram on cooling is shown in Figure 3.10. The crystallization exotherm temperatures were less reproducible than the endothermic melting temperatures for P(HB–HV) polymers. The major causes for variation in results were thought to be impurities such as dust particles which can induce surface nucleation in polymer samples. They can act as nucleating agents and at a given temperature, initiate crystallization at a rate faster than would be seen for a pure sample .

The inclusion of drugs in polymers may act in a similar way to impurities such as dust. The influence of a number of model drugs on the glass transition, crystallization exotherm and melting temperature is shown in Table 3.6.

Table 3.6. The effect of model drugs on the DSC transitions of PHB43K at programmed heating rate of 20K/min.

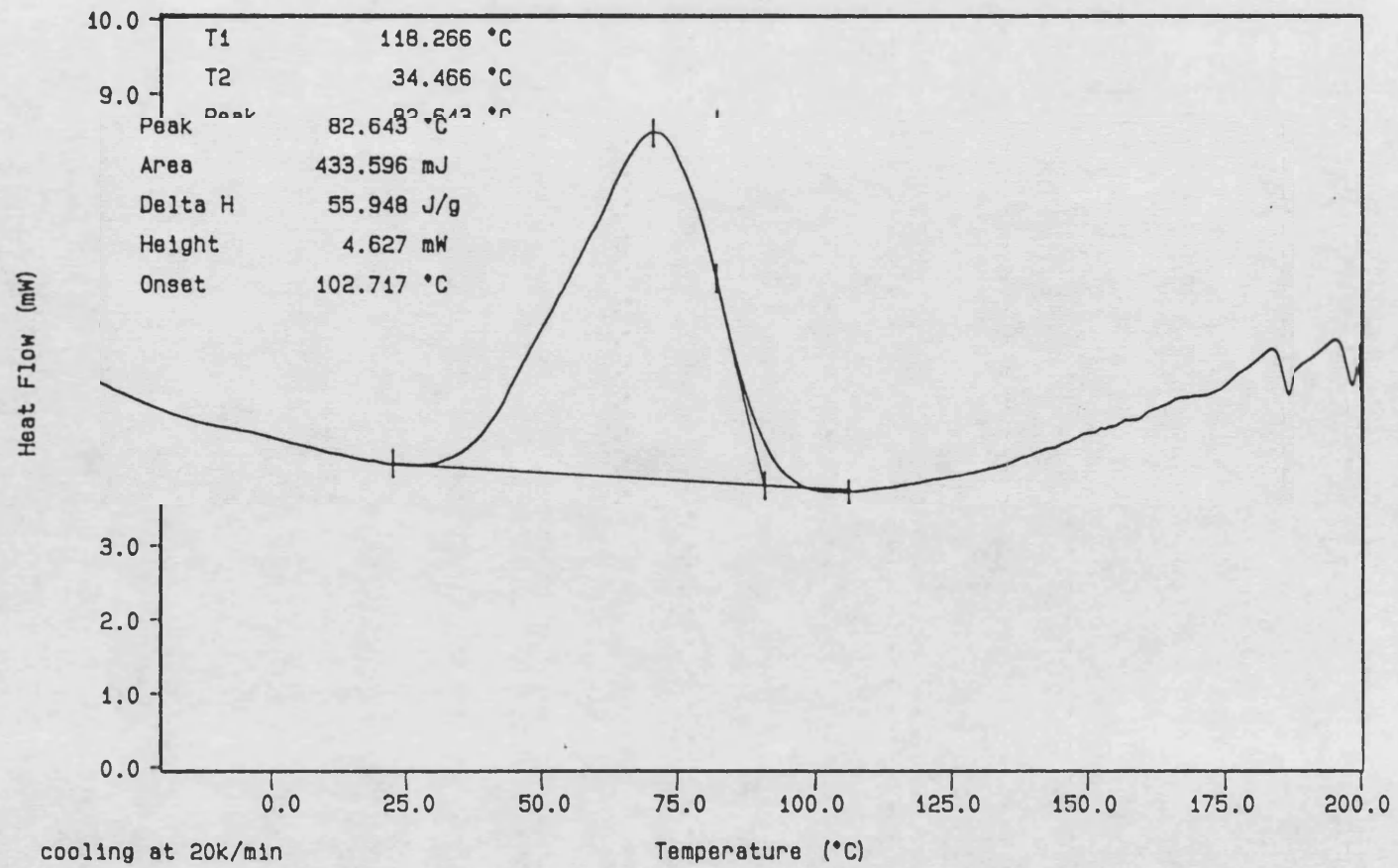| Model Drug Concentration (%w/w)	Temperature (°C)		
	Tg (onset)	crystallization (peak)	melting (peak)
PHB43K alone	6.5	63.4	176.6
+ 1% Methyl Red	4.3	53.9	173.4
+ 10% Methyl Red	4.5	76.6	167.7
+ 1% quinine	2.0	53.9	163.2
+ 1% sodium fluorescein	1.4	61.1	155.5

Figure 3.10. The crystallization of PHB43K during a cooling DSC run.

116

The inclusion of all drugs lowered the peak T_m of PHB. However, the magnitude of the effect was dependent on the concentration (10% Methyl Red depressed T_m by a greater amount than 1% of the same drug) and the nature of the drug (Sodium Fluorescein had a greater effect than quinine which had a greater effect than Methyl Red in depressing T_m of PHB43K). The presence of drugs in PHB lowered the T_g in the same way as T_m but the effect on the crystallization exotherm was variable. The effect of drugs at low concentration (1%) was to reduce the peak crystallization temperature but Methyl Red at higher concentrations (10%) actually increased this value. This may have been due to the higher concentration of drug in polymer reducing thermal conductivity in the sample and thereby introducing a temperature lag.

3.4.4 Thermal stability of P(HB – HV) biopolymers by TGA.

The classic way of assessing thermal stability of polymers is by thermal gravimetric analysis (TGA). This technique detects mass losses within a sample as volatile decomposition products are evolved. The degradation process is characterised by the onset degradation temperature (T_d) [399]. This is determined from the intersect of tangents drawn on the degradation profile as shown for PHB380K in Figure 3.11. For PHB 380K, T_d was approx. 310°C and 100% mass loss was complete within a temperature range of about 50°C at a heating rate of 20K/min. Results from TGA were found to very reproducible and typically, were within $\pm$ 2°C.

The decomposition of PHB can also be monitored by DSC. Programmed heating of PHB380K up to 500°C is represented in Figure 3.12. The peak at around 300°C following the endotherm of melting (175°C) was associated with the evolution of volatile degradation products from PHB. The peak temperature associated with degradation of PHB in the DSC was in agreement with the corresponding T_d values from TGA.

The reaction mechanism for the thermal degradation of PHB has been studied by Grassie *et al* [273]. The authors found that following the initial esterification of the terminal hydroxyl groups in PHB the main reaction involved random chain scission at the labile
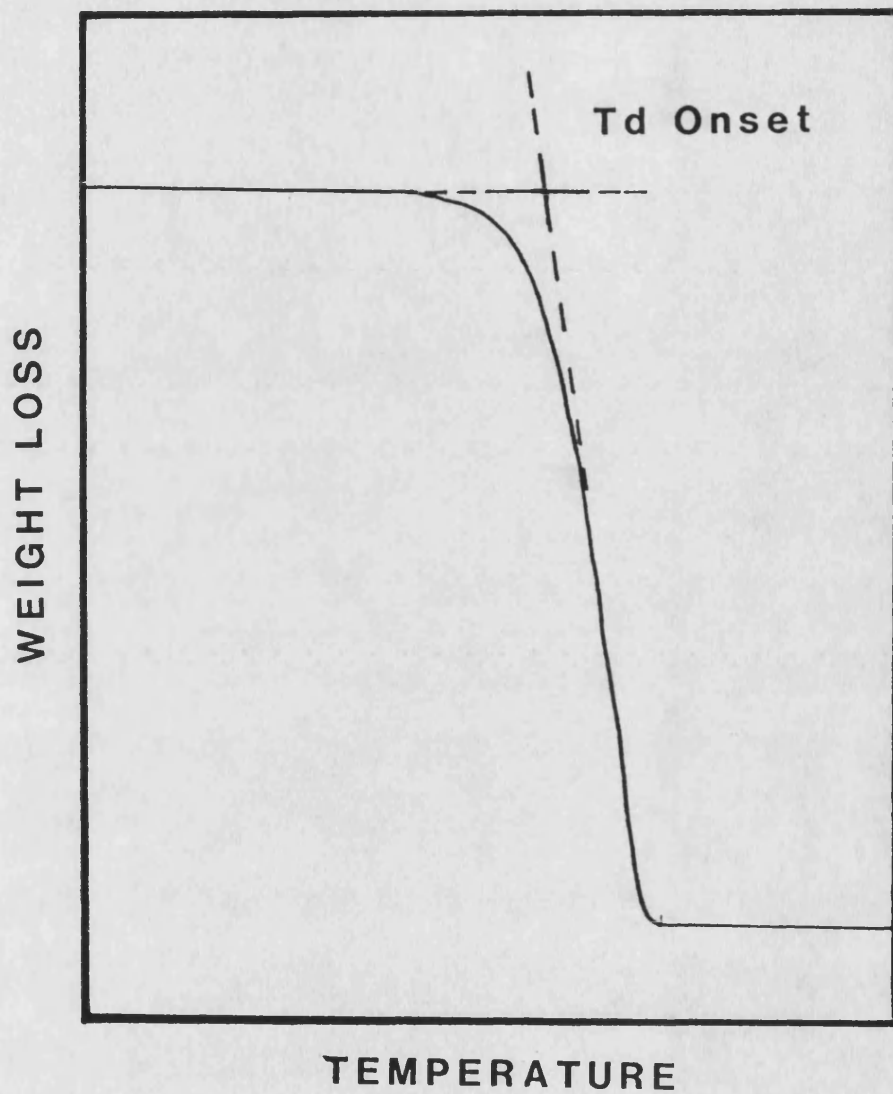
Figure 3.11. A TGA trace showing calculation of the degradation onset temperature.
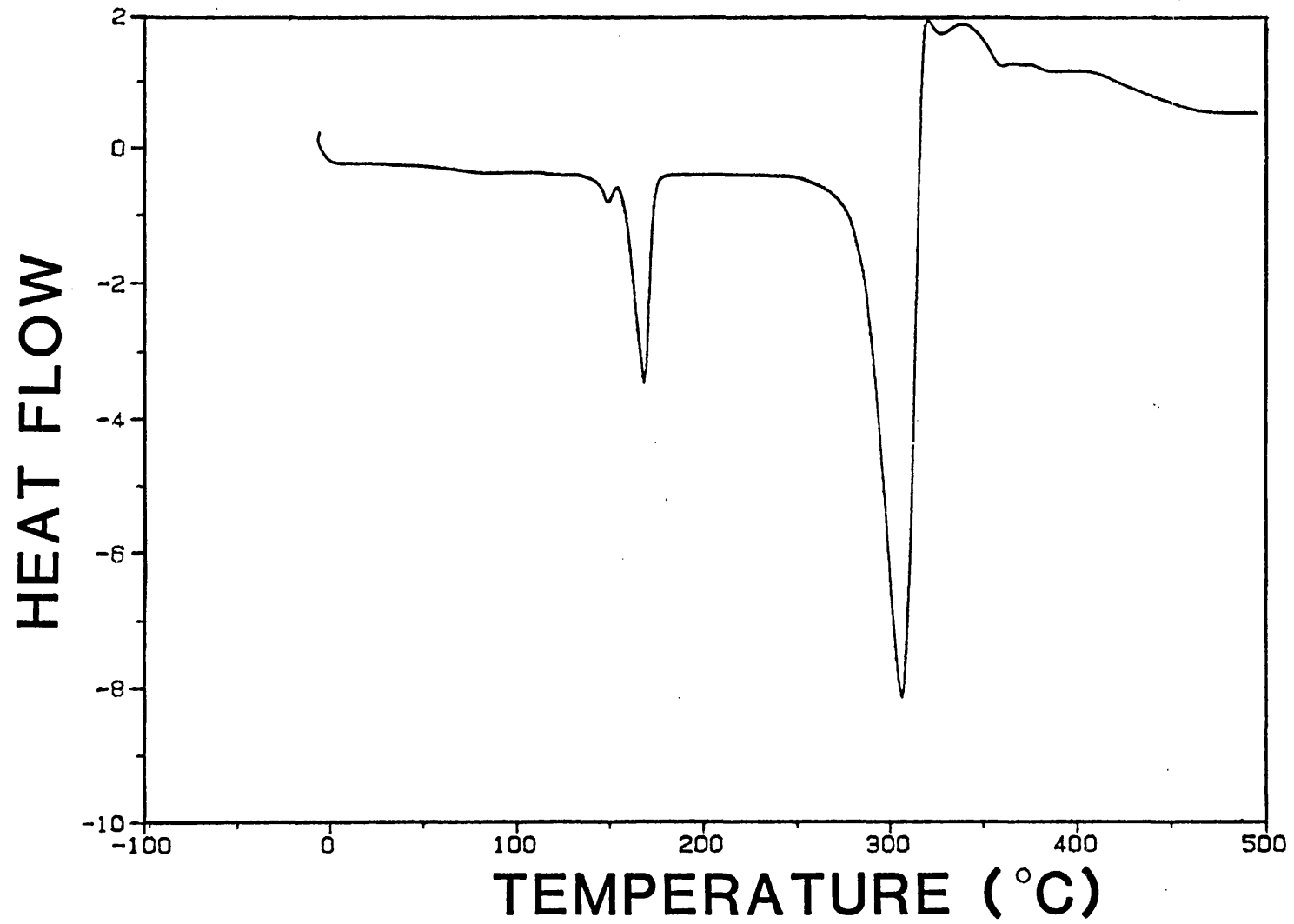
Figure 3.12. A DSC trace showing thermal degradation of PHB380K.

ester linkages. Grassie *et al* [272] found that the major volatile products for PHB were, in decreasing amounts, the dimer, crotonic acid, trimer, tetramer and isocrotonic acid. In addition, small amounts of carbon dioxide, propene, ketene, acetaldehyde and β-butyrolactone were also reported to be evolved but the authors showed that these were secondary products formed by further decomposition of the primary products.

Although a single stage mass loss of PHB was registered over a temperature range of approximately 300-350°C, thermal degradation of the polymer to non-volatile breakdown products may have occurred at lower temperatures without corresponding mass loss. Indeed, Grassie *et al* [401] have reported that although no significant weight loss occurs up to 190°C, molecular weight losses indicating degradation in PHB do occur even in this temperature range. The magnitude by which molecular weight changed at a particular temperature was dependant on the length of time the material was held at that temperature [401].

3.4.4.1 Effect of heating rate

The degradation profile and the T_d are dependent on the heating rate used in the TGA apparatus. Figure 3.13 shows that T_d for PHB43K increased with increasing heating rate. Increasing the heating rate from 5 to 20K/min resulted in a 20°C rise in the T_d. The explanation for this effect is the same as in DSC, where it was less pronounced, and is related to the residence time of the sample at a given temperature being shorter as the heating rate is increased.

3.4.4.2 Effect of polymer molecular weight

Figure 3.14 shows TGA curves for different molecular weights of PHB. The Td increased from PHB 140K ($T_d = 298$°C) to PHB380K ($T_d = 309$°C). However the value of 308°C for the T_d of PHB43K was not significantly different from that of PHB380K. The explanation for the apparently high value of PHB43K was not clear.
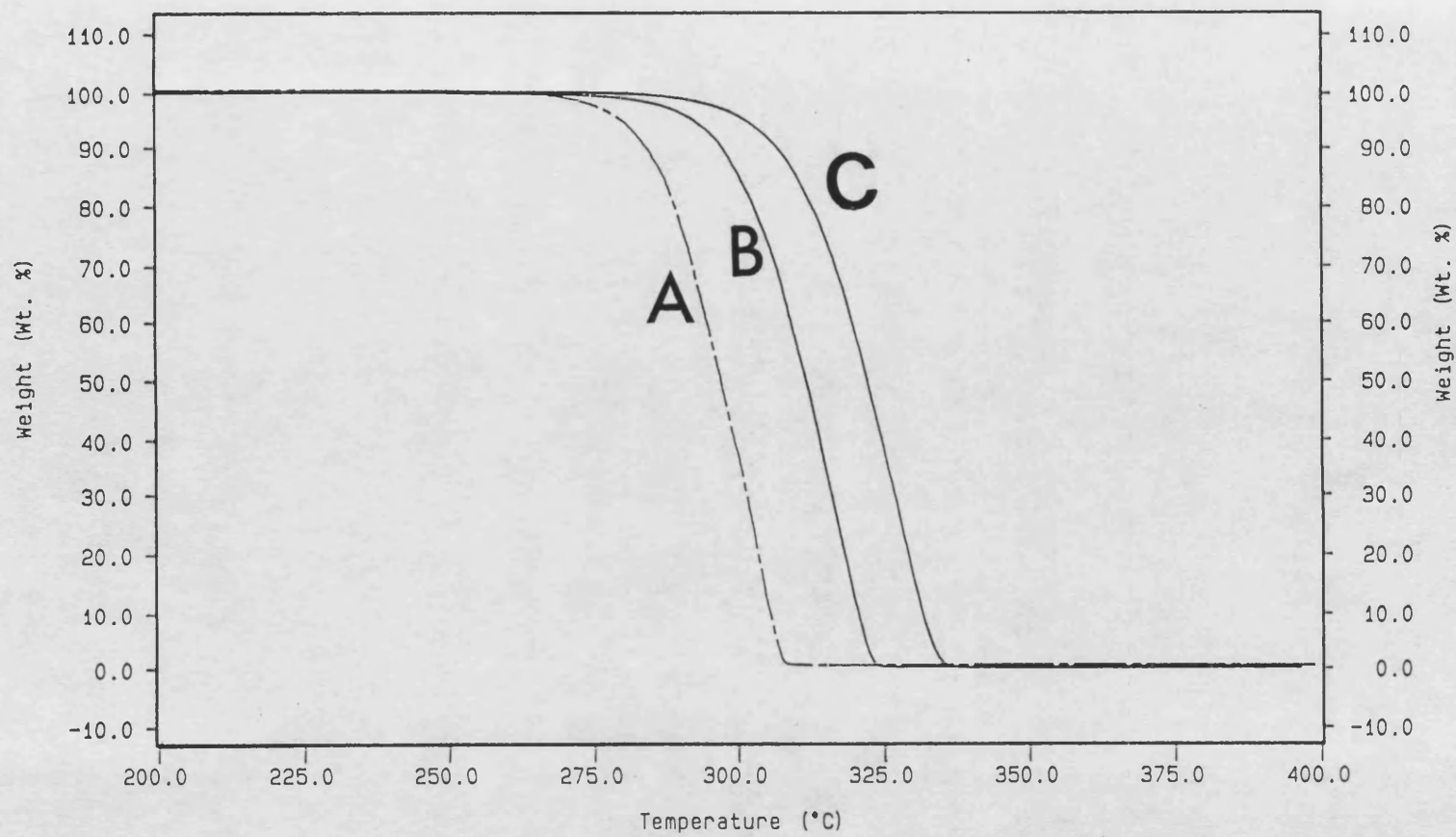
Figure 3.13. The effect of TGA heating rate on the degradation onset temperature for PHB43K (A = 5 K/min, B = 10 K/min and C = 20 K/min).
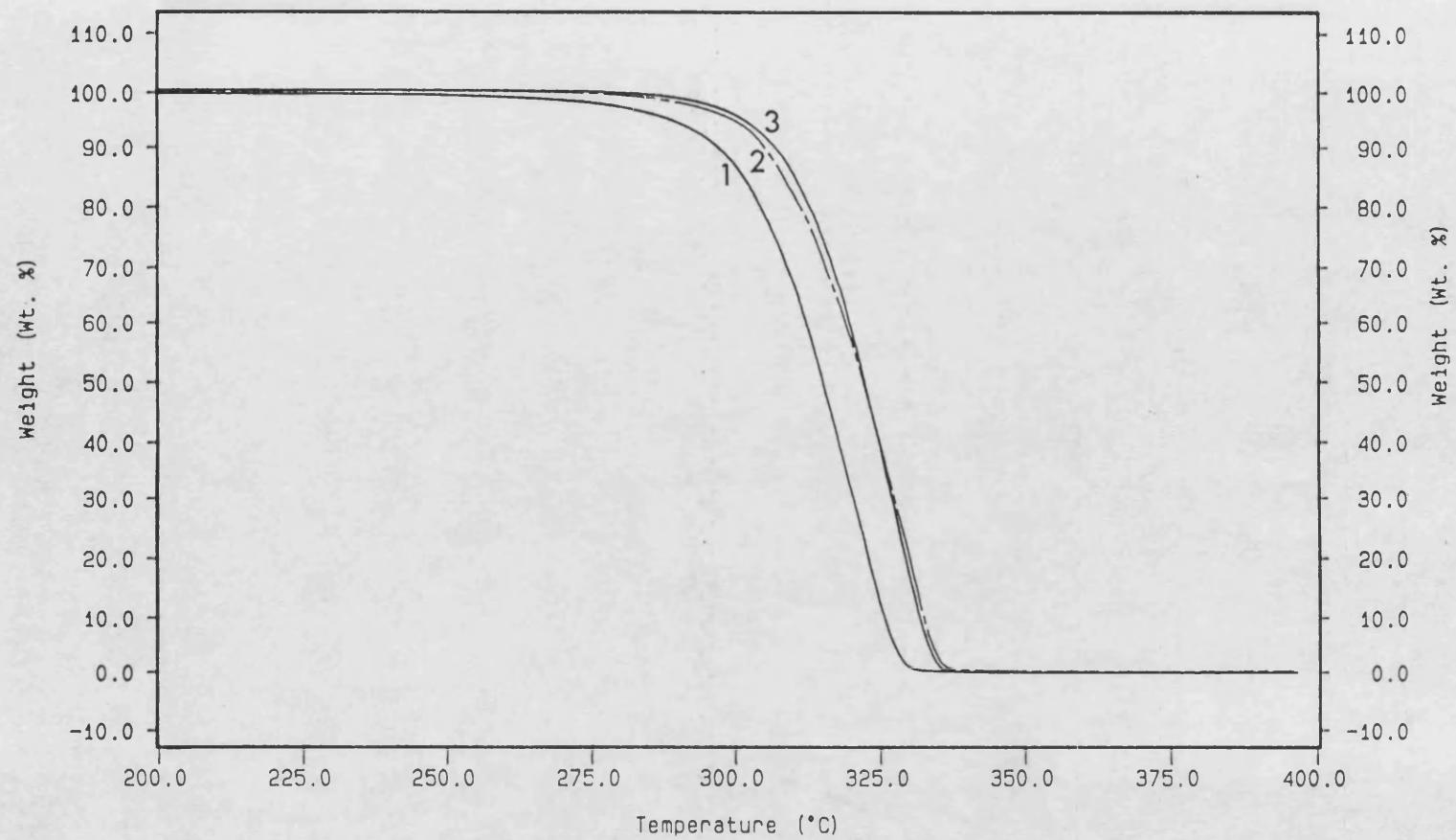
Figure 3.14. TGA traces showing the effect of polymer molecular
on the degradation onset temperature (1 = PHB140K, 2 = PHB43K and
3 = PHB380K).

3.4.4.3 Effect of copolymer composition.

The T_d for P(HB–HV) copolymers is given in Table 3.7. The results showed that for up to 12 mole% HV the T_d decreased with increasing HV content. Figure 3.15 shows the TGA curve for PHV12 compared to that of PHB43K. However, the T_d values for higher HV content copolymers were similar to those found for PHB.

Table 3.7 The effect of P(HB–HV) copolymer composition on T_d values.

Polymer	Td (oC)
PHB43	308.6
PHB380K	309.3
PHV6	298.3
PHV12	286.6
PHV20	308.9
PHV24	310.7

The DSC thermograms for the degradation of P(HB–HV) copolymers were similar to those obtained for the homopolymer. Figure 3.16 shows a representative DSC thermogram for PHV20. It was noted that although PHV20 had a much lower melting temperature than PHB no such difference was found in either T_d determined by TGA or the peak temperature of the DSC degradation endotherm. This may be due to their similar degrees of crystallinity [210–211].

Although the T_d was around 300°C for all the P(HB–HV) polymers studied, the progressive fall in their melting points (chapter 2) suggested that the window for safe thermal processing increased with increasing HV content. Materials which do not degrade until temperatures are very much above the melting point are preferable for manufacture by melt–processing. The copolymers therefore offer potential advantages of greater stability during melt processing when compared with the homopolymer.
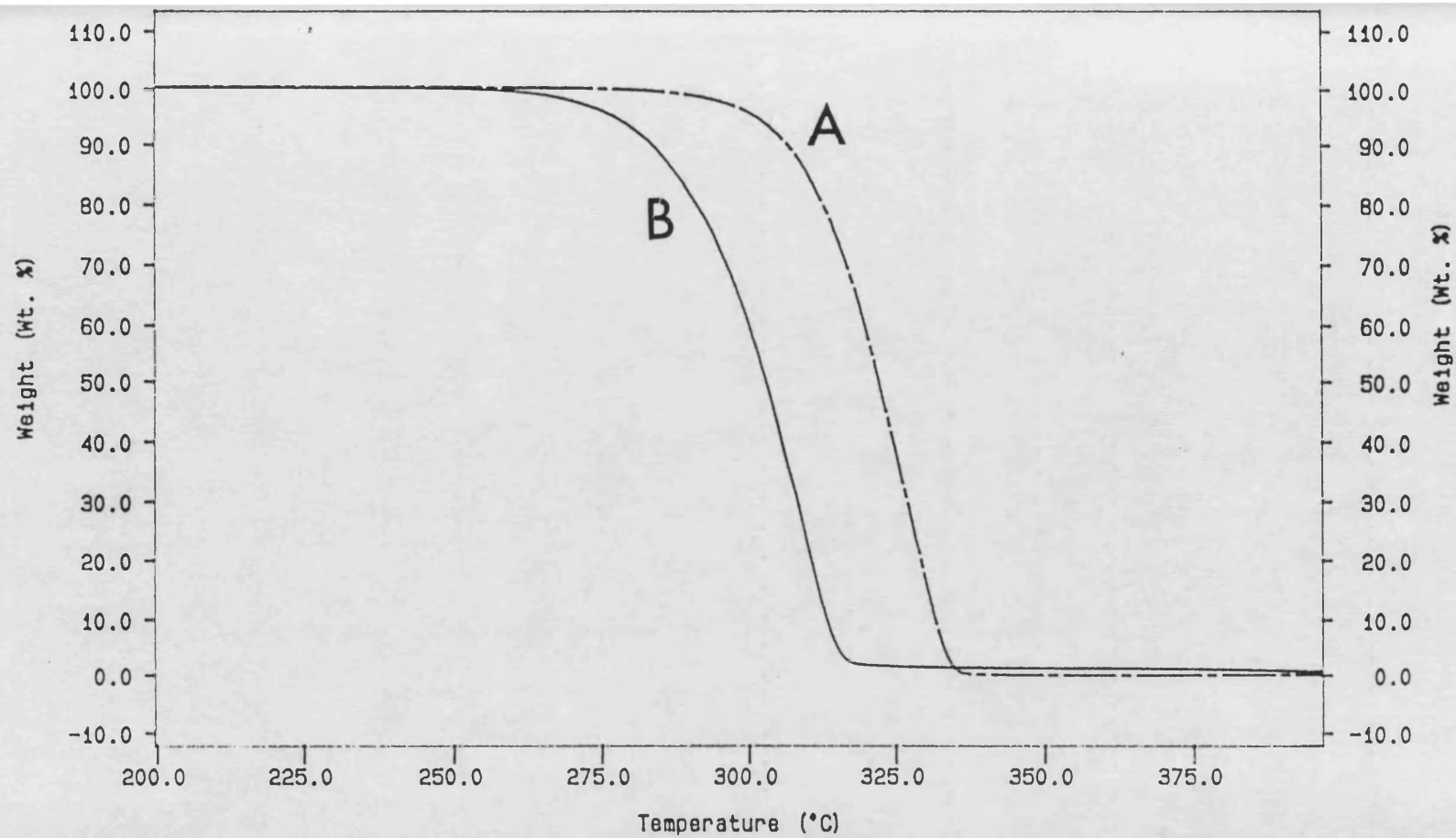
Figure 3.15. A comparison of the TGA traces for PHB43K (A) and PHV12 (B).
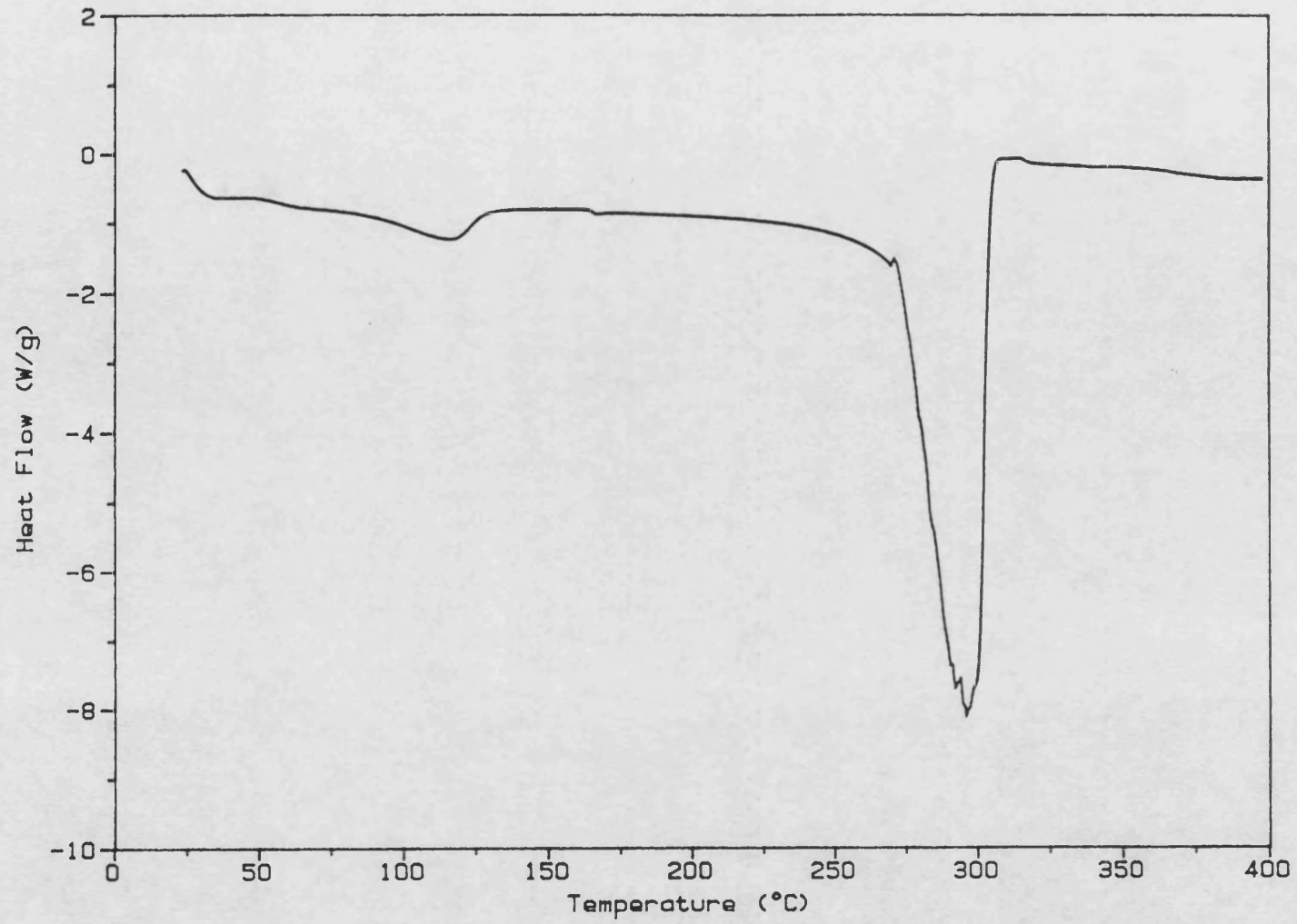
Figure 3.16. A DSC trace showing thermal degradation of PHV20.

3.4.4.4 Comparison with poly – L – lactide (PLA).

Figure 3.17 shows TGA degradation profiles for PLA and PHB. The degradation profile of PLA consisted of a single stage mass loss (as for PHB) and this was consistent with the findings of Gupta and Deshmukh [402] and Gilding and Reed [97]. Lactide has been reported to be the major decomposition product of PLA [97].

The value of T_d for PLA (303°C) was lower than PHB (309°C) but the major difference in the TGA degradation profile of the polymers was in the range over which mass loss occurred. Complete mass loss occurred for PHB within a range of approximately 50°C whereas for PLA, mass loss occurred over a wider temperature range of approximately 100°C. This suggested that the rate of thermal degradation of PHB (and P(HB – HV) copolymers) was much faster than that of PLA. Gupta and Deshmukh [402] have proposed that, under isothermal conditions, PLA degradation kinetics follow the Avrami – Erofeev equation for solid gas equilibria:

$$[-\ln(1-\alpha)]^{1/n} \; = \; kt$$

where α is the fractional weight loss, n is an exponent and k is the rate constant. The authors report that the Avrami – Erofeev equation kinetics suggest that the decomposition of PLA is due to nucleation and growth of decomposition sites [402].

The above results suggest that PHB has a similar temperature range for melt – processing as PLA. Both polymers melt and degrade at similar temperatures but once degradation is initiated or nucleated then degradation appears to more rapid in PLA than in PHB. This may be advantageous in melt processing of PHB but needs to be further investigated at temperatures close to the melt which are more likely to be used during thermal processing.
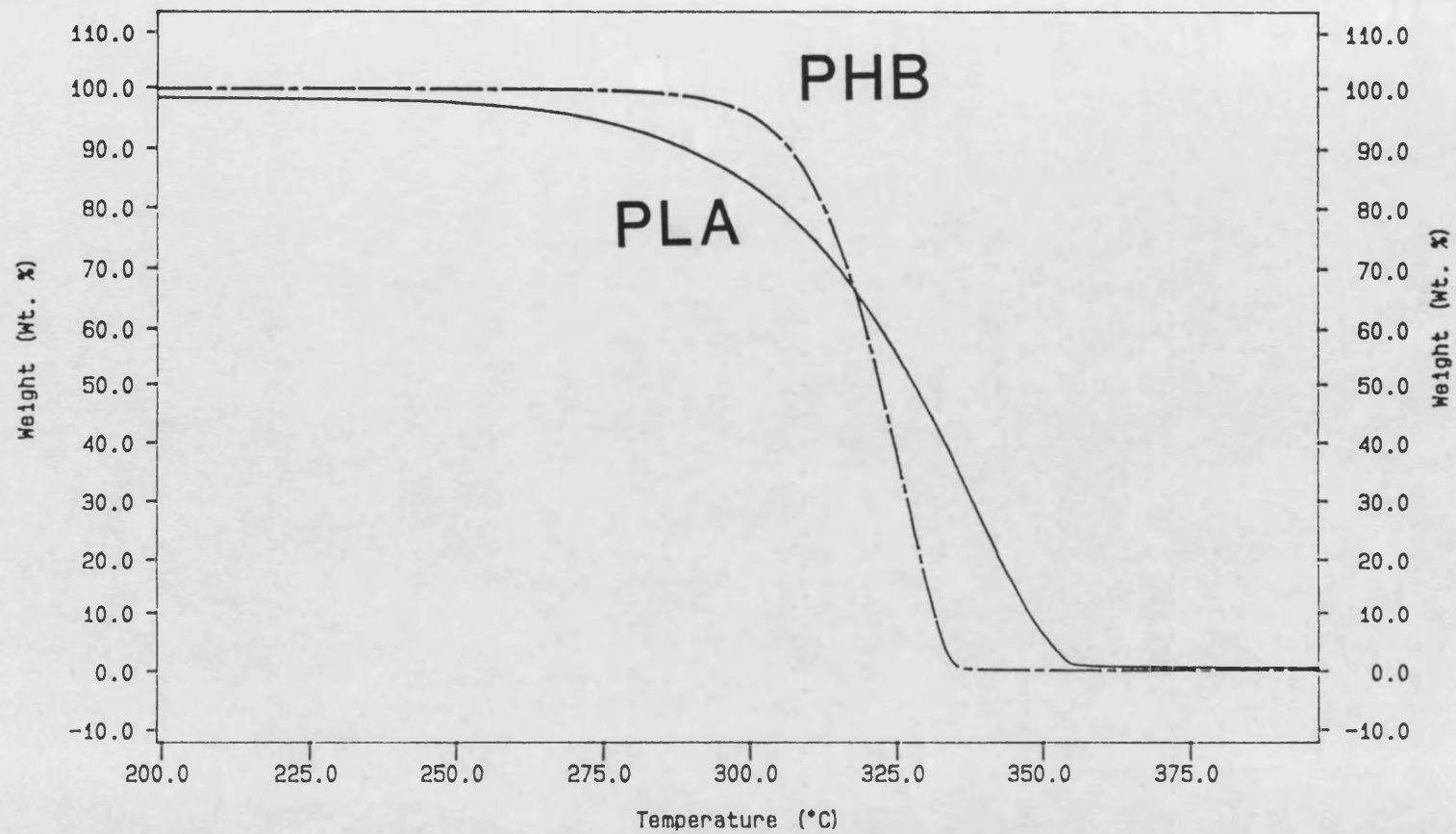
Figure 3.17. TGA traces comparing thermal degradation behaviour of PHB380K and PLA.

3.5 CONCLUSIONS

Results from both TGA and DSC were influenced by the programmed heating rates of the instruments.

The peak melting temperature was dependent on P(HB–HV) copolymer composition.

The glass transition temperatures for P(HB–HV) polymers were variable over the range −5 to 20°C and no correlation was established between T_g and HV content. The T_g values of P(HB–HV) polymers studied were all lower than body temperature.

Thermal degradation of P(HB–HV) polymers occurred over a narrow range (approximately 50°C) from around 300°C. The values for T_d were influenced by molecular weight and HV content but the relationships were not linear. PLA also degraded at around 300°C but over a wider temperature range than PHB.

CHAPTER 4

AGEING PROPERTIES

4.1 INTRODUCTION

Physical ageing of polymers refers to changes in their physical properties with time following manufacture. Ageing has been reported to occur in a number of materials and significant changes in both their physical and mechanical properties have been reported on storage [404–407].

Physical ageing has been widely studied by Struik [404–406] and in recent years ageing has been reported to occur in both amorphous and crystalline polymers [405]. Ageing has been demonstrated in a number of commercial semicrystalline polymers, including polypropylene and high density polyethylene, at temperatures above and below their glass transitions [405].

Physical ageing is a phenomenon characteristic of the glassy state because of its non–equilibrium character. In the glassy state (below T_g for semicrystalline polymers) residual short range mobility of molecules exists which produces molecular rearrangements that drive the thermodynamic variables closer to their equilibrium values. With increasing ageing time the free–volume, for instance, decreases and all physico–mechanical properties dependent on this variable will also change with time. The changes are faster at short rather than long ageing times because ageing is a self–delaying process in which the state of equilibrium (zero mobility) is reached asymptotically [269,404–405].

At temperatures above T_g in semicrystalline polymers, Struik [404–405] has shown that part of the amorphous phase remains glassy and consequently these polymers continue to exhibit ageing at temperatures above T_g, a behaviour not normally observed in purely amorphous polymers. Struik [404–405] also proposes that in semicrystalline polymers the crystalline phase reduces segmental motion of amorphous regions close to the crystal surface but the bulk amorphous regions remain undisturbed. Therefore, the amorphous phase no longer has a single T_g but a T_g–distribution. This may therefore explain the variations in the T_g values for P(HB–HV) and other polymers reported in chapter 3 and

the dependence of T_g on ageing and thermal history of the material.

The change in physical properties of polymers with time following fabrication or ageing will be an important consideration in determining the potential applications of such materials. Furthermore, knowledge of the behaviour of polymers on storage at specified conditions following manufacture (from solution or melt) will be important in determining methods of accelerating ageing and thereby producing devices with stable or at least known properties. Indeed, recent work by Kandil et al [407] on the effects of ageing on the mechanical properties of dental polymeric composite materials enabled the authors to develop a simple equation to predict the strength of composites when aged over a limited range.

Ageing properties of research materials are not always fully investigated and can often become an additional but unknown variable. A clear example of where this can occur is in the use of mechanical properties to monitor in vitro or in vivo degradation of polymeric materials. In such cases if the polymeric material is not allowed to age sufficiently (i.e. to a storage time when properties reach equilibrium) then any changes detected in the mechanical properties will not be solely due to the degradation but also a function of ageing. Clearly the ageing properties of polymers need to investigated if erroneous interpretations of results are to be avoided.

4.1.1 AIMS AND OBJECTIVES

1. To investigate the effect of physical ageing on the mechanical and crystalline properties of P(HB – HV) polymers.

4.2 MATERIALS

P(HB – HV) copolymer containing 16 mole% HV (PHV16; Mw = 41K) was purchased from Marlborough Biopolymers Ltd, UK.

All other materials used were identical to those given in chapters 2 and 3.

131

4.3 METHODS

4.3.1 Preparation of films

P(HB–HV) polymer films (30–50um) were prepared by solvent casting as in chapter 2. Polymer films cast from chloroform were initially dried under ambient conditions for 1 hour in a level drying cabinet. Films were removed from the glass after this period and then stored either at 25°C over silica gel or at 65°C in a vacuum oven before analysis at timed intervals. In all cases, only films within a narrow thickness range (40 ±10um) were used such that thickness of films could effectively be eliminated as a variable in the interpretation of results.

4.3.2 Mechanical testing

Mechanical properties of polymer films were determined using static tensile tests (ASTM 882–80a) as described in chapter 2.

4.3.3 Differential Scanning Calorimetry (DSC)

Bulk crystallinities of ageing films were monitored by DSC as described in chapter 3. A programmed heating rate of 20K/min was used unless otherwise stated.

4.3.4 X–ray diffraction studies

Polymer films (30–50um) were cast onto a glass slide and periodically analysed by X–ray diffraction (CuK–alpha source) as a function of time over a diffraction angle of 4–30°. A Philips PW 1820/00 computer controlled vertical goniometer with a Philips PW1710 diffractometer control was used. Intensity measurements were made using a Xenon proportional counter (Philips PW1711/10) with graphite monochromator and automatic divergence slit assembly. For the crystallinity index, the instrument was programmed to provide a step scan acquisition of data. Intensity data were acquired by scanning for 10s at 0.2° steps in diffraction angle over the range 10–30°. Data acquisition was carried out using the COMSTAR software package run on a BBC Master Microprocessor interfaced with the X–ray diffractometer.

4.4 RESULTS AND DISCUSSION

4.4.1 Mechanical Properties

In the course of the earlier investigation on the mechanical properties of P(HB – HV) polymers (chapter 2), it was found that mechanical properties of films varied with time following solution casting. In the present chapter, mechanical properties of P(HB – HV) polymer films were monitored at 25°C over a 42 day period following casting from chloroform solution.

The mechanical properties of all P(HB – HV) biopolymer films stored at 25°C appeared to change at first but stabilised to equilibrium values within 14 days. The Elastic Modulus (EM), a measure of polymer rigidity, changed rapidly at first before reaching equilibrium value for all polymers within 3 – 5 days ageing (Figure 4.1). The %Elongation (%E), a measure of polymer ductility, stabilised within a similar period of time (3 – 5 days) for all polymers except PHV12 which reached equilibrium within 14 days (Figure 4.2). The anomalous behaviour of PHV12 may be due to secondary crystallization following reorientation of polymer chains in crystallites or crystal domains.

The equilibrium %E and EM values for P(HB – HV) copolymers were dependent on the copolymer composition. The EM decreased and the %E increased with increasing HV content of copolymers at equilibrium. Their respective values at equilibrium were similar to those reported in chapter 2 (Figures 2.12 and 2.13).

The tensile strength (TS) of ageing P(HB – HV) films (Table 4.1) reached an equilibrium value for all polymers within 166 hours (approximately 7 days). There was some evidence to suggest that time taken to reach stable TS values was a function of HV content. The TS data for PHB380K and PHV12 exhibited large standard deviations and appeared to stabilise within approximately 2 days (46 h) whereas PHV20 and PHV27 stabilised within approximately 5 days (122 h) and 7 days (166 h) respectively. The equilibrium TS values of all polymers were similar to those reported in chapter 2.

Figure 4.1. The effects of ageing at 25°C on the Elastic Modulus
of solvent cast films of P(HB – HV) polyesters (Mean ± S.D; n = 5).

Figure 4.2. The effects of ageing at 25°C on the % Elongation of solvent cast films of P(HB – HV) polyesters (Mean ± S.D; n = 5).

The rapid changes in mechanical properties over the first few days following film casting were thought to be due to primary crystallization during solvent evaporation. Although all the films had dried sufficiently after 1 hour for them to be removed from the glass plate, crystallization was thought not to be complete until the majority of the solvent had evaporated from the polymer film. This was thought to have largely occurred within 3 – 7 days for films aged at 25°C. Small amounts of residual solvent, which may have remained trapped within the film matrix, could contribute to secondary crystallization processes allowing limited chain mobility and reorganization of polymer chains within the formed crystallites. This may have explained the delayed stabilization of %E in PHV12.

Table 4.1. The tensile strength of P(HB – HV) polyesters stored at 25°C as a function of ageing time.

Time (hours)	Tensile Strength (MPa); (Mean ±S.D; n=5).			
	PHB380K	PHV12	PHV20	PHV27
21	19.3 ±4.4	19.2 ±1.1	17.9 ±0.8	12.4 ±0.2
46	23.5 ±2.0	25.6 ±0.4	19.6 ±0.5	13.8 ±0.4
122	21.0 ±7.8	27.5 ±0.8	22.3 ±0.4	14.6 ±0.3
166	22.4 ±4.0	25.8 ±0.9	– – –	15.9 ±0.6
240	20.3 ±1.9	23.8 ±5.1	– – –	– – –
336	20.5 ±5.3	25.1 ±2.1	22.0 ±1.1	16.5 ±0.6

The effect of film storage at a higher temperature (65°C) on the mechanical properties of P(HB – HV) films is shown in Figures 4.3 – 4.5. A temperature of 65°C was chosen because it represents a temperature in excess of the boiling point of chloroform (62°C) and would accelerate solvent evaporation. It was found that mechanical properties had stabilised to equilibrium values within 24 hours. This suggested that ageing effects could be accelerated by controlling the temperature of storage.

4.4.2 Differential Scanning Calorimetry

4.4.2.1 Solvent cast films

Solvent cast films of PHB,PHV12 and PHV 27 stored at 25°C were analysed by DSC at timed

Figure 4.3. The effects of ageing at 65°C on the % Elongation of solvent cast films of P(HB–HV) polyesters (Mean ± S.D; n=5).
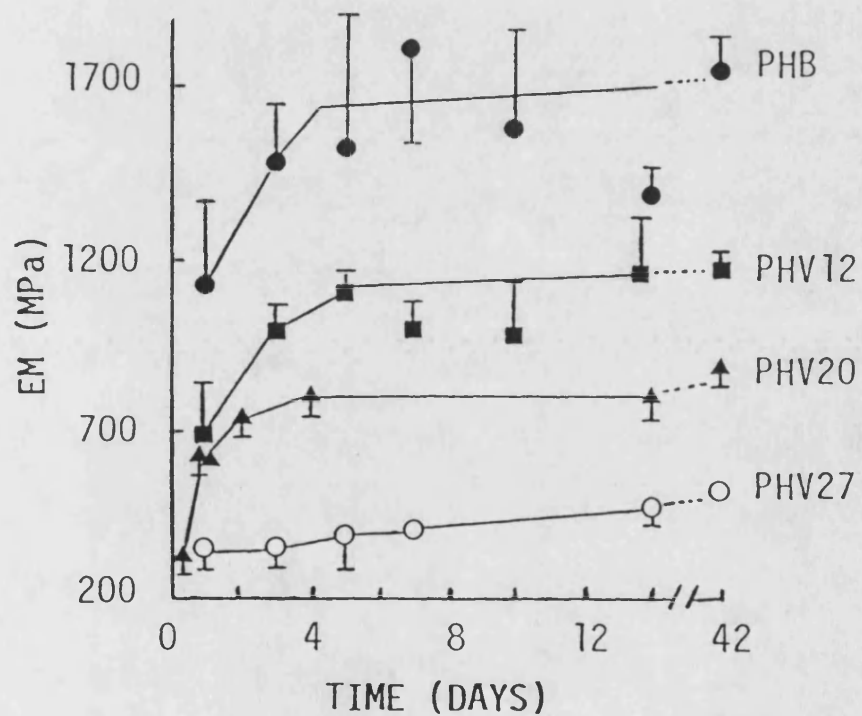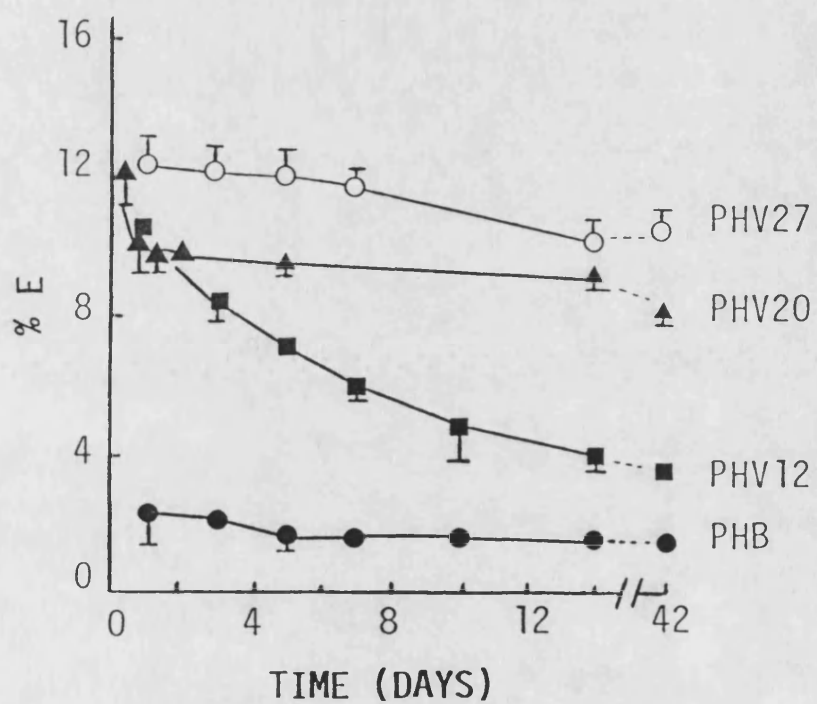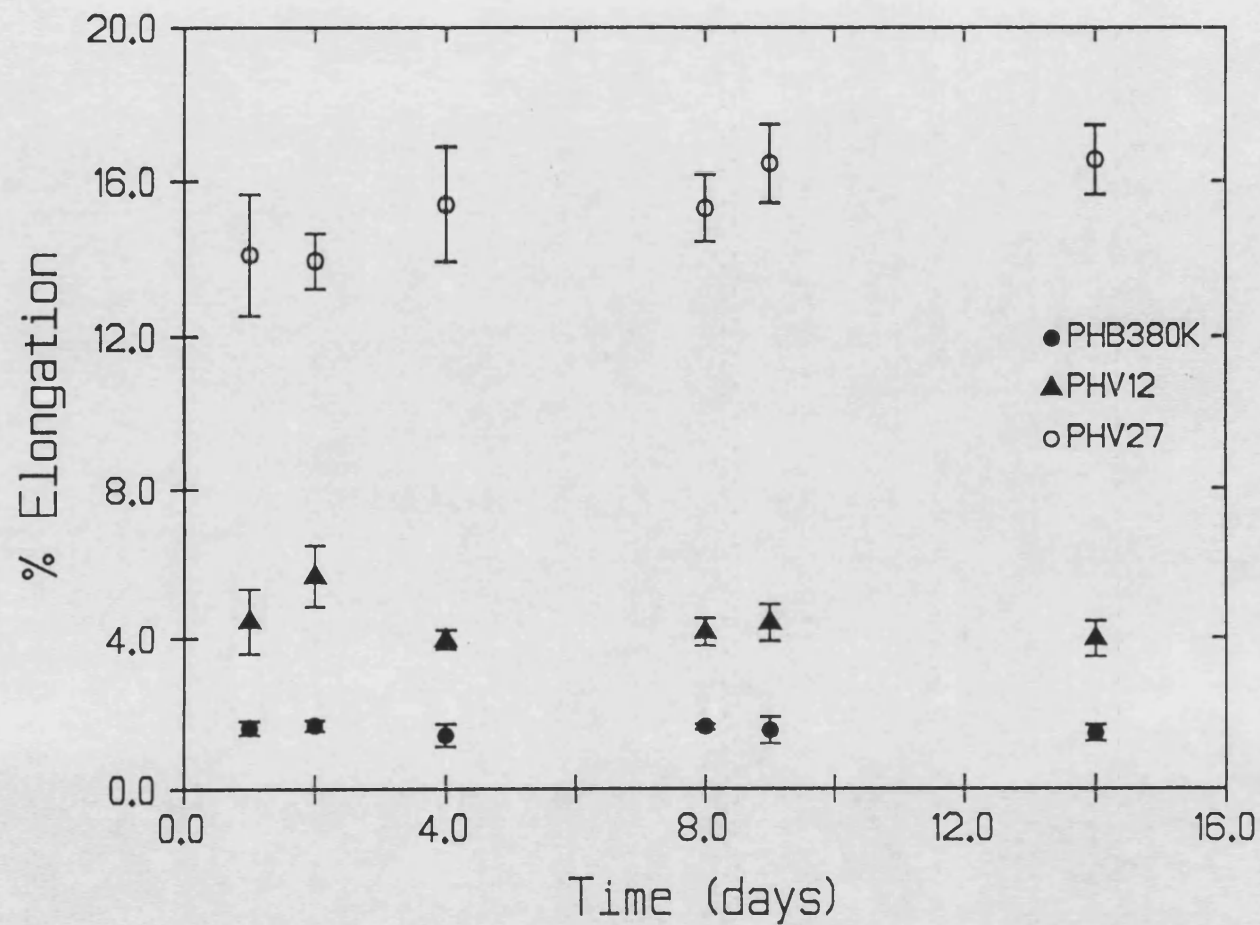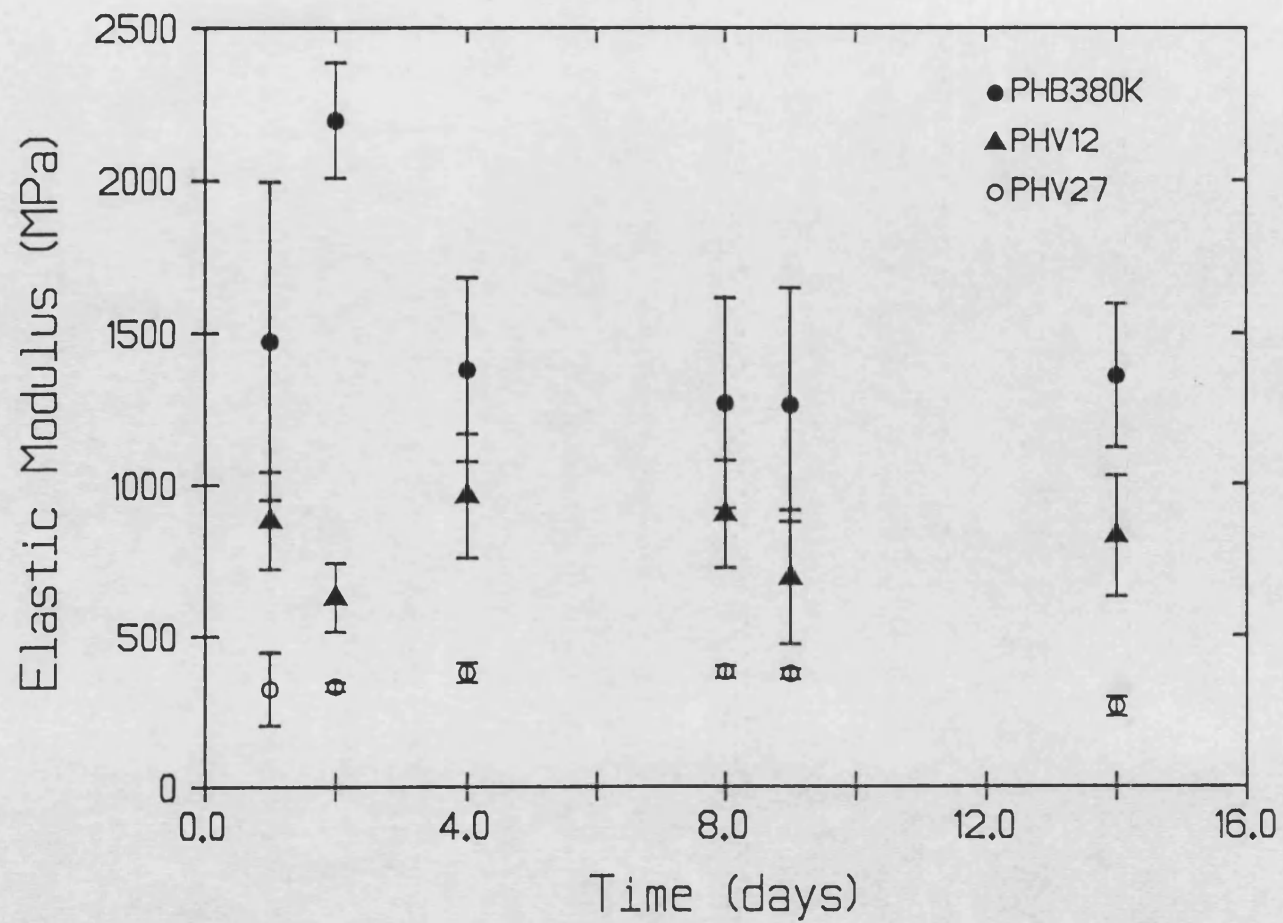
Figure 4.4. The effects of ageing at 65°C on the Elastic Modulus of solvent cast films of P(HB – HV) polyesters (Mean ± S.D; n=5).
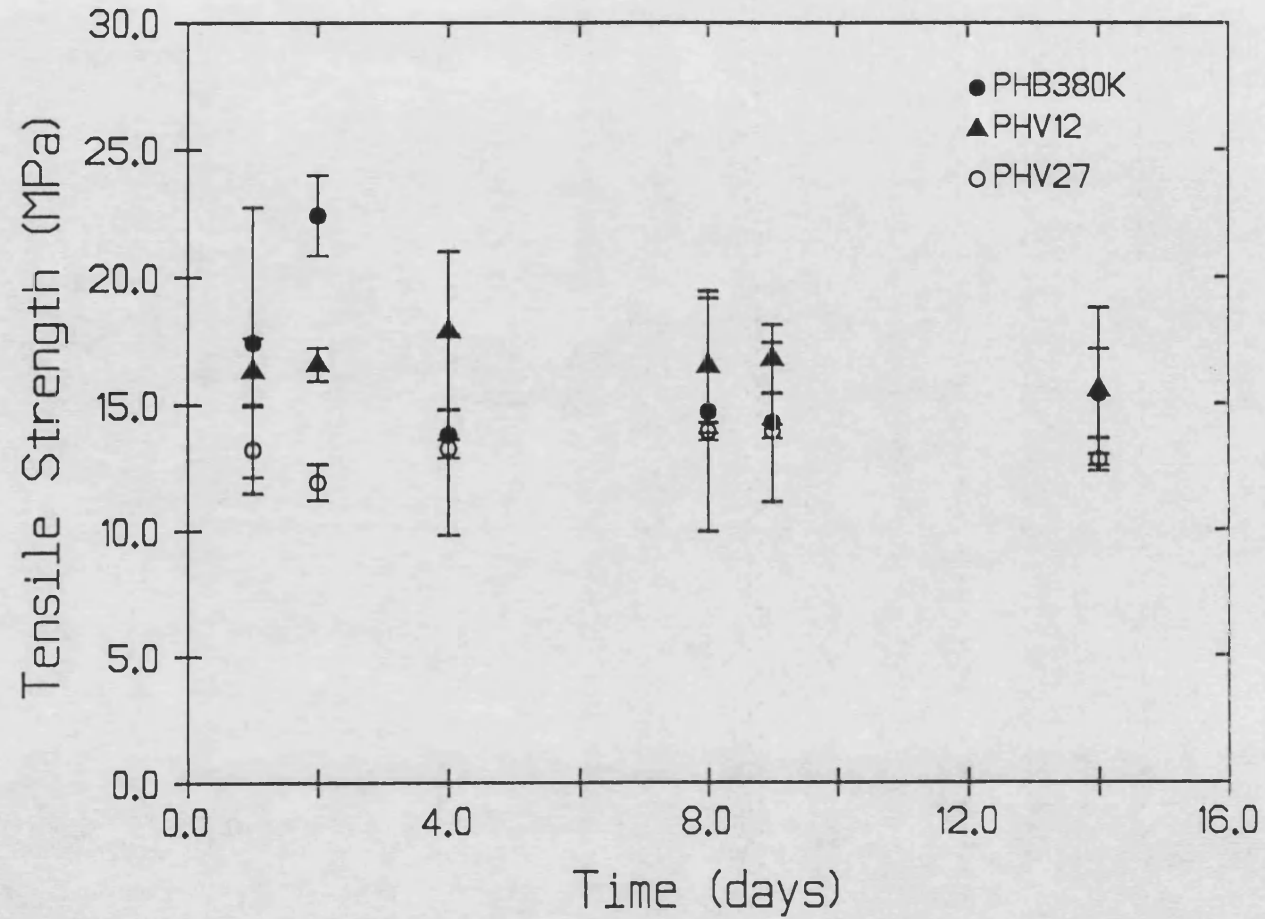
Figure 4.5. The effects of ageing at 65°C on the Tensile Strength of solvent cast films of P(HB – HV) polyesters (Mean ± S.D; n = 5).

intervals.

Figure 4.6 shows the variation in the heat of fusion for PHV27 on ageing. The heat of fusion, a measure of bulk crystallinity, initially increased rapidly with time but reached an equilibrium within 3 – 5 days for PHV27. This suggested that the degree of crystallinity of PHV27 increased to stable values within 3 – 5 days and largely mirrored mechanical property changes at 25°C. However Figure 4.7 shows that the shape of the DSC thermograms for PHV27 stabilised after longer periods of storage. The shape of DSC thermograms can be indicative of crystalline morphology in polymers [389]. The crystalline morphology is concerned with the size and arrangement of polymer crystals [408]. According to Shalaby [393] the shape of the DSC trace is determined in general by two competing processes: melting of the sample according to type, size and perfection of crystallites and reorganization of the sample as it is heated up during the scan. The results for PHV27 suggested that, although bulk crystallinity changed little after approximately 3 – 5 days storage at 25°C, the morphology of polymer crystals continued to change for longer periods of time. DSC thermograms for PHV27 stabilised within 31 days.

It was noted that DSC thermograms of PHV27 exhibited a double melt endotherm and these were seen in all P(HB – HV) copolymers (see chapter 3; Figure 3.5). The phenomenon of multiple melting endotherms in polymers is complex and attempts to explain their occurrence have been based on many hypotheses including variable crystallite sizes [393,413], different polymer morphologies [409 – 410] and melting and recrystallization of a single polymer morphology [411 – 412]. Double melt endotherms in bulk Nylon 66, polystyrene and poly(ethylene terephthalate) (PET) have been interpreted as a result of conversion of kinetically favoured lamellar crystals to thermodynamically favoured extended chain crystals [416 – 418]. The confusion over the best explanation for multiple melting peaks in polymers has recently been highlighted in a series of conflicting papers on the interpretation of multiple melting peaks in poly(ether ether ketone) (PEEK) [409 – 415]. The ongoing, and as yet unresolved, debate over the interpretation of multiple melting peaks in PEEK is of great interest as an analogy to the multimelting
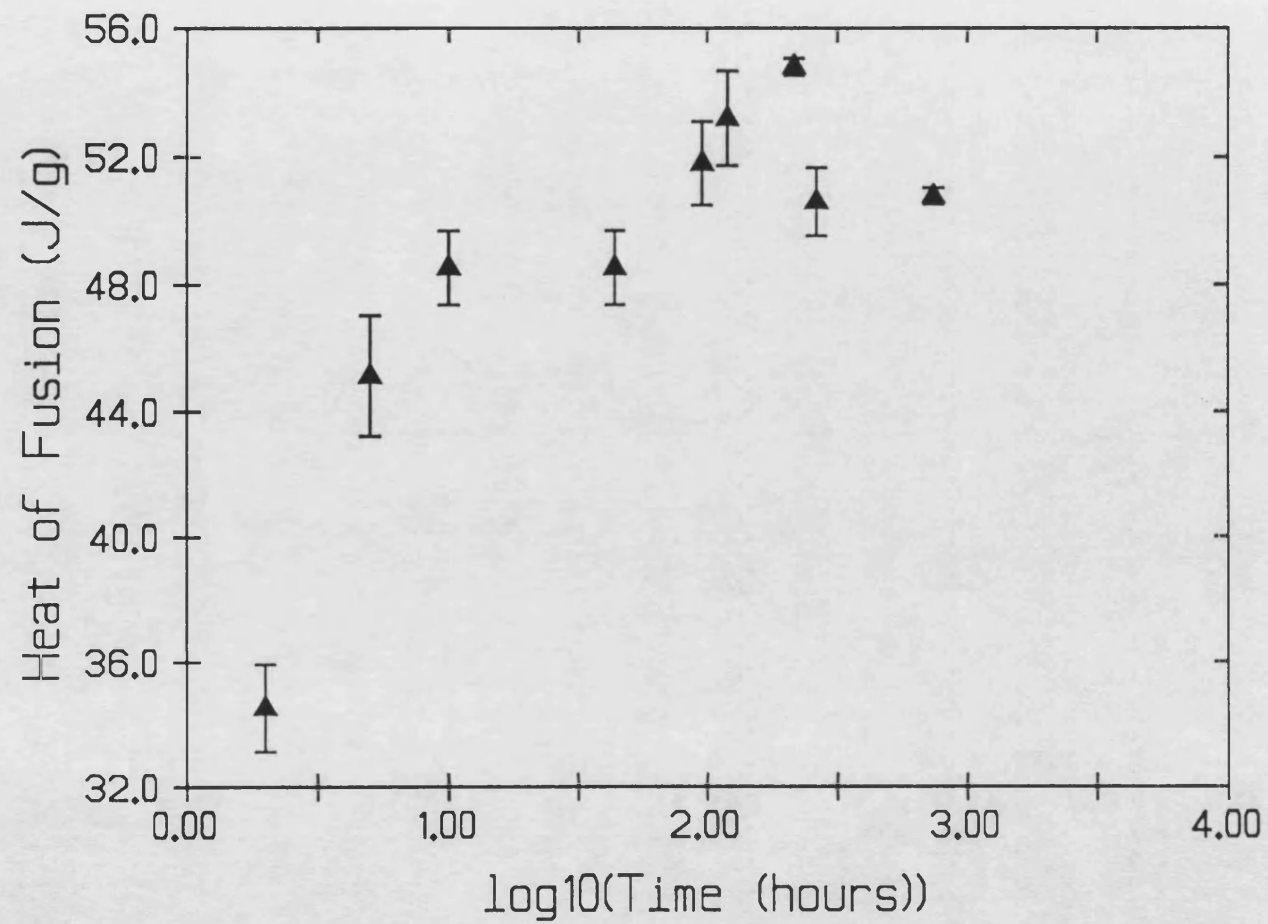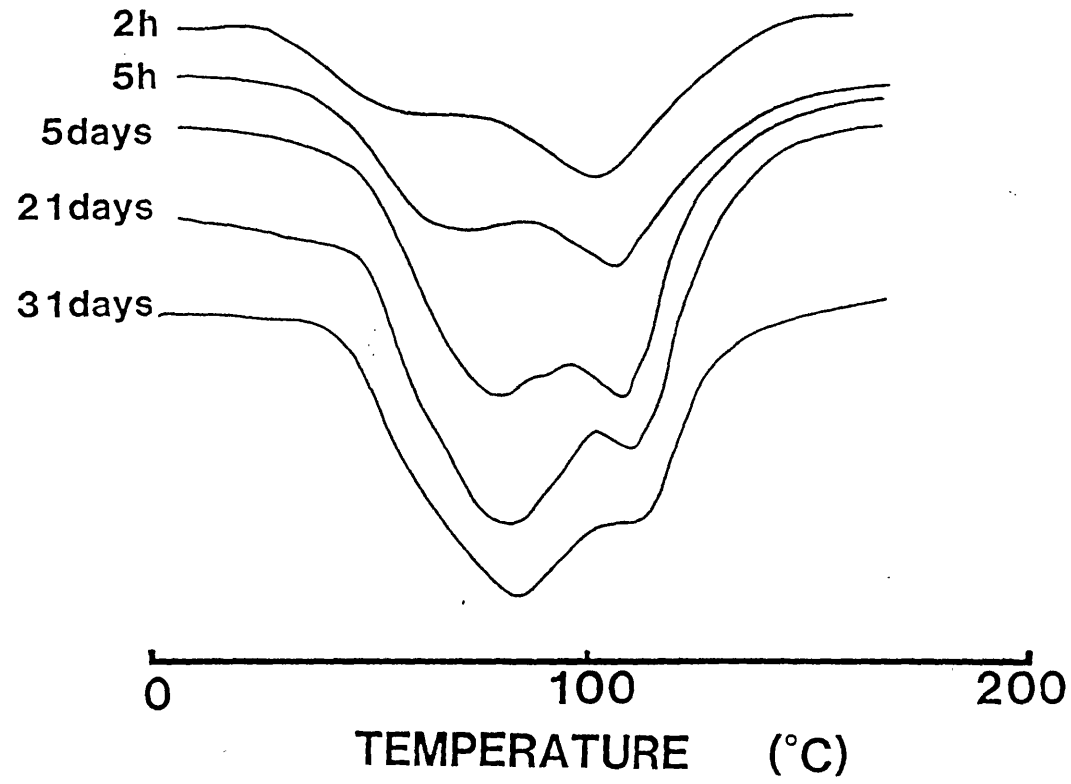
Figure 4.6. The variation in the heats of fusion for solvent cast films of PHV27 during ageing at 25°C. (Mean ± S.D., n=2)

Figure 4.7. The variation in the shape of DSC traces for solvent cast films of PHV27 during ageing at 25°C.

2h

5h

5days

21days

31days

0   100   200

TEMPERATURE   (°C)

142

endotherms seen in P(HB – HV) polyesters and a number of other polymers [419 – 420].

In the case of P(HB – HV) polyesters, the two melting peaks were thought to represent recrystallization of a single morphological form during the DSC heating program because this has been the most favoured of the hypotheses in studies with PEEK. This has been supported by observation of double melting peaks for isothermally crystallised P(HB – HV) polymer samples consisting of spherulites of the same size (one morphological form). Figure 4.8 shows that double melt endotherms were observed for P(HB – HV) spherulites isothermally crystallized at 60°C. Spherulitic crystallization is examined in more detail in chapter 5.

Ageing of PHV27 films at 25°C altered the shape and relative proportions of the two melting peaks until equilibrium was attained. Initially, peak II (the peak associated with melting at higher temperature) was the most prominent but on continued storage peak I (melting at a lower temperature) became the most prominent and appeared to be, thermodynamically, the more stable. The variation in peak melting temperatures for each peak (or crystal population) is shown in Figures 4.9 and 4.10. Peak I stabilised to a peak melting temperature of approximately 83°C (Figure 4.9) and peak II stabilised to approximately 110°C (Figure 4.10). A difference of approximately 27°C in the melting temperatures of the two peaks was observed at equilibrium.

Figure 4.11 shows changes in the relative proportions of the two peaks (or crystal populations) on ageing at 25°C. The relative proportions were calculated from the heats of fusion of each peak relative to the total heat of fusion for PHV27 and expressed as a percentage. Accurate results could not be obtained because the software did not allow deconvolution of the melt endotherms. However, estimates of the relative proportions of the two peaks were made using the Dupont thermal analysis software package which involved separating the two peaks by a perpendicular drop from the extrapolated baseline. Initially, peak II constituted 80% of the total melt endotherm. However this changed progressively over the first 4 – 6 days with peak I becoming more prominent. Note the cross over point, at about day 2, which represents the time when both peaks (or
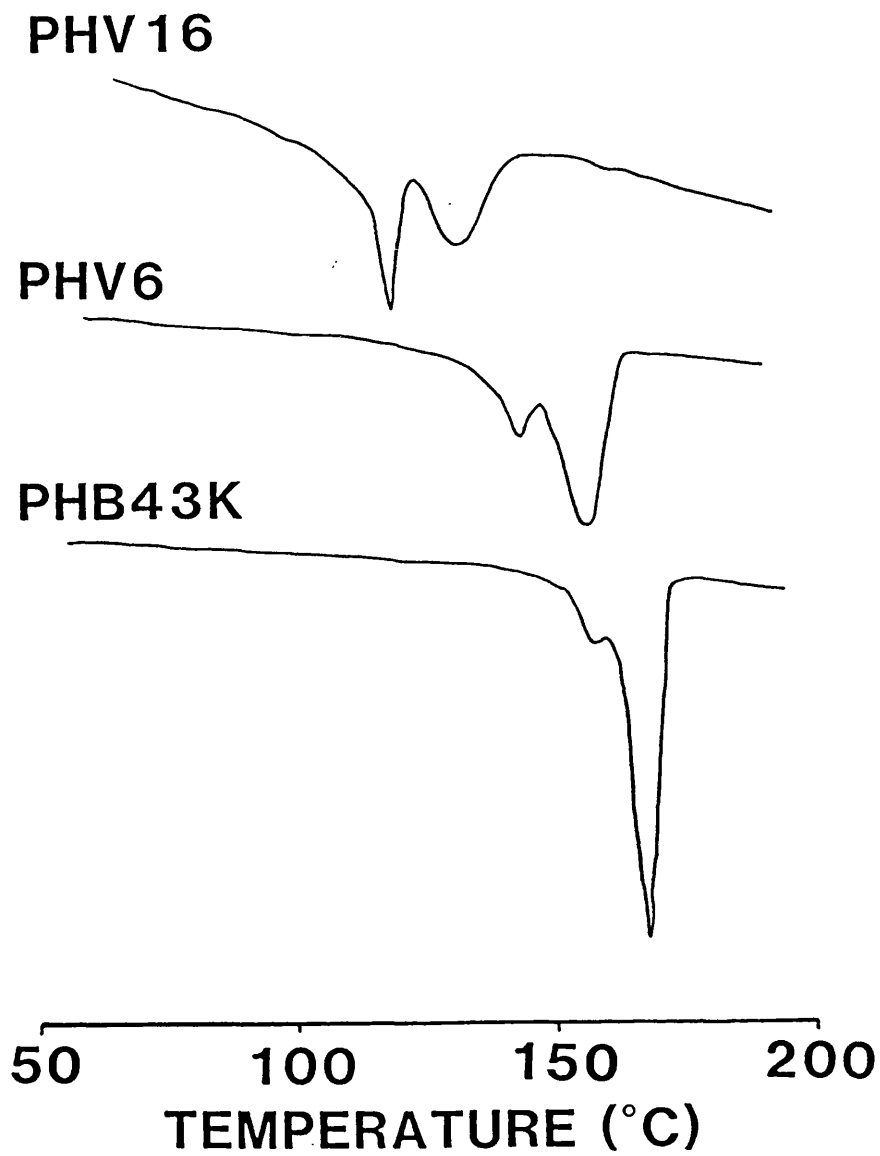
Figure 4.8. DSC traces showing double melt endotherms for P(HB – HV) spherulites crystallized isothermally at 60°C.
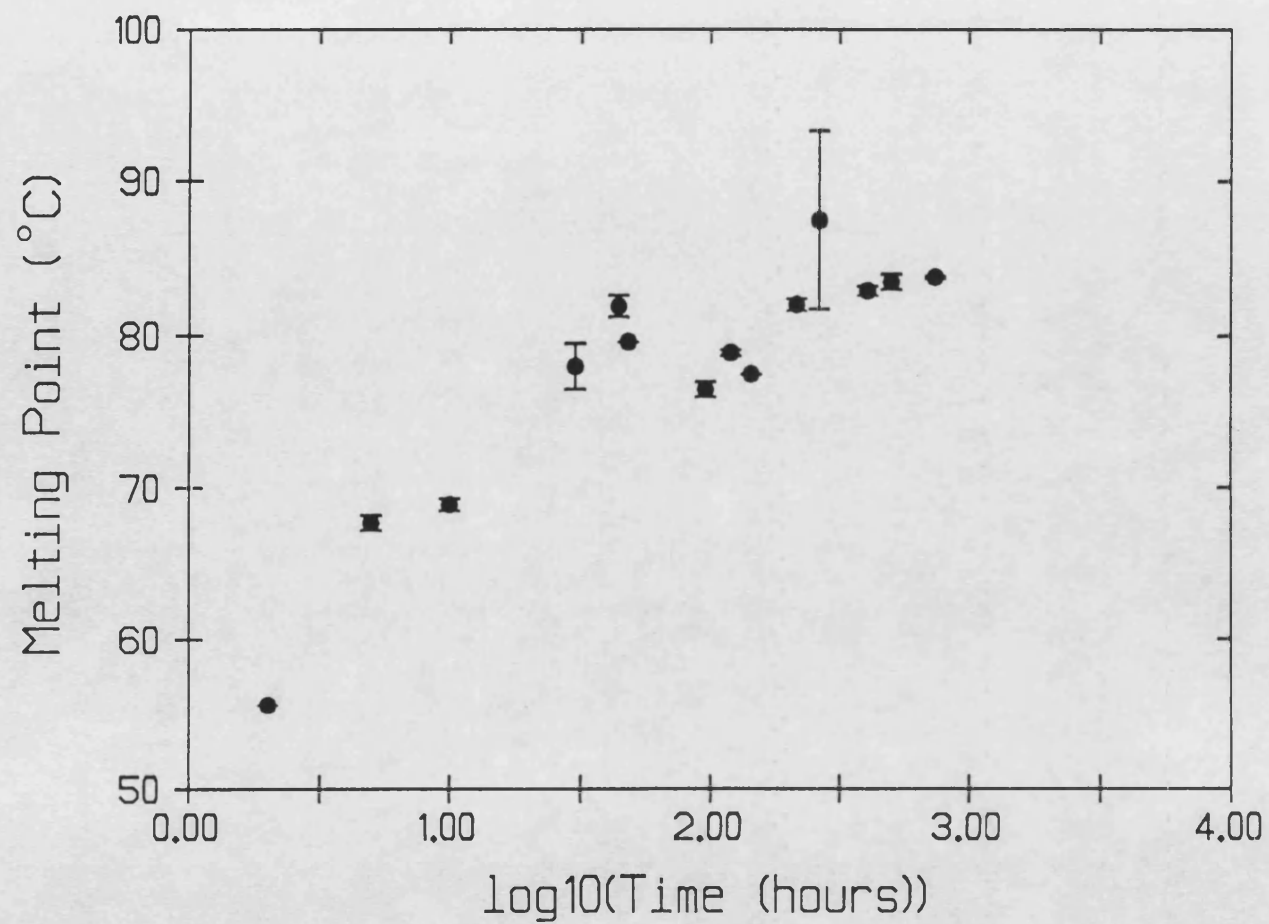
Figure 4.9. The variation in the melting temperatures of Peak I for solvent cast films of PHV27 during ageing at 25°C. (Mean ± S.D; n = 2).
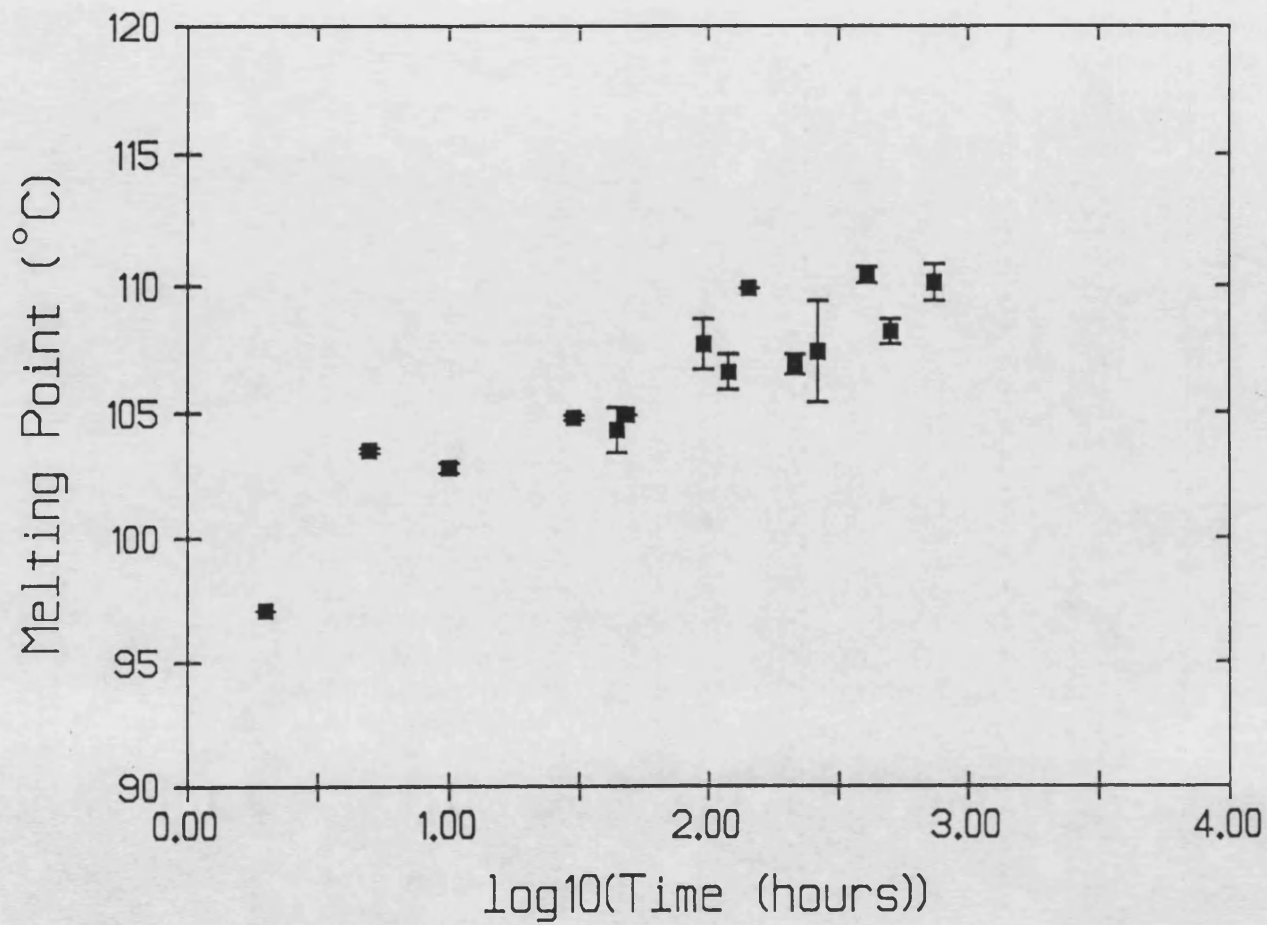
Figure 4.10. The variation in the melting temperatures of Peak II
for solvent cast films of PHV27 during ageing at 25°C.
(Mean ± S.D; n = 2).
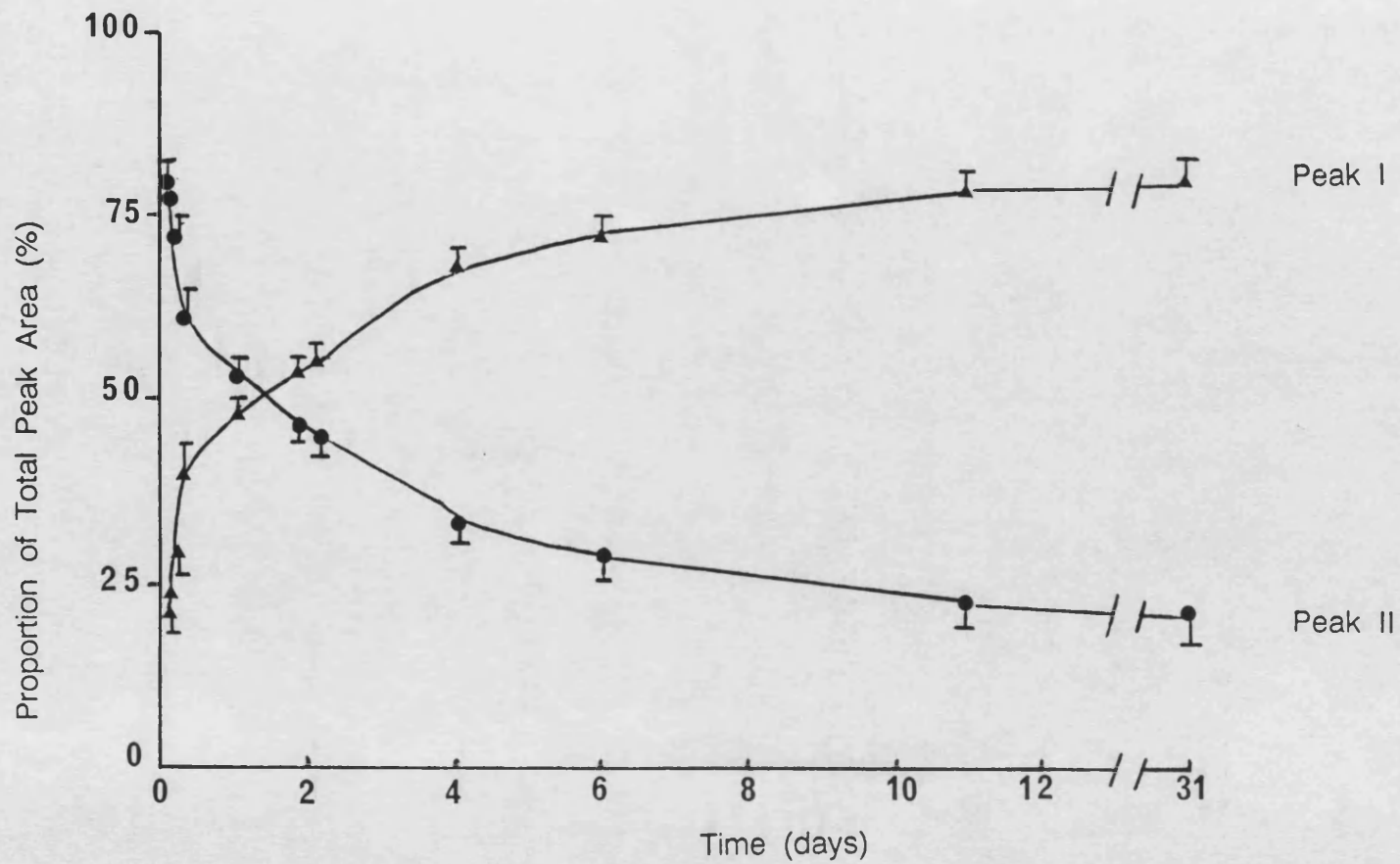
Figure 4.11. The variation in the relative proportions of the two melting peaks for solvent cast films of PHV27 during ageing at 25°C (Mean ± S.D; n = 2).

morphologies) were equal in magnitude. At equilibrium, the situation had reversed and peak I constituted about 80% of the total melt endotherm.

Table 4.2 shows that PHB films achieved stable values for the heat of fusion within 24 hours storage at 25°C. Figure 4.12 shows that the DSC thermograms of PHB also stabilised within a similar period of time. These results showed that the heat of fusion and shape of DSC thermograms for PHB stabilised more rapidly than PHV27 and also PHV12 (see Figure 4.13). In the case of PHV12, DSC traces stabilised within 19 days of ageing at 25°C. These results were in general agreement with those reported by Bloembergen et al [211] who showed that solution crystallization of P(HB – HV) copolymers occurs more slowly than in PHB. Crystallization of P(HB – HV) polymers from the melt showed similar results (see chapter 5). The explanation for the slower rates of crystallization was thought to be due to the additional methyl group in HV retarding crystallization kinetics in copolymers.

Table 4.2. Heats of Fusion for PHB380K as a function of ageing time.

Ageing Time	Heat of Fusion (Jg^{-1}) (Mean $\pm$ Range; n = 2)
4 hr	61.2 $\pm$ 5.1
8 hr	74.3 $\pm$ 4.3
11 hr	81.6 $\pm$ 2.3
1 day	89.5 $\pm$ 1.7
4 days	90.6 $\pm$ 1.0
6 days	89.6 $\pm$ 0.9
17 days	87.4 $\pm$ 2.0

The DSC thermograms of aged PHB films (solvent cast) also exhibited double melt endotherms. The double melt endotherm was characteristic of aged samples prepared from both melt and solution.

Figure 4.12.The variation in the shape of DSC traces for solvent cast films of PHB380K during ageing at 25°C.
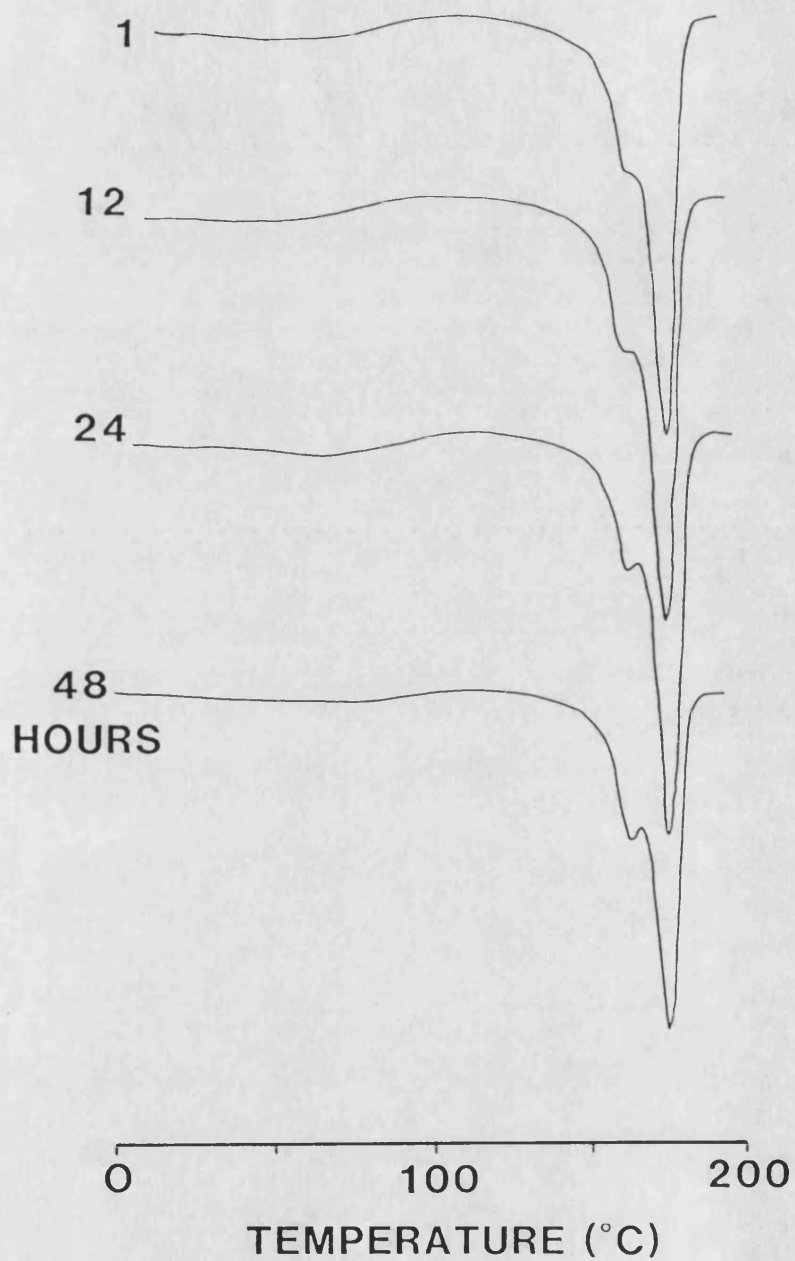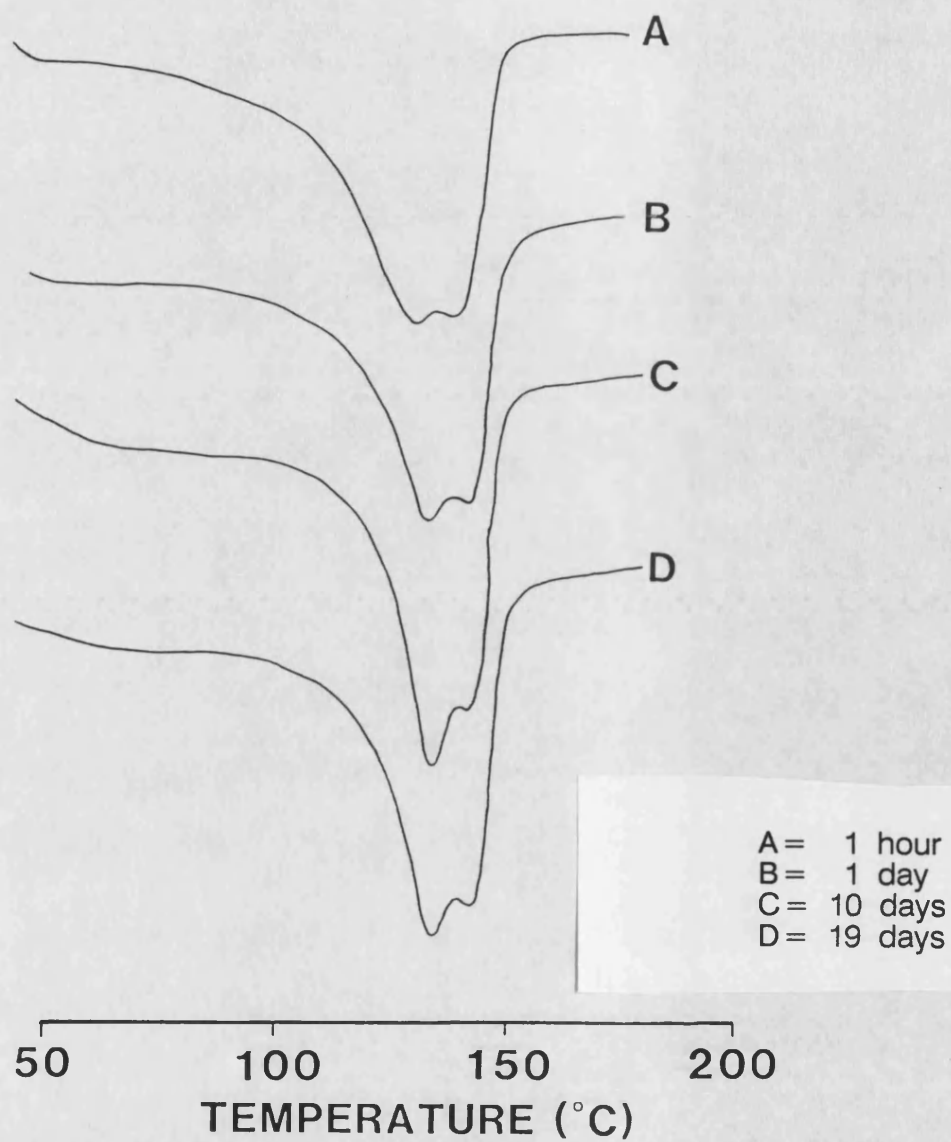
Figure 4.13. The variation in the shape of DSC traces for solvent cast films of PHV12 during ageing at 25°C.

4.4.2.2 Ageing of melt quenched PHB.

The immediate remelting of melt quenched samples of PHB resulted in a single melt endotherm following complete recrystallization during the DSC heating program. However if melt quenched PHB samples were aged at 25°C before remelting, then a double melt endotherm would result on melting (Figure 4.14a and e).

At 25°C, PHB was above its glass transition temperature (T_g) and sufficient mobility of chains existed for the polymer to rapidly crystallize by chain reorientation. In the DSC the crystallization process at 25°C for PHB was monitored by the progressive disappearance of the crystallization exotherm at around 50°C. As crystallization progressed during the ageing process, the heat of crystallization progressively decreased from an initial maximum value, of approximately 70% of the heat of fusion, to zero when the crystallization process was complete. Using this method of monitoring crystallization, PHB was found to crystallize rapidly at 25°C and crystallization was usually complete within 2 hours. The crystallization of melt quenched PHB samples aged at 25°C is represented by the DSC thermograms in Figure 4.14. The copolymers were found to crystallize more slowly (Table 4.3).

Table 4.3. Overall Crystallization times for P(HB–HV) polymers as estimated from DSC measurements.

Polymer	Overall Crystallization Time (hours)
PHB380K	< 2.0
PHV12	< 6.0
PHV20	<21.0

Ageing of poly–L–lactide (PLA) at 25°C did not produce any crystallization outside of the DSC run and the heat of crystallization, which occurred at around 116°C, remained essentially constant for the entire study period of 60 days (Figure 4.15). The value for the heat of crystallization of PLA (58 ± 5 Jg^{-1}) closely resembled that of the heat of
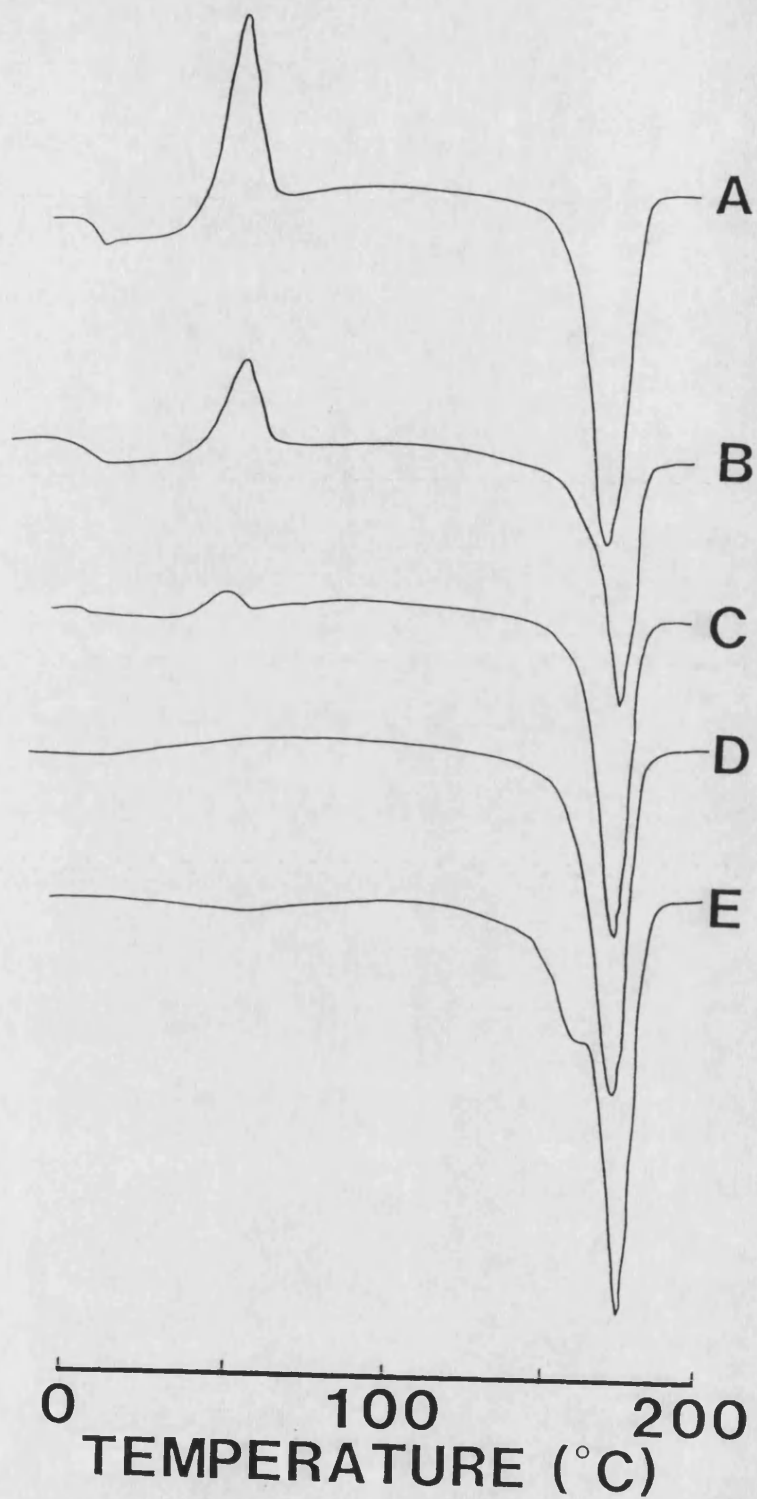
Figure 4.14. DSC traces showing crystallization and ageing
effects in melt–quenched PHB380K samples as a function of time.
(A = 1 min, B = 30 mins, C = 65 mins, D = 2 hours, E = 7 days).
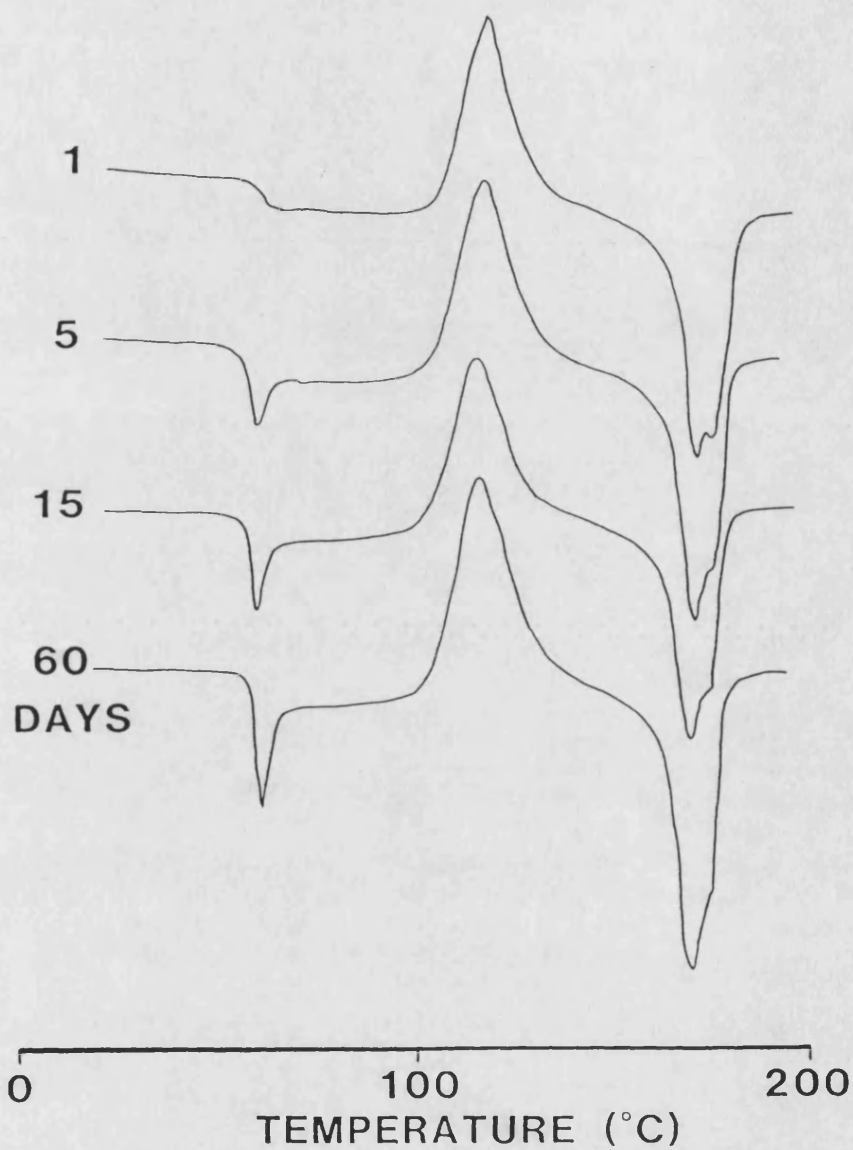
Figure 4.15. DSC traces for melt–quenched samples of PLA as a function of time during ageing at 25°C.

fusion (54 $\pm$ 4 Jg^{-1}). This was in contrast to findings with P(HB–HV) polymers where heats of crystallization were typically 50–70% of the heats of fusion for the range of copolymers studied (see chapter 3). The absence of crystallization for PLA at 25°C was due to its high T_g (56–59°C). At 25°C PLA was well below its T_g and existed in the glassy state. The polymer was, therefore, unable to crystallize because of insufficient chain mobility in this frozen glass. However, the glass transition for PLA, as shown in Figure 4.15, became more pronounced with time suggesting some stress relaxation or mobility of polymer chains on ageing. The position of the T_g was maintained within the range 56–59°C throughout the 60 day study period.

This DSC method detects the overall crystallization of the polymer which is a combination of both nucleation rate and spherulite growth rate. A more comprehensive report of the crystallization growth rates determined from polarized light microscopy measurements is presented in Chapter 5.

4.4.3 X–ray Diffraction

X–ray diffraction traces of ageing P(HB–HV) polymer films (solvent cast) changed with time when stored at 25°C. A representative trace showing changes with time for PHB is given in Figure 4.16. The amorphous state is characteristic of films cast from solution that have not completely dried. As crystallinity of the films progressed the sharp peaks, indicative of crystalline order, developed on the amorphous halo. The peak heights continued to change until equilibrium crystallinity was attained. At equilibrium the X–ray diffraction traces for P(HB–HV) polymers were similar in appearance (Figure 4.17) but this *per se* does not necessarily mean similar crystallinities. The amorphous component of each polymer needs to be assessed and for the degree of crystallinity to be independent of copolymer composition, the amorphous component must also be similar in each case. Although preliminary assessment of the amorphous components of the copolymers using X–ray diffraction on melt–quenched samples suggested that crystallinity was indeed similar for the copolymers, this can only be a tentative suggestion and further work is required in this area.

Figure 4.16. The variation in the shape of X-ray diffraction traces for solvent cast films of PHB380K during ageing at 25°C.

Equilibrium aged

Aged for 1/2 hour

Amorphous

30   26   22   18   14   10   6

2θ ANGLE
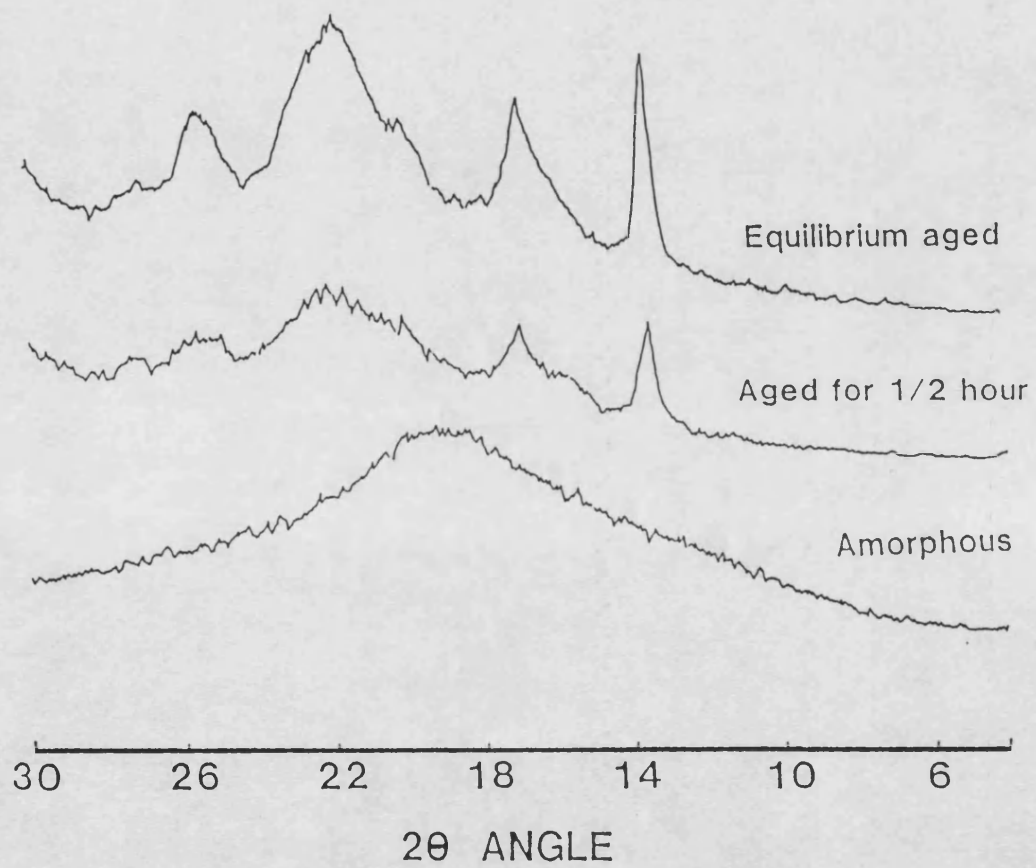
Figure 4.17. X – ray diffraction traces for equilibrium aged P(HB – HV) solvent cast films.

A = PHB380K
B = PHV6
C = PHV12
D = PHV20
E = PHV27

A

B

C

D

E

30   26   22   18   14   10   6

2θ ANGLE (DEGREES)
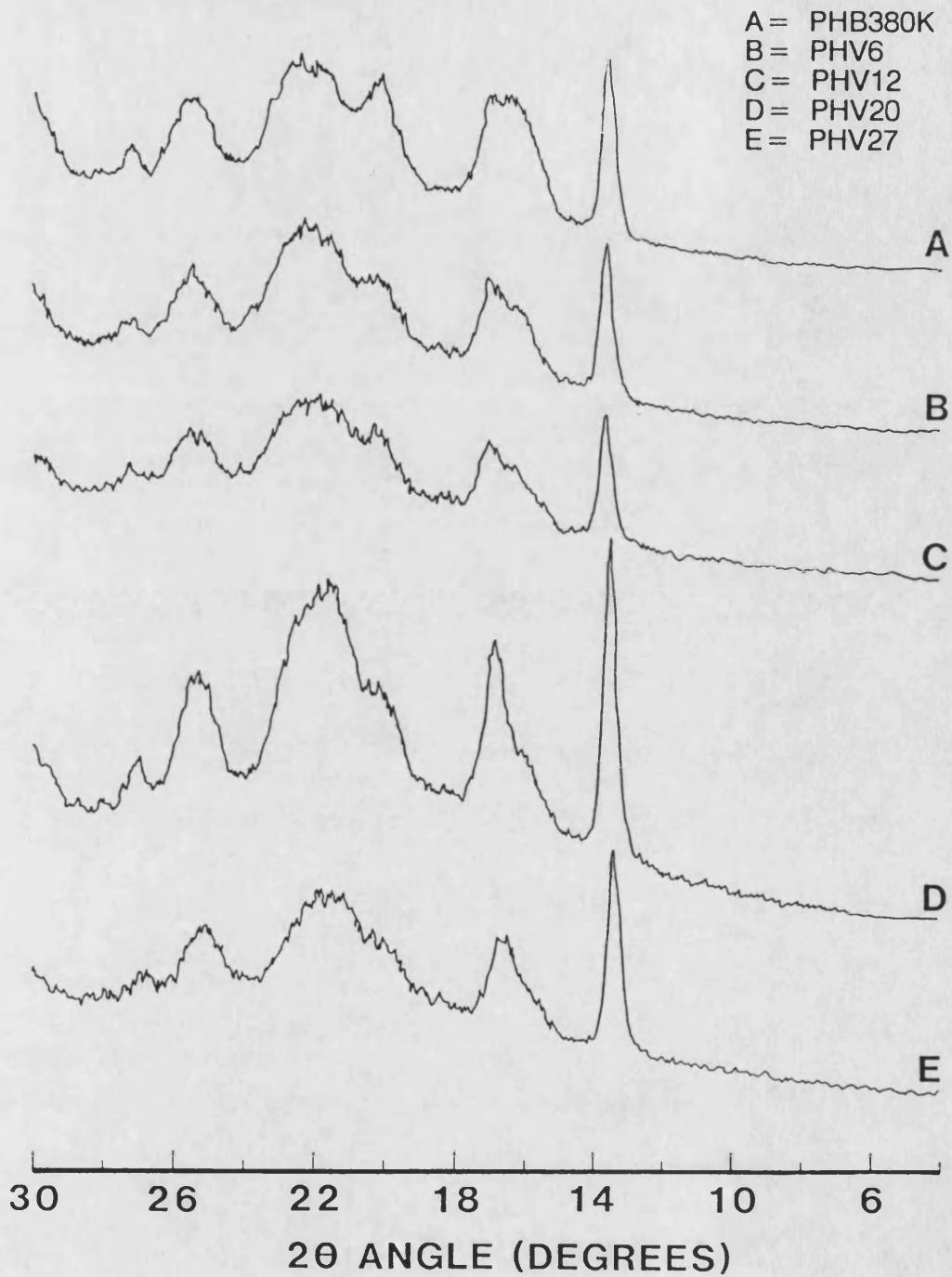
4.4.3.1 The crystallinity index

In order to quantify the changes in crystallinity observed for P(HB–HV) polymers during storage, a crystallinity index was developed. It is obvious from even a cursory inspection of the physics of diffraction from polymers that calculation of an absolute crystallinity value from X–ray data is a formidable task and and one which is prone to errors [421–422]. If an absolute value is determined, it is frequently open to debate as to whether certain assumptions that were used are actually valid [421]. It is often adequate to calculate a reproducible value from the X–ray data, which will compare, on an arbitrary basis, the crystallinity of different samples of the same polymer. Such a relative evaluation is termed a 'crystallinity index'. This approach of assessing crystallinity was suitable for this investigation in which degrees of crystallinity were being compared after samples of the same polymer had been aged for varying periods of time.

The differential intensity measurement method of Statton [421] was used in this study because of the advantages it offered over other methods of quantifying crystallinity. It is applicable to polymers having complex scans with several strong reflections [422]. The method requires no resolution or estimates of amorphous and crystalline scatter.

The method involved scanning two reference samples or standards between set limits of diffraction angle. One standard was for a highly crystalline sample and the other for a very amorphous sample. The unknown sample was then also scanned between the selected limits of the diffraction angle. The three scans were then normalized to the same total intensity between the selected limits of diffraction angle. An example of these scans for PET is reproduced from the original work of Statton [421] and is shown in Figure 4.18.

In the case of P(HB–HV) polymer films, the crystalline standard was the equilibrium aged (>2 months at 25°C) solvent cast film (30–50um) of the respective polymer. The amorphous standard was a 4%w/v chloroform solution for each of the respective polymers. By default

Figure 4.18. Representative X–ray diffraction traces for polyethylene terephthalate showing the principles involved in obtaining a crystallinity index (after ref. 421).
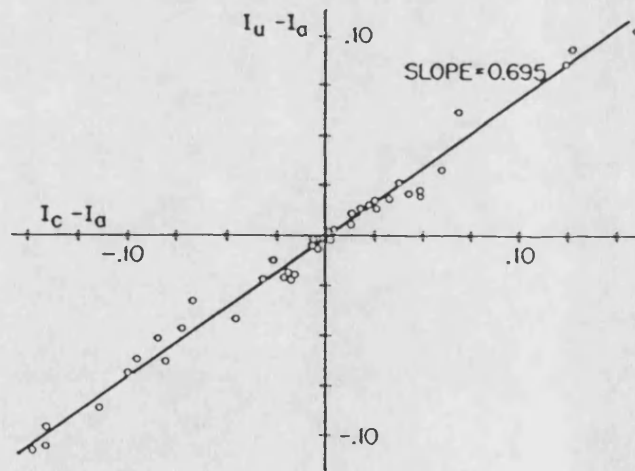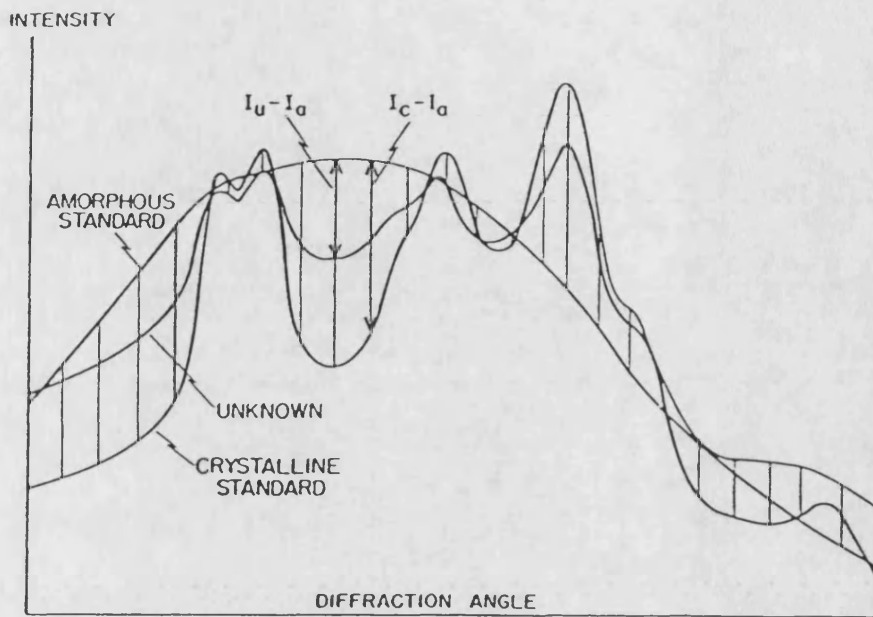
Figure 4.19. A typical plot of X–ray intensity data for PET from which the crystallinity index value is obtained (after ref. 421).

the standards represent 100% and 0% crystallinity respectively. The set limits for diffraction angle were $10-30°$. At increments of $0.2°$, the differences between the intensity values were determined: $(I_u - I_a)$ and $(I_c - I_a)$; where I is the intensity value and the subscripts represent the unknown sample (u), amorphous standard (a) and the crystalline standard (c). The increments were carefully chosen to coincide with the maximum height of peaks seen in the X-ray traces and at the same time to provide sufficient data for a statistically accurate result. The Philips diffractometer control was programmed to carry out a step scan at $0.2°$ with a 10s time interval for intensity accumulations. Increments of $0.2°$ yielded 100 data points from each X-ray diffraction trace.

According to Statton [421] there are two different methods of handling the data obtained from such scans. The first method results in an 'integral' crystallinity index and is calculated from

$$X = \frac{(I_u - I_a)}{(I_c - I_a)} \ (\times \ 100)$$

However, this method was quite sensitive to errors in experimental technique and Statton found lower precision for PET samples using this technique compared to the slope or correlation index method [421]. The latter is the second method and that used in this study. In this second method, the data were treated to obtain a 'correlation' crystallinity index from a linear regressional analysis of the expression

$$(I_u - I_a) = X(I_c - I_a) + B$$

The plot of $(I_u - I_a)$ against $(I_c - I_a)$ for a series of diffraction angle increments is expected to yield a straight line. Figure 4.19 shows the results obtained for PET by Statton [421]. By linear regression, the slope of the straight line was the crystallinity index (X). Although more calculations are required in this method it is preferred over the 'integral' crystallinity index method.

Figure 4.20 shows a typical graph of $(I_u - I_a)$ against $(I_c - I_a)$ for P(HB-HV) polymers
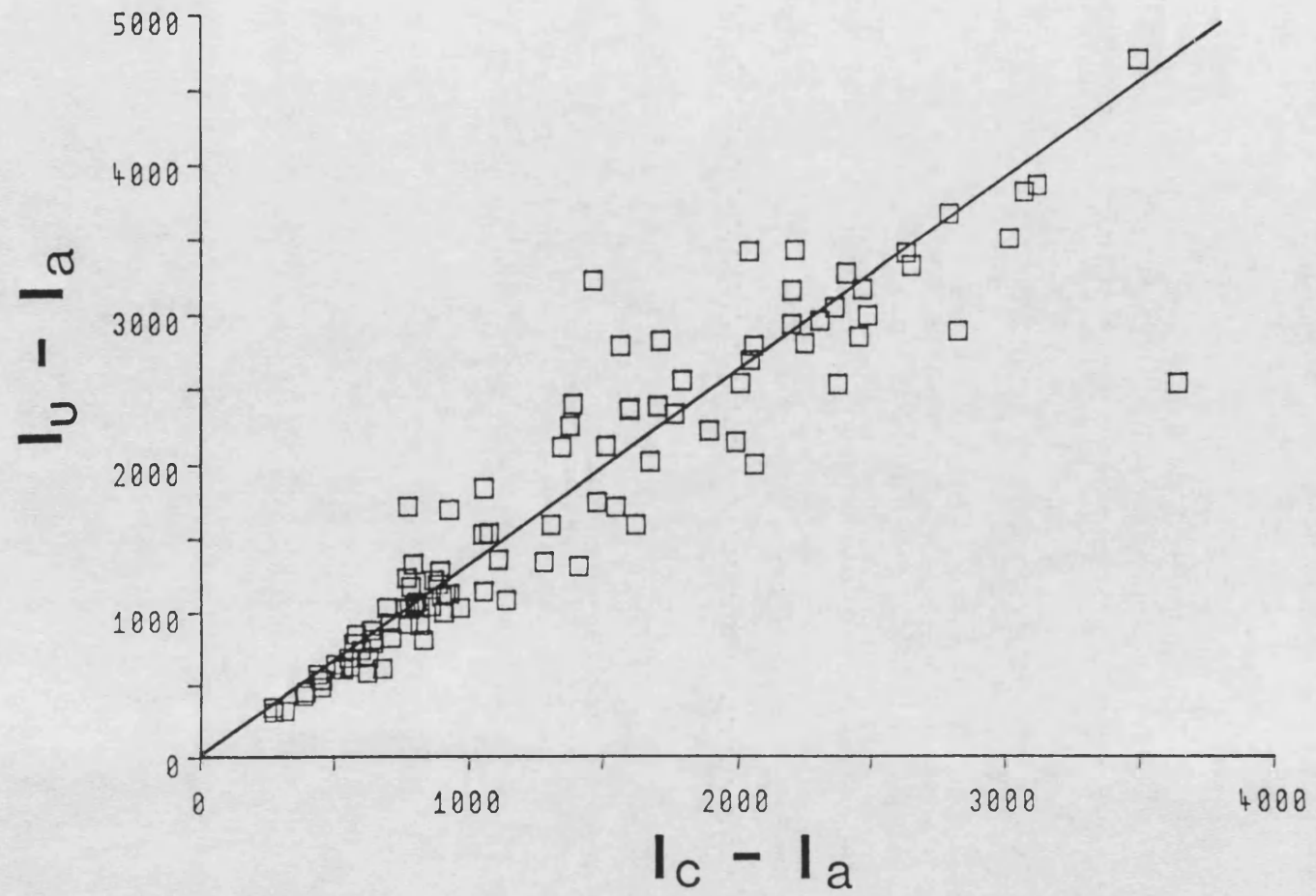
Figure 4.20. A typical plot of X−ray intensity data for PHB380K from which the crystallinity index was determined.

obtained using the above method. There was a large degree of scatter between the points and regressional analysis of the data gave values of r^2 consistently below 0.97.

Table 4.4 summarizes the crystallinity results for PHB380K, PHV12 and PHV27 on storage of films at 25°C. Contrary to the findings with the mechanical properties, the crystallinity of all polymer films (solvent cast) studied using X–ray diffraction, appeared to stabilise within 24 hours of fabrication. It appeared that crystallization was progressively retarded on increasing HV content. The crystallinity index reached equilibrium within approximately 2–4 hours for PHB380K, 4–8 hours for PHV12 and 12–24 hours for PHV27. No significant changes in the index were noted after this period but results may have been complicated by the large scatter of the acquired data. This was largely attributed to a greater variation in final film thickness (20–50um) of polymers used in the x–ray diffraction study.

Bloembergen et al [211], who used solvent cast films of an unknown thickness, have also studied ageing of solvent cast films. Using FTIR (Fourier Transform Infra–Red Spectroscopy) to measure crystallinity, they found that copolymer films stored at ambient stabilised more slowly than the homopolymer. The authors found that crystallinity of copolymers containing 7–47 mole% HV had not stabilised after 3 weeks of storage. They attributed this to the slower crystallization of copolymers which may involve secondary crystallization processes [211].

Table 4.4 Variation in Crystallinity Index as a function of ageing time for P(HB–HV) polymers.

Ageing Time (hours)	Crystallinity Index (Mean ± Range; n = 2)		
	PHB380K	PHV12	PHV27
0.33	0.30 ±0.29	0.27 ±0.21	0.13 ±0.10
0.67	0.65 ±0.14	0.45 ±0.33	0.42 ±0.12
1.00	0.48 ±0.11	0.85 ±0.24	0.25 ±0.22
2.00	0.91 ±0.17	0.74 ±0 21	0.55 ±0.31
4.00	0.97 ±0.52	0.90 ±0.11	0.65 ±0.21
8.00	1.10 ±0.21	0.98 ±0.20	0.74 ±0.15
12.00	1.01 ±0.44	1.11 ±0.10	0.67 ±0.41
24.00	0.92 ±0.46	1.12 ±0.22	0.94 ±0.21
48.00	1.00 ±0.20	0.99 ±0.13	1.10 ±0.10

The fact that polymer properties stabilized more rapidly when measured by X-ray diffraction than those measured by DSC or mechanical testing may be explained by the fact that X-ray diffraction is primarily detecting surface properties whereas the other two techniques are concerned with the bulk. The surface of the polymer film crystallized more rapidly than the bulk because drying proceeds from the surface inwards. The results are therefore consistent with the drying process.

These results have highlighted the fact that crystallinity must be determined by more than one technique for the results to be meaningful. Furthermore, bulk properties of P(HB – HV) polymers were found to change for longer periods than surface properties during ageing.

A recent report by Scandola et al [269], who investigated the ageing phenomenon in melt processed PHB by monitoring dynamic mechanical properties with time at 30°C, found that the dynamic mechanical spectrum (DMS) of PHB in the glass transition region continued to change throughout the 720 hour study period. At the same temperature the DMS for a copolymer containing 30 mole% HV continued to change throughout a 1120 hour study period [269].

Clearly ageing can occur in P(HB – HV) polymeric devices fabricated from both solution and melt and must be accounted for in biomedical and other applications of these polymers. Significant ageing effects were not evident in PLA when stored at 25°C and this may be due to its high glass transition temperature (56 – 59°C), which is well above room temperature. DSC traces for PLA stored at 25°C remained essentially unchanged but the glass transition became more pronounced with increasing ageing time.

4.5 CONCLUSIONS

The crystalline and mechanical properties of P(HB – HV) polymer films changed with time following fabrication. The bulk crystallinities and mechanical properties of P(HB – HV) films appeared to stabilise within 3 – 5 days, whereas surface crystallinities stabilised

within 24 hours for the polymers studied. These changes may have been related to either solvent evaporation and/or secondary crystallization effects.

Despite PHV20 and PHV27 films having stable crystallinities (DSC and X-ray diffraction) after a maximum of approximately 7 days, the morphology of these films, as detected by DSC, continued to change for up to 19 and 31 days respectively. These results suggest that some chain reorganizaion or stress relaxation may be occurring during storage. The reason why this occurred with the copolymers and not PHB remains unclear but may be related to the slower rates of crystallization observed in the copolymer. There was some evidence in terms of TS, stabilization of DSC traces and crystallinity index data from X-ray diffraction to suggest that ageing effects were progressively prolonged with increasing HV content.

CHAPTER 5

CRYSTALLINE PROPERTIES

5.1 INTRODUCTION

A knowledge of the crystalline properties of polymers is important because they influence all other bulk properties (thermodynamic, physical, mechanical and optical) [213] and in order to explain bulk properties fully it is essential to have a clear understanding of the nature and extent of crystalline regions. The degree and rate of crystallinity and the morphology of polymer crystals will be important parameters when considering the processing of semicrystalline polymers. In the biomedical and pharmaceutical applications of such polymers, the way in which these properties are modified on incorporation of drugs or additives will influence not only the manufacture but also the potential uses of the material. Furthermore, in drug delivery applications, the way in which drugs are trapped and distributed within the semicrystalline polymer and the way in which this influences polymer morphology may provide valuable information on the rates and mechanisms of drug release.

Polymer morphology concerns the shape and arrangement of crystals [408]. However, semicrystalline polymers in their solid state are reported to have very complex morphologies [219]. This is attributed to the chainlike nature of their constituent molecules, which leads to crystallization behaviour and morphologies that are in most aspects only rarely encountered in more traditional "small molecule" solids, and in other aspects are unique to polymers [219].

Evidently, the study of polymer morphology has a great deal to offer but, despite major advances in the last thirty years, with one or two notable exceptions, its full impact has yet to be realized. This applies especially to melt–crystallized polymers, i.e. many commercial products, whose morphologies have hardly been established or may still be controversial [423]. The morphology of crystalline polymers has been the subject of a number of reviews including notably those of Keller [6], Bassett [227,424], Geil [425], Vaughan and Bassett [229] and Khoury and Passaglia [219].

Many such reviews also consider morphology and crystallization behaviour from dilute

polymer solutions. The principles of which have been briefly covered in chapter 1. This chapter is primarily concerned with the crystallization and morphology of polymer melts. The crystalline morphology of polymers crystallized from the melt is thought to closely resemble that seen in polymers crystallized from concentrated solutions [220]. However, crystals grown from dilute solution are thought to be more perfect than polymer crystals produced from the melt [219,229]. Studies on crystalline morphology have shown that polymers do not attain perfect crystalline order [229] and even polymer single crystals are not 100% crystalline [425].

Closely related to polymer morphology is the subject of crystallization kinetics and this has also been reviewed by a number of authors including Hoffman *et al* [220], Bassett [424], Sanchez [426] and Ross and Frolen [427].

One of the simplest and direct methods of studying both morphology and crystallization kinetics in polymers is from bulk or melt crystallized samples. Polymers crystallize from the melt most commonly in the form of spherulites, which, as described later, are symmetrical arrays of chain-folded lamellae. The study of the morphology of polymers crystallized from the melt is therefore predominantly concerned with the determination of fine structure of spherulites and of the mechanism of growth [219,227].

5.1.1 Spherulitic Crystallization

Crystallization is the process whereby an ordered structure is produced from a disordered phase, usually a melt or dilute solution [408]. Crystallization from the melt to form spherulites is called "spherulitic crystallization". When the temperature of the melt is reduced to the melting temperature there is a tendency for the random tangled molecules in the melt to become aligned and form small ordered regions. This process is known as nucleation and the ordered regions are called nuclei. These nuclei are only stable below the melting temperature of the polymer since they are disrupted by thermal motion above this temperature [408]. Nucleation has been classified as either homogeneous or heterogeneous [408]. During homogeneous nucleation in a polymer melt (or

solution) it is envisaged that small nuclei form randomly throughout the melt (i.e. on the polymer itself). Although the process has been analysed in detail from a theoretical viewpoint [220,426] it is thought that in the majority of cases of crystallization from polymer melts (and solutions), nucleation takes place heterogeneously on foreign bodies such as dust particles or the surfaces of the containing vessel.

The second step in crystallization is growth whereby the crystal nuclei grow by the addition of further chains. In polymers it is recognised that the growth kinetics result not from diffusion of material away from the growing interface, but rather from a nucleation process occurring at the tip of the lamellar crystal [428 – 429]. Crystallization is therefore a process which takes place by two distinct steps, nucleation and growth, and these are often considered separately. Barham [215] has investigated the nucleation behaviour of PHB polymer melts and for that reason this study will primarily be concerned with spherulitic growth and its kinetics. Only qualitative observations on nucleation have been made where relevant.

Spherulitic crystallization is not confined to polymers but also occurs in minerals [430]. Spherulites in polymers superficially appear similar to the mineral counterparts but are generally smaller. Although in special cases, such as PHB, where polymer spherulites up to a few millimetres have been grown, they are usually of the order of 100um or less in diameter [219,424]. Examples of PHB spherulites observed in thin films under the optical microscope with crossed polarizers are shown in Figure 5.1. The three essential minimum attributes of spherulites can be inferred from their appearance [424]. The bright contrast derives from birefringence and indicates a crystalline entity. Superimposed on this is the black Maltese cross with arms lying parallel to the extinction directions of the polarizer and analyser. When the specimen is rotated in its own plane the cross remains stationary. This implies, as will be explained later, that all the radii are crystallographically equivalent to the resolution employed.

Historically, Bunn and Alcock [223] were the first to report the presence of spherulites in synthetic polymers in 1945. They also showed by birefringence measurements that the
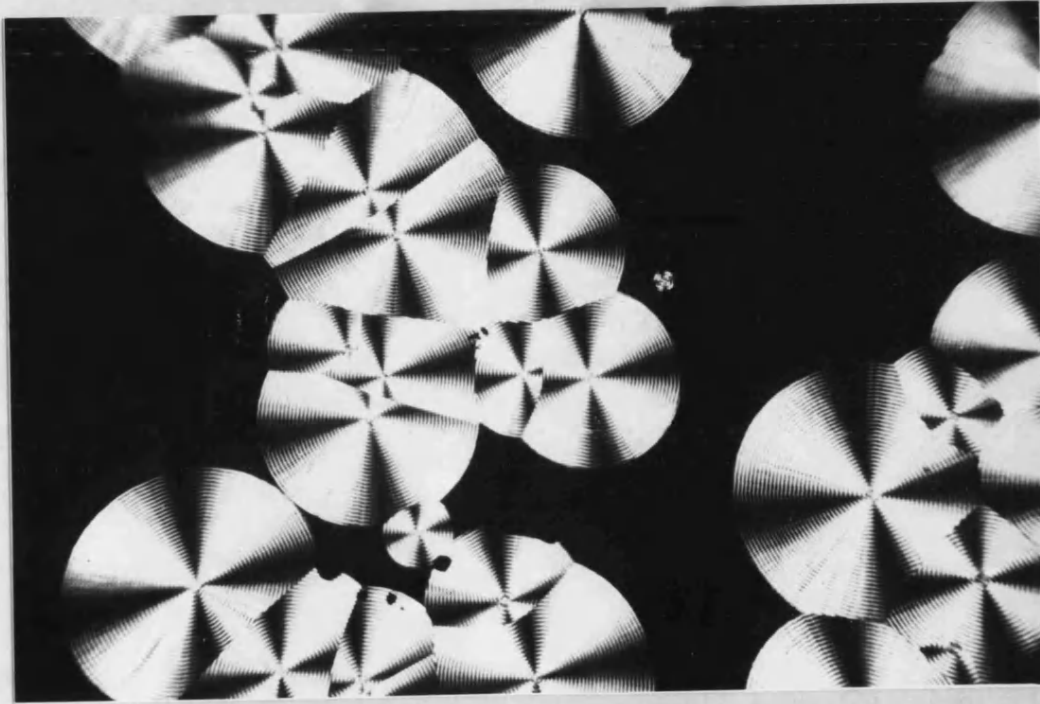
Figure 5.1. A optical photomicrograph showing PHB spherulites.

chain axes were perpendicular to the spherulite radius. Further early work on their structure was performed using a microbeam X-ray diffraction technique by, amongst others, Point [431] and Keller [432]. These studies showed that in polymeric spherulites the unit cell orientation is such that the molecular chains are normal to the radial direction, or nearly so, and that a crystallographic direction is parallel to the radius, and this clearly demonstrates the spherical symmetry of the spherulite. In many cases including polyethylene [432] and PHB [214] the molecular chains are normal to the radius and according to Khoury and Passaglia [219], no polymer is known, other than in the case of some species of polypropylene spherulites, for which the molecular axis makes an angle of less than 60°C with the radius. For this reason the molecular orientation in spherulites is said to be "tangential". In the exceptional case seen in certain species of spherulites of the alpha-monoclinic form of polypropylene, Binsbergen and De Lang [433] have observed twinning of chain folded lamellae within the fibrils. This twinning leads to the development of daughter lamellar branches at approximately right angles to radially orientated lamellae. Consequently, the molecules in the daughter branches are orientated with the chains parallel to the radius.

The tangential orientation of molecules in spherulites defied explanation by the then existing fringed micelle model and was not fully understood until Keller's [224] discovery of chain-folded polymer crystals in 1957. Fischer [225] was the first to clearly show the existence of lamellar structures in melt-crystallized polymers. However, the question as to whether these lamellae contained chain-folding was not answered. Perhaps, the most direct evidence for the presence of chain-folded lamellae came from the etching experiments on polyethylene by Palmer and Cobbold [434] and Keller and Sawada [435]. Microscopic fragments of a lamellar appearance were formed by selective oxidation using fuming nitric acid. Electron diffraction studies of these fragments showed that the chain molecules had similar orientations relative to the surface of the fragments as with molecules in chain-folded lamellae grown from solution [434-435]. Although the selective oxidation technique etched out the folds of the

molecules In the fragments, the experiments provided strong evidence that In the untreated solid polymer, the lamellae in the spherulites existed as chain-folded crystals.

Although no extensive etching studies have been performed on melt-crystallized PHB, Keller et al [436] have recently used gaseous methylamine to selectively degrade surface folds In freeze-dried solution-grown crystals of PHB. The authors have used the technique together with gel permeation chromatography to determine fragment lengths and therefore, fold lengths In solution-grown crystals. More recently, a preliminary report by Organ and Barham [437] suggests that this etching technique can also be successfully applied to melt-crystallized PHB and offers great potential for examining the underlying microstructure of P(HB-HV) polymer spherulites.

Clearly, the structure of spherulites remains an area of Intense study. However a summary of the current knowledge suggests that spherulites consist principally of radial arrays of chain-folded lamellae that are highly elongated In the radial direction. The stacks of lamellae radiating from a central nucleus have somewhat the appearance of fibrils. This Is represented schematically In Figure 5.2. In Figure 5.3 the crystal axes are superimposed on a PHB spherulite and a diagram of the molecules In the PHB unit cell are given for completeness.

5.1.2 Theory of optical extinction patterns and polarized microscopy

The study of spherulites by the polarizing microscope Is the most common [219] and historically, the oldest of methods [223]. A great deal has been learned about the grosser features of spherulitic structure from its application and when coupled with the fine details observed by electron microscopy, it serves as a unified picture of the structure of polymer spherulites.

The polarizing microscope itself Is a standard Instrument fitted with a pair of polarizing filters, one above and one below the specimen. When the two polarizers are In the crossed position with their permitted vibration directions orthogonal, then no light
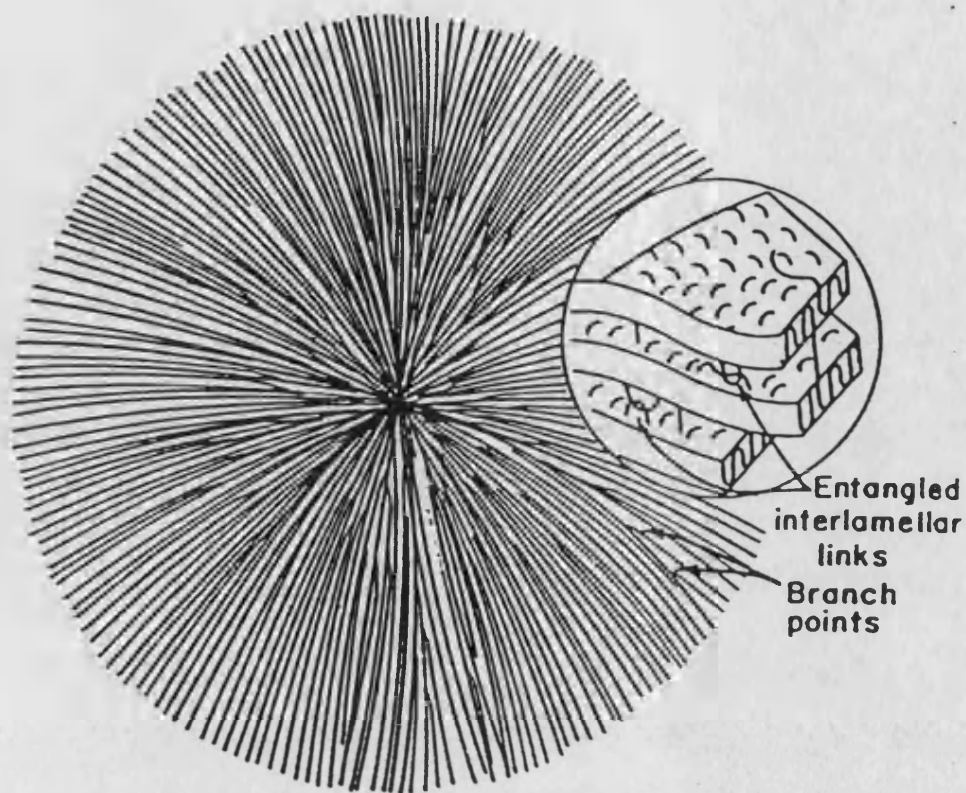
Polymer spherulite with chain-folded lamellae (schematic). Spherulite consists of chain-folded lamellae radiating from central point. Polymer chain axes in lamallae are more or less perpendicular to radius of spherulite. Branching causes spherulite to become spherical in shape after sufficient growth. Noncrystallizable material (not shown) when present accumulates between lamellae and at outer boundary. Twist of lamellae when present causes rings in optical extinction patterns

Figure 5.2. A diagramatic representation of a polymer spherulite showing the underlying morphology (from ref. 220).
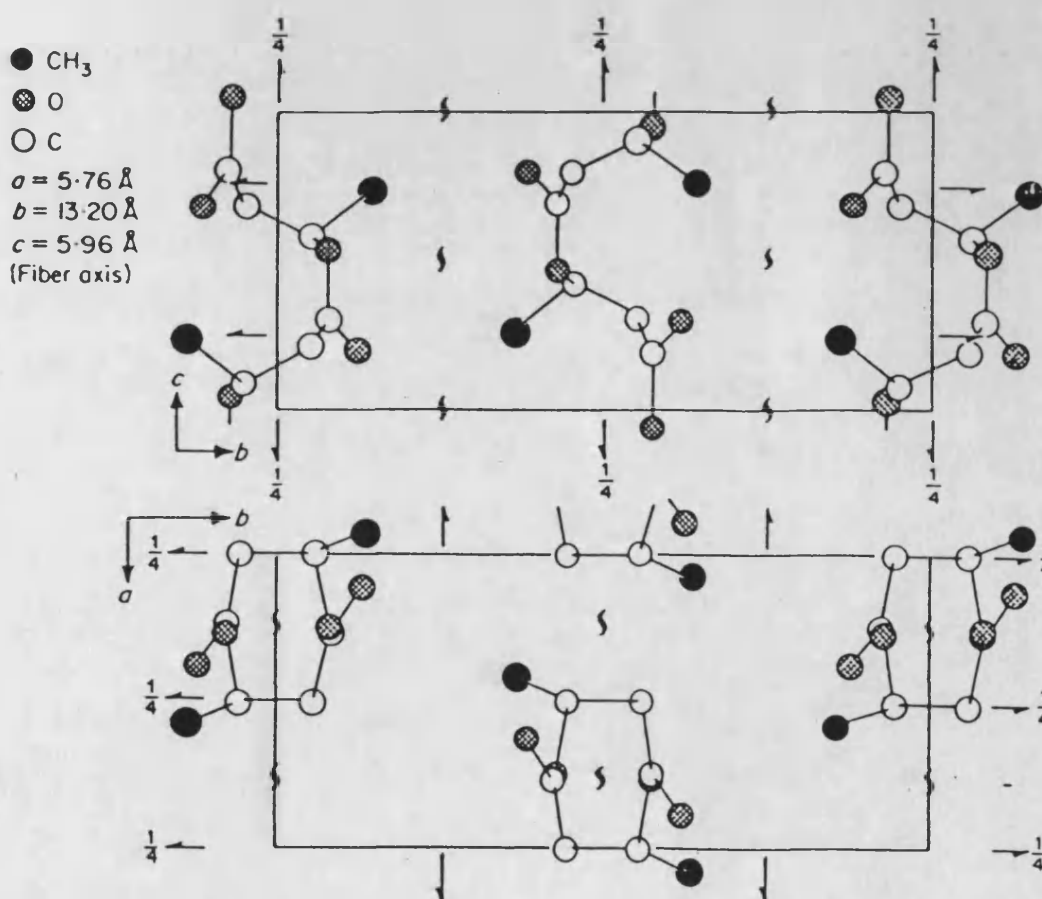
Figure 5.3. A diagram indicating the crystal axes in a PHB spherulite. Above, the crystal axes are superimposed on an optical micrograph of a spherulite; below, a diagram of the molecules in the unit cell of PHB is reproduced (after ref. 214 and 235).

passes through the microscope in the absence of a specimen, or if the specimen is isotropic. Inserting a doubly refracting (birefringent) specimen gives rise to beam splitting and interference phenomena which allow light to pass through the instrument. Such specimens will appear bright, even coloured, against a dark background [438].

The utility of the observations with the polarizing microscope stems from the fact polymer crystals are anisotropic with respect to their optical properties. The polarizability in the direction of the chain axis is usually different from that normal to the chain direction [439 – 440]. This results from birefringence, which is defined as the difference between the refractive indices of light with its electric vector parallel to the chain axis and light with its electric vector normal to the chain axis.

The interpretation of the characteristic extinction patterns for spherulites viewed between cross polars has had an important bearing on the determination of their structure [219]. In favourable cases the sign and magnitude of birefringence can provide information on the molecular orientation [227]. The sign of birefringence is usually determined using an accessory plate (1 or 1/4 wavelength optical path difference) which is inserted into the microscope above or below the specimen. A spherulite is considered positive in sign if the radial refractive index is higher than the tangential [438]. This is done by observing the change in polarizing colours produced. Barham *et al* [214] have found that PHB spherulites are negatively birefringent and the derived crystallographic axes have been shown in Figure 5.3.

The simplest and most common extinction pattern seen in spherulites is the Maltese cross with its arms parallel to the polarizer and analyser vibrational directions. This is usually superimposed on the 'fibrillar' texture of spherulites. The fact that in some cases spherulites exhibit more complex extinction patterns was first reported in 1952 by Keller [441]. These are of four types: 1) a pattern in which, in addition to the Maltese cross, concentric extinction rings with regular periodicity are seen, 2) a pattern as above but with rings paired so that there is double periodicity, 3) a pattern in which

the Maltese cross is replaced by a zig–zag, and 4) a pattern in which concentric extinction rings are seen in addition to the zig–zag.

The patterns were originally explained by Keller [441] and by Point [431] to arise from a periodic variation in the orientation of the constituent birefringent structural units along the radius. This was not a novel explanation and the concept had been suggested and discussed many years earlier by, for example, Wallerant [442] in the case of nonpolymeric spherulites. However following the discovery of chain–folding in polymer crystals, the patterns were fully analysed and explained in a set of interesting papers published simultaneously in 1959 by Keith and Padden [443–444], Price [445] and by Keller [446]. The explanation, substantiated by electron microscopy observations, showed that the concentric extinction rings arise because the crystal orientation rotates about the radius in progressing from the centre of the spherulite outward. This was due to the fact that fibrils twist as they grow. Even more remarkable was the fact that neighbouring fibrils twist with the same period and same phase, that is, they twist cooperatively. Keith and Padden [444] found that the hand, however, may be different along different radial paths and at rather well defined radial boundaries the hand changes discontinuously from right to left.

Cooperative twisting and the resultant complex extinction patterns have been observed in various polymers including polyethylene, poly(ethylene adipate) and poly(ethylene terephthalate), and while it has been extensively studied, its origins remain one of the unsolved problems of polymer morphology [219]. The reason for the twisting of chain folded lamellae is still unclear. In the same polymer it sometimes occurs and sometimes does not. Point [431] found that at relatively high undercoolings in polyethylene, ringed (or banded) spherulites were formed but at higher temperatures, unringed spherulites were formed.

The period of twist (ring or band spacing) depends upon the temperature of crystallization [431] and has been found to increase with increasing temperature [440,478]. In polyethylene, the ring spacing varies from about 1um to some tens of

micrometres [219]. Various mechanisms have been proposed to explain twist [447] but it is fair to say that none of them account convincingly for the experimental findings [219].

5.1.3 Formation and evolution of spherulites

The formation of spheulites is a feature of crystal growth which is still not well understood [229]. Precisely how a spherulite develops depends, in the first instance, on how it is nucleated. A common progression, but not essential, is that shown in Figure 5.4, beginning with a fibre or a single crystal and evolving through sheaf-like embryos (bundles) before attaining a sphericle envelope [424]. Following the discovery of chain folding, studies by Bassett et al [448] showed that these sheaf-like precursors were multilayered, chain-folded structures akin to the crystalline objects which had been variously and collectively referred to as axialites and/or hedrites. The latter are formed when polymers are crystallized from concentrated solution and from the melt at low undercoolings (undercooling refers to the difference between equilibrium melting and crystallization temperatures of the sample) [219]. The term axialite was first coined by Bassett, Keller and Mitsuhasi [448] to apply to multilayered objects grown in relatively concentrated solutions of polyethylene in xylene. The lamellae in these objects formed diverge apparently from a central axis and the objects exhibit polygonal or sheaf-like appearances, depending on the direction in which they are viewed. The term hedrite was first coined by Geil [425] to distinguish polygonal objects formed in melt-crystallized polymers from the more common spherulites. The reason as to why these structures diverge and fan out to form spherical entities remains unclear. Khoury and Barnes [449] have suggested that the lamellae are intrinsically curved and that the sheaving in axialites is a phenomenon of curved crystal formation but this has not been fully examined.

The spherulite growth sequence given in Figure 5.4, represents, according to Keith and Padden [428-429,450], successive stages in the evolution of an initially formed lamellar chain-folded crystal which degenerates progressively as it grows under the
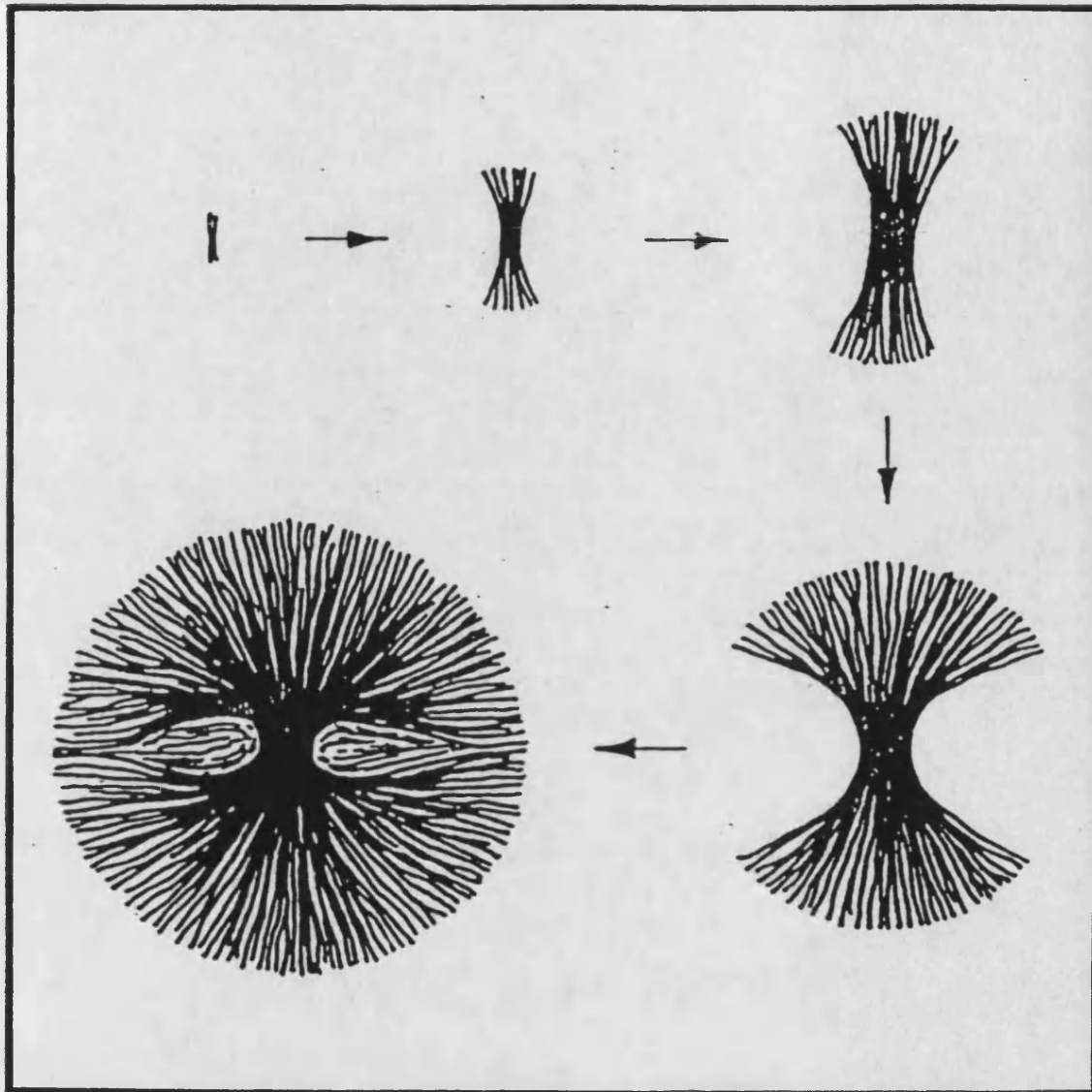
Figure 5.4. Schematic development of a spherulite from small fibres through sheaving outlines to the mature form (from ref. 227)

influence of impurities (such as low molecular weight polymer fractions) rejected at its lateral growth fronts. This classic theory of Keith and Padden [428–429] is based on diffusional segregation of impurities at interfaces and between lamellae. It has been used to account for the radiating fine fibrillar texture seen in fully evolved spherulites. According to the theory, the fibrillar texture develops from the sheaf–like objects because of a change in the habit of the lamellae [428–429]. This change in habit, from the polygonal single crystal habit to the fibrillar habit has been explained by Keith [451] as being a consequence of cellulation at the periphery of the polygonal lamellae during the early stages of spherulitic growth and is due to diffusional segregation of impurities. Although the theory of Keith and Padden [428–429,450] was developed almost 30 years ago and based primarily on optical observations, it has commanded widespread support, not least for the subtlety of textures for which it could account [227]. However, modern techniques of etching coupled with the greater detail of the fine structure now possible with electron microscopy has led to some modifications to the original theory [227]. A recent report by Vaughan and Bassett [229] suggests that the internal fibrillar texture is due to a spherulitic framework of individual dominant lamellae which branch and splay. This is qualitatively different from the cellulation model of Keith and Padden [428–429,450]. Furthermore, Vaughan and Bassett [229] have concluded that there is no clear evidence in favour of habit changes due to cellulation. This subject and the theory of Keith and Padden will be further discussed in relation to drug distribution in melt processed polymers (section 5.5.7).

5.1.4 Kinetic Growth Theory and Crystallization Kinetics.

The kinetics of polymer crystallization can be divided into three aspects [219]: a) the overall crystallization kinetics of the transformation of liquid to solid; b) the radial growth rate of spherulites; and c) the interfacial kinetics concerning the molecular details of the kinetic processes that occur at the crystal growth front (as described later).

There have been many attempts to develop theories to explain these important aspects of

crystallization but to date, none are thought to have been completely successful [452].

The two approaches used most commonly for analysis of crystallization data are those described by Avrami [453-454] and by Hoffman and coworkers [220,455].

5.1.4.1 Avrami equation

The overall crystallization kinetics of polymers in bulk is invariably treated using the Avrami approach which considers the evolution of the volume fraction crystallized [456]. Avrami published two papers relating to the kinetics of phase change in general [453-454]. His fundamental relationship as applied to the crystallization process was:

$$X = 1 - \exp(-Kt^n)$$

where X is the degree of crystallinity, K is the crystallization rate constant, t is the elapsed time and n is the Avrami exponent, usually an integer, characteristic of the type of nucleation and crystallization mechanism.

However, the Avrami model was not intended for polymers [457] and depends on a large number of assumptions which severely limit its applicability. These assumptions, as given by Grenier and Prud'Homme [457] include: constancy of shape of the growing spherulite; constant rate of radial growth; lack of induction time; complete crystallinity of the sample; random distribution of nuclei; primary nucleation process (no secondary nucleation); and absence of overlap between the growing crystallization fronts.

Obviously, all these assumptions cannot be met simultaneously and some of these can hardly be met at all for polymers [457]. Consequently, it has often been found that, contrary to theoretical predictions, nonintegral values of n are obtained [457]. Serious deviations from the Avrami expression can be found particularly towards the latter stages of crystallization because secondary crystallization often occurs and there is usually an increase in crystal perfection with time [452].

Although the Avrami analysis is still regarded as fairly successful in explaining the

178

phenomenology of crystallization it does not give any insight into the molecular process involved in the nucleation and growth of polymer crystals [452]. For the reasons given above and because this study was concerned primarily with the kinetics of growth and not overall crystallization, the Avrami approach was not used in this study.

5.1.4.2 Kinetic Growth Theory

The kinetic theories of crystallization lead naturally to predictions of the temperature dependence of the growth rate of a crystal [424]. The most widely accepted of the kinetic theories is that of Hoffman, Lauritzen and others [220,447] which has been used to explain nucleation and growth of polymer crystals (from solution and melt). Providing the spherulites are formed through the process of heterogeneous nucleation, the primary nucleation is developed from a solid surface such as a dust particle. It is then postulated that growth of polymer crystals takes place by a process of secondary nucleation on the pre-existing crystal surface. This process is similar to primary nucleation but differs somewhat because less new surface per unit volume of crystal is created than in the primary case and so the activation energy barrier is lower [452].

The first step in the secondary nucleation is the laying down of a portion of the polymer molecule on an otherwise smooth chain-folded lamellar crystal surface to form a stable folded nucleus. However, the manner in which this initial polymer stem is laid down is a matter of controversy. It still remains unclear as to whether the stem is attached onto the growth surface in a single process as a whole unit or in successive segments (or flexibility units) [458]. Following the formation of such a nucleus the rest of the long chain molecule is "reeled in", crystallizing with a fixed, temperature-controlled fold distance. This type of nucleation-controlled growth seems very consistent with the current knowledge of the fibrillar growth of spherulites [229,427].

The basic thrust of the theory is that the rate of formation of a chain-folded surface nucleus, i.e. the net flux, simultaneously governs the crystal growth rate and the initial lamellar thickness and has been outlined by Hoffman et al [220]. Applying the

179

flux equation approach to the theoretical idea of Turnbull and Fisher [459] on the crystallization kinetics of small molecules, Hoffman [220,455] has given the linear growth rate (G) of polymer spherulites as:

$$G = G_o \exp[-U^*/R(T-T_\infty)] \times \exp\left[-K_g\left(\frac{1}{T \triangle Tf}\right)\right] \qquad ....5.2$$

where G_o is a constant, U^* is an activation energy for transport of molecules to the growth front, R is the gas constant, T is the crystallization temperature, T_∞ is the temperature below which molecules become immobile, $\triangle T$ is the supercooling,

also where $f = 2T/(T^\circ_m + T)$ $\qquad ....5.3$

and $K_g = Kb_o \sigma\sigma_e T^\circ_m/k\triangle H_f$ $\qquad ....5.4$

where T°_m is the equilibrium melting temperature (melting temperature of infinitely thick, defect-free crystal), k is the Boltzmann constant, b_o is the monomolecular layer thickness, $\triangle H_f$ is the heat of fusion, $\sigma\sigma_e$ is the product of the lateral and end surface free energies, and K may have the value of 2 or 4 depending on the growth mechanism.

Hoffman et al [220] originally proposed two different growth regimes in polymer crystals depending on the relative rates of formation and spreading of new secondary nuclei at the growth front (Figure 5.5). Regime I is thought to occur at low supercoolings when the rate of spreading is so large compared to the rate of nucleation that a nucleus once formed spreads right across the growth front. Regime II occurs at higher or intermediate supercoolings when several secondary nuclei form and spread across the growth front together, the separation between them decreasing as the supercooling increases.

More recently, Hoffman [460] has proposed a third regime of growth in polymer crystals. Regime III is thought to occur at sufficiently high supercoolings when the separation between secondary nuclei is of the order of a molecular width and no more spreading takes place. The three regimes may be distinguished by the value of the constant K in the equation for K_g (equation 5.4); in Regimes I and III it takes the value 4 and in

Growth front morphology for regime I and regime II growth (schematic). Regime I: diagrams at left. Single nucleus forms on surface, rapidly completes new layer. Folds are all parallel to edge of crystal; $K_g = 4b\sigma\sigma_e T_m^0/(\Delta h_f)k$. Regime II: diagrams at right. Many new surface nuclei form before previous layer is complete, leading to reentrant or crenelated growth front. Some folds are now parallel to direction of overall growth; $K_g = 2b\sigma\sigma_e T_m^0/(\Delta h_f)k$.
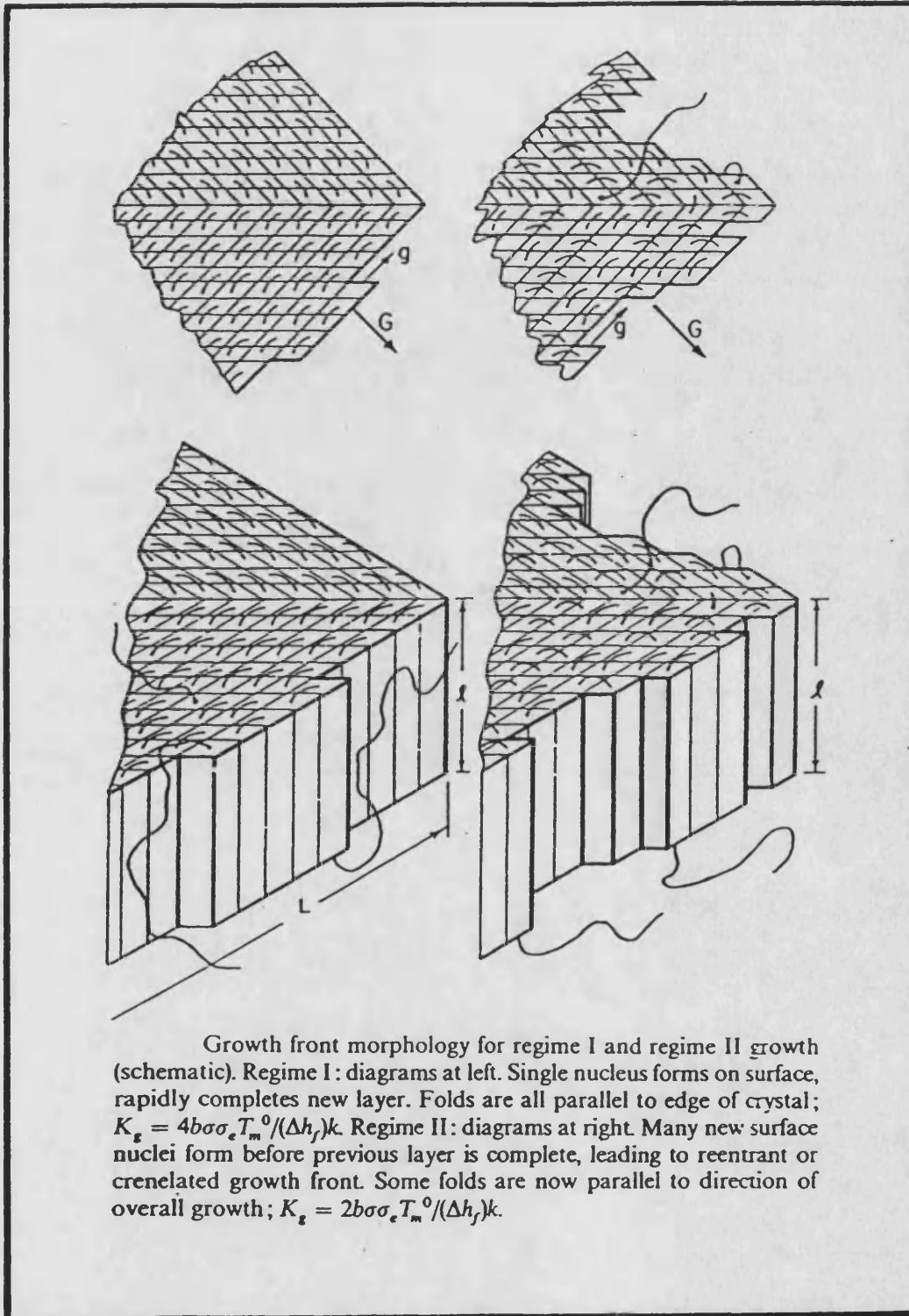
Figure 5.5. A schematic diagram of growth regimes in polymer crystals (from ref. 220).

181

Regime II it takes the value 2. The derivation of the equations, which involves complex mathematics based on the thermodynamic flux theorem, can be found in the work of Hoffman and others [220] or in the book by Bassett [424] and will not be included here.

The type of growth exhibited by a polymer system can be determined by converting equation 5.2 into a linear plot. The use of the equation for the data on spherulitic growth of P(HB-HV) polymers is described in the discussion (section 5.5.6).

The kinetic theory of Hoffman and coworkers [220] (also known as HL theory) has largely been based on knowledge from solution-grown crystals but continues to be used for melt-crystallized polymers in ways analogous to those for solution crystallization [424]. Much of the reason for this has been the considerable difficulty in producing firm facts to show how the behaviour differs in the two cases [424]. Although the theory is still widely used it has been modified on several occasions [220,461-462] since the original work [463]. Major criticisms of the HL theory have been made by Point [458,464-465] and by Sadler [466] who have proposed alternative theories to explain crystallization. In a very recent paper Point and Dosiere [465] have radically questioned the validity of the HL theory and concluded that regime I does not exist in practice and is completely hypothetical. The authors suggest that even the latest version of the HL theory [462] cannot account for kinetic crystallization data on polyethylene, the interpretation of which was a keystone in developing the original HL theory of polymer crystallization. They report that various characteristic lengths (such as the mean persistence length, L_p) are inconsistent with the modern versions of the HL theory and thus highlight some conceptional shortages of the kinetic theory [465]. It is thought that with the current advances in bulk polymer morphology, further modifications of the theory may result from renewed theoretical activity in this important area.

5.1.5 Theory relating to equilibrim melting temperature

The equilibrium melting temperature (T°_m) of a polymer has been defined as the melting temperature of an infinitely thick crystal [467] or a crystal with no surface [408] or

the melting of a large perfect crystal in an extended – chain configuration [427]. The concept of T°_m was introduced because of the variability in the melting behaviour of polymers [408] (see chapter 3). The experimentally derived melting point is usually much lower than this value because of the thinness of the polymer crystals [427] due to chain folding. This is particularly disturbing because accurate values of T°_m are required to test the theories of crystallization quantitatively, for example undercoolings are taken from T°_m.

T°_m can, however, be determined by a number of extrapolation methods [467]. The most commonly used method is that described by Hoffman and coworkers [220,468]. These authors showed that the lamellar thickness, I, of polymer crystals is a function of the temperature of crystallization. They also showed that when such crystals remain at the crystallizing temperature their initial lamellar thickness, l_g^*, increases by a factor, y, to the final thickness, I, according to equation [468] :

$$I = yl_g^*$$

They found that, with certain simplifying assumptions, the melting of thickened crystals could be represented by the following equation [220]:

$$T_m = T^{\circ}_m [1 - (1/y)] + (T_c/y) \qquad \ldots\ldots\ldots\ldots 5.5$$

where T_m = the experimentally determined melting point

T_c = temperature of crystallization

Equation 5.5 shows that the observed melting is always greater than the crystallization temperature and that a plot of T_m against T_c is always linear. Since T_m can never be lower than T_c the line $T_m = T_c$ will represent the lower limit of the melting behaviour. The point at which extrapolation of the upper line meets the $T_m = T_c$ line then represents the T°_m.

An interesting melting point relationship which requires fewer assumptions and that has a straightforward theoretical basis is the following [469]:

$$T_m = T^{\circ}_m [1 - (2\sigma_e/l\triangle H_f)] \qquad \ldots\ldots\ldots\ldots 5.6$$

where σ_e = end surface energy

$\triangle H_f$ = heat of fusion

l = lamellar thickness

Typically from equation 5.5 a plot of T_m against 1/l will result in a straight line. The intercept of which gives an estimate of T°_m. However, because l needs to be determined from complex procedures involving small angle diffraction or electron diffraction this method was not used in this study. The extrapolation of a plot of T_m against T_c to the $T_m = T_c$ line is a much simpler approach and is that used in this study.

5.2 AIMS AND OBJECTIVES

1. To study the crystallization kinetics and morphology of melt-crystallized P(HB-HV) polymers.

2. To study the effect of molecular weight and HV content on crystallization growth curves for P(HB-HV) polymers.

3. To study the effect of model drugs on crystallization kinetics and morphology of P(HB-HV) polymers.

5.3 MATERIALS

P(HB-HV) containing 16mole% HV (PHV16; Mw=41k) was purchased from Marlborough Biopolymers Ltd, UK.

All other materials were identical to those given in chapters 2 and 3.

5.4 METHODS

5.4.1 Measurement of radial growth rates of P(HB-HV) spherulites by polarized light microscopy

All polymer samples were used as solution cast films except for PHB43K and PHV16 which

were used in purified powder form.

Samples (2-3mg) of PHB and P(HB-HV) copolymers were heated to melt between two thin glass slides at 195°C for 30-60 seconds on a Monotherm hot plate (Rodwell Scientific Instruments Ltd). Polymer samples were then rapidly transferred to a Mettler FP82 hot stage linked to a Mettler FP80 central processor programmed for isothermal heating at a chosen crystallization temperature, T_c. The hot stage was connected to a polarizing optical microscope (Vickers) and radial growth of spherulites was recorded onto video tape (Scotch, Magnetic Media Division/3M, UK) using a Hitachi colour video camera with a V102 Vertical enhancer (Hitachi Denshi Ltd, Japan) and a Panasonic AG6200 VHS video cassette recorder. Spherulite radius, R, was measured directly from a calibrated flat monitor screen as a function of time, t. Radial growth rates, G, were then calculated from the relationship:

$$G = \delta R / \delta t$$

The value for G was, therefore, derived from the slope of the linear plot of R versus t.

5.4.2 Preparation of PHB samples containing model drugs

P(HB-HV) polymer films containing Methyl Red were prepared by solvent casting as described in chapter 2.

5.4.3 Melting points of crystallized samples in the estimation of the equilibrium melting temperature

Isothermally crystallised spherulites of polymers were heated to melt in the Mettler FP82 hotstage at a programmed heating rate of 10K/min. The point at which birefringence just disappeared was taken as the melting point of the sample.

5.4.2 DSC of isothermally crystallized P(HB-HV) spherulites

Polymer samples (2-3mg) were placed in DSC aluminium pans and heated to melt in a Mettler hot stage at 195°C for 30-60 seconds.
The samples were isothermally crystallized at the different crystallization temperatures

until crystallization was complete. The spherulites thus obtained were subsequently heated to melt at 20K/min in a Dupont DSC 910/9900 Thermal analyser.

5.4.3 X−ray diffraction of isothermally produced spherulites

Solvent cast films (3cm x 1cm; 30−50um) of polymers were heated to melt on a glass slide at 195°C for 30−60s and isothermally crystallized in a Mettler hot stage as before. The glass slide containing the film of spherulites was then analysed by X−ray diffraction (CuK−alpha source) over a diffraction angle of 4−30°. A Philips PW 1820/00 computer controlled vertical goniometer with a Philips PW1710 diffractometer control was used. Intensity measurements were made using a Xenon proportional counter (Philips PW1711/10) with graphite monochromator and automatic divergence slit assembly.

5.5 RESULTS AND DISCUSSION

5.5.1 Linear radial growth rates of spherulites

Spherulites nucleate and grow radially from a central nucleus until impingement occurs. They form by nucleation at different points in the sample and grow as spherical entities. Figure 5.6 shows the progressive growth of PHB spherulites under isothermal conditions. Note that they lose their spherical outline on impingement, at which point it becomes polyhedral. The type of outline or shape of spherulites on impingement is governed by the relative nucleation rate of adjacent spherulites. If neighbouring spherulites are nucleated simultaneously then they will have a planar interface, otherwise a common boundary will be a hyperboloid of revolution. As a result of variations in shape, morphology of spherulites was characterized in terms of their average size and internal fine structure.
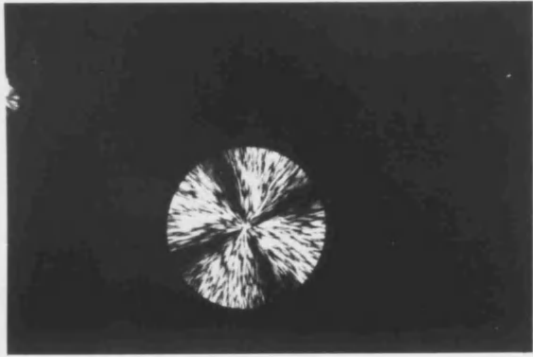
Figure 5.7 shows the linear growth rate of PHB spherulites crystallized isothermally at 90°C. The rate of growth (or velocity of radial advance) of spherulites prior to impingement was remarkably linear with time at a constant temperature. This is a common finding in polymers and deviations from linear radial growth have only been detected when spherulites near impingement or when the viscosity of the melt is deliberately

Figure 5.6. A series of optical micrographs showing the progressive growth of PHB spherulites under isothermal conditions as a function of time (A − F) over a period of 30 s at 75°C.
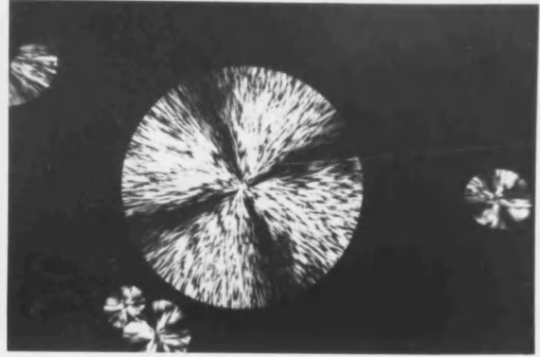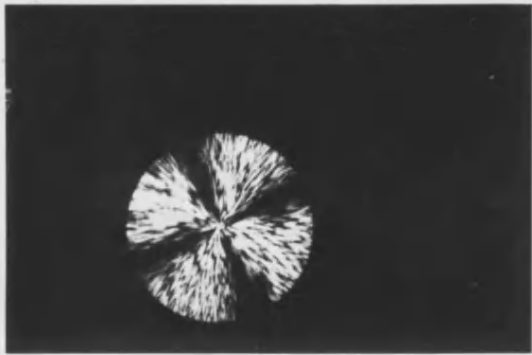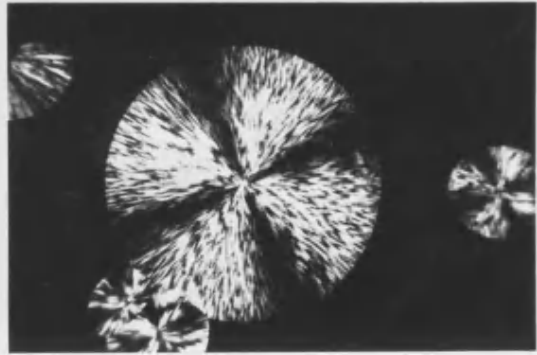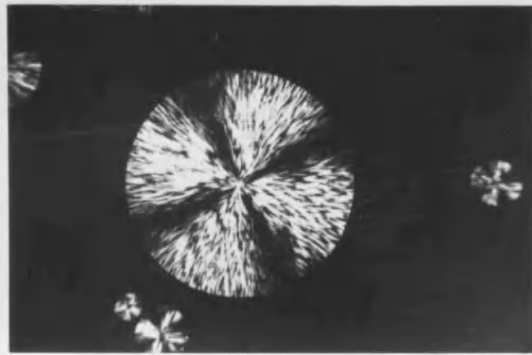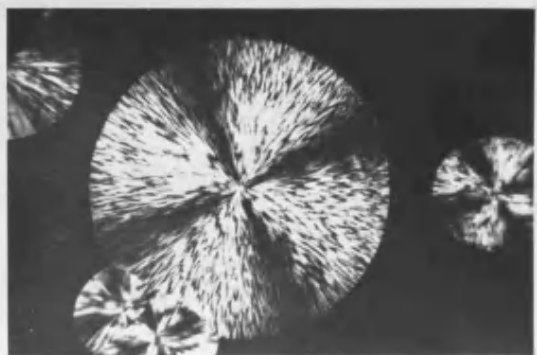
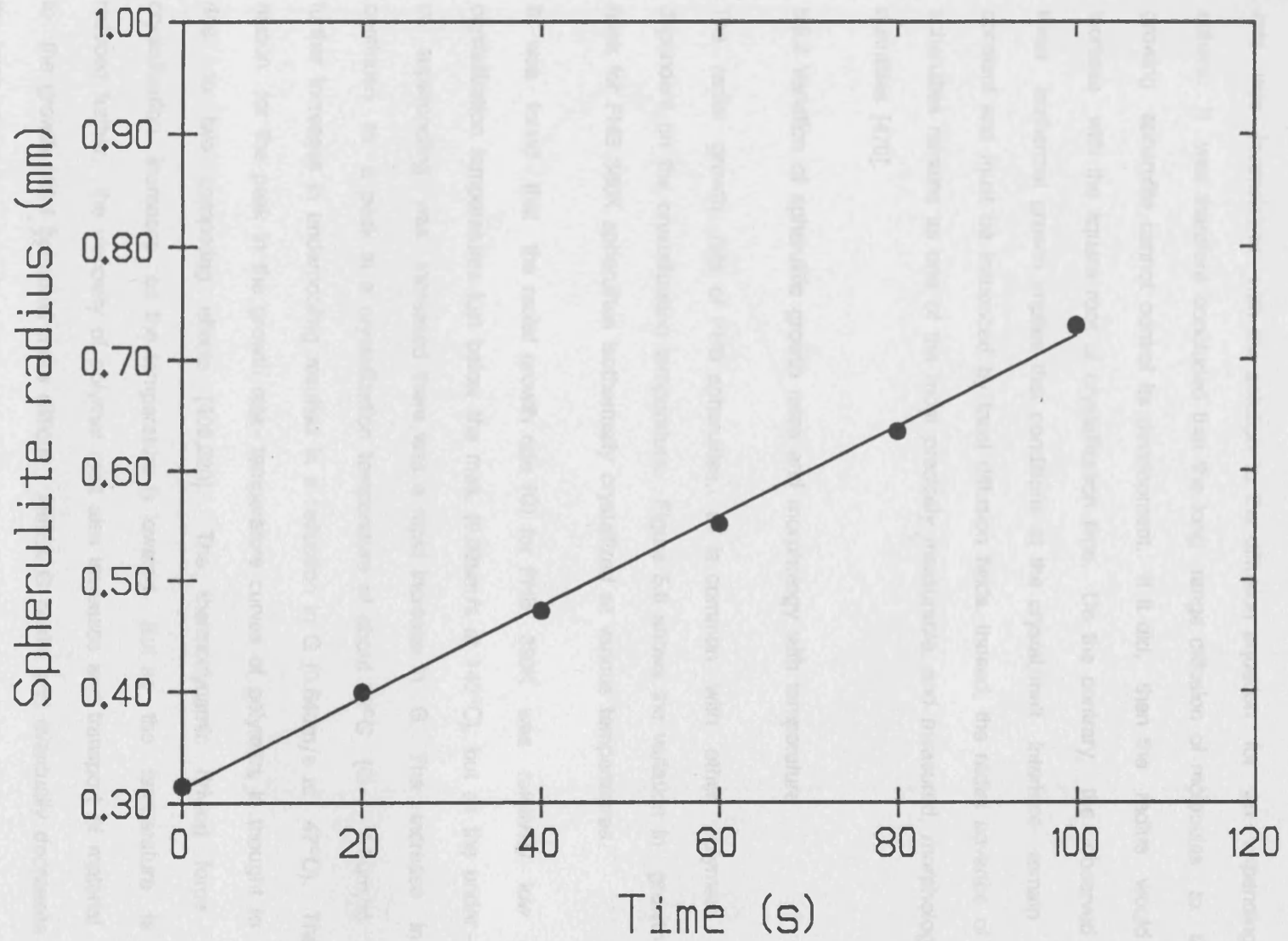Scale bar (A − F) = 500um.   ├────────┤

A

B

C

D

E
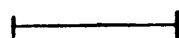
F

Figure 5.7. Linear growth rate of PHB380K spheulites grown
isothermally at 90°C (Mean; n = at least 2).
(S.D = less than 5% of Mean)

reduced [424]. It was pointed out by Keith and Padden [450] that this constant growth rate was inconsistent with the solution to the diffusion equation for an expanding sphere. It was therefore concluded that the long–range diffusion of molecules to the growing spherulite cannot control its development. If it did, then the radius would increase with the square root of crystallization time. On the contrary, the observed linear isothermal growth implies that conditions at the crystal/melt interface remain constant and must be influenced by local diffusion fields. Indeed, the radial advance of spherulites remains as one of the most precisely measurable, and measured, morphological quantities [470].

5.5.2 Variation of spherulitic growth rates and morphology with temperature

The radial growth rate of PHB spherulites, as is common with other polymers. was dependent on the crystallization temperature. Figure 5.8 shows the variation in growth rates for PHB 380K spherulites isothermally crystallized at various temperatures.

It was found that the radial growth rate (G) for PHB 380K was relatively low at crystallization temperatures just below the melt, (0.02um/s at 140°C), but as the under– or supercooling was increased there was a rapid increase in G. The increase in G continued to a peak at a crystallization temperature of about 90°C (G= 4.5um/s) and further increases in undercooling resulted in a reduction in G (0.64um/s at 47°C). The reason for the peak in the growth rate–temperature curves of polymers is thought to be due to two competing effects [408,220]. The thermodynamic driving force for crystallization increases as the temperature is lowered. But as the temperature is reduced further, the viscosity of polymer melt also increases and transport of material to the growth point becomes more difficult. Hence G peaks and eventually decreases as the temperature is reduced even though the driving force continues to rise. The detailed thermodynamics of the growth rate–temperature profiles will be analysed in section 5.5.6.
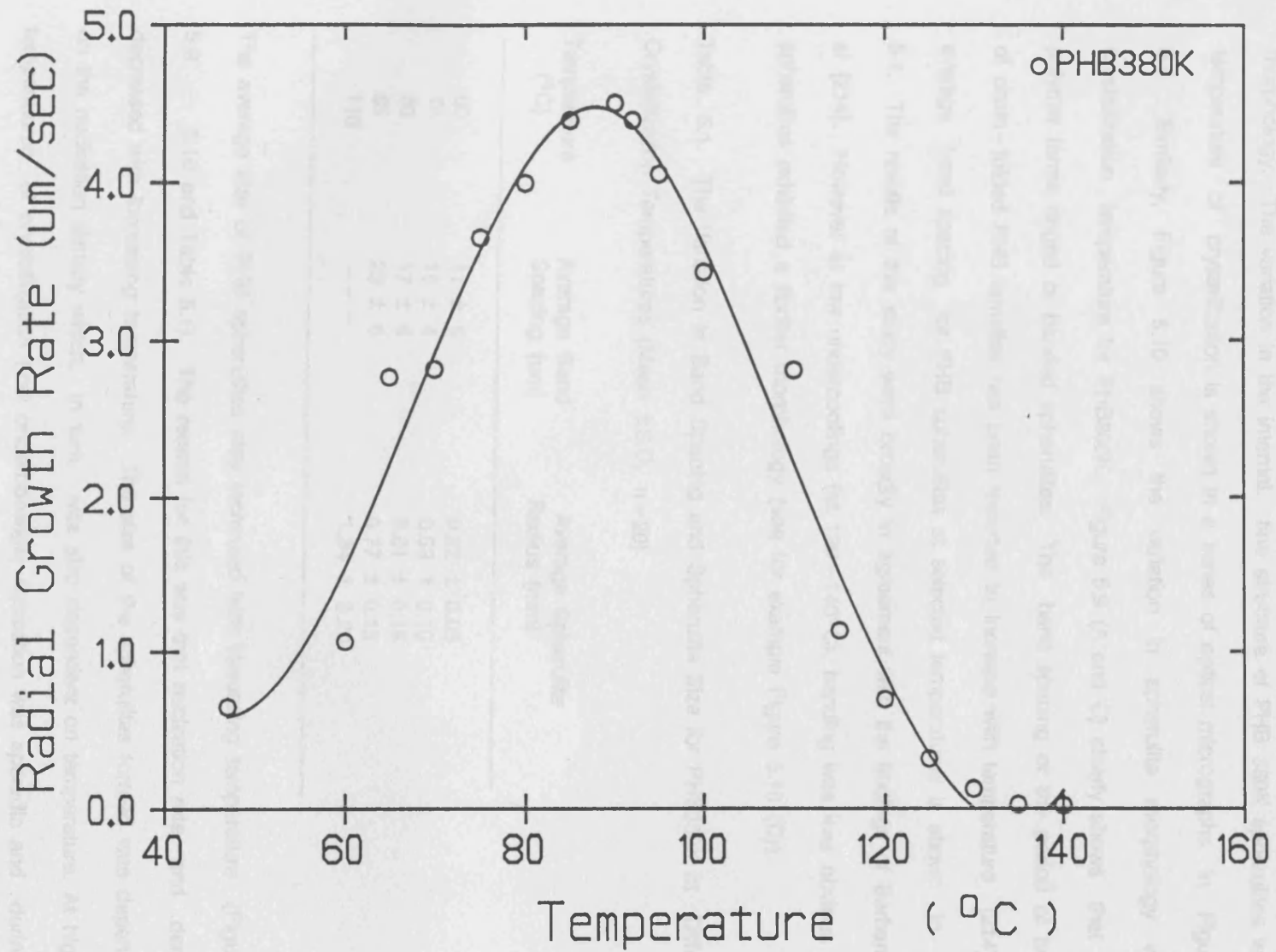
Figure 5.8. Growth rate – temperature profile for PHB380K
spherulites (Mean; n = at least 2).
(S.D = less than 5% of Mean)

Changes in growth rate of PHB 380K spherulites also resulted in changes in their

morphology. The variation in the internal, fine structure of PHB 380K spherulites with

temperature of crystallization is shown in a series of optical micrographs in Figure

5.9. Similarly, Figure 5.10 shows the variation in spherulite morphology with

crystallization temperature for PHB800K. Figure 5.9 (A and C) clearly shows that the

polymer forms ringed or banded spherulites. The band spacing or the period of twisting

of chain-folded PHB lamellae has been reported to increase with temperature [214]. The

average band spacing for PHB spherulites at selected temperatures is shown in Table

5.1. The results of this study were broadly in agreement with the findings of Barham et

al [214]. However at low undercoolings (at 120-140°C), banding was less obvious and PHB

spherulites exhibited a fibrillar morphology (see for example Figure 5.10 (D)).

Table 5.1. The Variation in Band Spacing and Spherulite Size for PHB380K at Different

Crystallization Temperatures (Mean ±S.D, $n = 20$)

Temperature (°C)	Average Band Spacing (um)	Average Spherulite Radius (mm)
60	11 ± 5	0.22 ± 0.05
70	15 ± 4	0.53 ± 0.10
80	17 ± 4	0.61 ± 0.15
85	29 ± 6	0.77 ± 0.13
110	– – –	1.34 ± 0.20

The average size of PHB spherulites also increased with increasing temperature (Figures

5.9 - 5.10 and Table 5.1). The reason for this was that nucleation rate and density

decreased with increasing temperature. The size of the spherulites formed was dependent

on the nucleation density which, in turn, was also dependent on temperature. At higher

temperatures of crystallization (low undercoolings) nucleation was sporadic and during

melt crystallization of PHB, a relatively small number of large spherulites were

formed. However, at lower temperatures many more nuclei formed (higher nucleation rate

and density) and a large number of smaller spherulites were obtained. A reduction in the

rate of nucleation was also found to decrease with increasing temperature, thereby

Figure 5.9. Optical micrographs of PHB380K spherulites isothermally crystallized at various temperatures

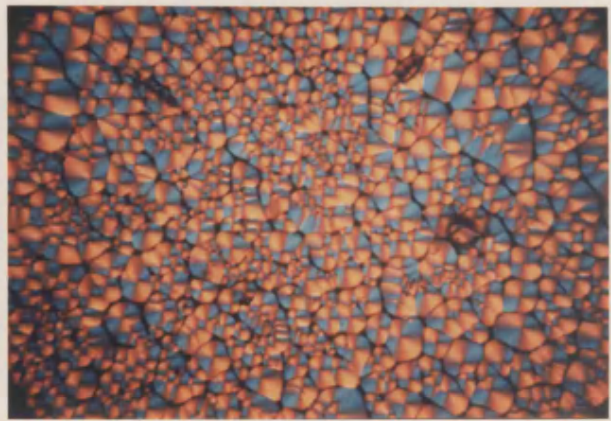(A = 60°C, B = 90°C and C = 110°C).

Scale bar (A–C) = 1mm

Figure 5.10 Optical micrographs of PHB800K spherulites isothermally crystallized at various temperatures

(A = 42°C, B = 60°C, C = 95°C and D = 135°C).

Scale bar (A – D) = 1mm.
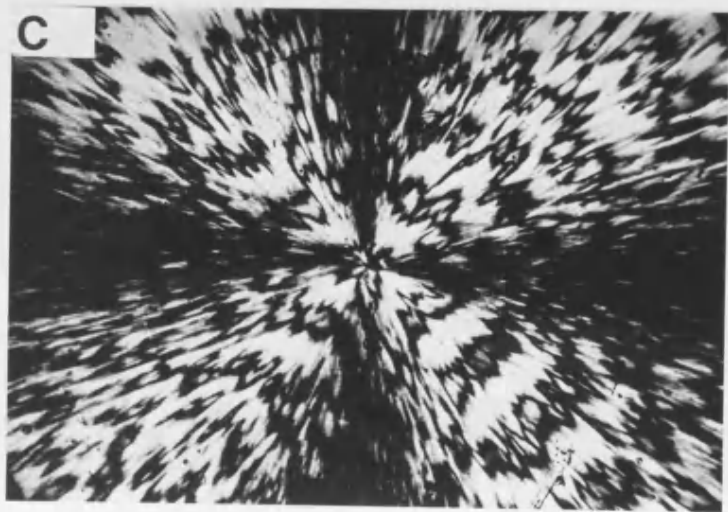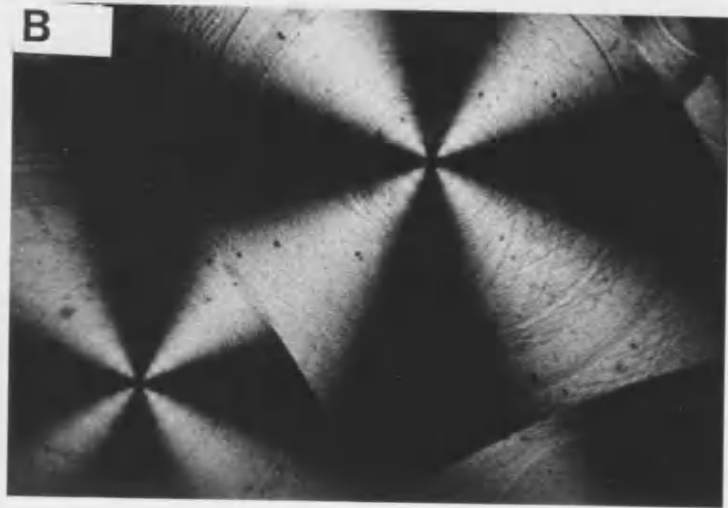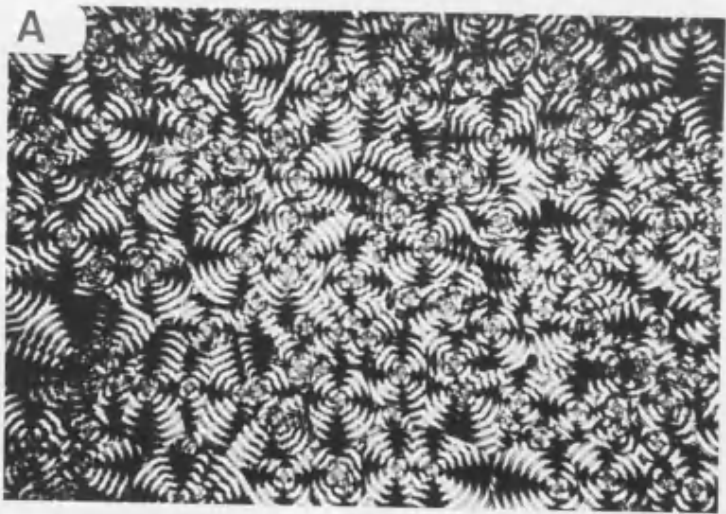
reducing overall crystallization time, but this was not quantified.

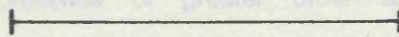At low undercoolings, nucleation of PHB spherulites was, in this study, found to be heterogeneous. This was confirmed by spherulites reappearing at the same sites following melting and recrystallization of PHB. Barham and coworkers [214 – 215] have carried out preliminary studies on the nucleation and crystallization behaviour of PHB spherulites. The results on spherulite size and nucleation from this study are in agreement with the findings of Barham and coworkers [214 – 215].

It should be noted that, unlike polyethylene [424], a complete growth rate profile could be obtained for PHB. For polyethylene, growth is so fast that only for the higher end of the curve (low undercoolings) can growth rates be accurately measured. Other polymers for which the whole curve can be measured include isotactic polypropylene and isotactic polystyrene [424]. This fact, coupled with the highly pure nature of bacterial PHB resulting in large spherulites (up to several millimetres at low undercoolings), make it an ideal model for studying polymer crystallization [214]. The large spherulite size can be disadvantageous because it confers brittleness to specimens but the size can be controlled by the addition of suitable nucleating agents [215].

5.5.2.1 X – ray diffraction and DSC of spherulites

X – ray diffraction and DSC were used to assess changes in the crystalline nature of spherulites with the temperature of crystallization. Crystallinity clearly increases as the spherulites form and grow but this study was concerned with examination of fully formed spherulites, i.e. at impingement and when all the available space in sample had been occupied.

Figure 5.11 shows the X – ray diffraction traces for PHB samples fully crystallized (where spherulites occupied all available space in sample) under isothermal conditions at 60, 90 and 110°C. The peaks in X – ray diffraction traces become sharper with increasing temperature suggesting the presence of greater order at the higher temperatures. This was confirmed with increases in heats of fusion of PHB samples from

Figure 5.11. X – ray diffraction traces for PHB380K spherulites isothermally crystallized at various temperatures.
(A = 60°C, B = 90°C and C = 110°C).
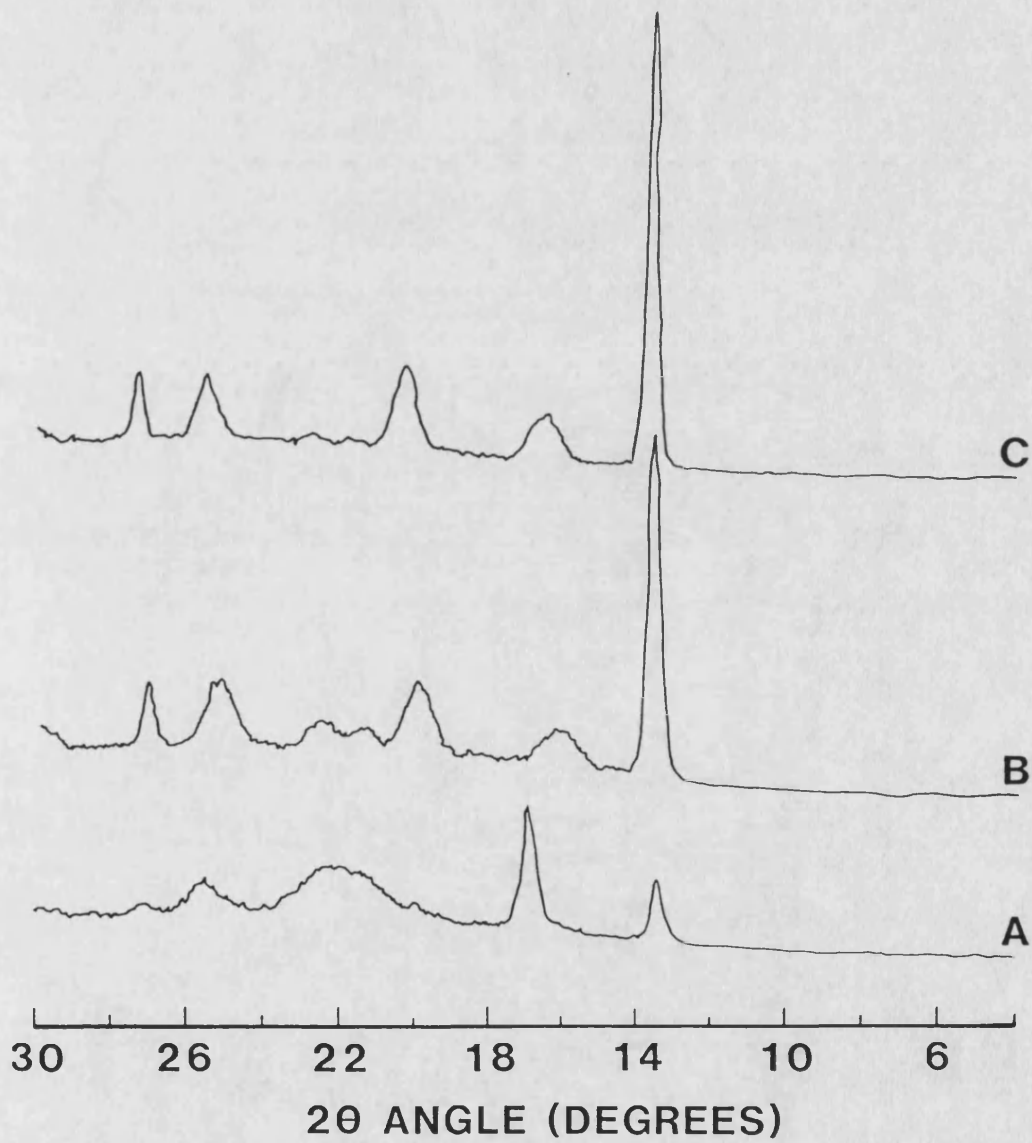
DSC studies (Table 5.2). Although these results suggested that the degree of crystallinity increased with increasing temperature, they may also be interpreted to indicate an increase in the perfection or quality of crystals. This perfection was primarily thought to be due to increases in lamellar thickness and although not determined in this study, it has been found to increase with other polymer systems crystallized or annealed at elevated temperatures [471 – 472].

Table 5.2 Heats of fusion for melt crystallized PHB380K as a function of crystallization temperature (Mean $\pm$ Range; n = 2)

Temperature (°C)	Heat of Fusion (Jg^{-1})
60	87.7 $\pm$ 2.2
90	90.3 $\pm$ 1.4
110	93.1 $\pm$ 1.1

5.5.3 The effect of molecular weight of PHB on spherulitic growth rates

Figure 5.12 shows the growth rate – temperature profiles for three different molecular weights of PHB. The curves appear to be similar for the molecular weights of PHB employed (43K, 380K and 800K). However, the maximum growth rate (G_{max}) for PHB43K spherulites was significantly higher ($p < 0.05$) than the two higher molecular weights (see also Table 5.3). This may be due to a lower viscosity of PHB43K providing less resistance to the radial advance of spherulites.

The polydispersity or molecular weight distribution of polymers has an interesting significance in crystallization in that at a given temperature below the equilibrium melting temperature, the larger molecules tend to crystallize more rapidly than the smaller ones [220]. The polydispersity of the PHB samples used in this study was about 2 but in some polymers, possibly where polydispersity is greater, separation of molecules on the basis of molecular weight can occur during the crystallization process [428]. The short chain lengths tend to accumulate, without crystallizing, near the growing crystal
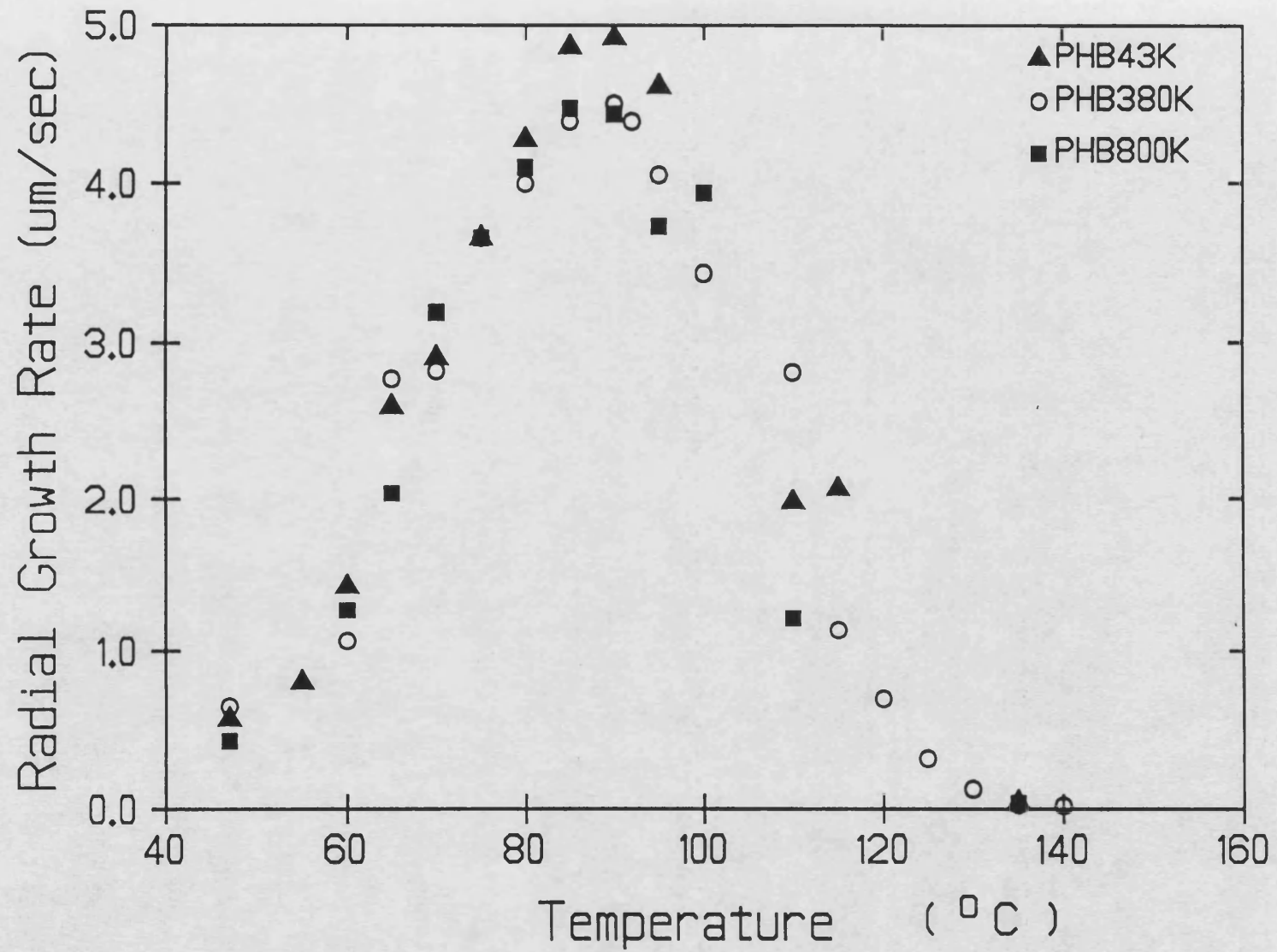
Figure 5.12. The influence of polymer molecular weight on growth rate – temperature profiles for PHB spherulites (Mean; n = at least 2) (S.D = less than 5% of Mean)

boundary [428].

The morphology of spherulites for the different molecular weights of PHB were found to be different. The morphology of PHB43K, PHB380K and PHB800K spherulites crystallized at 90°C is compared in Figure 5.13 (A-C). Furthermore, the morphology of PHB380K and PHB800K at different temperatures can be compared in Figures 5.9- 5.10. The findings of this study do not agree with those reported by Barham *et al* [214] who compared morphologies of PHB samples with different molecular weights. Although Barham *et al* [214] did not compare growth rates for different molecular weights of PHB they did make the following observation, as quoted from their paper, "In general we may say that the lower molecular weight polymer gives a similar morphology to that obtained at higher crystallization temperatures, when using a higher molecular weight". No examples of spherulites grown at different temperatures for the different molecular weights were given by the authors in support of this conclusion. However, the results from this study over the full temperature range indicated that this relationship does not exist.

Table 5.3. Maximum radial growth rates of P(HB-HV) polymers (Mean ±S.D, n= at least 2).

Polymer sample	G_{max} (um/s)	T_c at G_{max} (°C)
PHB43K	4.92 + 0.09	90
PHB380K	4.50 + 0.07	90
PHB800K	4.47 + 0.04	85
PHB380K		
+ 2%w/w MR	3.61 + 0.06	90
+ 8%w/w MR	2.66 + 0.05	80
PHV6	1.42 + 0.04	80
PHV12	0.48 + 0.02	75
PHV16	0.24 + 0.02	70

MR = Methyl Red

5.5.4 The effect of P(HB-HV) copolymer composition on spherulitic growth rates

Figures 5.14-5.15 show the growth rate-temperature profiles for P(HB-HV) copolymers. At any given T_c, the rate of spherulite growth was progressively lowered as the HV content was increased.

Figure 5.13. A series of optical micrographs comparing the morphology of spherulites isothermally crystallized at 90°C.

A = PHB43K
B = PHB380K
C = PHB800K
D = PHV6
E = PHV12
F = PHV16

Scale bar (A – F) = 500um |————————|
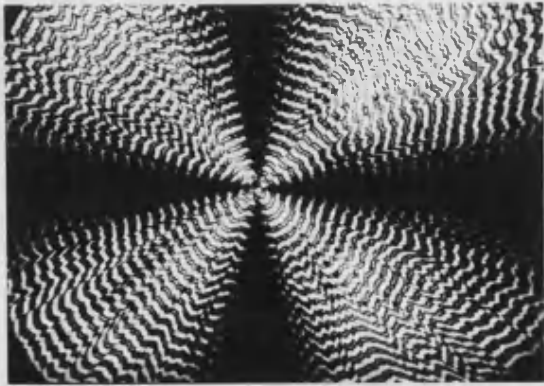
A
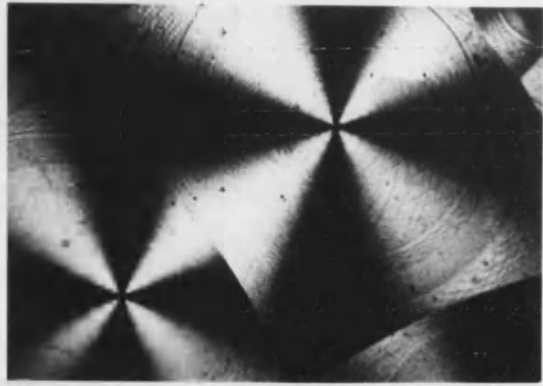
B
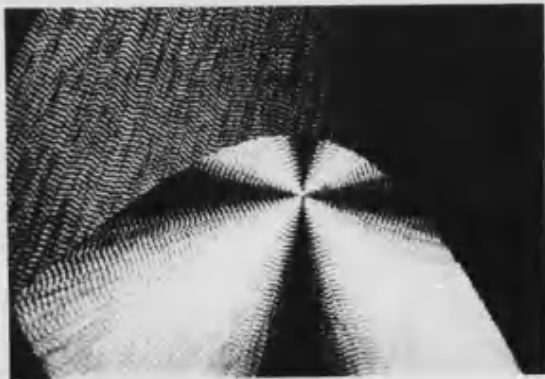
C
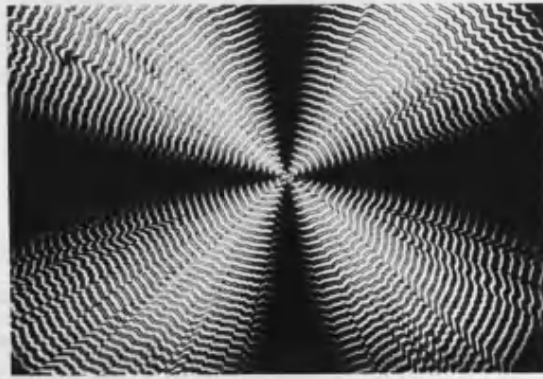
D
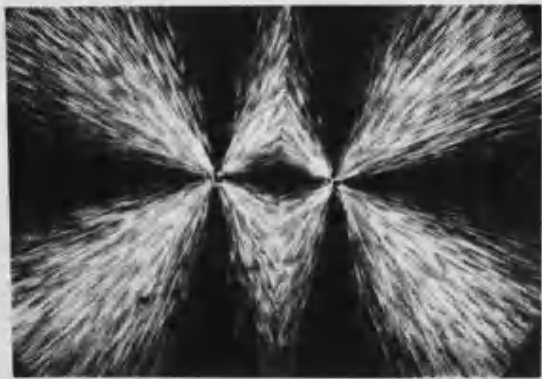
E
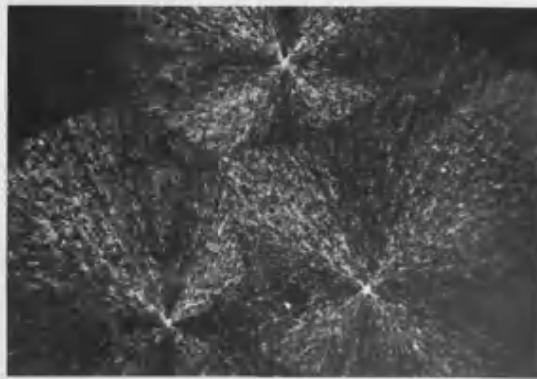
F
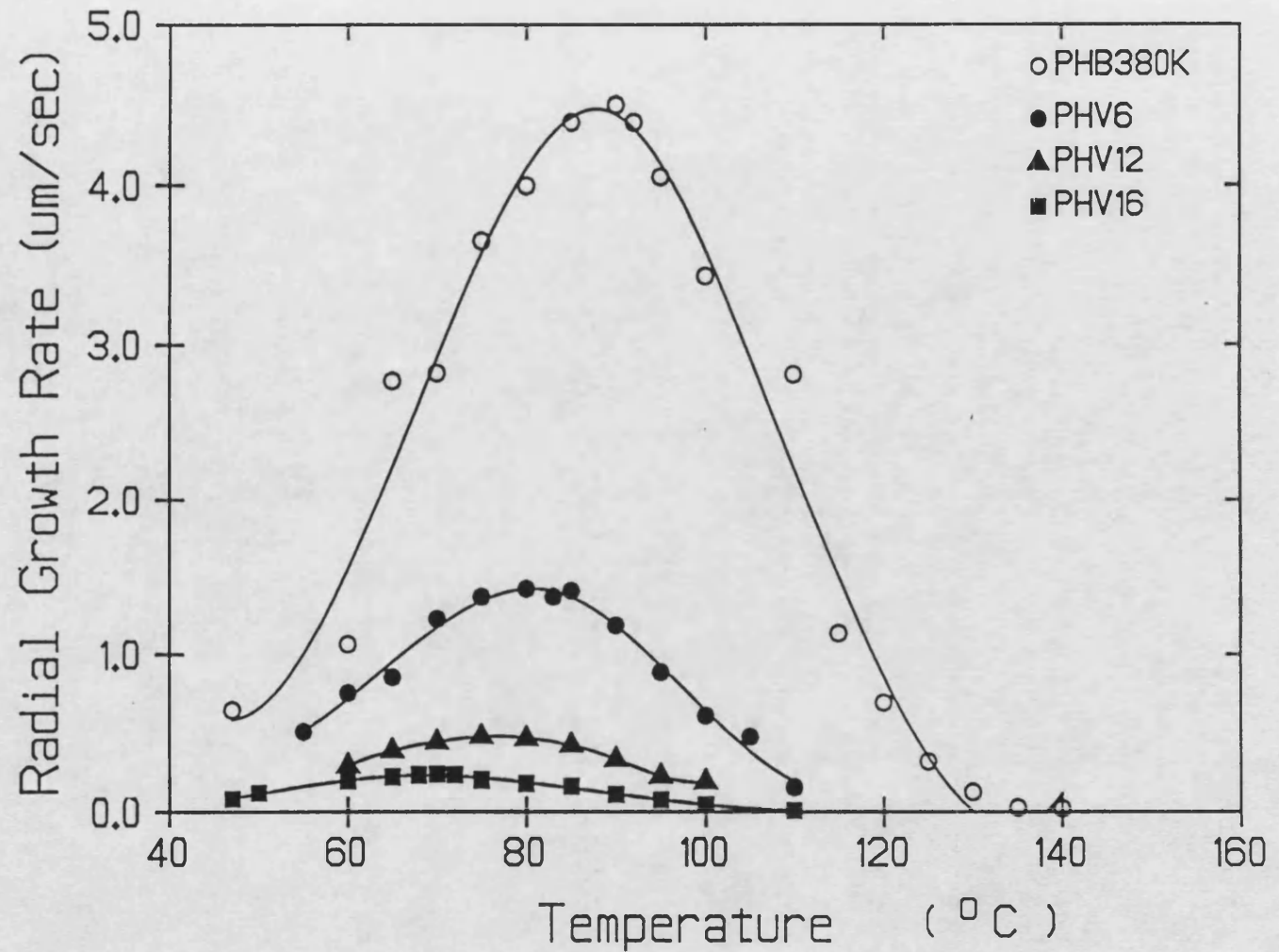
Figure 5.14. A comparison of the growth rate – temperature profiles for PHB380K and P(HB – HV) copolymer spherulites (Mean; n = at least 2). (S.D = less than 5% of Mean)
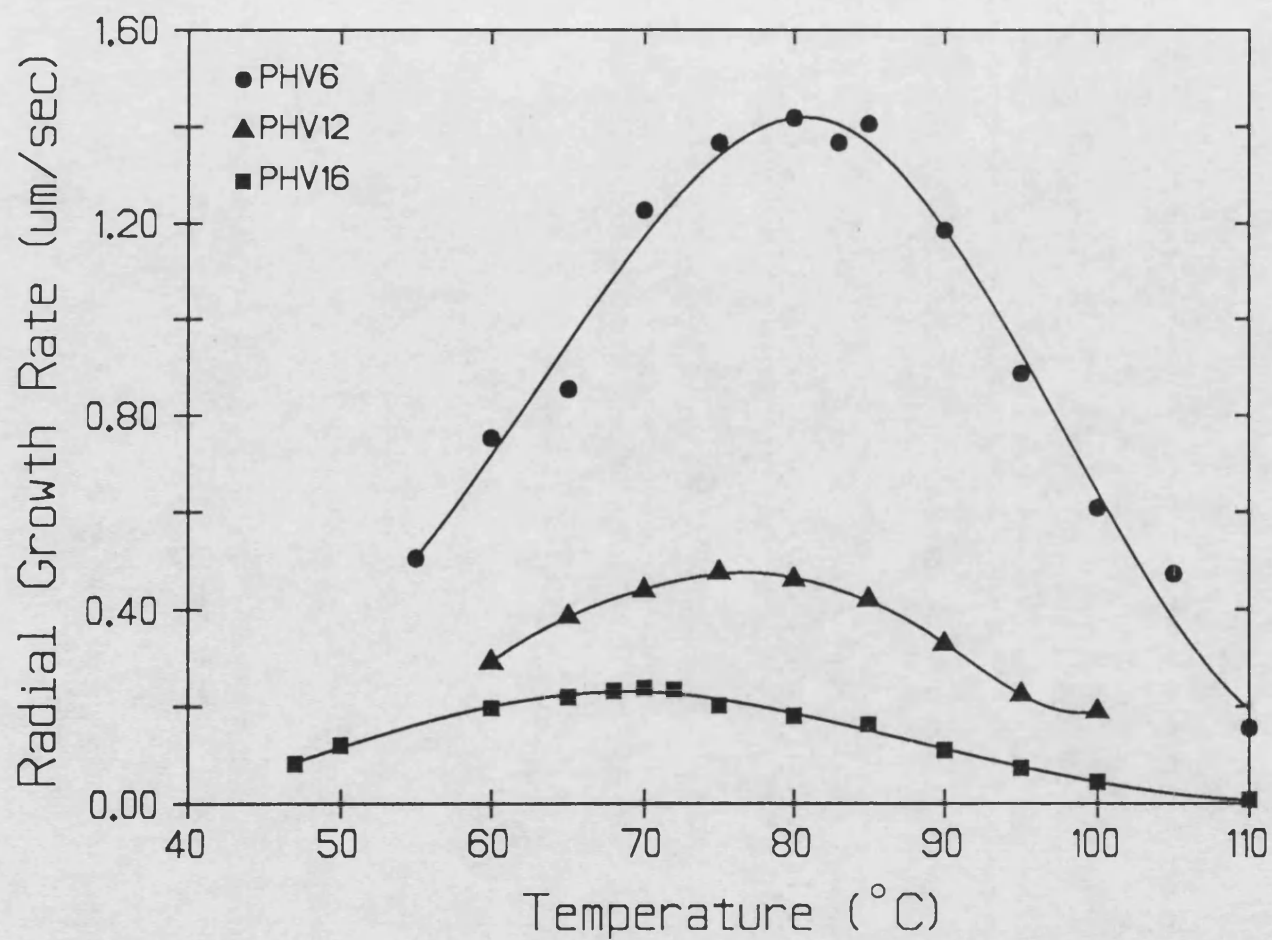
Figure 5.15. Spherulitic growth rate – temperature profiles of P(HB – HV) copolymers (Mean; n = at least 2).
(S.D = less than 5% of Mean)

Figure 5.16 shows the variation of G_{max} as function of HV content. The relationship was not linear and G_{max} decreased to 32% for PHV6, 11% for PHV12 and 5% for PHV16 when compared to G_{max} in the homopolymer, PHB380K. In addition to the reduced rate of spherulitic crystallization, G_{max} was also achieved at progressively lower crystallization temperatures with increasing HV content in copolymers (Table 5.3). The peak in the growth curve for PHB occurred at 90°C whereas for PHV16 the growth curve reached a peak at 70°C. This reflects the depression in equilibrium melting point in the copolymer (see section 5.5.5) and emphasizes the fact that G_{max} is governed by the undercooling (as postulated by Hoffman et al [220]). Figure 5.17 shows growth rates of copolymers plotted as a function of undercooling. G_{max} or the peak in the growth profile of all the copolymers occurred at a similar undercooling to that observed for the homopolymer PHB380K (Figure 5.18).

The progressively slower crystallization for P(HB – HV) copolymers with increasing HV content was thought to be due to the retarded incorporation of the HV components into the common crystal lattice. This was thought to be largely due to the slower transport of chain segments containing HV components to the crystal growth front, possibly because of the larger molar mass of this component resulting from the additional methyl group in the side chain. However the extent to which HV components are incorporated into the PHB crystal lattice remains unclear. Although Marchessault and coworkers [210] suggest that P(HB – HV) copolymers are isodimorphic and therefore the HV components would be expected to be equally distributed between the amorphous and crystalline domains, recent evidence has questioned this hypothesis [249 – 250]. If the degree of crystallinity of the copolymers is similar then equal distribution of HV components between crystal and amorphous domains cannot account for the decreasing density of copolymer samples with increasing HV content [249]. There may be some exclusion of HV from crystals. This would not be unexpected. If the theory of Keith and Padden applies in this case, then HV units may be regarded as impurities and may become, to some extent, segregated and therefore accumulate within amorphous domains in the crystallites or at the interfacial boundaries
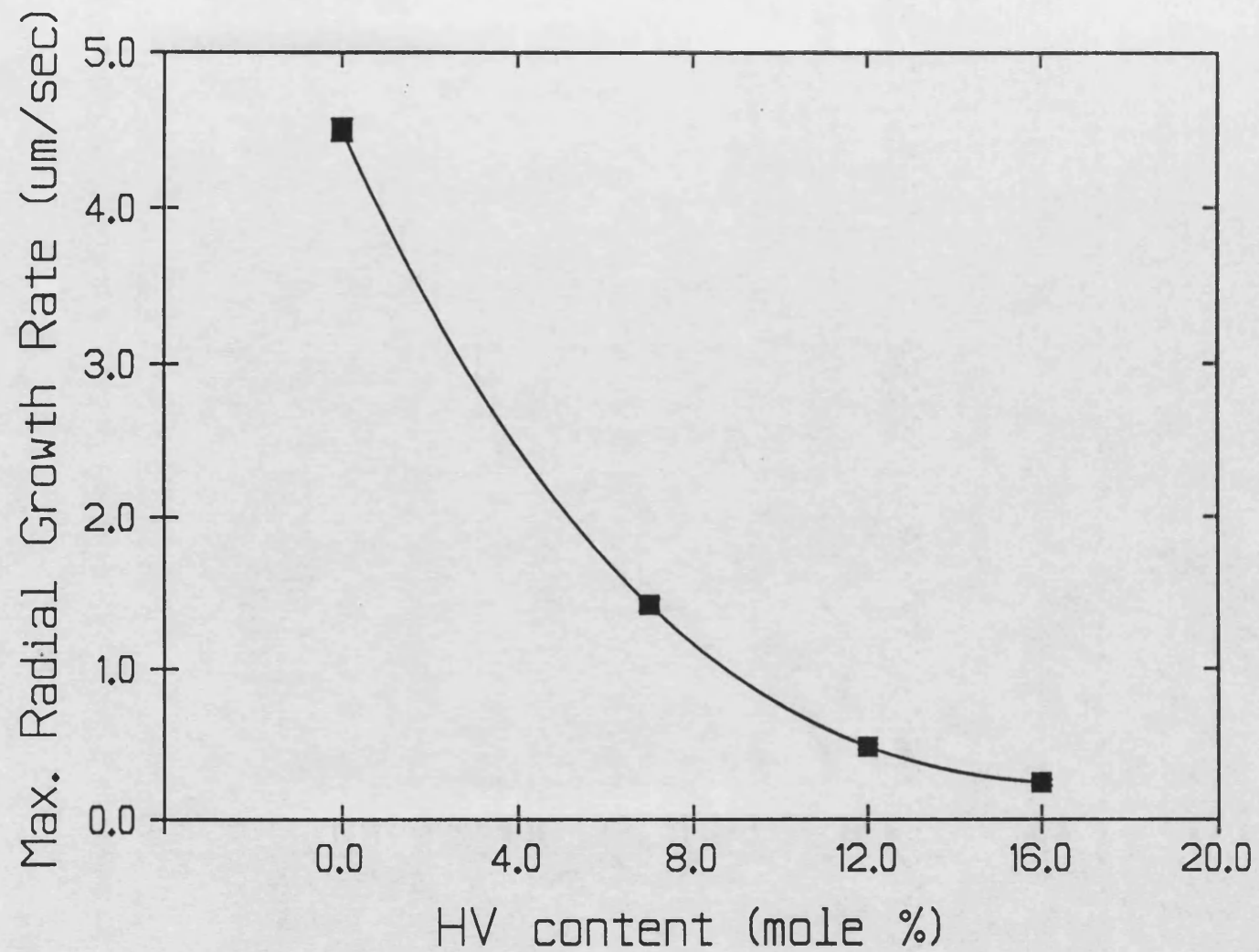
Figure 5.16. The variation in maximal growth rate of polymer spherulites as a function of copolymer composition (Mean; n = at least 2). (Data from Table 5.3).
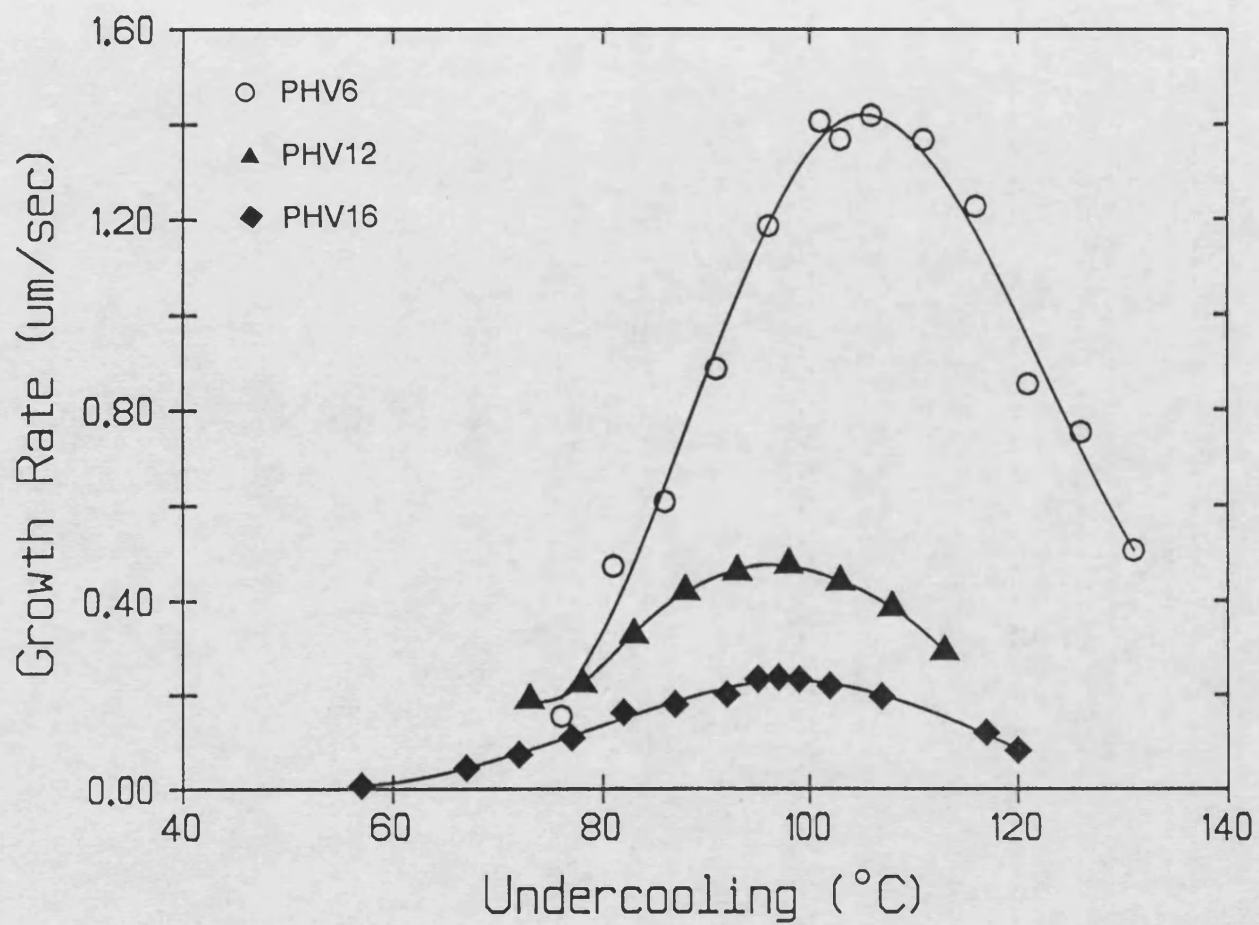
Figure 5.17. Spherulite growth rates as a function of
undercooling for P(HB – HV) copolymers (Mean; n = at least 2).

(S.D = less than 5% of Mean)
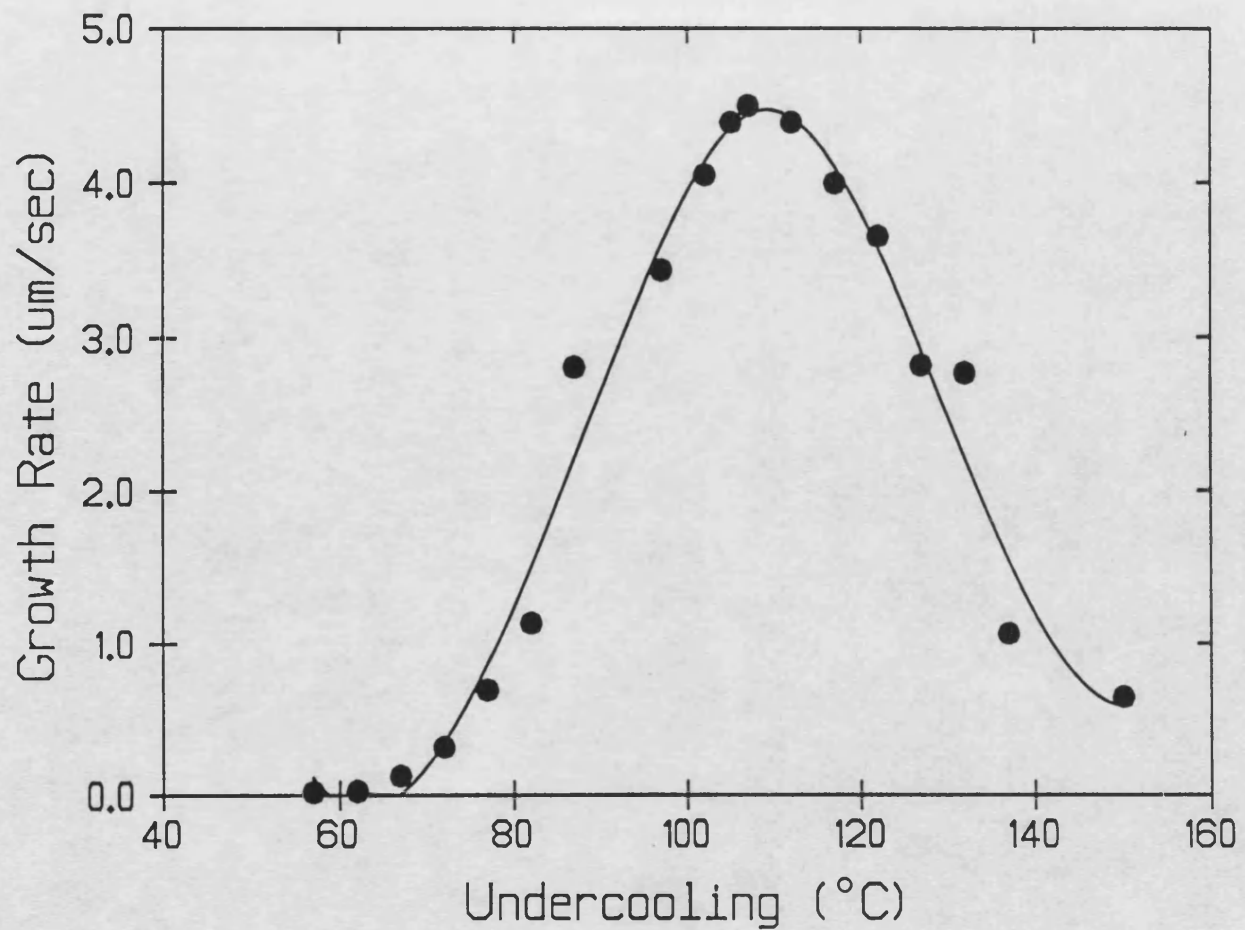
Figure 5.18. Spherulite growth rates as a function of undercooling for PHB380K (Mean; n = at least 2). (S.D = less than 5% of Mean)

of growing spherulites.

At a constant crystallization temperature, the morphology of the copolymers varied with HV content. Figure 5.13 compares the spherulite morphology of P(HB-HV) polymers crystallized isothermally at 90°C. The nucleation rate and density was also progressively reduced on increasing HV content and is reflected in the size of spherulites (Figure 5.13 (D-F)). As a result, at constant temperature the overall crystallization time decreased with increasing HV content but this was not accurately quantified.

5.5.5 Estimation of the equilibrium melting points for P(HB-HV) polymers

Estimation of equilibrium melting temperature (T°_m) was made from extrapolation of linear plots of T_m against T_c to intersect with the $T_m = T_c$ line. Such a plot is shown for PHB380K in Figure 5.19 and for the copolymers in Figure 5.20. Each datum point represents the mean of two replicate experiments. A summary of the values for T°_m are given in Table 5.4.

Table 5.4. Equilibrium melting temperatures of P(HB-HV) polymers.

Polymer	T°_m (°C)
PHB43K	193
PHB380K	197
PHB800K	197
PHV6	186
PHV12	173
PHV16	167

5.5.6 Thermodynamic parameters from spherulitic growth kinetics

The equation of Hoffman given below and in section 5.1.4.2 governs the spherulite growth rate-temperature profiles as seen, for example in Figure 5.14.

$$G = G_o \exp[-U^*/R(T-T_\infty)] \times \exp[-K_g\left(\frac{1}{T \triangle Tf}\right)] \qquad \ldots\ldots\ldots 5.2$$
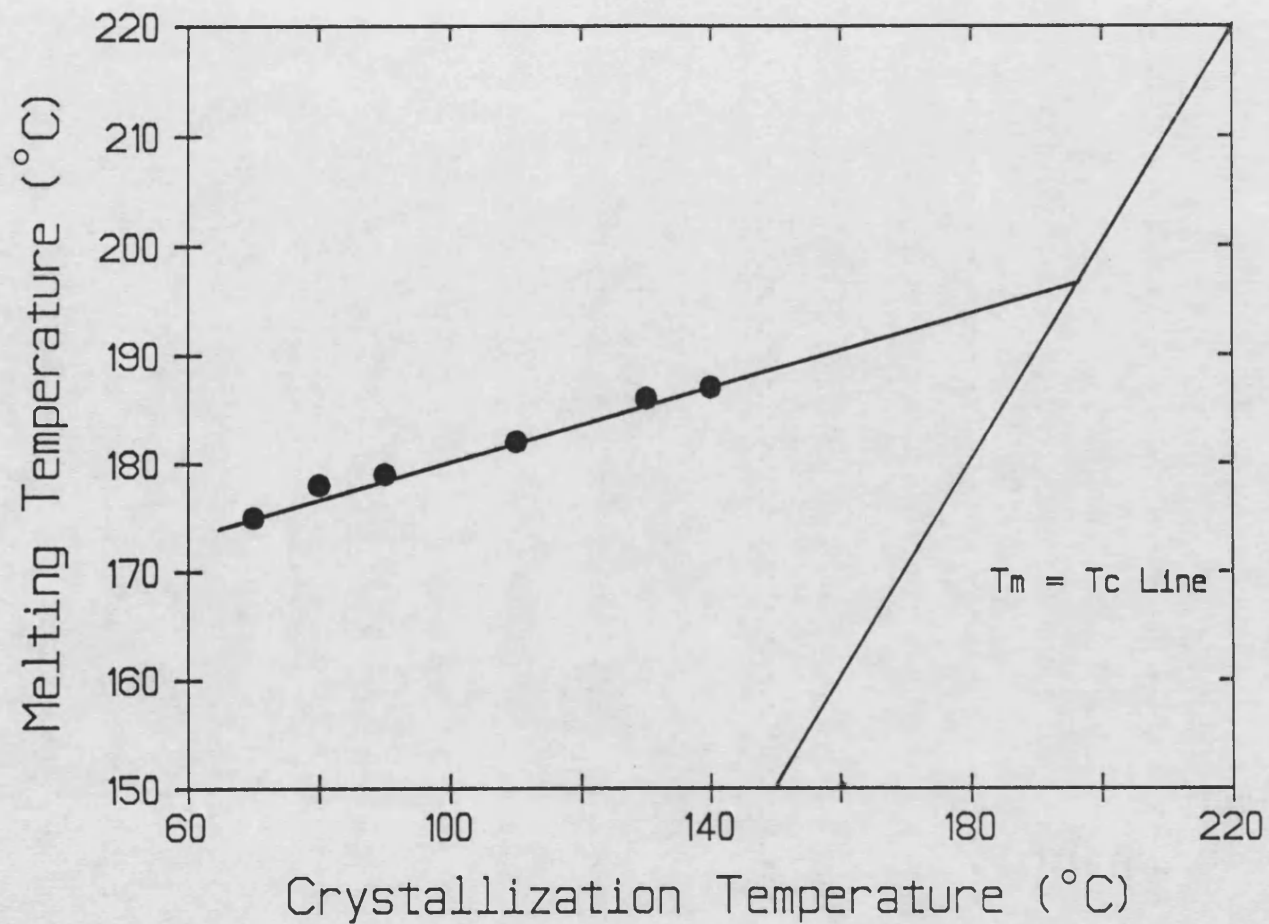
Figure 5.19. A plot of equilibrium melting point data for
PHB380K (Mean; n = at least 2). (S.D = less than 5% of Mean)
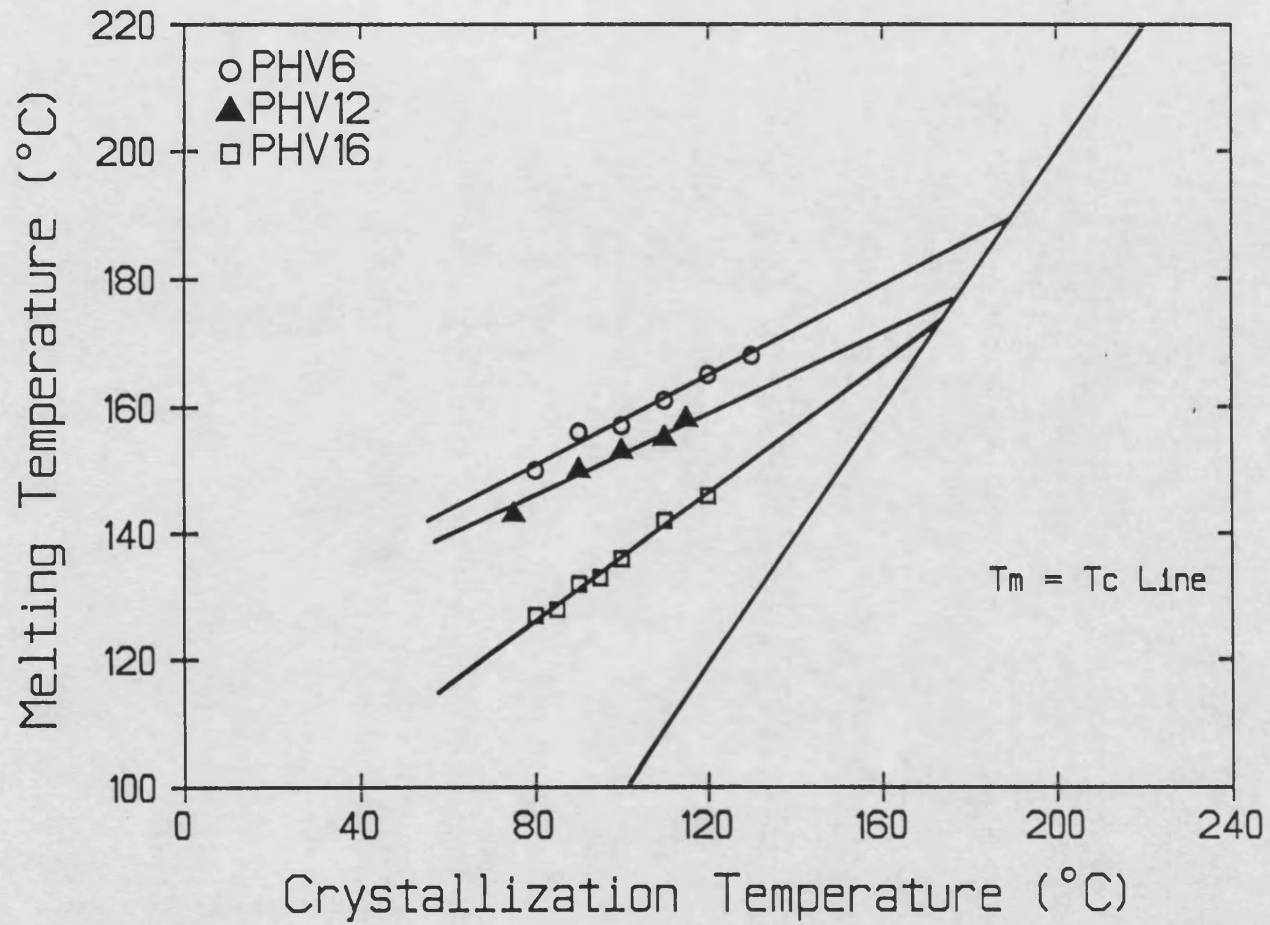
Figure 5.20. A plot of equilibrium melting data for P(HB – HV) copolymers (Mean; n = at least 2). (S.D = less than 5% of Mean)

The rise in growth rate as the undercooling is increased is governed by the expression $\exp[-K_g(1/T\triangle Tf)]$ and the fall after G_{max} is controlled by the opposing factor $\exp[-U^*/R(T-T_\infty)]$ [220,427].

The value for K_g reflects the type of growth occurring at the crystal interface. The growth regime, according to Hoffman et al [220], can be determined experimentally by fitting growth rate data to equation 5.2.

The data represented in the growth curves for P(HB-HV) polymers crystallized at high temperatures (beyond G_{max}) were used in an attempt to fit Hoffman's equation. In order to model this equation values of T°_m, U^*, and T_∞ needed to be estimated. T°_m values were deduced from T_m v T_c plots and are summarized in Table 5.4. Estimates of K_g and hence an insight to the molecular mechanism of growth for PHB and P(HB-HV) copolymers were made by obtaining best linear fits for the growth data when plotted in the form: $\log G + U^*/R(T-T_\infty)$ against $1/T\triangle Tf$. Hoffman et al [220] found that for a fairly large number of polymers values of U^* in the vicinity of 1000-1400 cal/mol and T_∞ values about $30^\circ K$ below T_g give excellent fits. Values of T_∞ of about $20-50^\circ C$ below T_g and values of U^* in the range $0.9 - 1.20 KJ/mol$ gave good fits for P(HB-HV) polymers and the results are summarized in Table 5.5.

Table 5.5. Best-fit values for various parameters in equation 5.2.

Polymer	U^* (KJmol^{-1})	T_∞ ($^\circ K$)	T°_m ($^\circ K$)	K_g (K^2) x 10^5	Regressional Analysis r^2
PHB380K	1.20	230	470	− 1.62	0.9852
PHV6	1.00	250	460	− 1.82	0.9802
PHV12	1.00	260	446	− 2.90	0.9901
PHV16	0.90	265	440	− 1.91	0.9791

The best-fit plots derived from the above parameters are plotted according to the Hoffman equation in Figure 5.21. The slope or K_g value derived for P(HB-HV) polymers from the growth data at high crystallization temperatures suggests that PHB380K
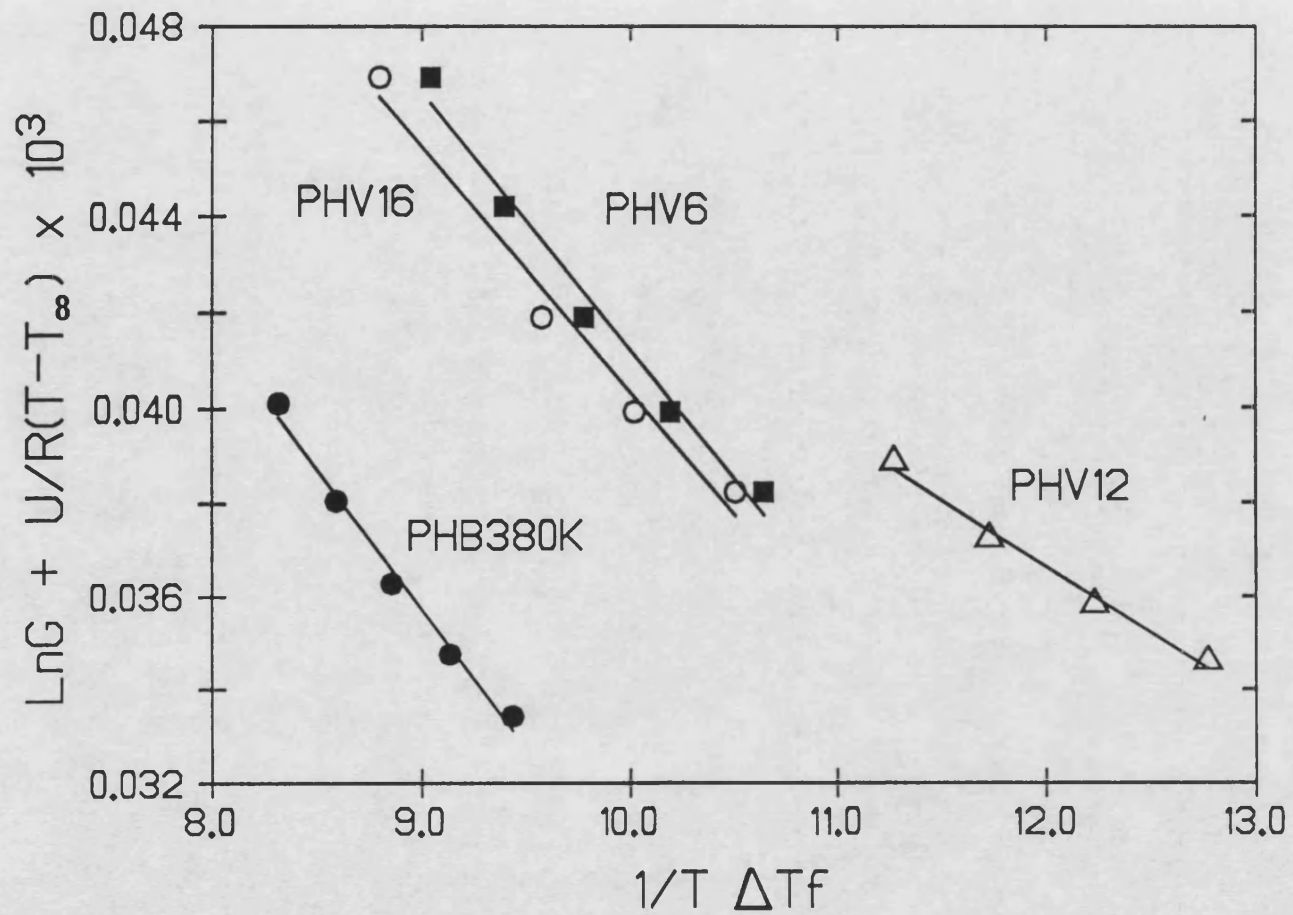
Figure 5.21. Best fits of crystallization data for P(HB – HV) polyesters plotted according to the Hoffman equation to determine growth regimes (see also Table 5.5).

crystallizes according to Regime II. Barham *et al* [214] found that PHB (Mw 358K) crystallized according to Regime III when crystallized at temperatures below 128°C and by Regime II at crystallization temperatures above 135°C. It was therefore concluded by the authors that PHB undergoes a Regime II – Regime III transition within the approximate temperature range 128–135°C [214]. Results from this study suggested that for PHB380K Regime II may actually extend to the lower crystallization temperatures used in this study (as low as 110°C). Regime I has not, as yet, been observed in PHB. This finding may lend support to the idea of Point and Dosiere [465], who in a recent paper, conclude that Regime I, as postulated by the HL theory [220], is hypothetical and does not occur in practice. Furthermore, the authors have severely criticised the use of In G versus $1/T\triangle T$ plots to establish Regime I and thereby have questioned the validity of the HL theory [220]. Clearly the theory needs to be reassessed in the light of comments made by Point and Dosiere [465].

In the case of P(HB–HV) copolymers, PHV6 and PHV16 exhibited similar K_g values to the homopolymer and therefore it must be concluded that they crystallized according to the same regime as PHB380K. However, the K_g value for PHV12 suggested that it may be crystallizing according to Regime III.

Attempts to fit the whole growth curve data for P(HB–HV) polymers according to Hoffman's equation (5.2) using curve fitting software (MINSQ; Micromath Scientific Software, USA and INSTAT; University of Reading, UK) were unsuccessful. The main problem was that G_0 estimates were very different for the different growth regimes (as predicted by HL theory) and no suitable estimate of the parameter gave a good fit. This further highlights the shortfalls of the HL theory which is clearly not ideal in explaining crystallization of polymers.

5.5.7 The effect of drug incorporation in P(HB–HV) polymers on spherulitic growth rates.

Methyl Red was used as a model crystalline drug which is chloroform soluble. Figure 5.22 shows that pure Methyl Red also crystallised from the melt as spherulites. The

Figure 5.22. An optical photomicrograph of Methyl Red
	spherulites.

spherulites exhibited a weak extinction cross and were difficult to detect. Consequently

no growth rate data were obtained for pure Methyl Red. In the presence of PHB, Methyl

Red did not crystallize as separate spherulites suggesting that the drug remained

amorphous and was mixed at a molecular level. The Methyl red was thought to be entrapped

within spherulite boundaries and within the interlamellar fibrils. A similar conclusion

has been derived for blends of PHB and poly(ethylene oxide), PEO [217]. Although PEO is

crystalline it fails to crystallize in the presence of PHB and is thought to remain

amorphous and possibly trapped within the interlamellar regions of PHB spherulites

[217].

Figure 5.23 shows the growth rate – temperature curves for PHB380K loaded with 2 and 8%w/w

of Methyl Red (MR) as a model drug. The G_{max} was substantially reduced on increasing

drug concentration. Loadings of only 2% w/w Methyl Red reduced G_{max} to 80% of that for

pure polymer and at 8% w/w loading the G_{max} was only 59% of that for the pure

homopolymer. An 8% loading of Methyl Red was sufficient not only to reduce the growth

rate of PHB but also to cause a shift in peak to a lower crystallization temperature

(Table 5.3). Again, this was related to the depression in the $T°_m$ of PHB380K containing

8% Methyl Red and therefore a function of the undercooling. For PHB380K containing 8%

MR, a $T°_m$ of 189°C was obtained (determined as in section 5.5.5). The undercooling at

which G_{max} occurred for PHB380K and PHB380K containing 8% MR was, therefore, similar.

The morphology of PHB spherulites was also influenced by the addition of Methyl Red.

Figure 5.24 compares spherulite morphologies of PHB380K containing 2 and 8%w/w drug

loadings at a crystallization temperature of 90°C. There were clearly differences in

spherulite morphology of polymer with increasing drug loading. Comparisons of morphology

with the unloaded polymer can be made by reference to Figure 5.13(B). At an 8% loading

of Methyl Red in PHB380K, there was some evidence to suggest exclusion of drug from

spherulites grown at 80 and 90°C (Figures 5.24(B) and 5.25). This suggested that under

such crystallization conditions a loading of 8% MR may have exceeded the capacity of

drug which can be effectively entrapped within the highly crystalline PHB. The rapid
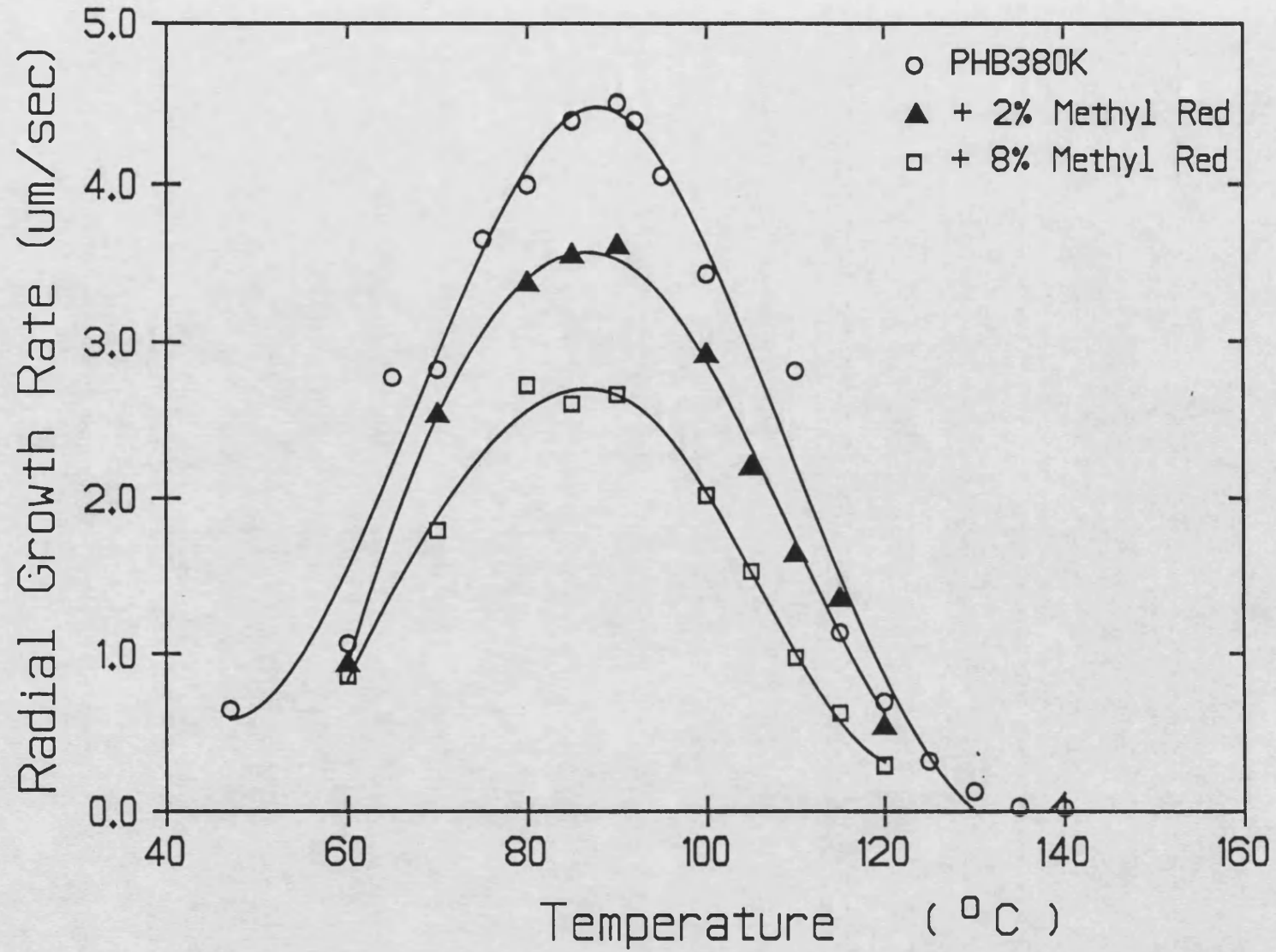
Figure 5.23. The influence of Methyl Red (MR) inclusion on growth rate – temperature profiles of PHB380K spherulites (Mean; n = at least 2). (S.D = less than 5% of Mean)

Figure 5.24. Optical micrographs showing morphology of drug loaded PHB380K spherulites isothermally crystallized at 90°C.

A = PHB380K + 2%W/W METHYL RED

   Scale bar = 250um

B = PHB380K = 8%W/W METHYL RED

   Scale bar = 500um
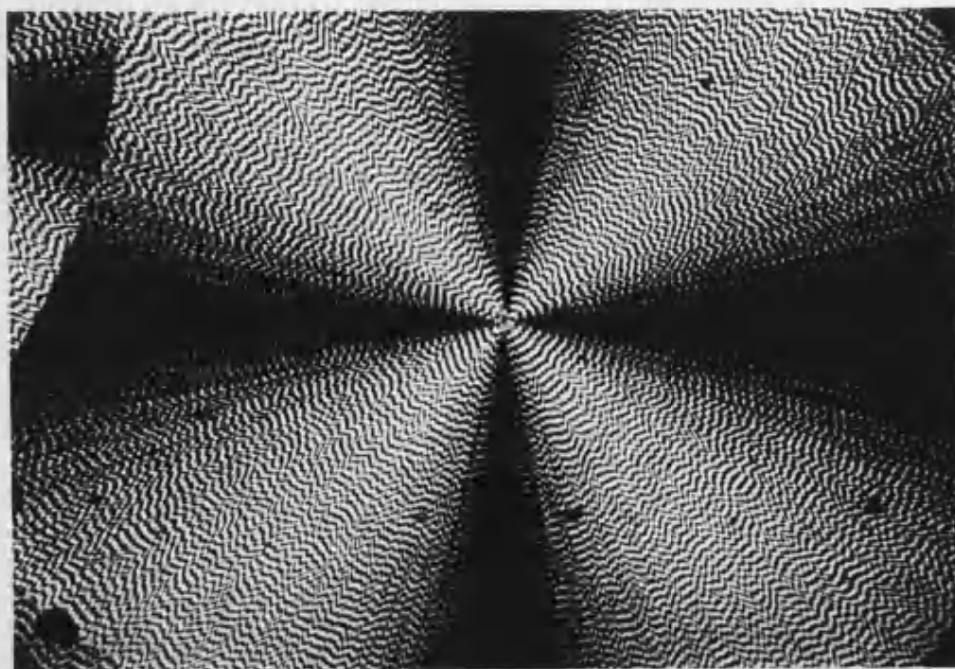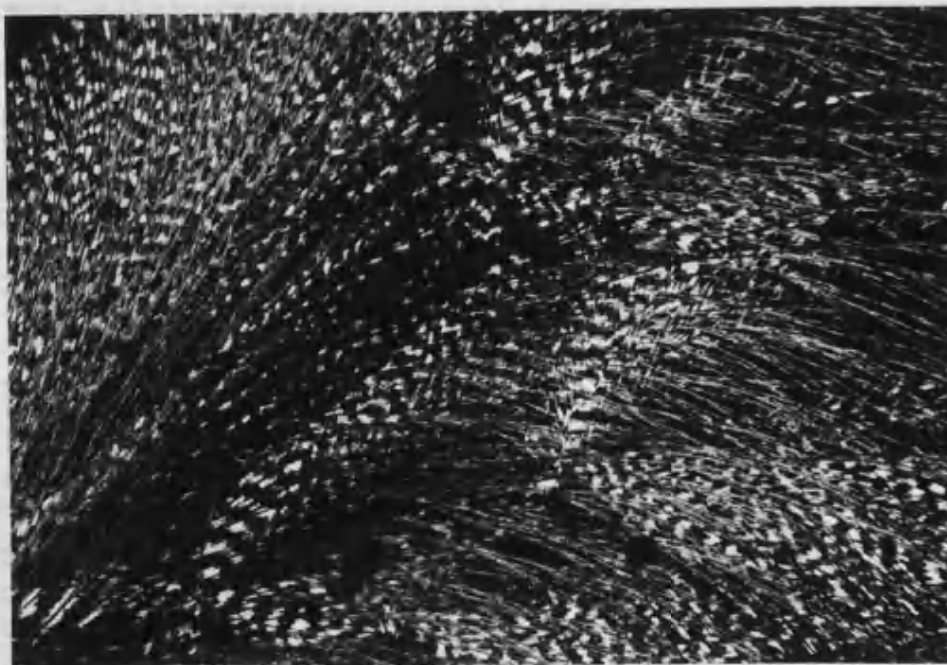
Figure 5.25. Optical micrographs showing morphology of PHB380K spherulites containing 8%w/w Methyl Red isothermally crystallized at 80°C (A) and 90°C (B).

Scale bar = 250um
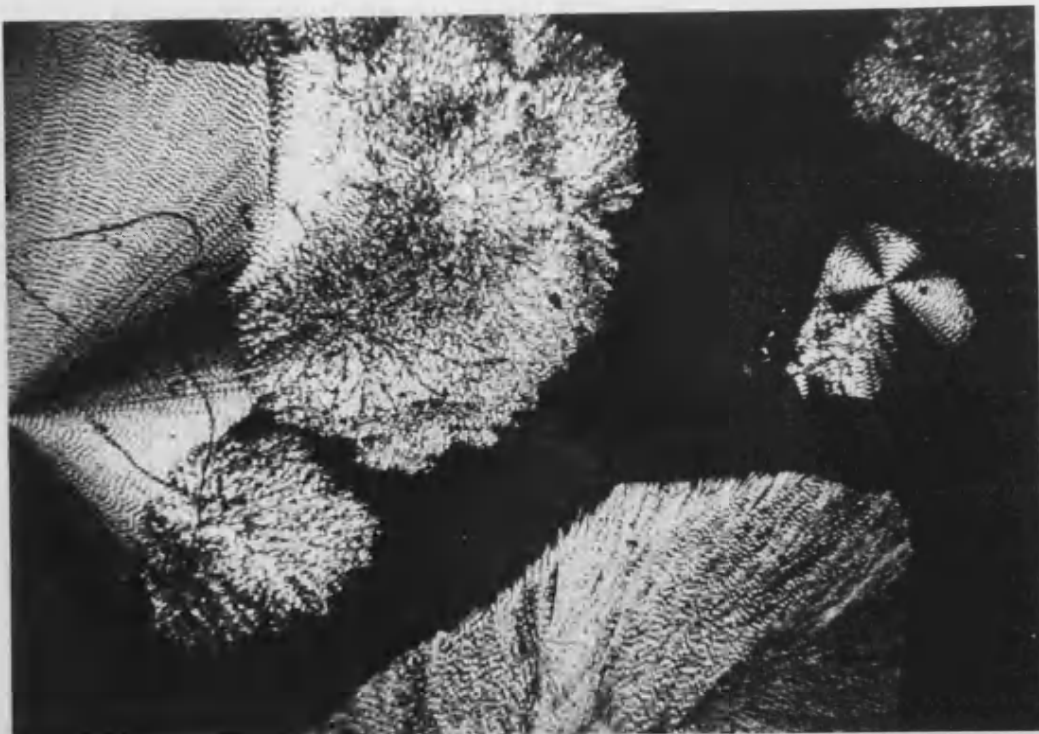
growth rates (close to G_{max}) at these crystallization temperatures may have prevented adequate redistribution and entrappment of the drug within spherulites. The subsequent exclusion of drug to the surface resulted in open, fibrillar morphologies of polymer as shown in Figure 5.25. It is expected that slower spherulitic growth rates would enhance drug exclusion from the polymer crystals. This is further discussed in terms of drug distribution in copolymers (which have slower crystallization rates) in chapter 7. No evidence of drug exclusion for 2% loadings of MR was obtained and at such low loadings the drug was thought to be adequately trapped within the spherulites.

The effects of drug incorporation on the morphology and rate of polymer crystallization may be explained according to the theory of Keith and Padden [428 – 429]. This phenomenological theory proposed that molecular species which crystallize slowly or cannot crystallize will be rejected at the growth fronts. The rejected species (drug or impurities) then accumulate to give enhanced local concentrations above average values in the melt to magnitudes controlled by local diffusion fields. This segregation of material within spherulites has been confirmed by autoradiography [428,473]. The addition of tracers and their subsequent location has shown segregation at interspherulite boundaries and along radii. The reduced growth rate is observed because the accumulated drug or impurities at the growth interfaces depress the equilibrium (liquidus) temperature of the melt and, therefore, the under– or supercooling at the isothermal interface. Keith and Padden [428] showed that when the rejected species are sufficiently mobile deviations from the linear growth rate were observed often giving rise to parabolic growth behaviour. This was not observed for the concentrations of Methyl Red used in this study and growth remained linear for all the undercoolings investigated.

The theory proposes that morphology of the spherulites is governed by the diffusion and distribution of accumulated impurities. In particular, the openess of texture is related to the concentration of the impurity (or drug) present; and coarseness of texture, which is a measure of the "diameters" of crystalline fibres between which impurities become

217

concentrated during crystallization, is determined by $\delta = D/G$, where D is the diffusion coefficient for impurities in the melt and G is the growth rate of the spherulites; δ has the dimensions of length.

Although excessively open structures were not generally observed in the Methyl Red – PHB 380K system, slightly open structures were observed at the higher concentration of drug (8%w/w). Extrapolation of Keith and Padden's theory suggests that the open structures would become more prevalent with increasing drug loadings. The type of polymer morphology obtained will be particularly important in determining drug release rates and mechanisms and is addressed in chapter 7.

The sensitivity of P(HB – HV) polyesters to electron beam damage has prevented direct observation of spherulitic morphologies by electron microscopy. However, very recent advances in etching techniques [224,437] and high resolution microscopy [474] specific to PHB have overcome some of these problems. The morphology of drug loaded polymer spherulites clearly invites much further study.

5.5.8 The incidence of cracking in aged spherulites.

In the course of this study it was noticed that the storage of spherulites at room temperature for several hours following complete crystallization resulted in cracking or fracture along radial and circumferential directions.

Figure 5.26 shows such cracking in PHB800K spherulites crystallized at 95°C and 110°C. At a crystallization temperature (T_c) of 110°C, cracks were observed in both the radial and circumferential directions for PHB800K, whereas at a T_c of 95°C only radial cracks were observed. However in the case of PLA, predominantly circumferential cracks were observed in spherulites crystallized at 135°C (Figure 5.27(C)). At the same temperature, cracking is less obvious in PHB380K (Figure 2.27(B)). No other reports in the literature were found on the incidence of cracking in PLA. Cracks were not observed for the high molecular weight P(HB – HV) copolymers. However, cracks were observed in PHV16
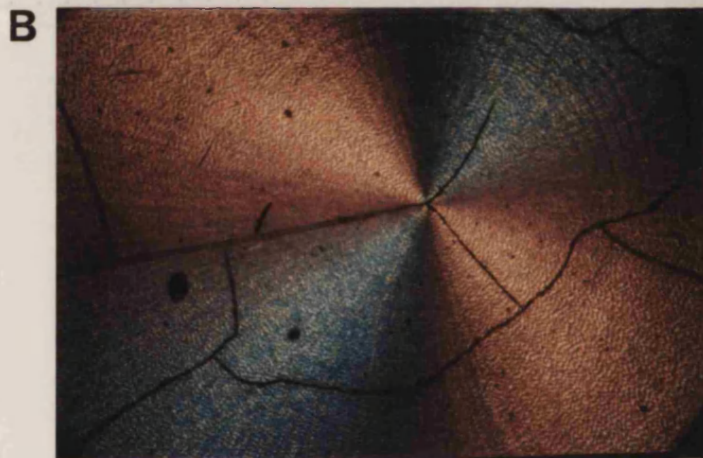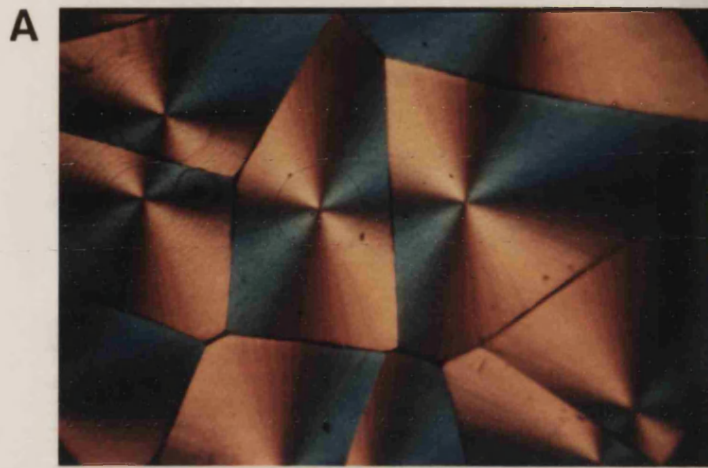
Figure 5.26. Optical micrographs showing cracking in PHB800K spherulites crystallized at 95°C (A) and 110°C (B).

Scale bar = 1mm
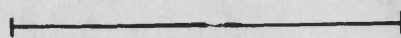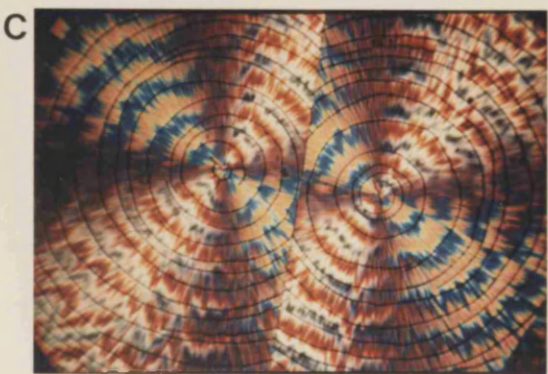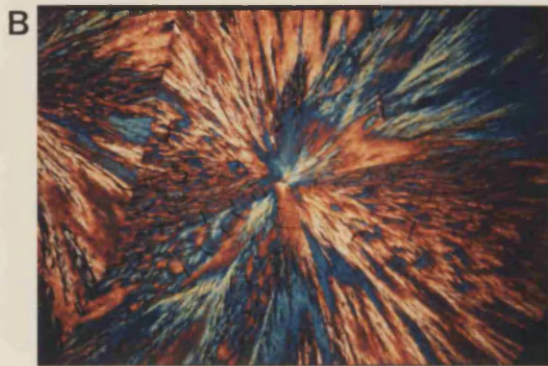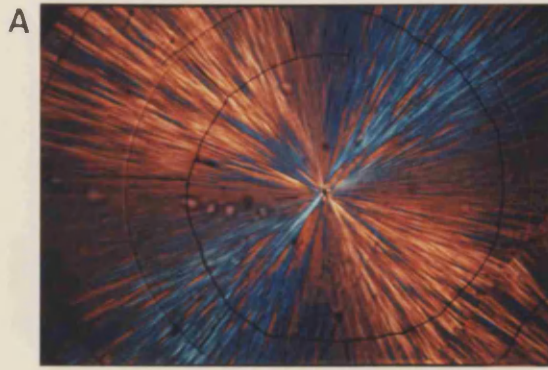
Figure 5.27. Optical micrographs showing cracking in polymer spherulites.

A = PHV16 spherulites crystallized at 100°C.

B = PHB380K spherulites crystallized at 135°C.

C = PLA spherulites crystallized at 135°C.

Scale bar = 1mm
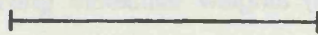
(Mw = 41K) spherulites. Figure 5.27(A) shows circumferential cracking in PHV16 spherulites crystallized at 100°C.

The explanation for the occurrence of cracking in PHB and PLA remains speculative. The radial and circumferential cracks in PHB may be due to the spherulites possessing different radial and circumferential thermal expansion coefficients which can result in the build up of sufficient internal stresses to initiate the cracks [475]. The variation in thermal expansion coefficients in the radial and circumferential directions of spherulites has previously been demonstrated for polyethylene but this did not result in cracking [476]. The fact that cracking is observed in spherulites crystallized at room temperature and the fact that crystallization temperature influences the type of cracking observed has led to a suggestion that there may be a link between crystal growth regimes and cracking [475]. However this has yet to be validated.

The absence of cracking in high molecular weight P(HB–HV) copolymers may be explained by the fact that the build up of thermally induced stresses, which causes cracks in PHB, is prevented either because of some internal rearrangement (as in polyethylene [476]) or because the differential expansion coefficients, simply, do not exist. This clearly invites further investigation.

The presence of cracks for the low molecular weight PHV16 suggests that cracking may be related to molecular weight. The fact that a minimum molecular weight of around 200K was required to produce a mechanically intact specimen of PHB from solution (chapter 2) may have some significance to this study. The incidence of cracking in PHV16 spherulites may correspond to the breaking up (into small pieces) of low molecular weight polymer films cast from solution upon drying. The number of tie–molecules present between radiating lamellae within the spherulite may therefore be critical in determining the occurrence and extent of cracking in polymers. However a recent report has suggested that cracking is not found in copolymers with HV contents in excess of 12 mole% [477]. These results were based on copolymers having molecular weights (Mw) in excess of 260 Daltons and the effect of varying molecular weight was not considered [477].

Cracking is known to occur in the spherulites of thin films fabricated by melt processing [475] and may explain the brittle nature of melt-pressed PHB (chapter 2). Whether the same explanation applies for the brittle behaviour in solvent cast films of PHB remains unclear. Cold rolling has been reported to heal the observed cracks and thereby improve the mechanical properties of melt-processed PHB films [475]. An alternative method of avoiding cracking in P(HB-HV) polymers is to limit the size of spherulites formed (e.g by increasing nucleation density) [475,477].

5.6 CONCLUSIONS

Polymer spherulites exhibited linear growth at any given crystallization temperature for all the systems studied. Growth rates were dependent on temperature. The growth rate-temperature profile was essentially independent of PHB molecular weight but dependent on P(HB-HV) copolymer composition. At any given crystallization temperature, the growth rate of copolymer spherulites was progressively reduced on increasing HV content.

Spherulite morphology was influenced by both crystallization temperature and copolymer composition. The variations in crystallite size and internal fine structure between copolymers may explain the dependence of physicomechanical properties on copolymer composition which cannot easily be explained by differences in the overall degree of crystallinity in P(HB-HV) systems.

The incorporation of increasing amounts of a model drug (Methyl Red) into PHB380K progressively reduced the rate of spherulitic crystallization. At a low loading (2%), the drug failed to crystallize and was thought to be distributed both inter- and intra-spherulitically in an amorphous state. At a higher loading (8%), some drug was excluded to the crystallite surface and dramatically influenced spherulite morphology. The extent to which drug-polymer morphology influences drug release is addressed in chapter 7.

Storage of polymer spherulites for a period of time at ambient conditions resulted in circumferential and radial cracking. The occurrence of cracking was thought to be dependent on both polymer molecular weight and copolymer composition.

CHAPTER 6

SPRAY DRIED MICROPARTICLES FOR PARENTERAL ADMINISTRATION

6.1 INTRODUCTION

The use of polymer microspheres for drug delivery and other commercial applications has been extensively studied. Microparticulate systems have been investigated for use in drug targetting [11] and for the controlled/sustained delivery of many therapeutic actives including local anaesthetics [98-99], steroids [101], and peptides [109-111]. This study is concerned with the use of biodegradable P(HB-HV) microparticulates as carriers or matrices for parenteral (intra-muscular and/or sub-cutaneous) drug delivery.

The preparation of drug loaded microspheres or microcapsules can be achieved by many different methods [479-480] and a list of typical processes is given in Table 6.1. The most widely used of these methods is solvent evaporation [481] and the subject of this investigation. Primarily, there are two classes of solvent evaporation processes which may be used to form microspheres:

a) solidification of emulsions (emulsion deposition)

b) spray drying of drug in solvent.

The emulsion deposition method of preparing microspheres is the most common method of solvent evaporation [481]. Indeed, previous work on PHB particulate carrier systems has involved the use of such single batch solvent evaporation techniques for producing microspheres [307-311]. Emulsion deposition generally produces discrete microspheres which are often of a narrow size distribution. Size ranges from submicron to 2000um can be produced by this method. Particle size can be controlled by a number of processing parameters such as rate of agitation and emulsifier concentration [481-482].

In contrast, spray drying, as a method of producing microspheres for controlled drug delivery, has received little attention in the pharmaceutical literature. This may, in part, be due to the volatile and often flammable nature of the solvents commonly used in dissolving hydrophobic polymers for drug delivery. The non-aqueous solvents can present problems in large scale drying because after solvent evaporation, exhaust gases have to be carefully vented out in a safe and appropriate manner or recovered for re-cycling. In

the mounting concern over environmental issues and strict governmental control, this may prove expensive in certain cases where solvent recovery is difficult.

However, spray drying has the advantage over emulsion deposition in being a rapid, single – stage operation suitable for batch or continuous production of large quantities of product. Heat sensitive materials, such as proteins and peptides, can be spray dried because exposure to elevated temperatures is short, normally ranging from 5 – 30 seconds [483]. With these advantages in mind spray drying was investigated as a method of producing P(HB – HV) microparticles for parenteral controlled release preparations.

Table 6.1. A summary of the processes used in preparing microparticles (After ref. 481).

Process	Description	Drugs Amenable to Process
A. Phase separation type		
1.Organic phase separation	Drug suspended or dissolved and polymer dissolved in solvent (CH_2Cl_2) with a phase inducer. Non – solvent added to harden microparticles.	Water – soluble drugs such as peptides, salts and drugs insoluble in the solvent.
2. Emulsion phase separation	Drug dissolved in aqueous phase of emulsion. Polymer in the organic phase. Non – solvent used to harden microparticles.	Water – soluble drugs.
3. Low – temperature phase separation	Drug suspended in solvent containing dissolved polymer. Alcohols used to precipitate microparticles.	Drugs insoluble in the solvent (e.g. toluene)
B. Solvent evaporation type		
1. Emulsion deposition	Drug and polymer dissolved in organic phase of an emulsion with the aid of a surfactant. Organic solvent evaporated to leave solid microparticles.	Drugs soluble or suspended in the organic phase (e.g. steroids).
2. Spray drying	Drug and polymer spray – dried in the usual manner.	Both water – soluble and organic soluble drugs.
C. Melt processing type		
1. Prilling	Drug and polymer co – melted and dropped from a small orifice through a tower.	Heat stable drugs (e.g. phenothiazines)

6.1.1 AIMS AND OBJECTIVES

1. To investigate the possible use of spray drying as a method of producing P(HB – HV) polymer microspheres for parenteral drug delivery.

2. To study the effect of operational variables in spray drying on the product morphology and release characteristics.

3. To study the effect of molecular weight and copolymer composition on release characteristics of the spray – dried product.

6.1.2 PRINCIPLES OF SPRAY DRYING

Masters [484] has defined spray drying as the transformation of feed (a solution, suspension or paste) from a fluid state into a dried particulate form by spraying the feed into a hot drying medium (usually hot air). For pharmaceutical microencapsulation and microsphere production the feed consists of a drug either dispersed or dissolved in a polymer solution (aqueous or organic). The final form of the resulting dried product depends upon the physical and chemical properties of the feed and on both dryer and operational variables.

There are many different types of spray dryers available, varying in design to suit the requirements of the feed material and product [485]. The most common type used in industry is the open cycle, co – current spray dryer and is represented in a schematic diagram in Figure 6.1. Co – current, as opposed to counter – current, refers to the direction of flow of the drying medium (hot air) being the same as that of the feed. Open cycle refers to the layout in which exhaust gases are vented out into the atmosphere. This is the standard layout of industrial dryers and the most widely used [486]. Closed cycle layouts in spray dryers involve re – cycling of exhaust gases and solvents.

Spray drying involves atomization of feed (polymer or polymer – drug solutions) into a

spray and contact between spray and drying medium resulting in solvent evaporation. The drying of the spray continues until solvent evaporation is complete and the dried product is then recovered from the drying medium [487].

Spray drying therefore consists of four different stages:

Stage 1 – Atomization of feed: Atomization involves the break up of liquid into millions of individual droplets forming a spray. The energy needed for this process is supplied by pressure, centrifugal, sonic or kinetc effects depending on the type of atomizer used [488].

The two most commonly used atomizers are the rotary and pressure nozzle atomizers. The former involves centrifugal energy to form a spray. This is commonly achieved by introducing the feed centrally onto a wheel or disc rotating at speed. The feed flows outwards over the surface, accelerating to the periphery and on leaving the wheel or disc the feed readily disintegrates into a spray of uniform sized droplets [488].

In the pressure nozzle atomizer the feed is fed into the nozzle under pressure. Pressure energy is converted to kinetic energy and the feed issues from the nozzle orifice as a high speed film that readily disintegrates into a spray due to the instability of the film [488].

The type of atomizer used can influence the dried product particle size and it has been reported by Masters [488] that rotary atomizers generally produce finer particles. However the final particle size will depend on a combination of other operational variables.

Stage 2 – Spray–air contact: During spray–air contact, droplets meet the hot air and solvent evaporation takes place from the droplet surfaces. Evaporation is rapid due to the vast surface of droplets in a spray. However, high evaporation rates may expand or fracture droplets to give non–spherical porous particles of low bulk density [488].

The manner in which the spray contacts the drying medium (hot air) is an important

factor in spray dryer design because it has great bearing on the properties of the dried product. The droplet residence time within the drying air will be determined by the position of the atomizer in relation to the drying air inlet. Co-current flow yields lower droplet residence times than counter-current flow and is widely used for heat sensitive materials [488].

The temperature distribution within the drying chamber will also influence dried product characteristics. The temperature distribution depends on whether the air disperser creates plug flow or swirling air conditions in the drying chamber. The greater the swirling motion the more uniform the temperature distribution throughout the chamber [488].

Stage 3 - Drying of spray (solvent evaporation): As soon as droplets come into contact with the drying air, solvent evaporation takes place from the saturated vapour film which is quickly established at the droplet surface. The temperature at the droplet surface approximates to wet-bulb temperature of the drying air [488].

Solvent evaporation at first occurs at a constant rate because there is sufficient solvent within the droplet to replace that lost at the surface. This is termed the constant rate period [488] which continues as long as saturated surface conditions are maintained. When the solvent content within the droplet becomes too low to maintain saturated surface conditions, the so-called critical point is reached and a dried shell forms at the droplet surface. In this second or falling rate period of drying, evaporation is dependent upon the rate of solvent diffusion through the dried surface shell. The thickness of the dried shell increases with time, causing a decrease in the rate of evaporation [488].

The droplet residence time governs the rate of evaporation from the droplet surface and this in turn, governs the morphology and particle size of the dried product [488]. Different materials exhibit different evaporation characteristics. Some tend to expand, others collapse, fracture or disintegrate leading to porous, irregularly shaped

particles. Others maintain a constant spherical shape or even contract so that particles become more dense [488].

Stage 4 – Separation or recovery of dried product: Product separation from the drying air follows completion of the drying stages, when the dried product remains suspended in the air [488]. Separation of dried product from the air influences particle properties by virtue of mechanical handling involved during the separation stage. Excessive mechanical handling can produce products having a high percentage of fines [488].

6.2 MATERIALS

P(HB–HV) copolymer containing 16mole% HV (Mw 14K) was purchased from Marlborough biopolymers Ltd, UK.

All other materials were identical to those used in chapters 2 and 3.

6.3 METHODS

6.3.1   Spray drying

6.3.1.1 Preparation of polymer–drug solutions

Polymers were dissolved by refluxing in chloroform (1%w/w). Accurately weighed amounts of a model drug (Methyl Red) were added to cooled polymer solutions. Suitable mixing of polymer–drug blends was achieved by either placing solutions in a sonic bath (Deakon FS100 Frequency Sweep; Deakon Ultrasonics Ltd, UK) for 5 minutes or by mechanical agitation with a glass rod for 5–10 minutes.

6.3.1.2 Spray drying of polymer–drug solutions

A co–current, open cycle Buchi B190 Minispray Dryer was used to spray dry polymer–drug solutions. Before solutions were dried, the spray dryer was heated and stabilised at the desired inlet (T_{in}) and outlet (T_{out}) temperatures. The inlet temperature was controlled by adjusting power supplied to the oven heater situated at the top of the drying chamber. Inlet temperatures up to a maximum limit of 220°C could be attained in the

Buchi B190. The outlet temperature could not be independently controlled but was largely dependent on T_{in} and the feed rate. In the Buchi B190 minispray dryer the inlet/outlet temperatures were monitored by PT-100 temperature sensors.

The polymer-drug solutions in chloroform were pumped into the pressure nozzle atomiser (0.7mm diameter) at a chosen feed rate. The feed rate could be controlled by a combination of the speed setting on the peristaltic pump and the diameter of the silicone feed hose. Pressure for the nozzle atomizer was provided by compressed air (5 - 8 bar). Cooling water was used to minimise temperature rises in the nozzle. Air was drawn through a heated oven to provide a co-current flow of drying air through the glass drying chamber (10cm diameter) and the rate of hot air flow was controlled by the aspirator setting. Recovery of product into a sample collector was achieved following product separation in the cyclone. The chloroform-air exhaust was vented out through a fume cupboard. A schematic diagram and photograph of this bench model spray dryer is given in Figures 6.1 - 6.2. Standard settings for operating variables are given in Table 6.2.

Table 6.2. Standard spray drying parameter settings.

PARAMETER	SETTING
Dryer	Buchi B190 minispray
Type	Open cycle, co-current
Atomiser	Pressure nozzle (0.7mm diameter)
Drying chamber	Glass, 10cm diameter, 50cm length.
Solvent	Chloroform
Temperature	125°C inlet; 85°C outlet
Feed Rate	14ml/min

Key:
1. Magnetic stirrer
2. Polymer feed
3. Peristaltic pump
4. Feed inlet
5. Compressed air inlet
6. Cooling water inlet
7. Pressure nozzle
8. Hot air heater
9. Inlet temperature sensor
10. Drying chamber
11. Trap
12. Outlet temperature sensor
13. Cyclone
14. Product collecting vessel
15. Exhaust gases
16. Control panel
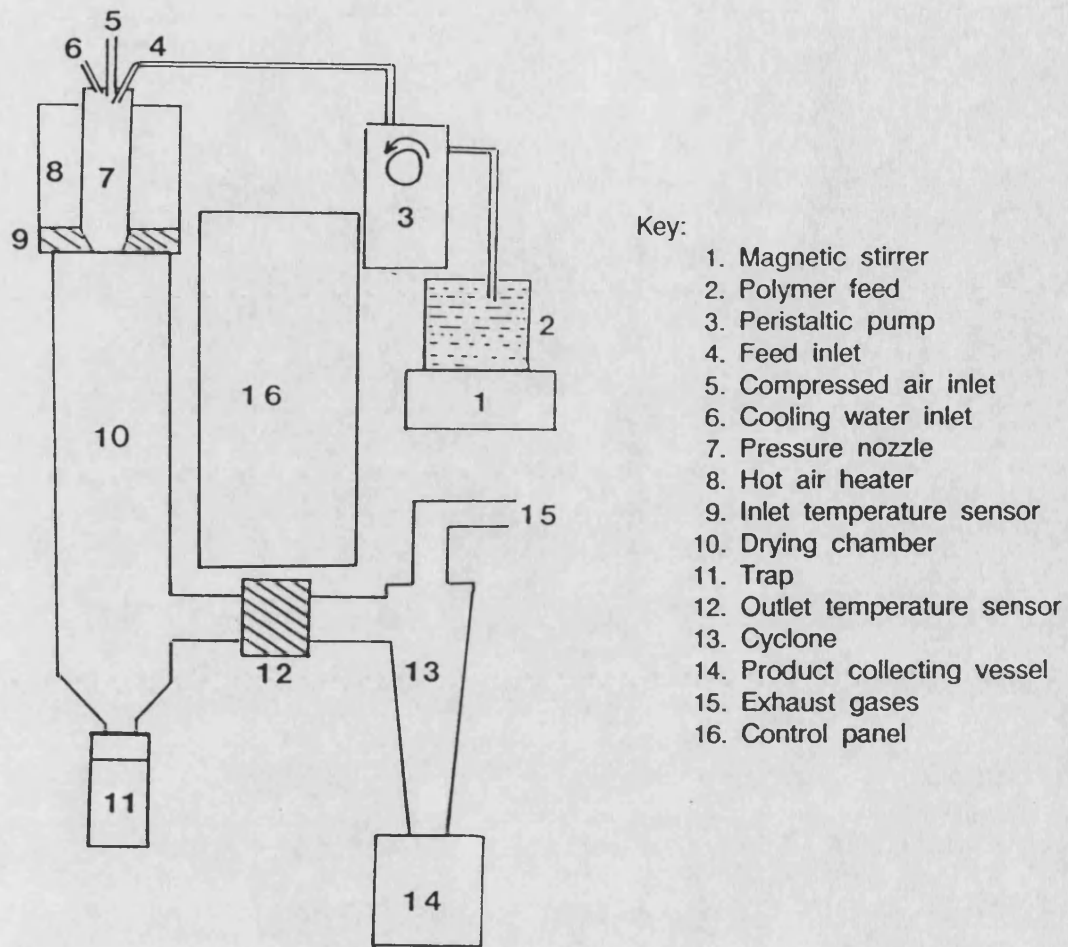
Figure 6.1. A schematic diagram of an open cycle, co – current Buchi spray dryer.

Figure 6.2. Photograph of the Buchi minispray dryer (see overleaf).
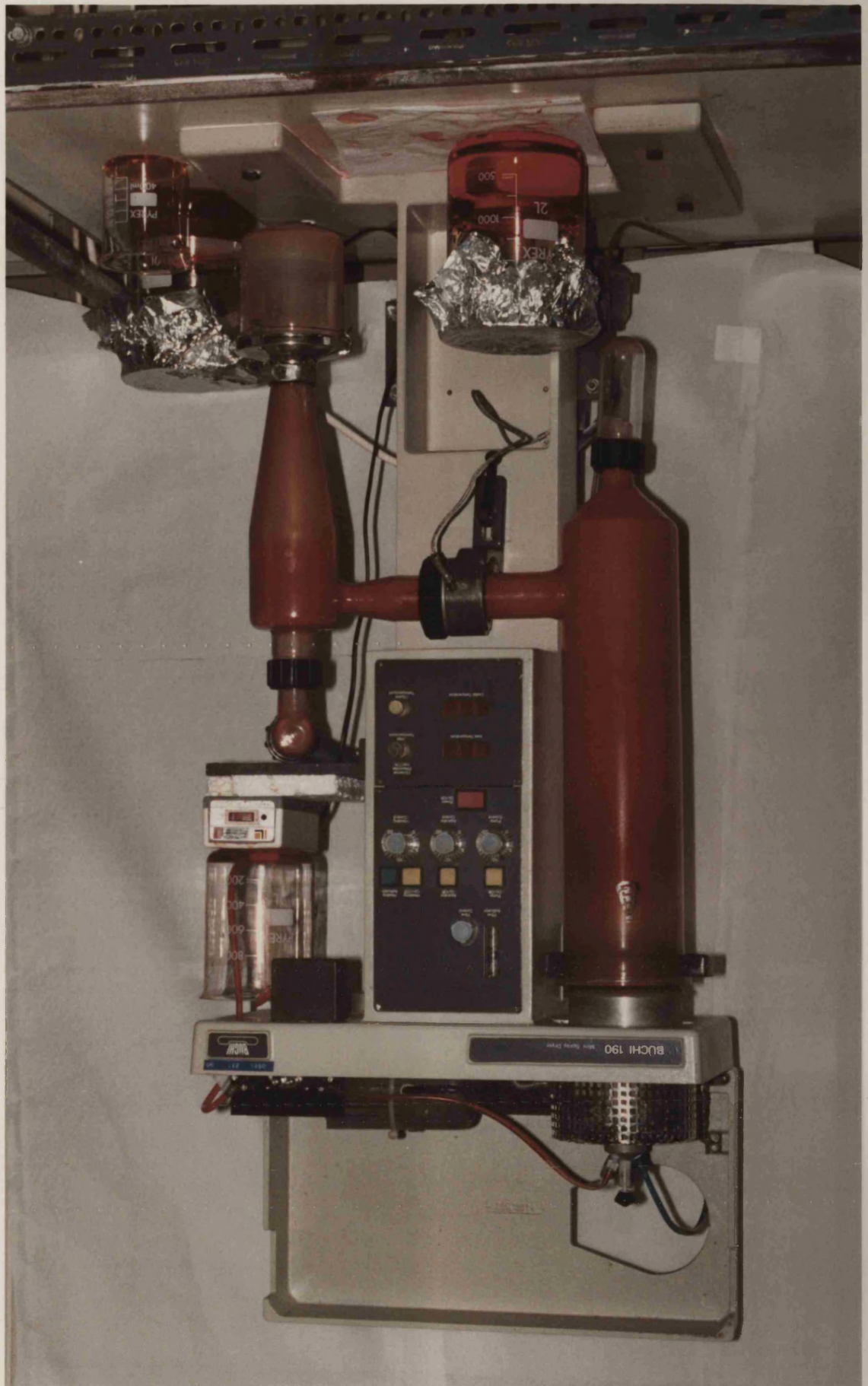
6.3.1.3 Preparation of replicate batches

A minimum of two batches were produced for each operating condition. Replicate batches were usually prepared on a separate day following thorough cleaning of the spray dryer. The air orifice and nozzle tip were cleaned with a sponge between batches and clean glass parts were used for new batch preparation.The spray dryer was re-heated from ambient to the desired operating temperatures for each batch as described above.

6.3.2   Characterization of spray-dried product

6.3.2.1 Particle size

Particle size of spray dried material was determined using a Malvern 2600/3600 Laser Particle Size Analyser VF.6 fitted with a 100mm focal length lens and a stirred sample cell.

The samples were suspended in a light grade paraffin, Puremor (Castrol Oil Co.UK), which was found to be a suitable non-solvent for the drug loaded particles. The light grade paraffin had been previously filtered through a 0.45um filter to remove any extraneous matter. The suspensions were sonicated for 1 minute in the Malvern sonic bath to ensure breakdown of weakly held aggregates prior to size analysis.

The size distribution results were expressed according to the following parameters:

$$\text{Volume Mean Diameter (VMD)} = \frac{N(x).x^4}{N(x).x^3} = \frac{V(x).x}{V(x)}$$

where N(x) is the number frequency

       V(x) is the volume frequency

       x   is the particle diameter

$$\text{Sauter Mean Diameter (SMD)} = \frac{N(x).x^3}{N(x).x^2}$$

$D_{10\%}$, $D_{50\%}$ and $D_{90\%}$ represent the sizes at which 10%, 50% and 90% of the volume (weight) of material is of smaller diameter. These values were obtained by linear interpolation of the cumulative volume (weight) undersize data.

6.3.2.2 Morphology by scanning electron microscopy

Small amounts of spray-dried product were mounted onto aluminium stubs (2.6cm diameter) coated with colloidal graphite (Conductive Carbon Cement; Leit C, FRG) as adhesive. The samples were sputter coated with gold using an Edwards sputter coater (Edwards S150B; Edwards High Vacuum, Crawley,UK). Typically samples were coated for 6 minutes in a vacuum (100m of mercury) with a current of 20mA and a voltage of 1.4KV.

The particle size and surface morphology of sputter coated samples were examined using a Jeol JSM 35C Scanning Electron Microscope (Japanese Electron Optics Ltd, Tokyo, Japan) with an electron beam energy of 5kV or 10kV. The gold and colloidal graphite layers ensured that specimens were fully earthed and prevented overheating and accumulation of charge.

6.3.2.3 Differential scanning calorimetry

Samples were heated from ambient to melt at a programmed heating rate of 20K/min in a Dupont DSC 910/ 9900 Thermal Analyser as described in chapter 3.

6.3.3 Assay of drug content

Accurately weighed samples of Methyl Red loaded PHB microparticles (10mg) were dissolved in 50ml of chloroform and diluted for assay at an absorption maximum of 490nm (Molar Absorption Coefficient = 36098). Drug loadings were calculated as %w/w.

6.3.4 *In vitro* drug release

Accurately weighed samples of drug loaded microparticles (approximately 50mg) were sealed in Clinbritic vials (30ml capacity) containing 25ml phosphate buffer (pH 7.4; formula given in appendix C) at 37°C. Vials were agitated in a direction normal to their length at 180 oscillations/min in a constant temperature shaking water bath. Variable amounts of release medium were sampled periodically and replaced with fresh buffer to maintain conditions close to sink. To prevent loss of spray-dried particles on

sampling, vials were removed 5-10 minutes before sampling to allow settling down of particles and a plastic hypodermic syringe (10ml) fitted with a 22 gauge needle was used for sampling of medium. Release of Methyl Red in buffer was determined by spectrophotometric assay at 430nm using a Perkin Elmer uv-vis spectrophotometer (Molar Absorption Coefficient = 20263).

6.3.5 The Rotating basket method of agitation in release studies

This device consisted of a wire basket (40 x 40 x 20 cm) rotated about its central axis using a modified Kymograph motor. The Clinbritic release vials were positioned such that an end-on-end roll could be achieved to provide suitable agitation. The speed of basket rotation was set to provide a roll frequency of 2 cycles/min. Agitation was stopped periodically to remove samples. The device was kept in a 37°C incubation room in order to maintain constant temperature conditions.

6.4 RESULTS AND DISCUSSION

6.4.1 Preliminary studies on spray drying of P(HB-HV) polymers

The purpose of the preliminary investigation was to study the spray drying ability of PHB and the effect of polymer molecular weight (MW) on product characteristics. A series of molecular weights of PHB ranging from 23K to 800K were employed in this preliminary study. No drug was incorporated at this stage.

The results of this study (see Table 6.3) showed that low molecular weight PHB samples (140K and below) of concentration up to 2%w/v, could be spray dried to a product which appeared, at a macroscopic level, to be a fine, free flowing powder. The higher molecular weight PHB samples (275K and above) were more difficult to spray dry using the Buchi B190 minispray dryer. These higher molecular weight samples could only be spray dried from very dilute solutions (<0.5%w/v) and then only to form a fibrous end product. At higher concentrations the polymer tended to line the glass drying chamber and cyclone as thin fibrous strands and no product was recovered. Scanning electron micrographs (at low magnifications) comparing the spray-dried products obtained for low and high

molecular weights of PHB are given in Figures 6.3 and 6.4.

Table 6.3. The effect of molecular weight on the spray drying characteristics of PHB.

Mw	Feed Concentration	Product appearance
23K	Up to 2% w/v	Fine Powder
43K	Up to 2% w/v	Fine Powder
140K	Up to 2% w/v	Fine Powder
275K	Less than 0.5% w/v	Fibrous
380K	Less than 0.5% w/v	Fibrous
800K	Less than 0.5% w/v	Fibrous

A more detailed analysis of the low MW spray-dried product showed that it did not consist of discrete microspheres but aggregates (20-40um) consisting of smaller irreversibly fused microspheres (see Figure 6.5). Higher magnification of high MW PHB spray-dried product showed that this product consisted of even smaller particles irreversibly fused together to give a fibrous end product. In both cases, no pores were visible at the surface of particles at magnifications up to x3500. In contrast, PHB380K microspheres prepared by an emulsion deposition method using polyvinyl alcohol (2% w/v) as emulsifier resulted in discrete spherical particles with rough surfaces indicating a porous structure (Figure 6.6). Similar surface roughness was observed for PHB microspheres (170um) prepared by Juni et al [300] when using gelatin as emulsifier. However, Bissery et al [307], who prepared smaller PHB microspheres (1-12um) by a similar emulsion deposition method reported an absence of surface pores when examined under the scanning electron microscope at magnifications of up to x10,000.

The difficulty in preparing high molecular weight PHB microparticles by spray drying was thought to be a consequence of the highly crystalline nature of PHB. Values of up to 90% crystallinity have been reported for PHB [149,214]. It was noted that only the non-film forming molecular weights of PHB could be spray dried easily. This suggested that lower cohesive energies and fewer chain entanglements were necessary to form spray-dried microparticles compared to solvent cast films. A minimum molecular weight of

Figure 6.3 (A – B). Scanning electron micrographs of the low molecular weight (PHB43K) spray – dried product under low magnifications.

A 10KU   X200   100μm   0041

B 10KU   X350   50μm   0041
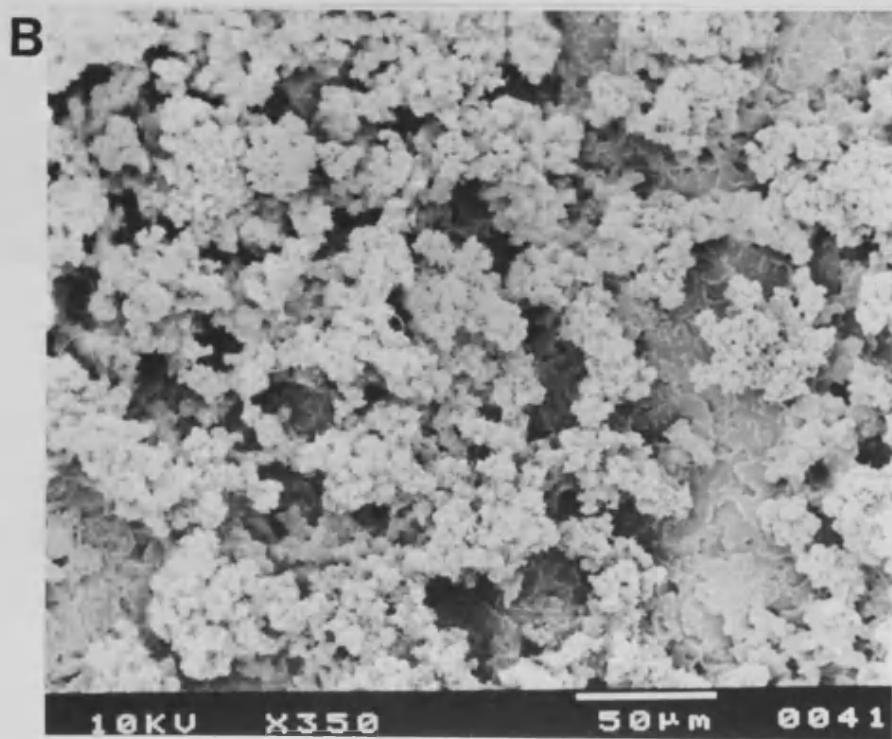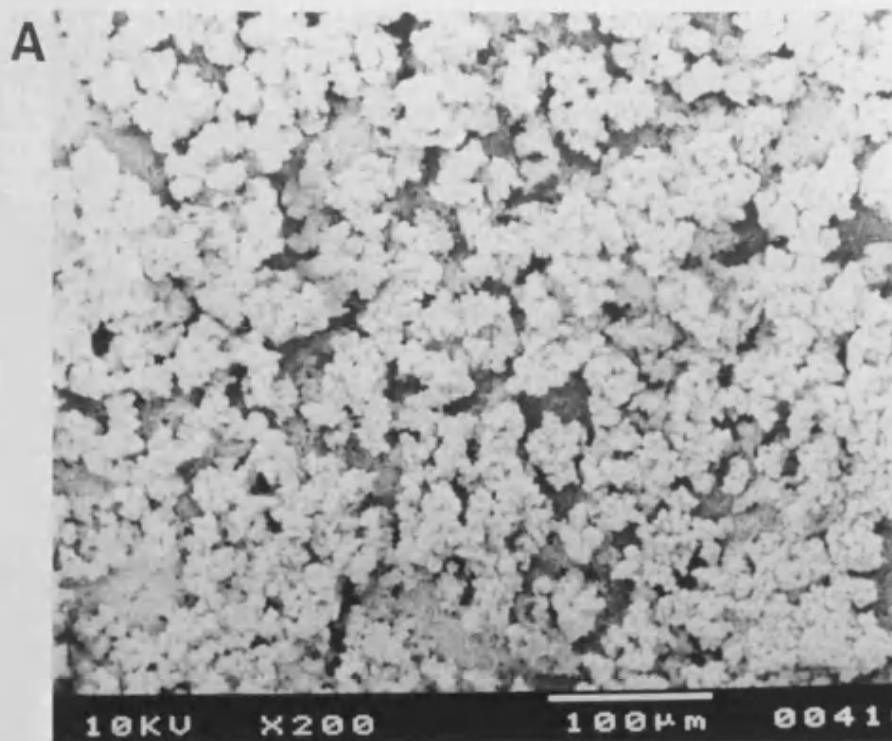
Figure 6.4. Scanning electron micrograph of the   high molecular
weight (PHB800K) spray – dried product.

Scale bar = 500um.

Figure 6.5 (A – B). Scanning electron micrographs of the low molecular weight spray – dried product under high magnifications.

A

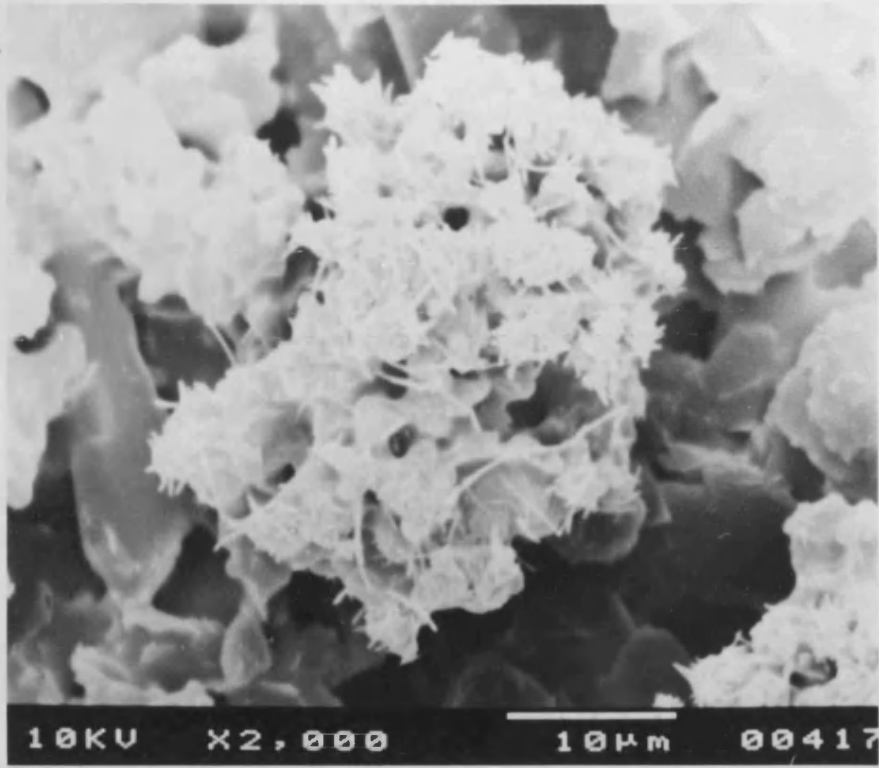10KU   X2,000   10μm   00417

B

10KU   X1,500   10μm   00417
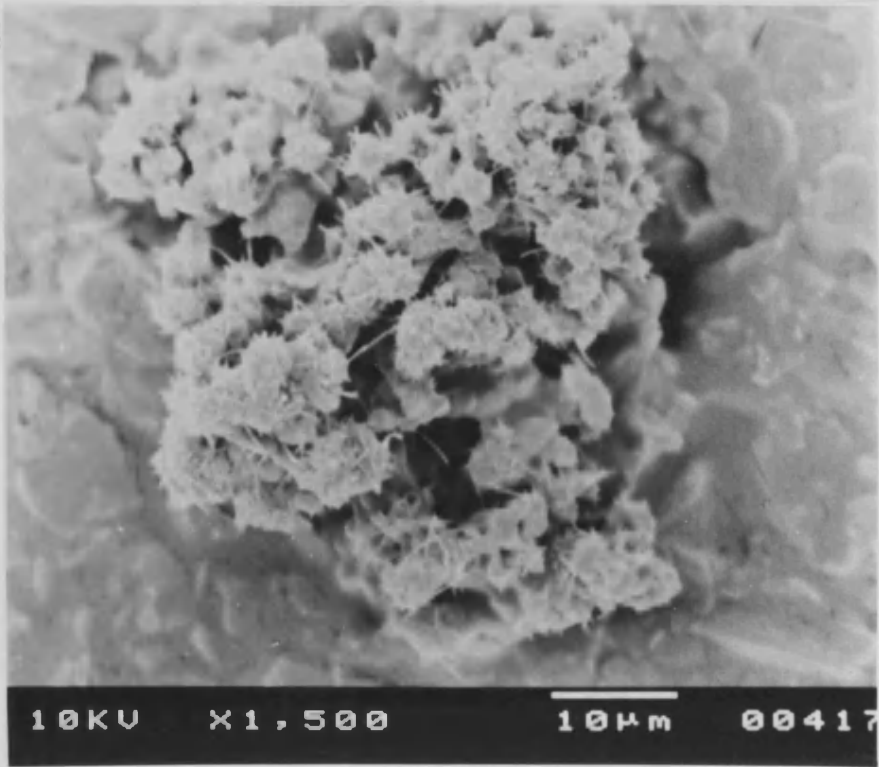
Figure 6.6. Scanning electron micrograph of PHB380K microspheres prepared by an emulsion deposition method.

10KU X350 50µm 000216
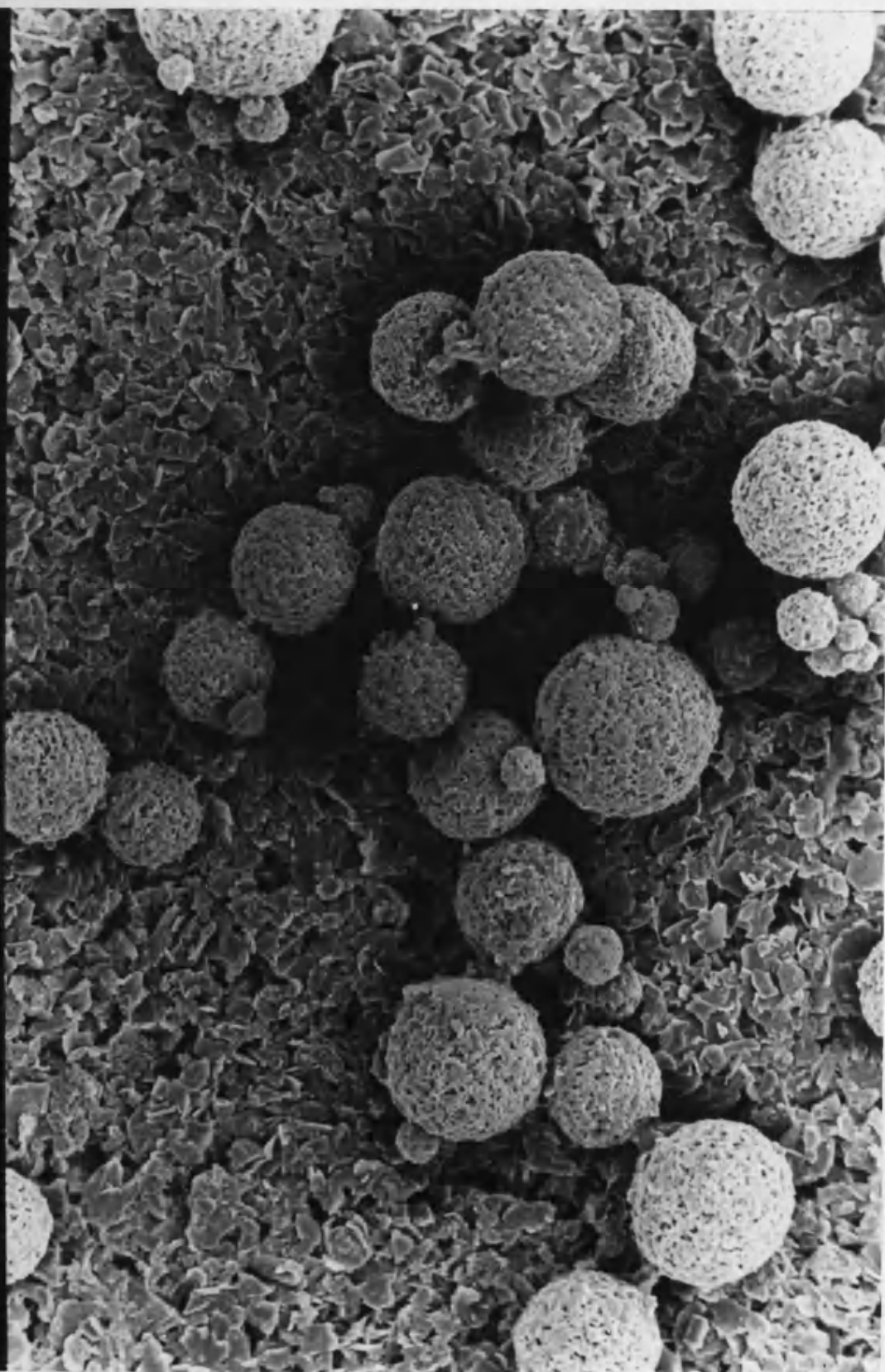
approximately 190–200K was necessary to form a film [264] as reported in chapter 2. Molecular weights above this threshold value appeared to be more difficult to atomize using the pressure nozzle and consequently formed a poor quality product. The higher viscosities for high MW's of PHB may have hindered formation of a good product but even at very low (<0.5%w/v) concentrations of PHB a poor product was recovered.

Rotary atomizers generally produce finer particles [488] but because of design constraints, a rotary atomizer could not be used in the Buchi B190 Minispray dryer. However, a study carried out using a pilot scale spray dryer (Mobile Minor Spray Dryer, chamber diameter 1 metre; Niro Atomizer, Denmark) equipped with a rotary atomizer showed similar results to those obtained with the Buchi model. Again, low molecular weights of PHB could be easily spray dried whereas no useful product could be recovered from higher molecular weights. Although the low molecular weight product again consisted of aggregates of smaller fused microspheres (similar to those shown in Figure 6.5), the aggregates were of smaller size (10–15um).

These preliminary results suggested that only low molecular weights of PHB could be spray dried to form a suitable product for possible use in parenteral drug delivery systems. Consequently further studies were limited to polymers with molecular weight of 140K and below.

6.4.2 Drug loaded microparticles from spray drying

6.4.2.1 Studies on batch–to–batch variation of product

Batch–to–batch variation of the spray–dried product was investigated using 3 batches of PHB 43K microparticles containing 4%w/w Methyl Red. The batches were prepared on different days using the standard spray dryer settings as shown in Table 6.2.

In order to assess product variation between batches, the spray–dried material was analysed in terms of particle size, product morphology and drug release characteristics.

The product morphology was investigated using scanning electron microscopy. The same

product morphology was seen for all 3 batches and was identical to that found in the preliminary studies using low molecular weights of PHB (see Figure 6.5). The size of the aggregates were determined using the Malvern (2600/3600) Particle Sizer and are given in Table 6.4.

Table 6.4. Product characteristics of 3 spray dried batches of PHB microparticles containing Methyl Red.

Batch Number	Drug:Polymer Ratio	Actual Drug Loading (%w/w)	SMD	Particle Sizes of Aggregates (um);(Mean $\pm$ Range; n = 2)			
				$D_{50\%}$	$D_{10\%}$	$D_{90\%}$	VMD
1	4:100	4.27	20.85 $\pm$0.08	32.81 $\pm$0.19	10.72 $\pm$0.11	69.27 $\pm$2.11	38.30 $\pm$0.63
2	4:100	4.27	20.73 $\pm$0.05	36.78 $\pm$0.26	9.90 $\pm$0.10	76.52 $\pm$1.32	41.48 $\pm$0.57
3	4:100	4.18	22.89 $\pm$0.89	38.40 $\pm$1.70	11.24 $\pm$0.54	84.28 $\pm$2.80	47.14 $\pm$1.89

The results showed that although there were some differences in the particle sizes of the 3 batches, these were considered to be sufficiently close for the purposes of regarding these batches as reproducible in terms of particle size. Batches were also considered reproducible in terms of drug content. However, drug release profiles obtained using the rotating basket method suggested some variance between batches (Figure 6.7). Each datum point, in Figure 6.7, represents the mean of 2 replicate experiments from the same batch. Intra–batch variation in terms of particle size and morphology was minimal and drug release was reproducible. Typically, standard deviations of intra–batch release data were within 5% of the mean.

The release of Methyl Red from PHB microparticles appeared to be biphasic. The drug was released rapidly at first (burst effect) and then release continued at a slower rate.
The variation between batches was greatest over the first phase of release. Table 6.5 shows that the standard deviation (S.D) expressed as a percentage of the mean release data for the three batches progressively decreased from a maximum value of 21% after 2.5 hours of release decreased to only 4% after 273.5 hours. This may be explained by variable distribution of drug at the surface of microparticles from different batches
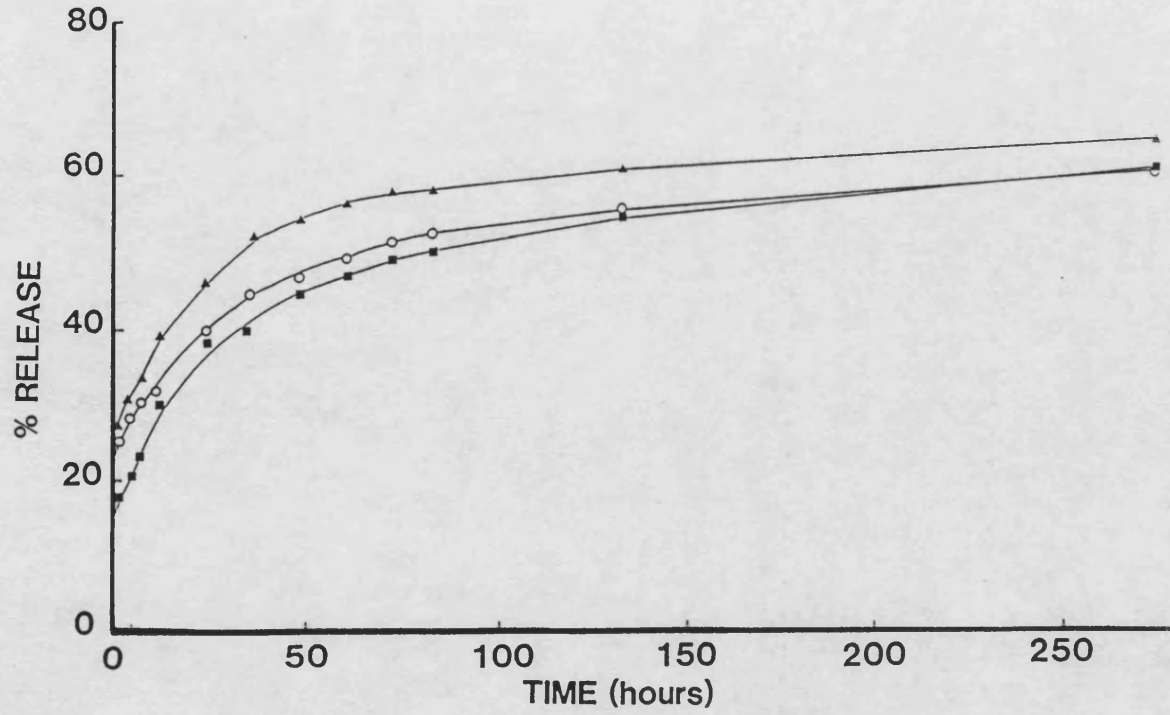
Figure 6.7. Release profiles of 3 spray–dried batches of PHB43K microparticles containing 4%w/w Methyl Red (Mean; n = 2). (S.D = less than 5% of Mean)

leading to variable drug release over the initial phase.

Table 6.5. The mean release data for the 3 batches of spray dried PHB microparticles containing 4% w/w Methyl Red.

Time (hours)	Mean % Release (of 3 batches)	Standard Deviation of mean (S.D)	S.D as a % of mean
2.5	23.2	4.9	21
5.0	26.5	5.1	19
7.5	29.0	5.0	17
12.0	34.9	4.3	12
24.5	41.6	4.2	10
36.0	45.9	6.3	14
48.0	49.0	5.3	11
60.0	50.7	5.1	10
72.0	52.9	4.8	9
84.0	53.4	3.9	7
132.0	56.9	3.5	6
273.5	61.6	2.7	4

In order to explain the mechanism of drug release from PHB microparticles attempts were made to fit the release data to the established models proposed by Higuchi [489] and a modification of this model as proposed by Brophy and Deasy [490]. Cardinal [491] has stated that the general equation required to describe drug release from a matrix device (slab or particles) will depend on a number of factors, including the design of the device, the geometry, the initial drug loading and the method of manufacture. Nevertheless, the basic elements of the release rate equation can all be found in the Higuchi model. The equation was originally utilized to define drug release from a porous ointment base and can be stated as:

$$Q = A [D Cs (2C_0 - Cs) t]^{1/2} \quad \text{...............} \quad (6.1)$$

where Q = fraction of drug released, D = diffusion coefficient, C_s = solubility of drug in matrix, C_0 = initial drug loading, A = Area of device, and t = time.

Although this equation describes release from a slab–type matrix, modifications of this

243

equation have been used to model release from other geometries [491 – 492]. The principle

of all is that drug release is proportional to the square – root – of – time. The derivation

of the Higuchi model is given in standard textbooks and will not be included here. In

the development of this equation a number of assumptions were made which can be

summarised as follows: a) infinite dimensions in two coordinates; b) a pseudo – steady

state exists; c) A >> C_s; d) the diffusion coefficient is constant; e) diffusion through

the polymer is the rate controlling step rather than dissolution of the crystal; and f)

the diffusional process occurs through the polymer matrix rather than through solvent

filled pores or channels within the matrix [491].

The Brophy and Deasy model is an extension of the square – root – of – time kinetics model

proposed by Higuchi. In their original paper [490], the authors have given a summary of

the complex mathematical derivation involved in their model but a more detailed

derivation has been given by Majid [286]. The model was originally used to describe the

in vitro release of sulphamethizole from PHB microparticles of general shape and can be

summarised as:

$$F(t) = B_1\ t^{1/2} - B_2\ t \qquad\qquad\qquad (6.2)$$

where f(t) is the fraction of drug released at time, t, and B_1 and B_2 are constants, the

values of which can be determined from the intercept and slope respectively of a linear

plot of equation 6.2 in the form $\left[\dfrac{F(t)^2}{t}\right]^{1/2}$ versus $t^{1/2}$.

This extended model was developed to account for release over a greater time period and

for release from a 3 – dimensional matrix.

Figures 6.8 and 6.9 represent the data of the three spray dried batches of PHB43k

containing 4%w/w Methyl Red plotted according to the Higuchi and Brophy and Deasy models

respectively. The data did not fit either of the proposed models. This suggested that

release of Methyl Red was not entirely controlled by passive diffusion but may have also

involved drug release through aqueous pores or channels created by dissolution of

adjacent drug particles. It is likely that more than one release mechanism was

Figure 6.8. Release profiles of 3 spray – dried batches of PHB43K microparticles containing 4%w/w Methyl Red plotted according to the Higuchi model (Mean; n = 2). (S.D = less than 5% of Mean)
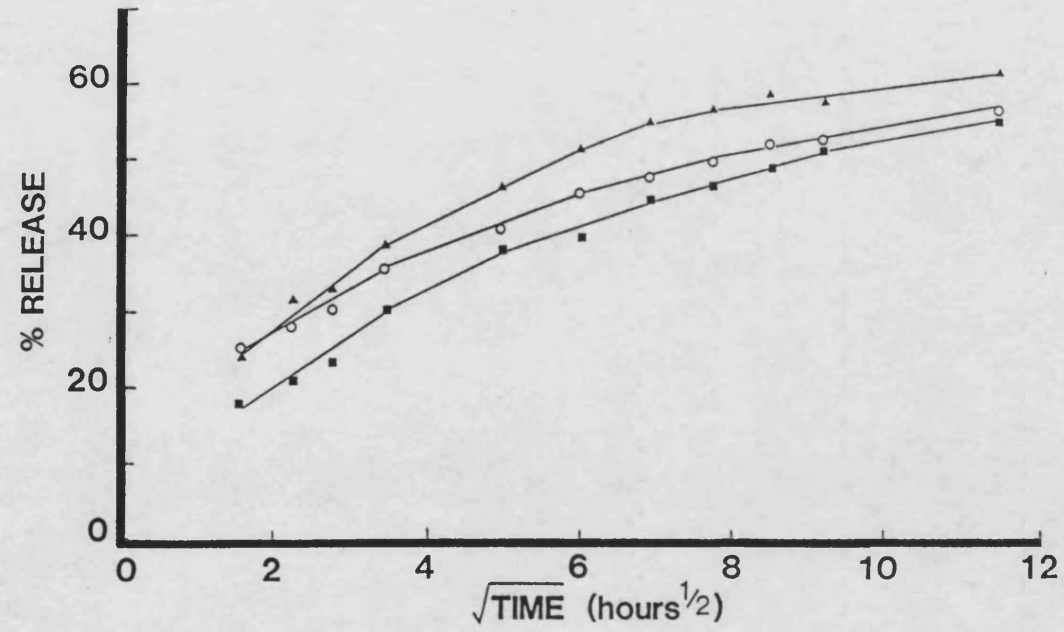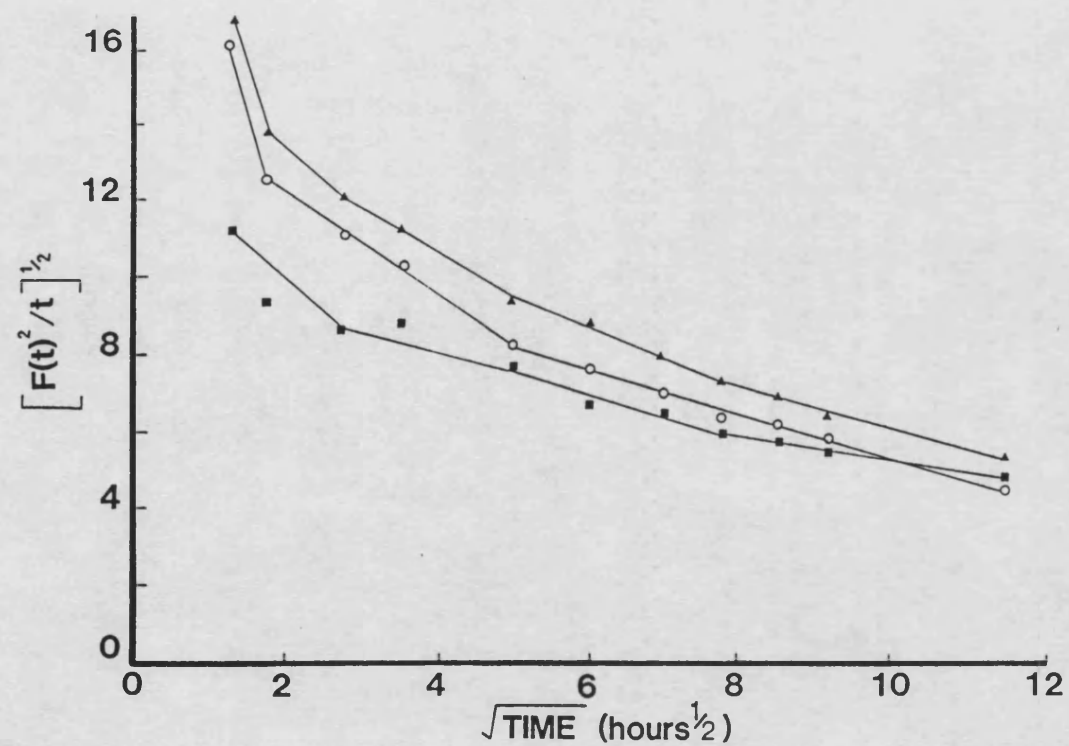
Figure 6.9. Release profiles of 3 spray – dried batches of PHB43K microparticles containing 4%w/w Methyl Red plotted according to the Brophy and Deasy model (Mean; n = 2).
(S.D = less than 5% of Mean)

operating at any stage of the release process. The initial burst effect was thought to be due to dissolution of the drug at the surface of particles followed by slower release via aqueous pore diffusion. Polymer degradation was not thought to control the release over the initial stages but may be a contributing factor in the latter stages of drug release where drug particles may become effectively trapped within the polymer matrix. The poor fit to the established models may also, in part, be due to difficulty in meeting all the assumptions of the respective models, such as achieving perfectly sink conditions.

Donbrow *et al* [493] have suggested that in polydisperse particulate systems the overall release profile recorded is a complex summation of release kinetics from individual particles. Using curve fitting mathematics, the authors found that drug release from ensembles of microparticles consisting of individual entities which release drug at constant rates may actually follow zero order, first order or biphasic equations. The release equation observed depends upon the statistical distribution of release determining parameters (such as drug loading) among the population. Donbrow *et al* [493] concluded that it is impossible to determine the true mechanisms or the nature of the heterogeneous distribution without extensive studies on individuals in populations.

It was beyond the scope of this study to assess whether the spray dried aggregates were homogeneous in release determining factors such as drug loading. In terms of particle size, spray dried aggregates of PHB exhibited normal size distributions as deduced from the Malvern particle sizer analysis. However in the case of the smaller irreversibly fused spheres making up these aggregates, it would be a near impossible task to assess heterogeneities in release determining factors. Such heterogeneities may have contributed to the deviation from the Higuchi square-root-of-time kinetics of Methyl Red loaded PHB microparticles.

6.4.2.2 The effect of drug loading

In · the study of drug loading on release characteristics, batches of Methyl Red-loaded

microparticles of PHB43K were prepared in replicate using the standard spray drying parameters listed in Table 6.2. A selection of drug-polymer ratios were spray dried to obtain a range of Methyl Red concentrations from 2 to 8%w/w in PHB 43K microparticles. Table 6.6 shows the particle sizes and actual drug loadings achieved after spray drying.

Table 6.6. The effect of drug loading on product characteristics (Mean $\pm$ Range; n = 2)

Nominal Drug loading (%w/w)	Actual Drug Loading (%w/w)	Particle size (um) SMD
2.0	1.97 ±0.15	22.07 ±0.59
4.0	4.24 ±0.06	21.49 ±0.76
8.0	7.85 ±0.32	20.07 ±0.67

In vitro release experiments for different drug loadings were carried out at 37°C in the shaking waterbath (180 oscillations/ min). Release profiles of microparticles agitated in this way showed that release was more rapid than found with the rotating basket method. This may have been due to a reduction in the hydrodyanamic boundary layers around the particles. Figure 6.10 shows that at least 90% of drug release was complete within 2 days. Thus drug release was not controlled by polymer erosion. Figure 6.11 shows release of Methyl Red from the same experiment over the first 7 hours. Release was dependent on drug loading. As the amount of drug incorporated into the polymer microparticles was increased the percentage of drug released also increased. The time taken for 50% (t_{50x}) of the Methyl Red to be released increased from 1.5 hr for an 8% loading to 4 hr for a 2% loading.

The findings of this study on the effect of drug loading were in agreement with those reported for PHB by Brophy and Deasy [306], Juni et al [310], and Korsatko et al [304].

However, the data did not fit the models of Higuchi (Figure 6.12) or Brophy and Deasy (Figure 6.13). It was thought that release of methyl Red from these spray-dried

Figure 6.10. The effect of drug loading on release of Methyl Red from PHB43K spray – dried microparticles (Mean; n = 2). (S.D = less than 5% of Mean)
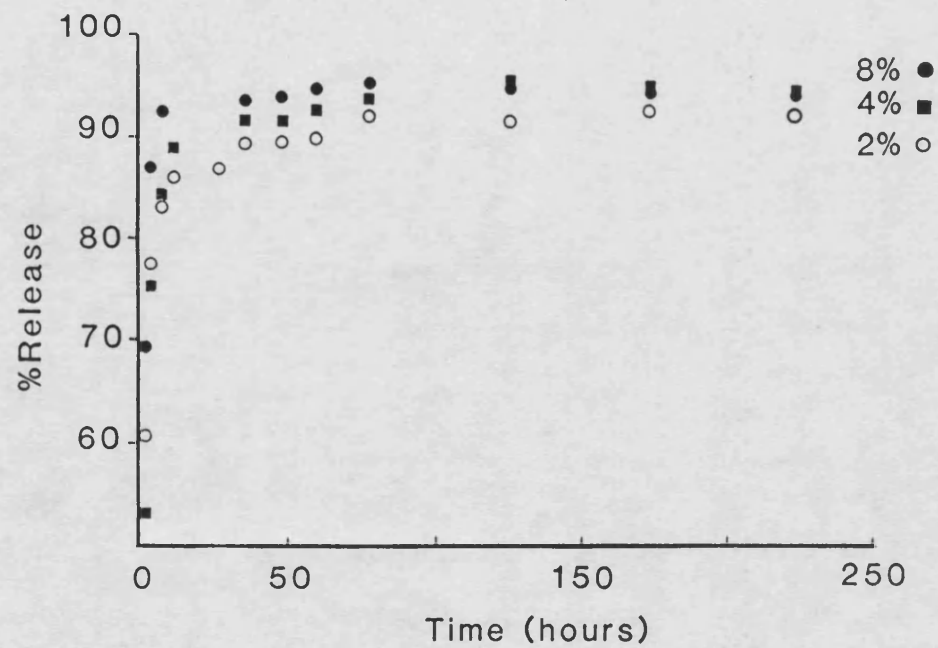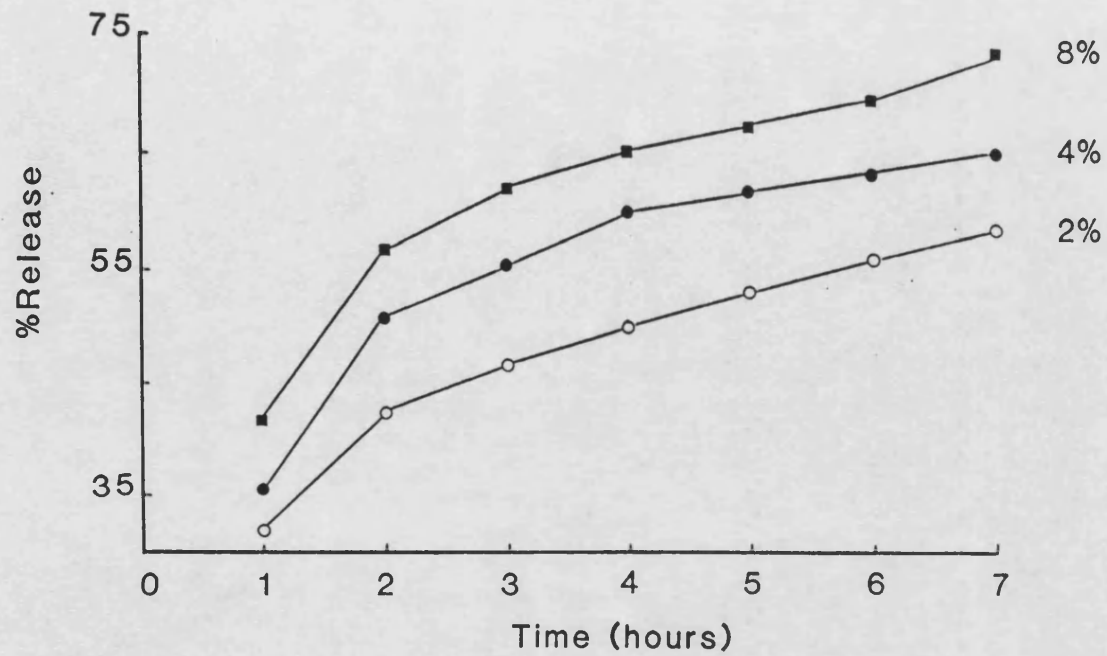
Figure 6.11. The effect of drug loading on the early phase of release of Methyl Red from PHB43K spray – dried microparticles (Mean; n = at least 2). (S.D = less than 5% of Mean)

Figure 6.12. The effect of drug loading on release of Methyl Red from PHB43K spray – dried microparticles plotted according to the Higuchi model (Mean; n = at least 2). (S.D = less than 5% of Mean)

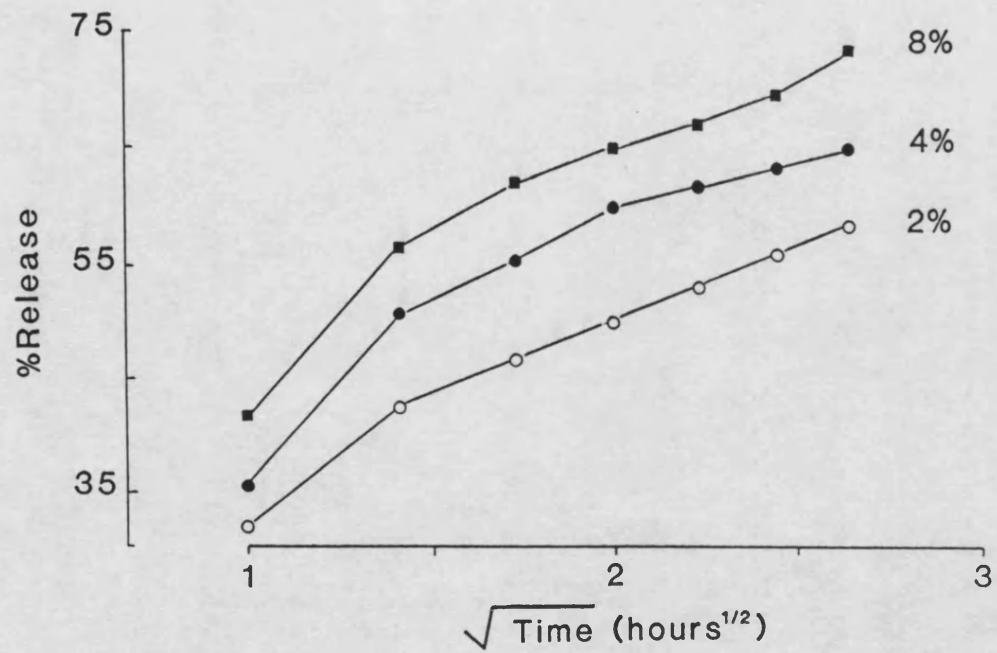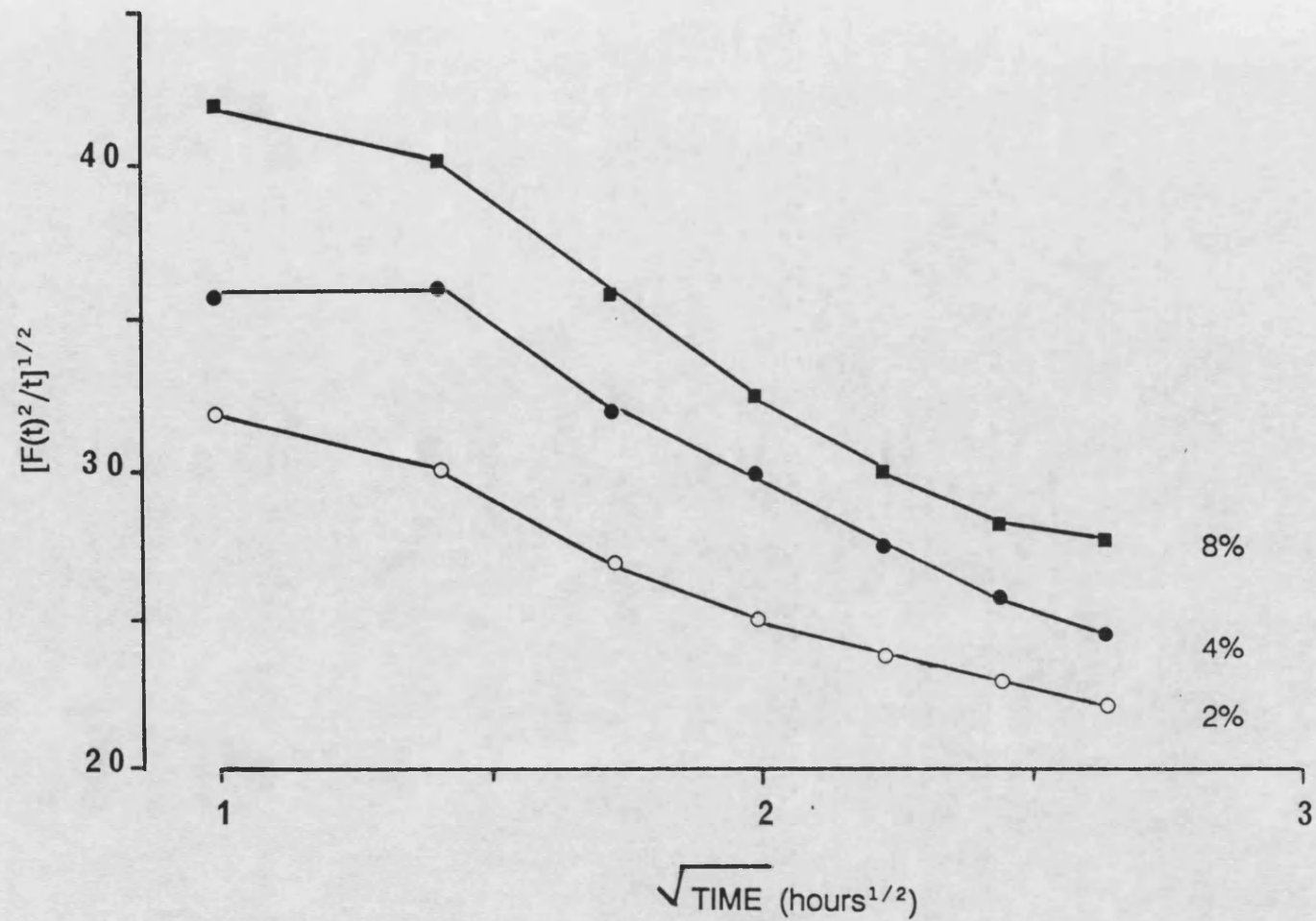Figure 6.13. The effect of drug loading on release of Methyl Red from PHB43K spray-dried microparticles plotted according to the Brophy and Deasy model (Mean; n = at least 2).
(S.D = less than 5% of Mean)

microparticles occurred according to a combination of passive diffusion and aqueous channel formation as proposed by Langer and coworkers [494]. This model is further discussed for thin film matrices in chapter 8.

In order to assess if the drug was dispersed physically as a separate phase or at a molecular level within the PHB matrix of the microparticles, differential scanning calorimetric studies were carried out. No separate peaks for the melting of the drug were seen in the DSC traces at drug loadings up to 8%. However, no firm conclusions could be drawn because of similar melting temperatures for both the drug and the homopolymer. In the case of copolymer films, which had lower melting temperatures compared to the drug, DSC traces were generally devoid of a melting transition for the drug and thus suggested a molecular mix of drug and copolymers (see chapter 7). It is therefore thought that a similar molecular mix of drug existed within the homopolymer.

6.4.3 The effect of polymer molecular weight on drug release

Figure 6.14 shows the release of 4%w/w loadings of Methyl Red from different molecular weights of PHB. The percentage of drug released increased when the molecular weight of PHB was increased from 23K up to 140K. The results were consistent with the findings of Brophy and Deasy [306]. The authors found that high molecular weight of PHB (500 – 1000k) released sulphamethizole at a more rapid rate than PHB of 140K MW.

6.4.4 The effect of copolymer content on drug release

High molecular weight P(HB–HV) copolymers could not be spray dried to form an acceptable product. A similar product to that obtained with high molecular weight PHB was observed. Problems were also encountered in spray drying PHV16 of molecular weight 41K. The only copolymer available in the study which formed a recoverable product was PHV17 of Mw 14K. The release profile of this copolymer with a Methyl Red loading of 4% w/w is compared with the equivalent product obtained with PHB 23K in Figure 6.15. Drug release from the copolymer appeared to be more rapid than from PHB 23K. No firm conclusions can be drawn from this study on the effect of copolymer composition on drug release from
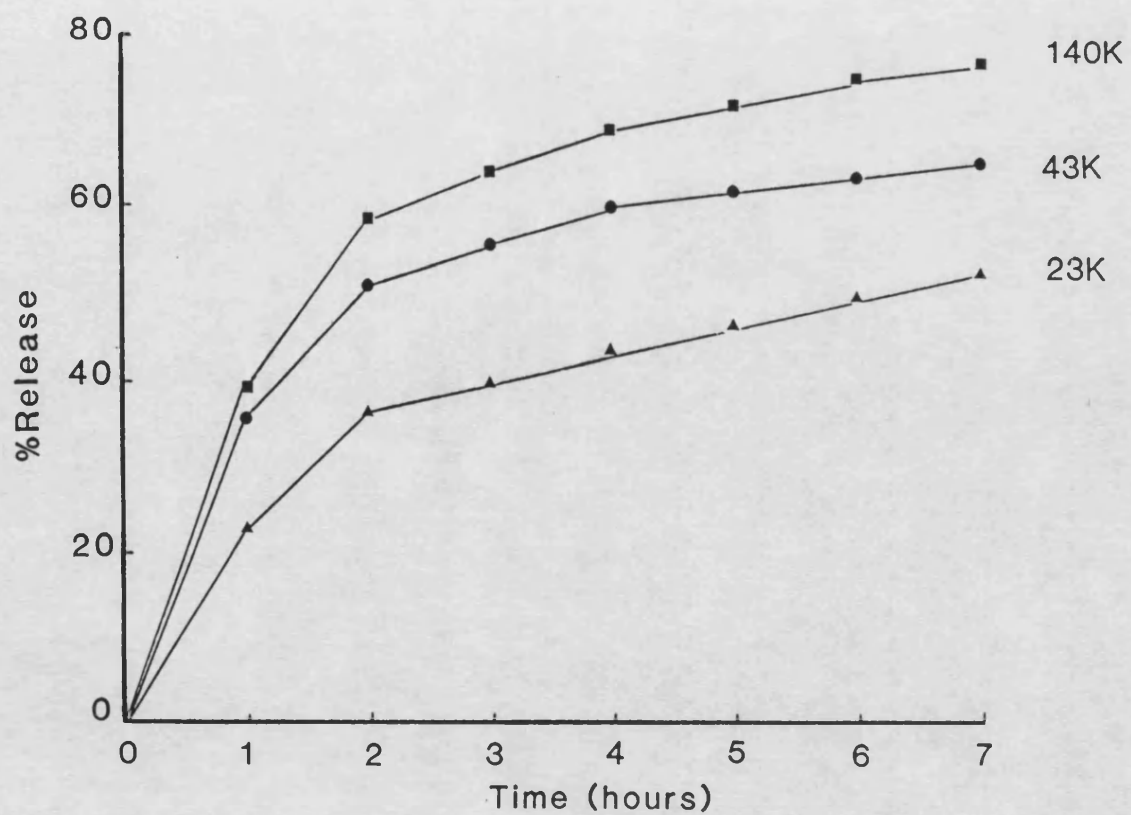
Figure 6.14. The effect of polymer molecular weight on release from PHB43K spray-dried microparticles containing 4%w/w Methyl Red (Mean; n = at least 2). (S.D = less than 5% of Mean)
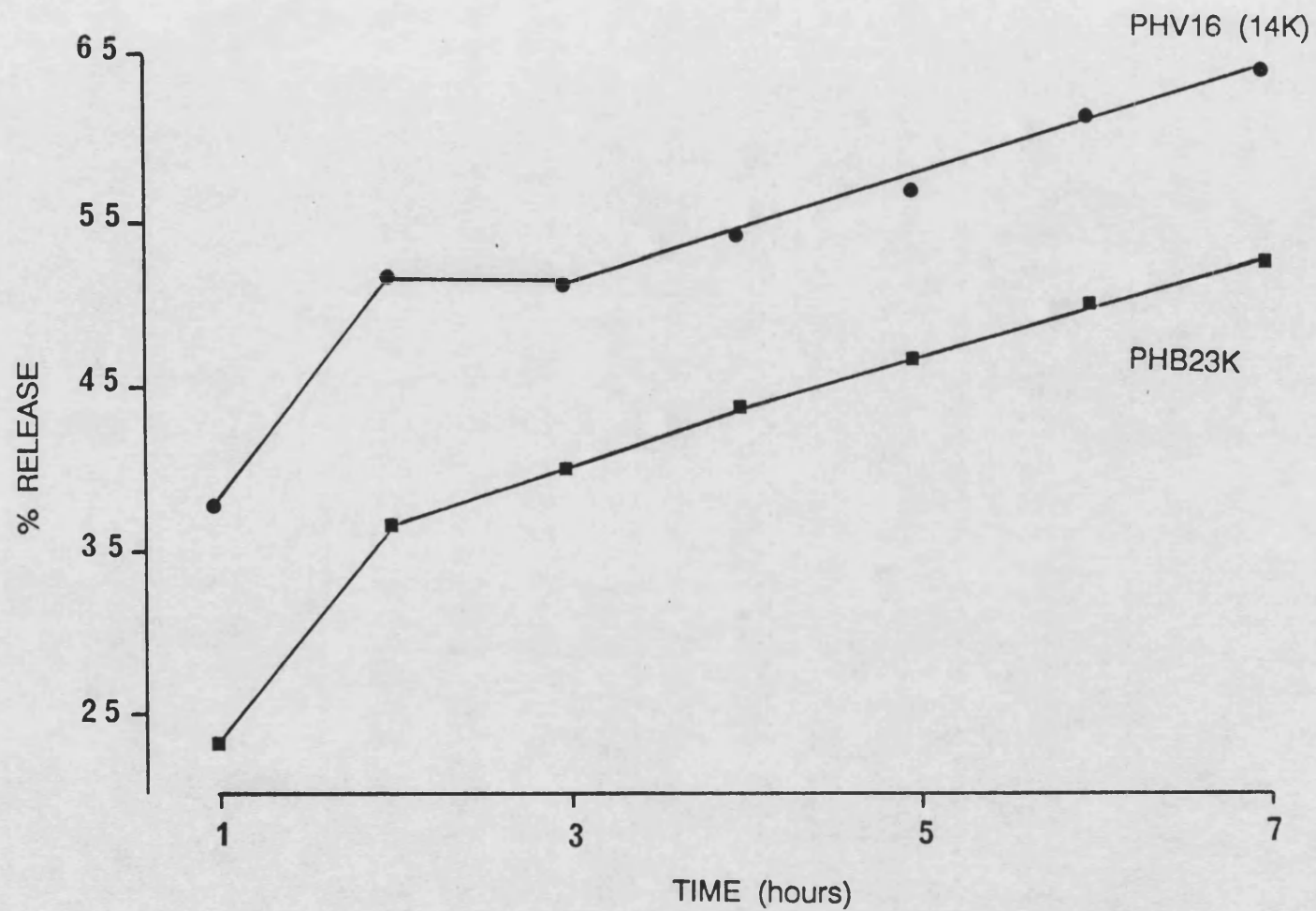
Figure 6.15. Release profiles of PHB23K and PHV16 (14K) containing 4%w/w Methyl Red (Mean; n = 2).

(S.D = less than 5% of Mean)

spray–dried particles since the molecular weights were not close enough to be considered equivalent. A study of drug release from P(HB–HV) copolymer films containing up to 28 mole% HV is presented in chapter 8.

6.4.5 The effect of spray drying processing parameters

The operational variables studied were polymer concentration, feed rate, inlet temperature and aspirator control. Each parameter was varied individually and the rest maintained as in the standard settings of Table 6.2. Release experiments were carried out using the rotating basket method.

6.4.5.1 The effect of polymer concentration.

The product morphology was similar for the different polymer concentrations used and was similar to that seen in Figure 6.5. The particle sizes, as shown in Table 6.7 increased with increasing polymer concentration and therefore, increasing the polymer concentration reduced the rate at which Methyl Red was released from PHB43K microparticles. The release profiles are given in Figure 6.16.

Table 6.7. Product characteristics of spray dried PHB43K microparticles containing 4% Methyl Red on changing polymer concentration (Mean $\pm$ Range; n = 2)

Polymer concentration (%w/v)	Actual Drug Loading (%w/w)	Particle size (um) SMD
0.5	4.07 ±0.11	18.07 ±0.20
1.0	4.24 ±0.06	21.49 ±0.76
2.0	4.15 ±0.12	25.98 ±1.02

6.4.5.2 The effect of feed rate

Variations in the feed rate did not significantly (p>0.05) affect drug loadings (Mean

Figure 6.16. The effect of polymer feed concentration on drug release from PHB43K spray-dried microparticles containing 4%w/w Methyl Red (Mean ± S.D., n=2)

±S.D = 4.09 ±1.2%; n=3), particle size (SMD ±S.D = 23.62 ±0.90um; n=3) or product morphology. The release data were similar for variations of feed rate from 14ml/min to 37.5ml/min and are given in Figure 6.17. An increase in the feed rate from 14ml/min to 37.5ml/min resulted in a reduction in the outlet temperature of approximately 10-15°C but this did not seem to modify product characteristics.

6.4.5.3 The effect of inlet temperature

Variations in the inlet temperature did not significantly (p>0.05) affect the particle size (SMD ±S.D = 21.60 ±0.91um; n=3), drug loadings (Mean ±S.D= 4.14 ±0.90%; n=3), or the microscopic morphology of the product. However macroscopic observations suggested that the product produced at an inlet temperature of 85°C appeared to be a 'wet mass' and not as free flowing as the product produced at 205°C. This was attributed to incomplete drying at low outlet temperatures resulting from the low inlet temperatures.

The release profiles of products containing 4%w/w Methyl Red produced at varying inlet temperatures are shown in Figure 6.18. The rate of drug release decreased as the inlet temperature was increased. As particle sizes were similar, this was thought to be due to increasing matrix porosity with decreasing inlet temperature. Incomplete drying of product at low inlet and outlet temperatures suggested greater solvent retention within the polymer matrix. The associated porosity resulted in more rapid release of Methyl Red. However, there was no evidence of pores at the surface of microparticles in scanning electron micrographs taken at magnifications up to x3500.

6.4.5.4 The effect of aspirator setting

The aspirator control adjusts the flow-through of hot air drawn in to the drying chamber. At a maximum setting of 10 on the dial of the aspirator control, the Buchi is designed to have a hot air flow-through of about 45m³/h.This value was supplied by the manufacturers and not confirmed. The settings on the dial could be adjusted on an arbitrary scale from 1 to 10.
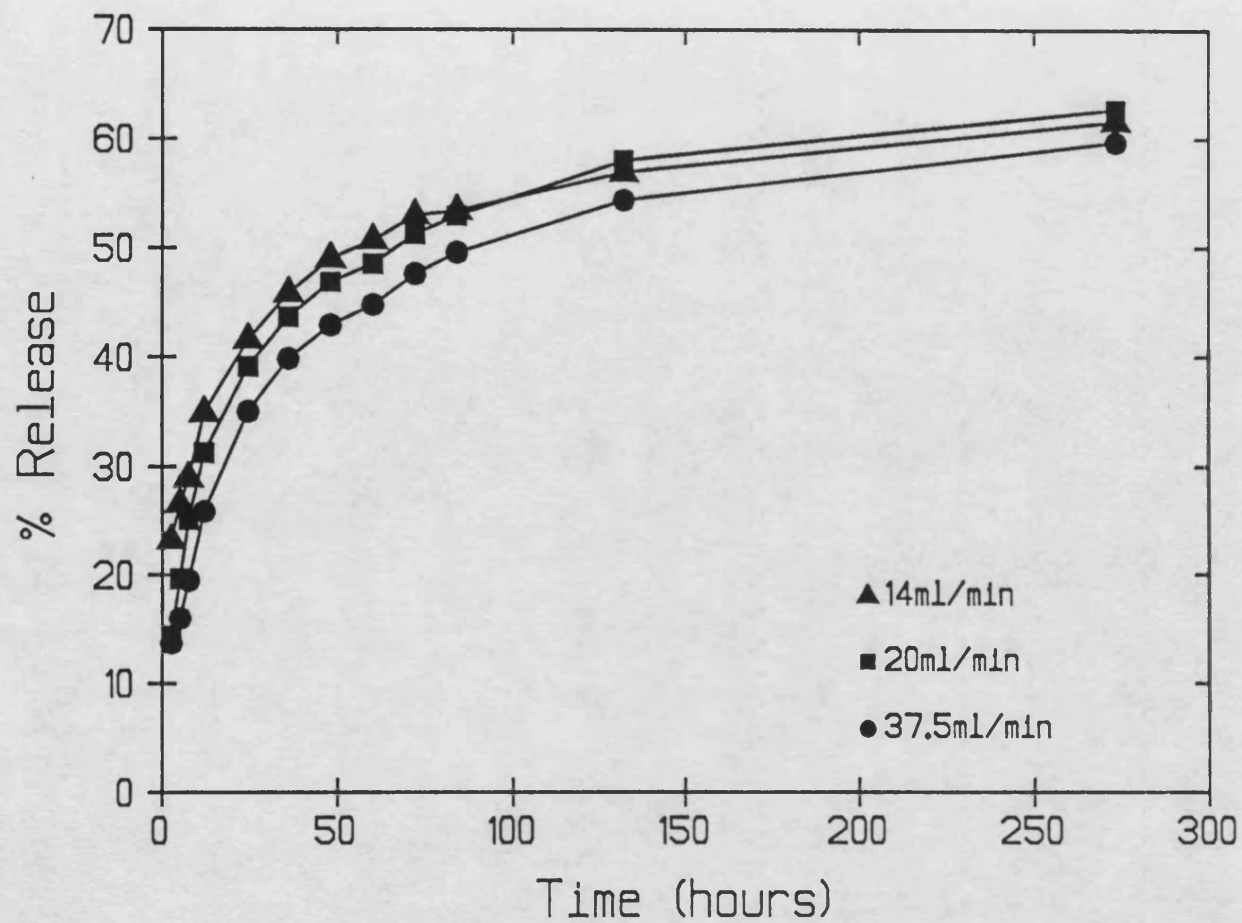
Figure 6.17. The effect of feed rate on drug release from PHB43K spray–dried microparticles containing 4%w/w Methyl Red (Mean; n = at least 2). (S.D = less than 10% of Mean)
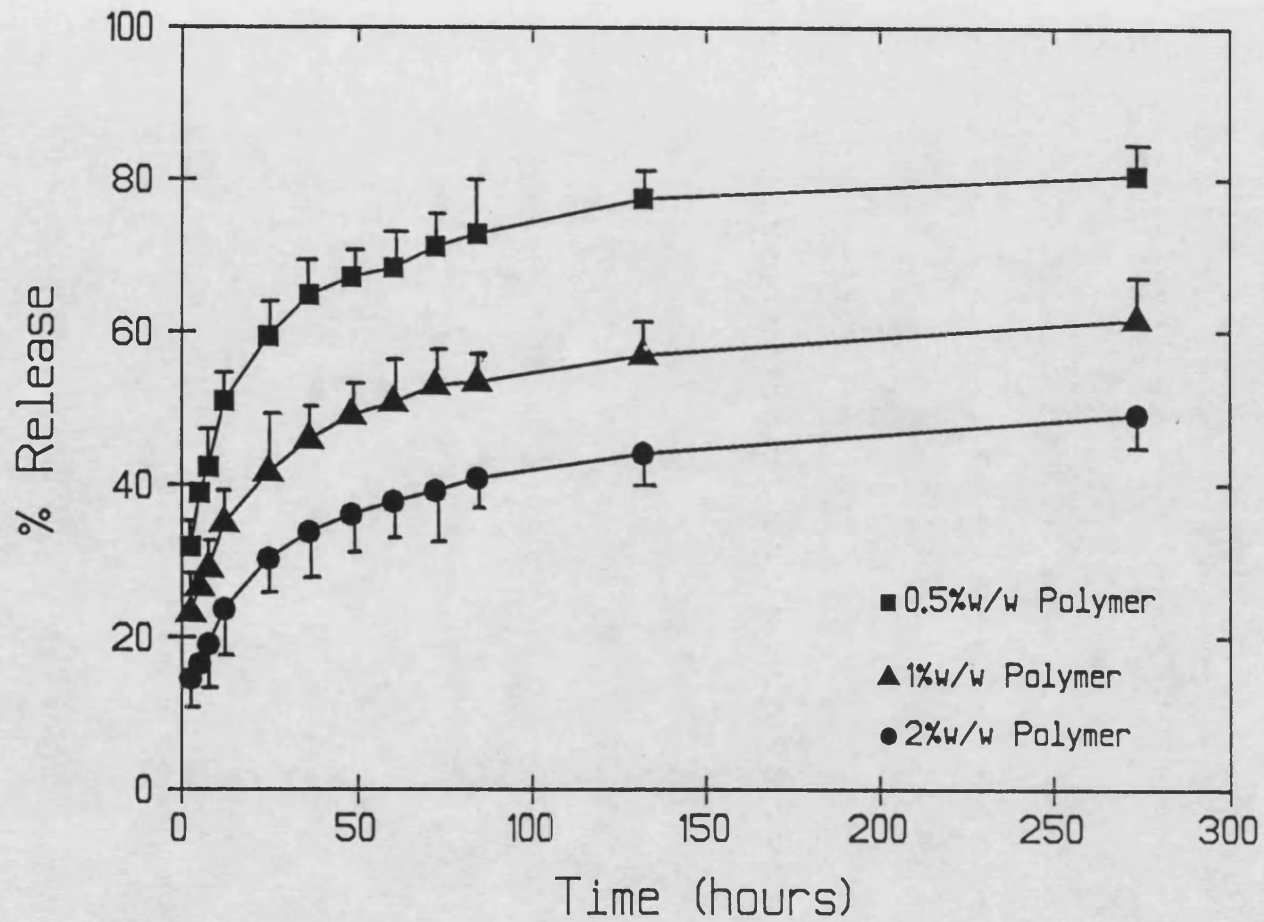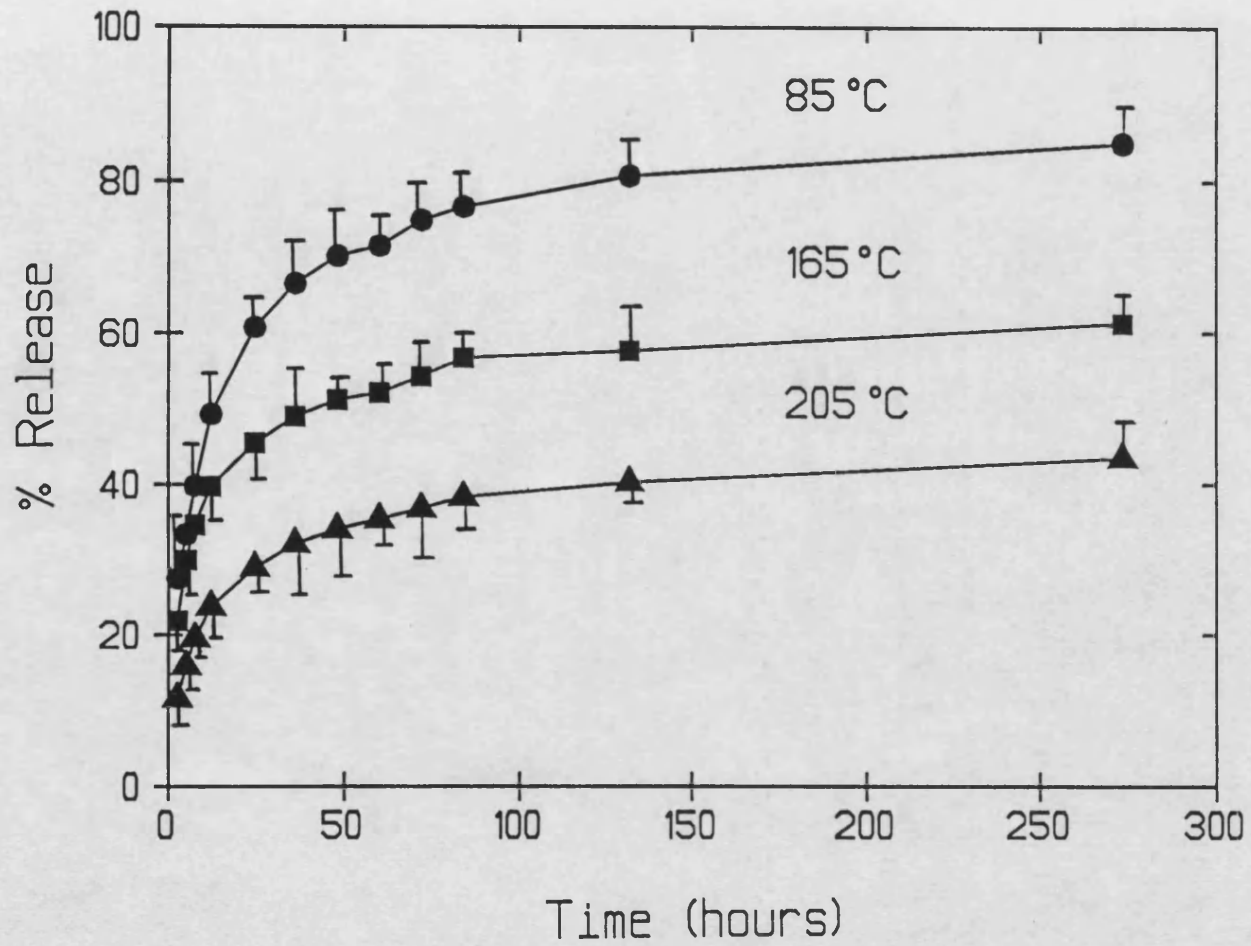
Figure 6.18. The effect of inlet temperature on drug release from PHB43K spray-dried microparticles containing 4%w/w Methyl Red (Mean ± S.D., n=2)
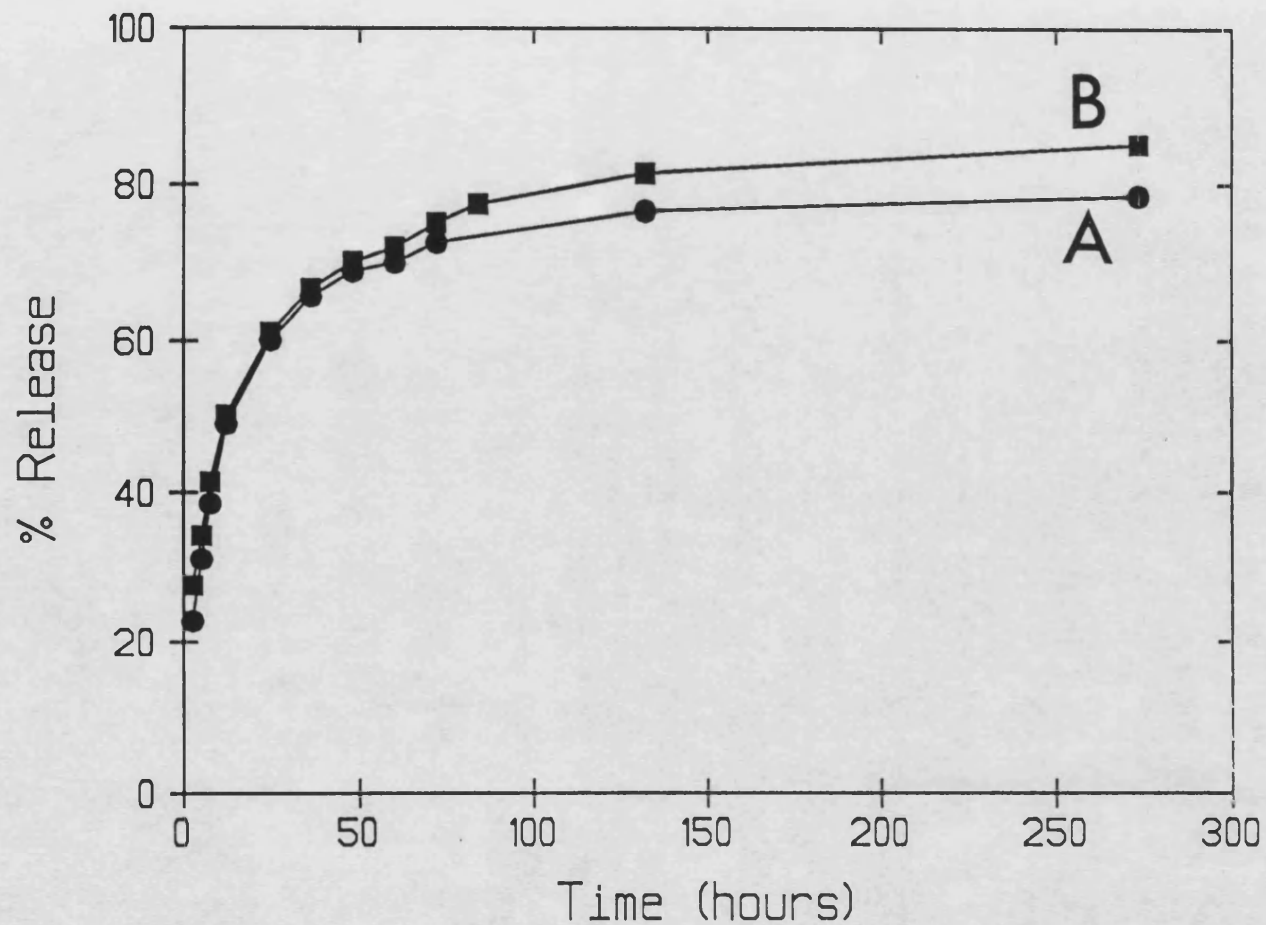
Figure 6.19. The effect of aspirator setting on drug release from PHB43K spray-dried microparticles containing 4%w/w Methyl Red (Mean; n = at least 2) A = setting 1; B = setting 10. (S.D = less than 10% of Mean)

Table 6.8 shows the variation in particle size with increasing aspirator setting. Although the particle size was significantly different ($p<0.05$) at the two settings the release profiles were similar as shown in Figure 6.19.

Table 6.8. The effect of aspirator setting on the spray–dried product characteristics. (Mean $\pm$ Range; n = 2).

Aspirator setting	Actual Drug Loading (%w/w)	Particle size (um) SMD
1	4.11 $\pm$0.15	16.49 $\pm$0.16
10	4.24 $\pm$0.06	21.49 $\pm$0.76

6.5 CONCLUSIONS

PHB of molecular weights up to 140K could be spray–dried to form a fine free flowing product. Film forming molecular weights of PHB could be spray dried from dilute solutions but the product was more fibrous.

Spray–dried microparticles were not spherical but fused aggregates (20–40um) of smaller spheres.

Release from microparticles was generally not controlled by polymer degradation. Drug release from PHB microparticles was dependent on drug loading and complete within 2 days under agitated conditions (180 oscillations/min in shaking water bath).

Release did not fit the Higuchi or Brophy and Deasy models and was thought to occur by aqueous channel formation between adjacent drug particles.

The Buchi spray dryer produced a similar product morphology irrespective of the operational settings chosen. Particle size could be controlled by varying the polymer concentration in the feed. The inlet temperatures chosen for spray drying in this study did influence release characteristics of the product. Some batch–to–batch variation in release profiles was observed.

CHAPTER 7

P(HB-HV) POLYMER FILMS AS IMPLANTABLE DRUG DELIVERY DEVICES

7.1 INTRODUCTION

The use of biodegradable polymer devices as implants for sustained or controlled drug delivery has received much attention over the last two decades. The major advantage of these systems is that the polymeric device will degrade and thus will not require surgical removal after drug release is complete. In addition to colloidal carriers in the form of microspheres and nanoparticles (see chapter 6), macroscopic matrices such as films, slabs and cylinders [31,38,40,42,44] have also been investigated as possible sub-cutaneous and/or intra-muscular implants. The major advantage of implanting large matrices is that they can be easily removed from the implant site should any complications arise during release.

In this chapter thin films fabricated by melt-processing and solution casting have been investigated as potential matrices for implantable drug delivery systems.

7.1.1 AIMS AND OBJECTIVES

1. To investigate and compare *in vitro* release of model drugs from solvent cast and melt processed P(HB-HV) films for implantation.

2. To study the mechanism of drug release from P(HB-HV) films containing low and high molecular weight drugs.

3. To study the effect of drug loading and P(HB-HV) copolymer composition on *in vitro* drug release

4. To fabricate drug-loaded thin films with known crystalline morphologies and to investigate the effect of film morphology on *in vitro* drug release rates and mechanisms.

7.2 MATERIALS

Azocasein was a gift from Dr. D.J.G. Davies, Head of School of Pharmacy and Pharmacology, University of Bath, Bath BA2 7AY.

All other materials were identical to those used in chapters 2 and 3.

7.3 METHODS

7.3.1 Preparation of P(HB-HV) polymer films

7.3.1.1 Solvent cast films

Polymer films (30-50um) were cast from chloroform solution (4%w/v polymer) as described in chapter 2. Methyl Red was incorporated into polymer films in variable amounts to achieve drug loadings of 2, 4 and 8%w/w. Films were stored for 2 weeks after casting and before use in release studies.

7.3.1.2 Incorporation of azocasein into solvent cast films

Azocasein was used as a model protein and macromolecule. Azocasein is the milk protein casein with an azo linkage added for easy assay by uv-vis spectroscopy. A suitable dispersion of the model protein could not be achieved from simple solvent evaporation of a drug-polymer suspension. A better distribution of drug within solvent cast films was achieved by using ethanol as a cosolvent. Incorporation of azocasein into polymers was achieved by firstly dissolving known amounts (approximately 6.4mg) of the drug in a mixture of 0.2ml distilled water and 0.4ml of ethanol. This was added to 7.4ml of a 4%w/v polymer solution in chloroform. The mixture was sonicated in a bath (Deakon FS100 Frequency sweep; Deakon Ultrasonics Ltd,UK) for 5mins and then left to stand for about 1 hour. Once the air bubbles had been removed the film was cast onto glass as described in chapter 2.

7.3.1.3 Melt pressed films

As-received polymer samples were size reduced in a pestle and mortar and blended with known amounts of drug (Methyl Red) to achieve a range of drug loadings up to 8%w/w. The powdered polymer-drug blends were melt pressed into films according to the method described in chapter 2. Films were stored for two weeks before use in release studies.

7.3.4 *In vitro* release studies

Solvent cast films (30 – 50um) containing Methyl Red or Azocasein were cut into 3 x 2 cm strips using a sharp scalpel and a glass template. Discs (1.5cm diameter) were cut out of the melt processed films using a cork borer. The thickness of melt pressed disks used in release studies was in the range 300 – 400um and mass of disks was in the range 30 – 40mg. Each disc was weighed individually before use.

Release was carried out in vials containing 25ml phosphate buffer (see appendix C) pH 7.4 at 37°C. Vials were shaken in a waterbath at a frequency of 180 oscillations/min. In order to maintain conditions close to sink, variable amounts of medium were periodically removed. Release of Methyl Red and Azocasein was determined by uv – vis spectroscopy at 430nm and 230nm respectively.

7.3.5 Assay of drug content
7.3.5.1 Methyl Red

In the case of both solvent cast and melt pressed films, a known weight of sample (20mg) was dissolved in 100ml of chloroform and assayed by uv – vis spectroscopy at 490nm.

7.3.5.2 Azocasein

Film samples (20 – 30mg) were dissolved in 50ml of chloroform. The azocasein was removed by repeated extraction with 2ml of phosphate buffer (at least 10 extractions) and the cumulative extractions were assayed by uv – vis spectroscopy at 230nm. The drug loadings achieved with both Methyl Red (MR) and Azocasein (AZ) are summarized in Table 7.1.

Table 7.1. Summary of Drug loadings (Mean ± Range; n = 2)

Sample	Nominal Drug loading (%w/w)	Actual Drug Loading (%w/w)
A. Solvent cast Films + MR		
PHB380K	2.0	1.98 ±0.21
	4.0	4.12 ±0.32
	8.0	7.89 ±0.21
PHV6	4.0	3.87 ±0.11
PHV20	4.0	3.92 ±0.27
PHV27	4.0	4.12 ±0.33
B. Solvent cast films + AZ		
PHB380K	2.0	1.91 ±0.24
PHV6	2.0	2.15 ±0.26
PHV12	2.0	2.04 ±0.19
PLA	2.0	1.89 ±0.23
C. Melt Pressed discs + MR		
PHB380K	2.0	1.82 ±0.20
	4.0	3.89 ±0.31
	8.0	7.75 ±0.26
PHV6	4.0	3.74 ±0.33
PHV20	4.0	3.97 ±0.17
PHV27	4.0	4.01 ±0.19

7.3.6 Scanning electron microscopy of films

Freeze – fractured samples were prepared by immersing films in liquid nitrogen until brittle and subsequent fracture with a single blow of a hammer. Both freeze – fractured and normal film samples were then sputter coated and examined by scanning electron microscopy as described in chapter 6.

7.3.7 Differential Scanning Calorimetry of films

Samples were heated from ambient to melt at a programmed heating rate of 20K/min in a Dupont DSC 910/ 9900 Thermal Analyser as described in chapter 3.

7.4 RESULTS AND DISCUSSION

7.4.1 Characterization of solvent cast films.

P(HB−HV) polymer films prepared by solvent casting were characterized in terms of their surface properties. Surface properties of materials for implantation are known to be important in determining the wettability and surface biocompatibility [496]. Furthermore, initial solvation and wetting of the film surface will depend on the surface propensity of the pendent hydrophilic functional groups (i.e. carbonyl) at the surface and this in turn will affect the susceptibility of the polymer surface to hydrolytic attack [497]. It is thought that the initial stages of degradation may alter the distribution of functional groups and this may in turn result in altered biological response to the eroding polymer [497].

Static Secondary Ion Mass Spectroscopy (SSIMS) and X−ray Photoelectron Spectroscopy (XPS) techniques have been used to investigate the surface composition of P(HB−HV) polymer films [497]. This work was carried out in collaboration with Nottingham and Surrey universities. The results of these studies are presented in appendix A. The XPS data confirmed the exceptional purity of P(HB−HV) polymers and gave good agreement between the theoretical and experimental elemental ratios. Similarly the functional group analysis was consistent with the stoichiochemistry. The SSIMS data also showed no evidence of any extraneous or organic contamination in the polyester surfaces. The fact that SSIMS is useful in detecting impurities at the surface of devices was recently highlighted when SSIMS was successfully used to determine residual concentrations of surfactant (sodium dodecyl sulphate) on the surface of solvent evaporated PHB microparticles [498]. The surfactant was found to be present at the surface of particles even after extensive cleaning by dialysis and ultracentrifugation [498]. SSIMS was also useful in determining the HV content at the surface of P(HB−HV) copolymers. Studies [499] on a range of P(HB−HV) copolymers showed that the HV content at the surface was identical to the bulk HV content as determined by ^{1}H−NMR (see chapter 2).

P(HB−HV) polymer films cast onto glass had two contrasting surfaces. The film surface in contact with glass was smooth and shiny whereas the surface of the film exposed to the air was dull and rough. Contact angle measurements on both surfaces of solvent cast films using the aqueous sessile drop method are described in appendix B. The results are summarized in Table A2.2 of appendix B. Contact angles were essentially similar for the shiny and dull surfaces of P(HB−HV) films. However the contact angles for the dull surfaces of PHV12 and PHV20 were significantly higher ($p < 0.05$) than the contact angle for their respective shiny surfaces.

The contact angles for all the P(HB−HV) polymers were in the range $67 - 85°$, suggesting that they are very hydrophobic. However for any given surface the contact angle appeared to be a complex function of HV content. The contact angles of PHB380K and PHV6 were similar to each other but significantly different ($p < 0.05$) to contact angles for PHV12, PHV20 and PHV27. The contact angles for the latter three copolymers were not significantly different ($p > 0.05$) from each other. The significance of these results in terms of surface biocompatibility is yet to be determined.

On examination of the film surfaces with the electron microscope, it was found that both surfaces (polymer−glass and polymer−air) were porous (Figures 7.1 and 7.2). The flatter, more compressed appearance of the shiny surface is clearly visible. Pores were visible on both surfaces of films. The pores appeared to be more open on the dull surface as this was the surface from which most of the trapped solvent had evaporated on drying of films. However, the number of pores appeared to be independent of copolymer composition in P(HB−HV) copolymers. This suggested that porosity of copolymer films was similar to that of the homopolymer. Electron micrographs of freeze−fractured film samples confirmed that the films were porous throughout their thickness (Figure 7.3(A)).

7.4.2 Solvent cast P(HB−HV) films containing Methyl Red

Preliminary studies showed that storage of films after casting resulted in morphological and mechanical property changes (Chapter 4). Films were therefore stored at 25°C for 14

Figure 7.1. Scanning electron micrographs showing surface pores in a solvent cast film of PHB380K on

(A) the shiny surface; glass – polymer interface and

(B) the dull surface; polymer – air interface.
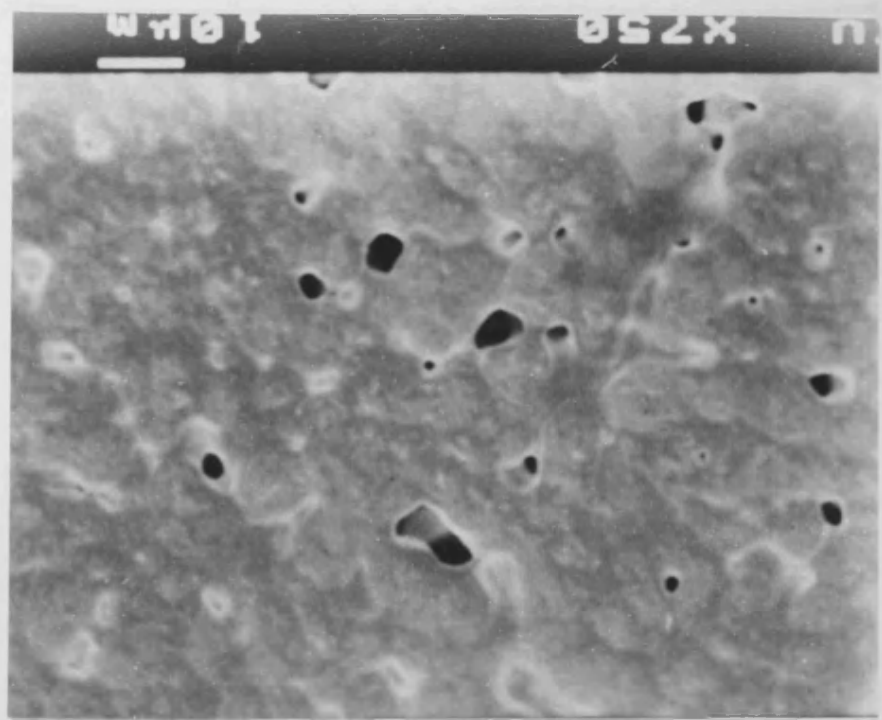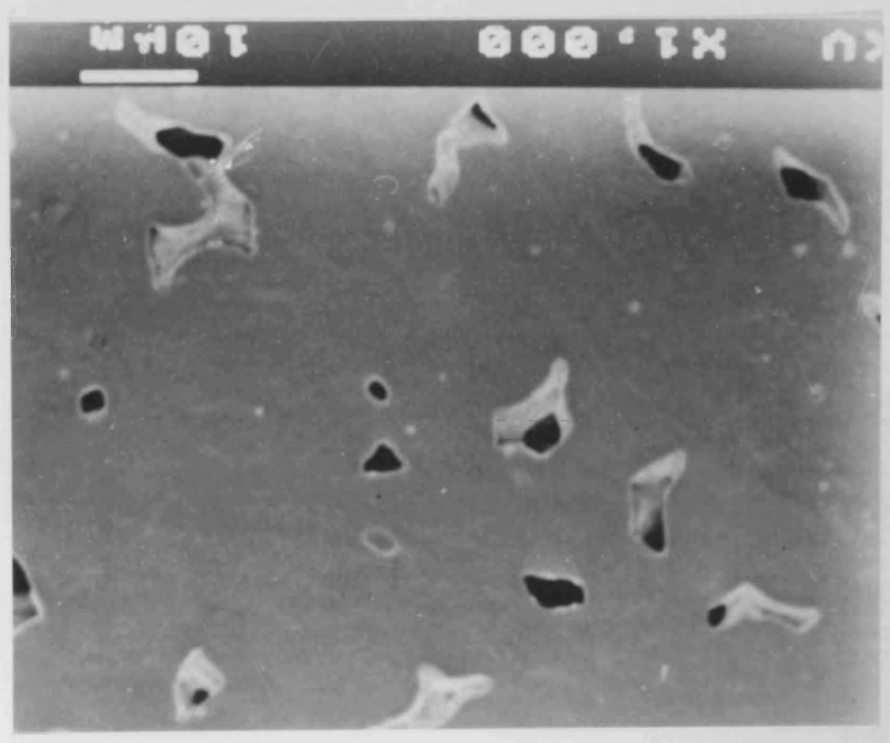
Figure 7.2. Scanning electron micrographs showing surface pores in a solvent cast film of PHV27 on

(A) the shiny surface; glass – polymer interface and

(B) the dull surface; polymer – air interface.

5KU   X1,000   10μm   005151

5KU   X2,000   10μm   005156
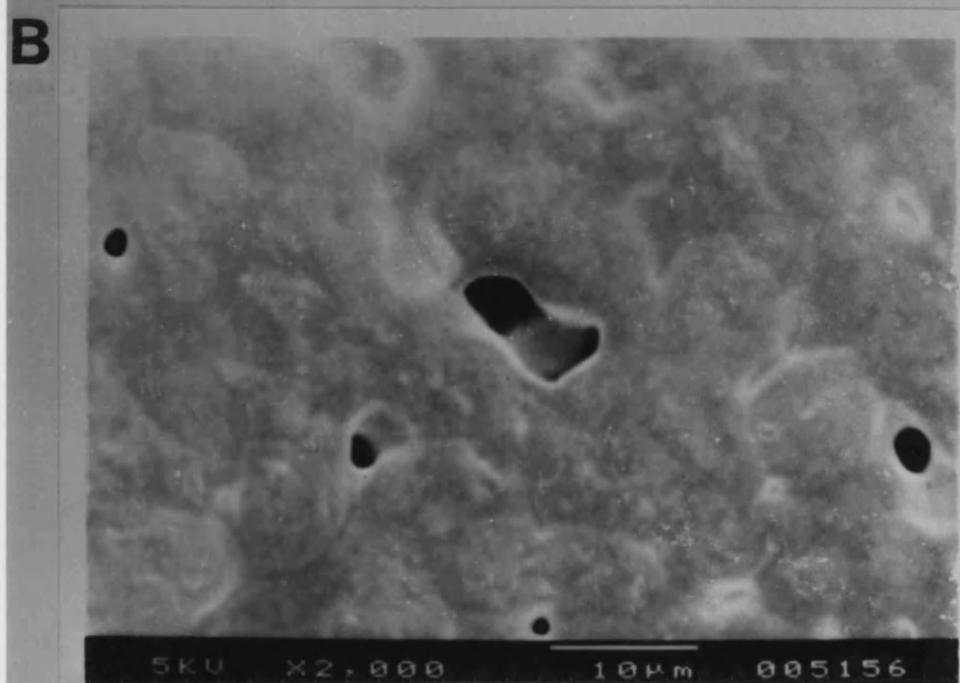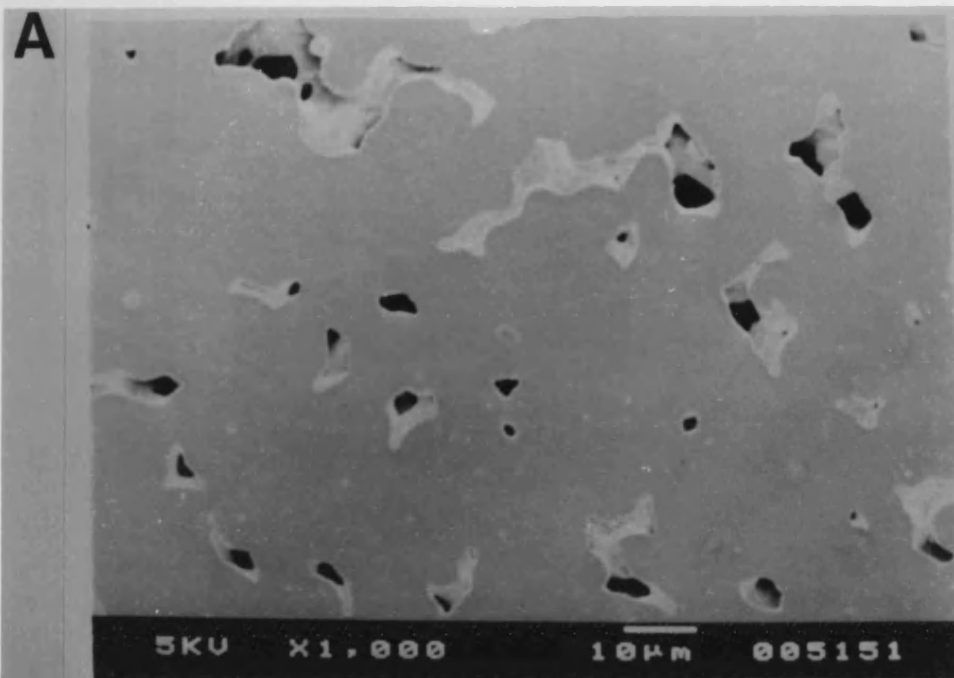
Figure 7.3. Scanning electron micrographs showing a freeze-fractured section (A) and Methyl Red on the surface (B) of solvent cast films of PHB380K.
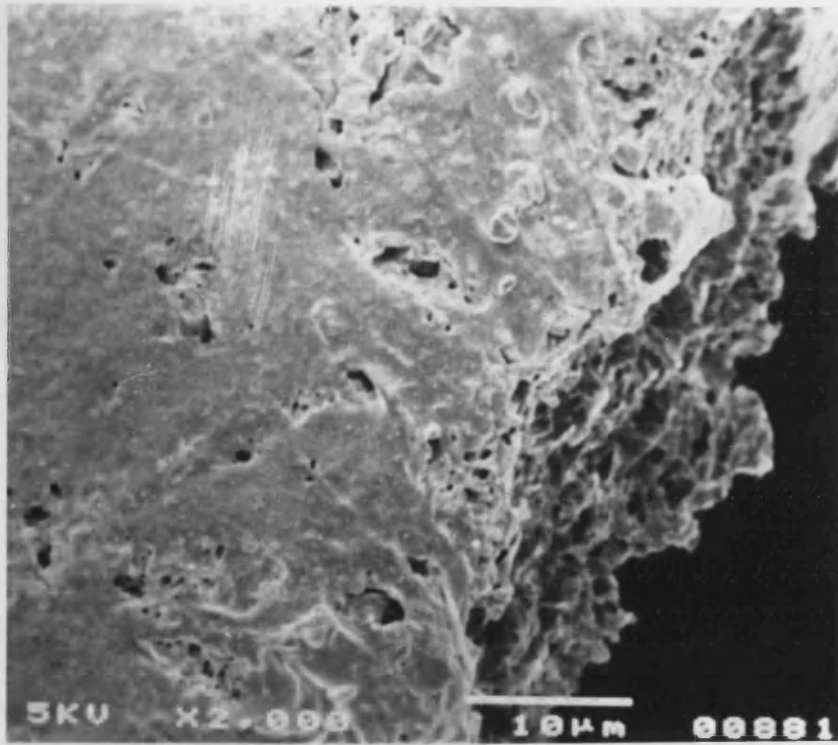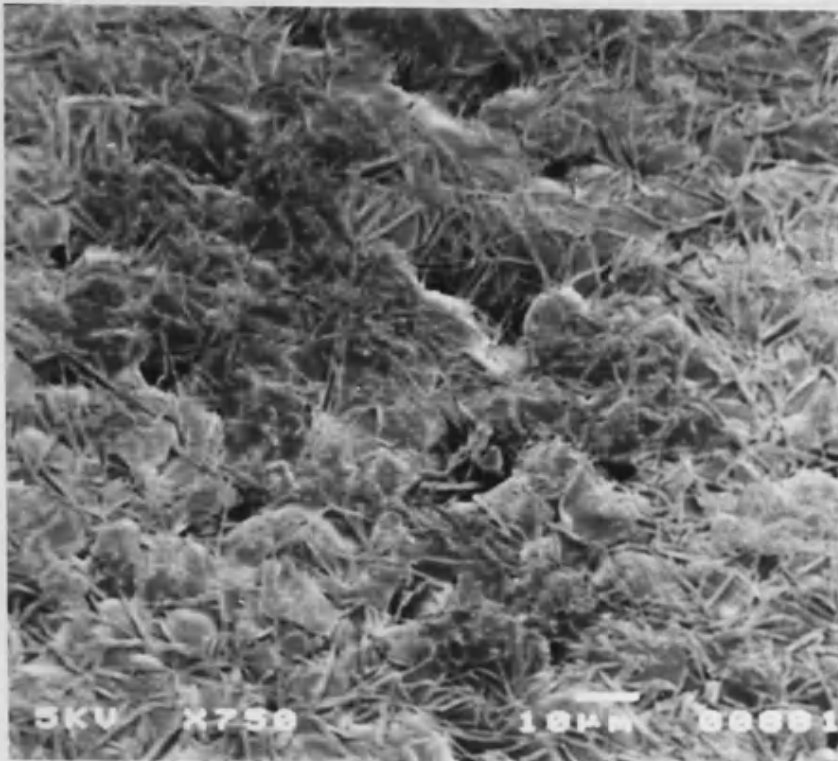
days prior to use in drug release studies. Ageing of Methyl Red loaded P(HB-HV) polymer films resulted in the accumulation of drug crystals at the surface. This was particularly noticeable at loadings in excess of 8% in PHB380K and loadings in excess of 4% in copolymers. This was thought to be related to secondary crystallization resulting from further rearrangement of polymer chains on storage which caused the exclusion of Methyl Red from the polymer crystals. Figure 7.3(B) shows an electron micrograph of Methyl Red crystals (filaments) on the surface of PHB380K film. This drug at the surface of films was removed by washing in distilled water prior to release experiments. Removal of excess Methyl Red was confirmed by observation of washed films under a light microscope.

7.4.2.1 The effect of drug loading in solvent cast PHB films

The effect of drug loading on release profiles was investigated using Methyl Red as the model drug in PHB380K films. Figure 7.4 shows that release was a function of drug loading. The percentage of drug released from PHB films increased with increasing drug loading. The amount of drug released after 177 hours from a 2% loading was about 14% compared to 21% for a 4% loading of drug and about 52% release from films loaded with 8%w/w Methyl Red. Although the release from solvent cast films was retarded to a greater extent than release from spray-dried particles (chapter 6), the bulk of the drug release for at least the high loading (8%) was not controlled by polymer erosion. The degradation half-life for the surface erosion of thin films (85um) at 37°C and pH 7.4 has been reported to be 152 weeks [286-287].

The release of Methyl Red from PHB380K films was biphasic. An initial rapid release of drug was followed by a much slower release of the remaining drug from the matrix. Release from PHB380K films did not fit the Higuchi square root of time kinetics [489] (Figure 7.5) or the model proposed by Brophy and Deasy [490] (Figure 7.6). The release of Methyl Red appeared to follow the mechanism proposed by Langer and coworkers [494] which was originally used to describe drug release from ethylene-vinyl acetate matrices. At low loadings of Methyl Red (4% and below), the drug was believed to be trapped in the

Figure 7.4. The effect of drug loading on the release of Methyl red from solvent cast films of PHB380K (Mean; n = 2) (S.D = less than 5% of Mean)
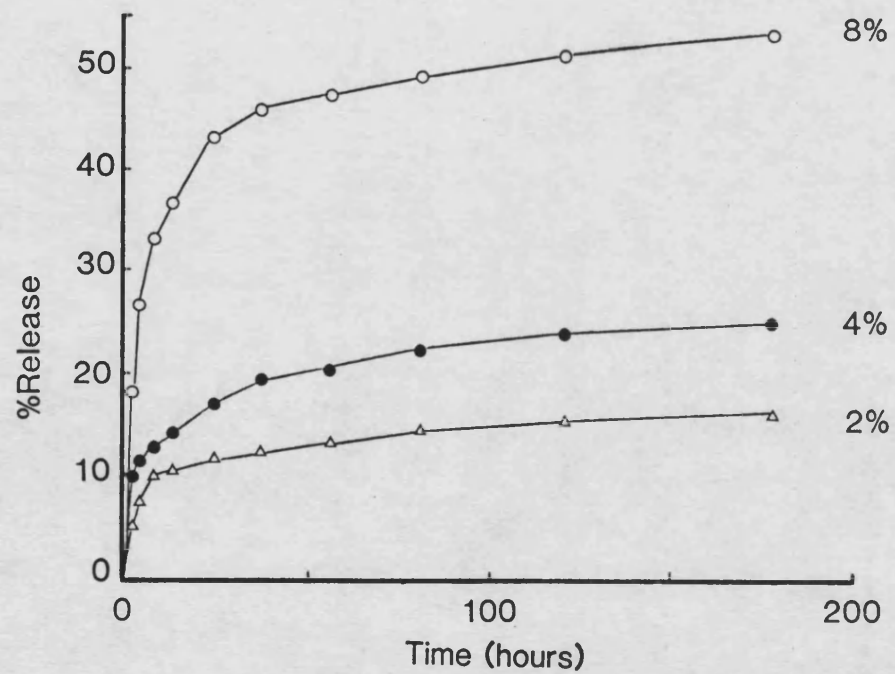
Figure 7.5. Release profiles of Methyl Red – loaded solvent cast films of PHB380K plotted according to the Higuchi model (Mean; n = 2). (S.D = less than 5% of Mean)
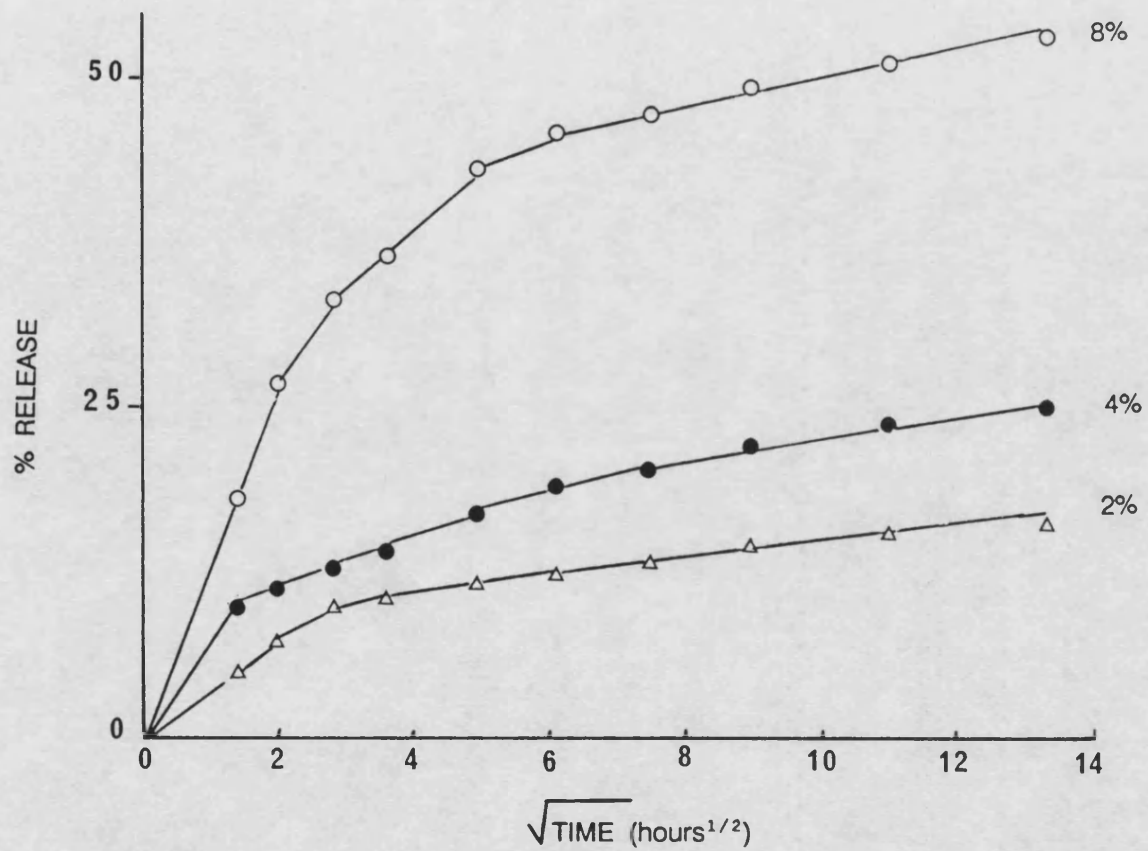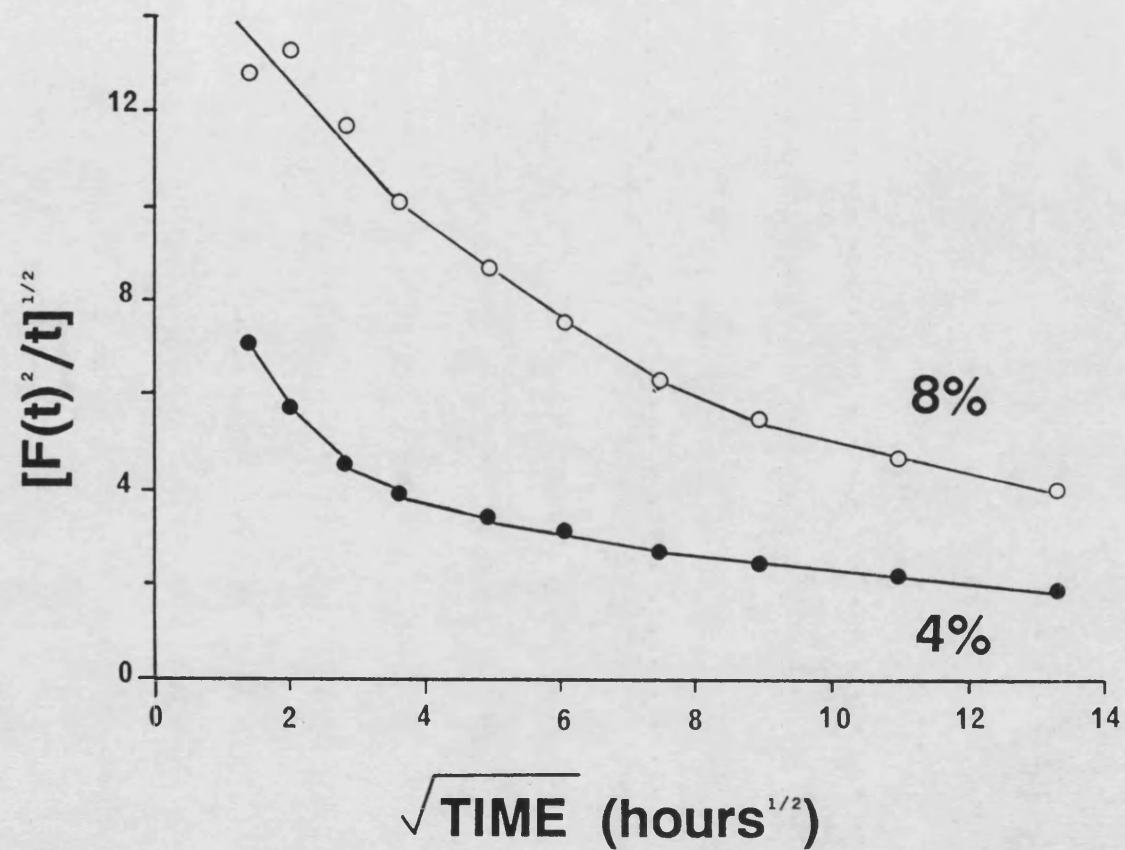
Figure 7.6. Release profiles of Methyl Red – loaded solvent cast films of PHB380K plotted according to the Brophy and Deasy model (Mean; n=2). (S.D = less than 5% of Mean)

matrix and release was essentially complete when all the drug particles at the surface had been released. A substantial proportion of drug can remain effectively trapped or surrounded entirely by a 'sea' of polymer (see Figure 7.7). At higher loadings, the particles were not thought to be distributed as well and may often be touching. In this case greater amounts of drug can be released and at much faster rates when water penetrates into pores created by dissolving drug particles. This eventually leads to the formation of an aqueous channel or a network of pores within the matrix. A small amount of drug can still remain trapped within the matrix and will only be released by either polymer erosion or by possible diffusion of drug through polymer.

In the case of both high and low drug loadings the fast phase of the release profiles was thought to be due to a combination of drug dissolution at the surface of the matrix and aqueous pore formation. The slow phase of the release profile corresponded to the release of trapped drug particles. This may be due to slow diffusion of drug or even polymer erosion. In non−biodegradable systems the way in which macromolecular drugs are released in the slow phase remains unclear [494]. At present, it is not known whether the slow phase is due to defects (microcracks) in the polymer or due to 'reptation' of the drug molecules through the polymer [494].

7.4.2.2 The effect of P(HB−HV) copolymer composition in solvent cast films

Figure 7.8 shows the effect of copolymer composition on the release profiles of solvent cast films containing 4%w/w Methyl Red. The release of Methyl Red was substantially more rapid than from PHB 380K. The percentage of drug released increased with increasing HV content. After 177 hours PHB380K films released only 21% of Methyl Red whereas 76, 92 and 94% of the drug was released from PHV6, PHV20 and PHV27 respectively.

The release of Methyl Red from P(HB−HV) copolymers did not fit the Higuchi model (Figure 7.9) and the mechanism of drug release was thought to be similar to that observed in PHB380K films (see above).

MATRIX RELEASE

278
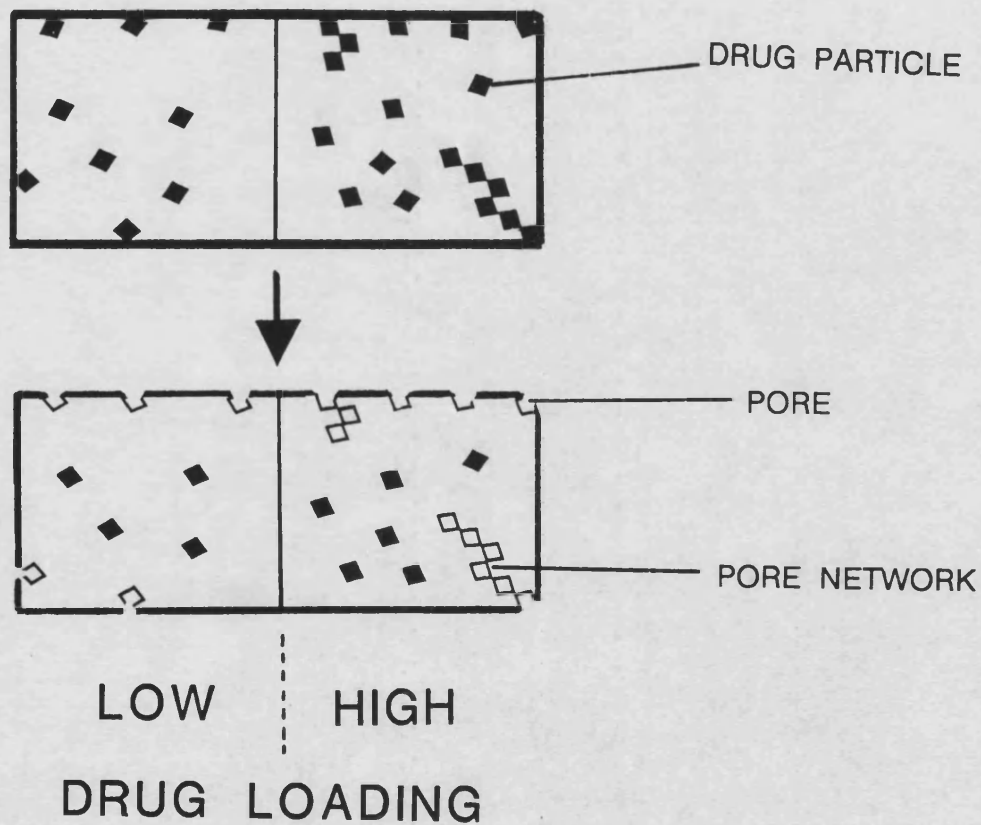
Figure 7.7. A schematic diagram showing matrix release patterns from low and high drug loadings.
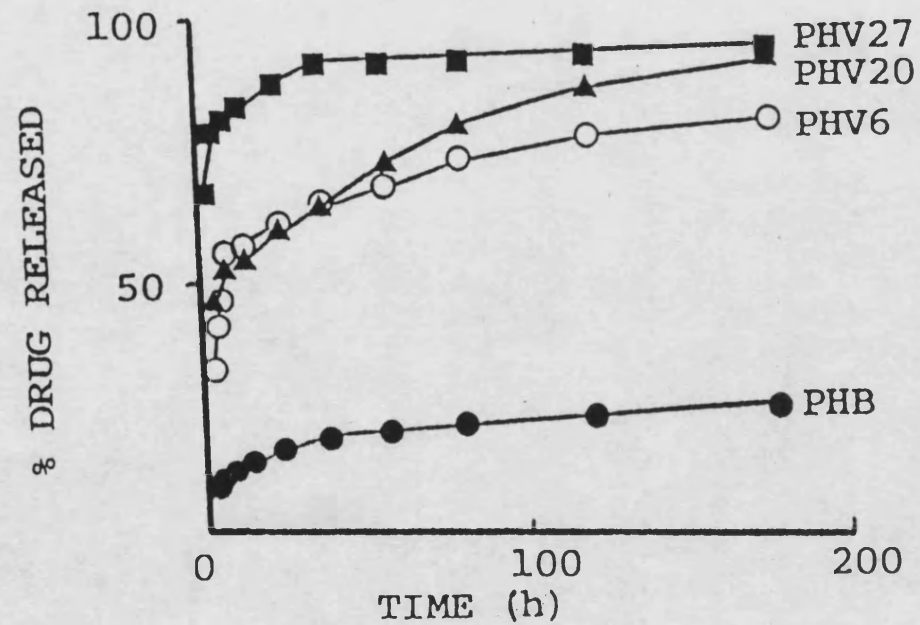
Figure 7.8.The effect of copolymer composition on drug release from solvent cast films of P(HB – HV) copolymers containing 4%w/w Methyl Red (Mean; n=2). (S.D = less than 5% of Mean)
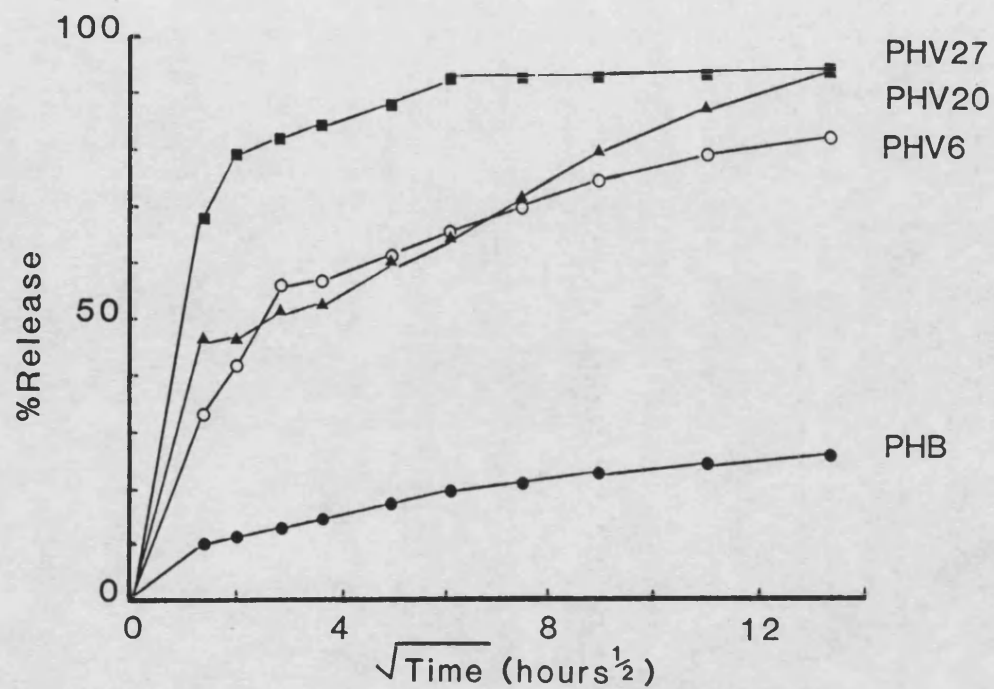
Figure 7.9. Drug release profiles of P(HB – HV) polyester films containing 4%w/w Methyl Red plotted according to the Higuchi model (Mean; n=2). (S.D = less than 5% of Mean)

The reason for the more rapid release of drug from copolymers could not be explained in terms of their overall degree of crystallinity. The copolymers have been reported to have similar degrees of crystallinity to the homopolymer (60 – 70%) [210 – 211]. Since the physical dimensions, drug loading and method of manufacture were all similar, it was thought that the explanation may lie in the nature of drug distribution within copolymers and/or in the crystalline morphology of copolymers.

Visual inspection and examination by light microscopy showed that although drug was less well distributed in PHV27, drug distribution in PHV6 and PHV20 films could not be distinguished from that in PHB380K films (see Figure 7.10). The drug in PHV27 appeared to be present as clusters or aggregates but the remaining copolymers had uniform distribution of the drug. This may have been due to poor solubility of Methyl Red in PHV27 or due to exclusion of drug during the much slower crystallization process in PHV27.

Analysis of drug distribution by DSC was carried out and DSC traces for the drug loaded copolymers are given in Figure 7.11. The DSC trace of PHV27 containing 4% Methyl Red was devoid of a separate peak corresponding to the melting of the drug at about 175°C. This suggested that although visual inspection showed that Methyl Red in PHV27 films appeared to be poorly distributed, DSC evidence indicated that the drug was generally well dissolved and well distributed in the films. Since melt endotherms for drug, PHV6 and PHV20 overlapped, no conclusions on drug distribution in these copolymers could be drawn form the available data. However, the shape and breadth of melt endotherms of copolymers were modified on the incorporation of drug (compare with DSC traces of pure polymers in Figure 3.5 of chapter 3). The drug generally acted as an impurity to lower the peak melt temperature and also to broaden the melt endotherm.

Crystallization studies have shown that the copolymers crystallize from the melt with different morphologies (chapter 5). It was thought that such morphological differences also existed in solution cast films and this accounted for the different release behaviour observed in P(HB – HV) copolymers. The morphology of solvent cast films cannot
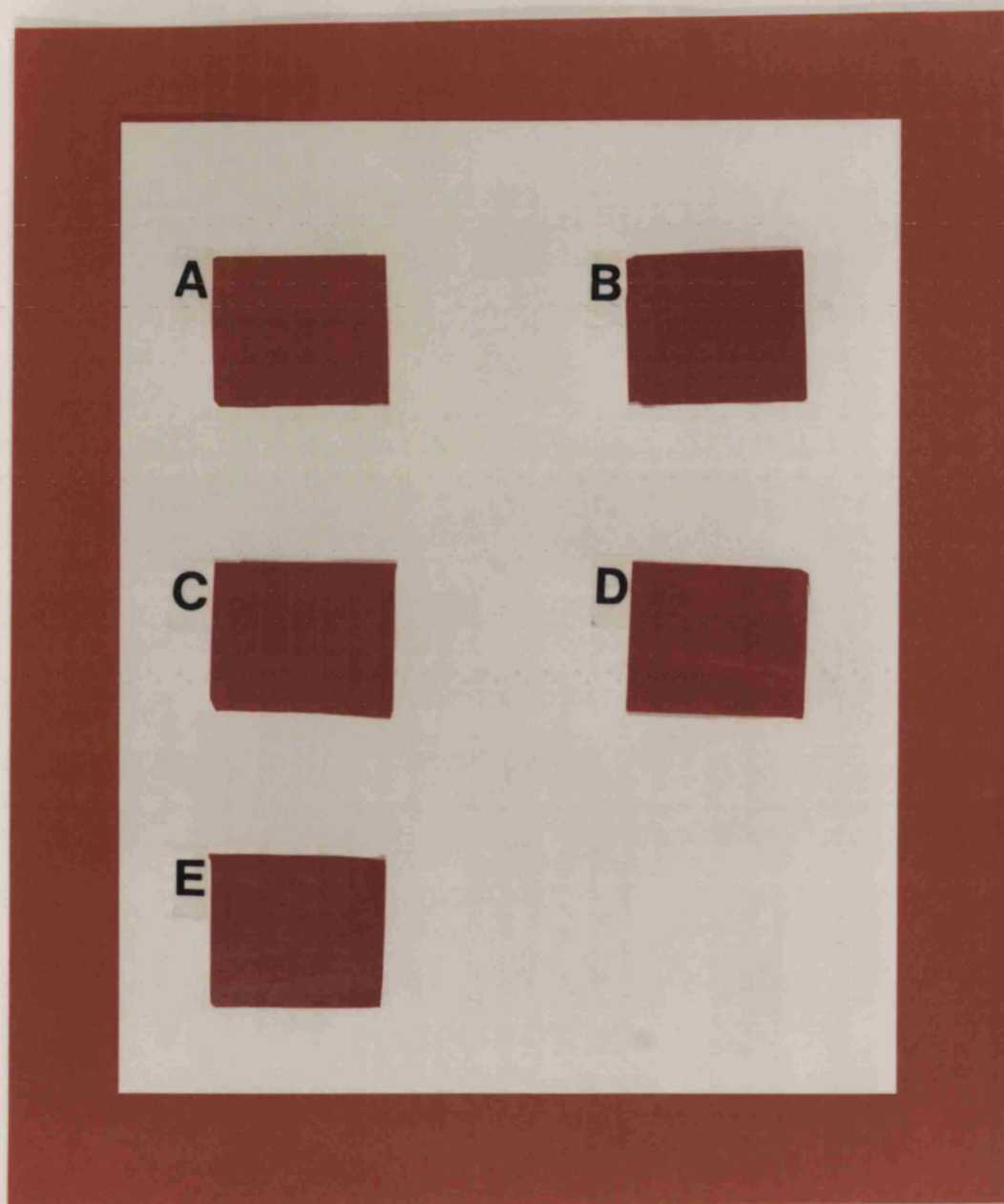
Figure 7.10. A photograph showing drug distribution in Methyl Red loaded solvent cast films of P(HB – HV) polymers.

A = PHB380K + 2%w/w Methyl Red
B = PHB380K + 4%w/w Methyl Red
C = PHV6   + 4%w/w Methyl Red
D = PHV20   + 4%w/w Methyl Red
E = PHV27   + 4%w/w Methyl Red
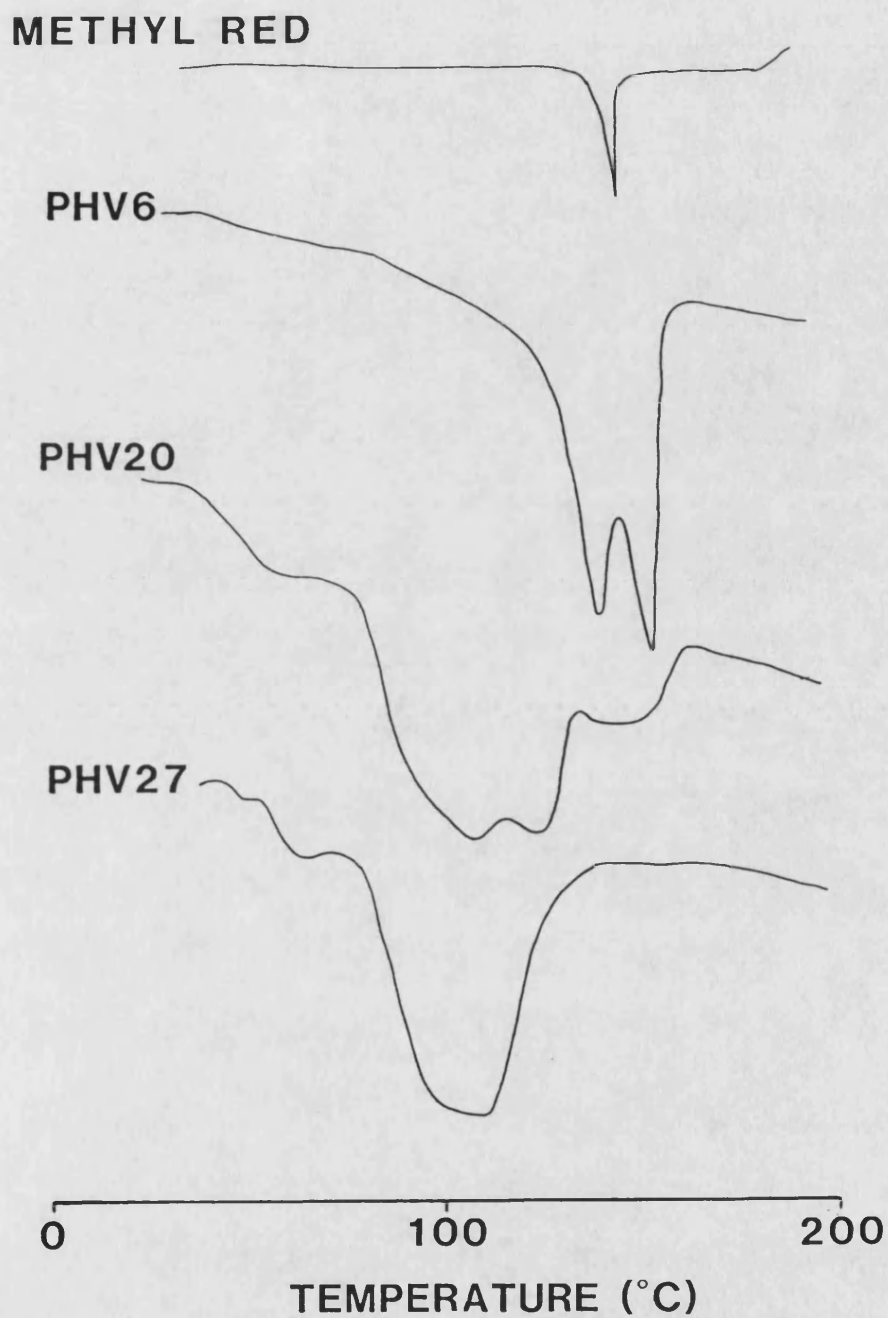
Figure 7.11. DSC traces of solvent cast films of P(HB – HV) copolymers containing 4%w/w Methyl Red.

easily be studied and certainly not with the same precision as melt–crystallized films. Therefore to examine this hypothesis further, release from Methyl Red–loaded copolymer films crystallized from the melt was examined. P(HB–HV) polymer films with known, yet different, morphologies were prepared and the release determined as before.

7.4.3. Release from Methyl Red–loaded films with different crystalline morphologies.

Solvent cast films (1.5cm x 1.5cm; 30–50um) of PHB380K containing 8%w/w Methyl Red (identical to those used above) were heated to melt at 195°C for 30–60 seconds and isothermally crystallized at 60, 90 and 110°C. Solvent cast films of PHB380K, PHV6 and PHV12 containing 4%w/w Methyl Red were also heated to melt and isothermally crystallized at 90°C for comparison. The spherulitic morphologies of the drug–loaded PHB380K films are shown in Figure 7.12. Note the differences in the internal fine structure of the respective spherulites.

Figure 7.13 shows drug release from PHB380K films with two different crystalline morphologies prepared at 60°C and 110°C. There is clearly a difference in the release profiles from the two morphologies. There appears to be a greater percentage of Methyl Red present at the surface of the films prepared at 110°C (approximately 13%) when compared with those prepared at 60°C (approximately 7%). This was evident in the photomicrographs of Figure 7.12 but the reason for this remains unclear. The release from the different film morphologies appeared to converge to similar values in the latter stages of the measured release.

Figure 7.14 shows drug release from these two morphologies and that prepared at 90°C over a period of 600 hours. The release from films crystallized at 60 and 110°C converged to similar values after 600 hours but the release from films crystallized at 90°C was significantly different ($p < 0.05$) to the release from the other two morphologies.

The release from P(HB–HV) copolymer films crystallized at 90°C with a 4%w/w loading of

Figure 7.12 Optical micrographs showing variation in spherulite morphology of isothermally crystallized films of PHB380K containing 8%w/w Methyl Red as s function of crystallization temperature.

A = 60°C, B = 90°C and C = 110°C.

Scale bar (A–C) = 500um   ├─────────────┤
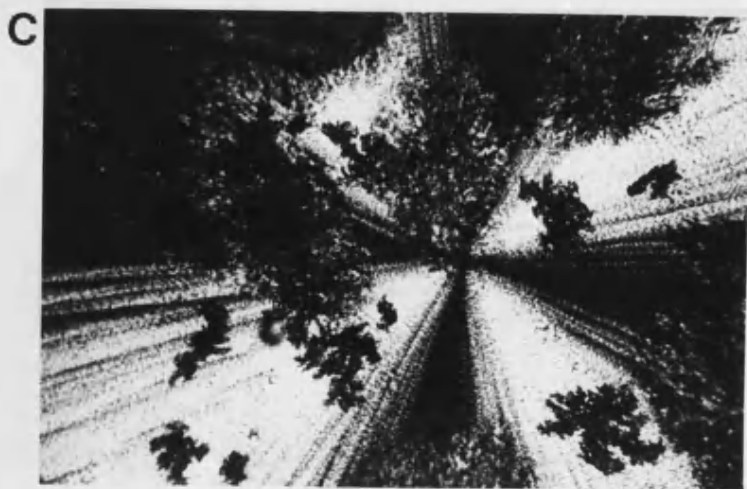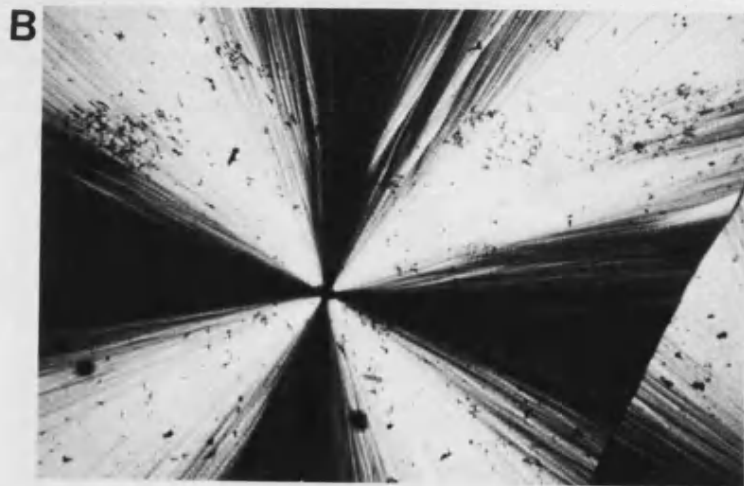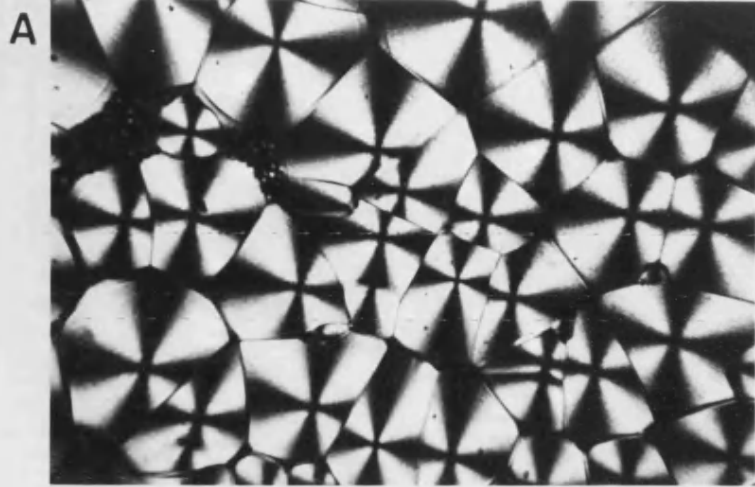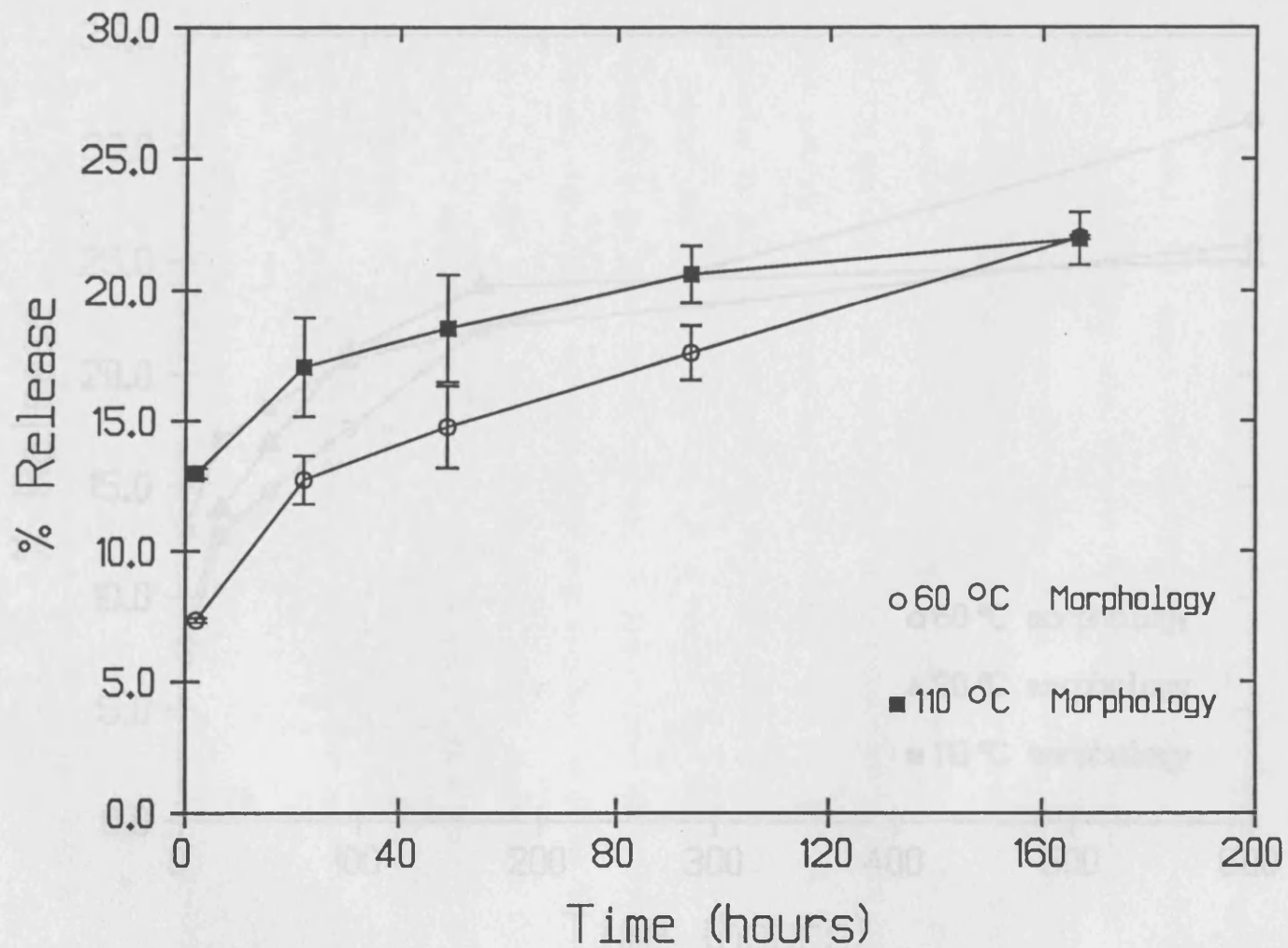
Figure 7.13. Drug release profiles of PHB380K films containing 4%w/w Methyl Red isothermally crystallized at 60°C and 110°C (Mean ± S.D; n=2).
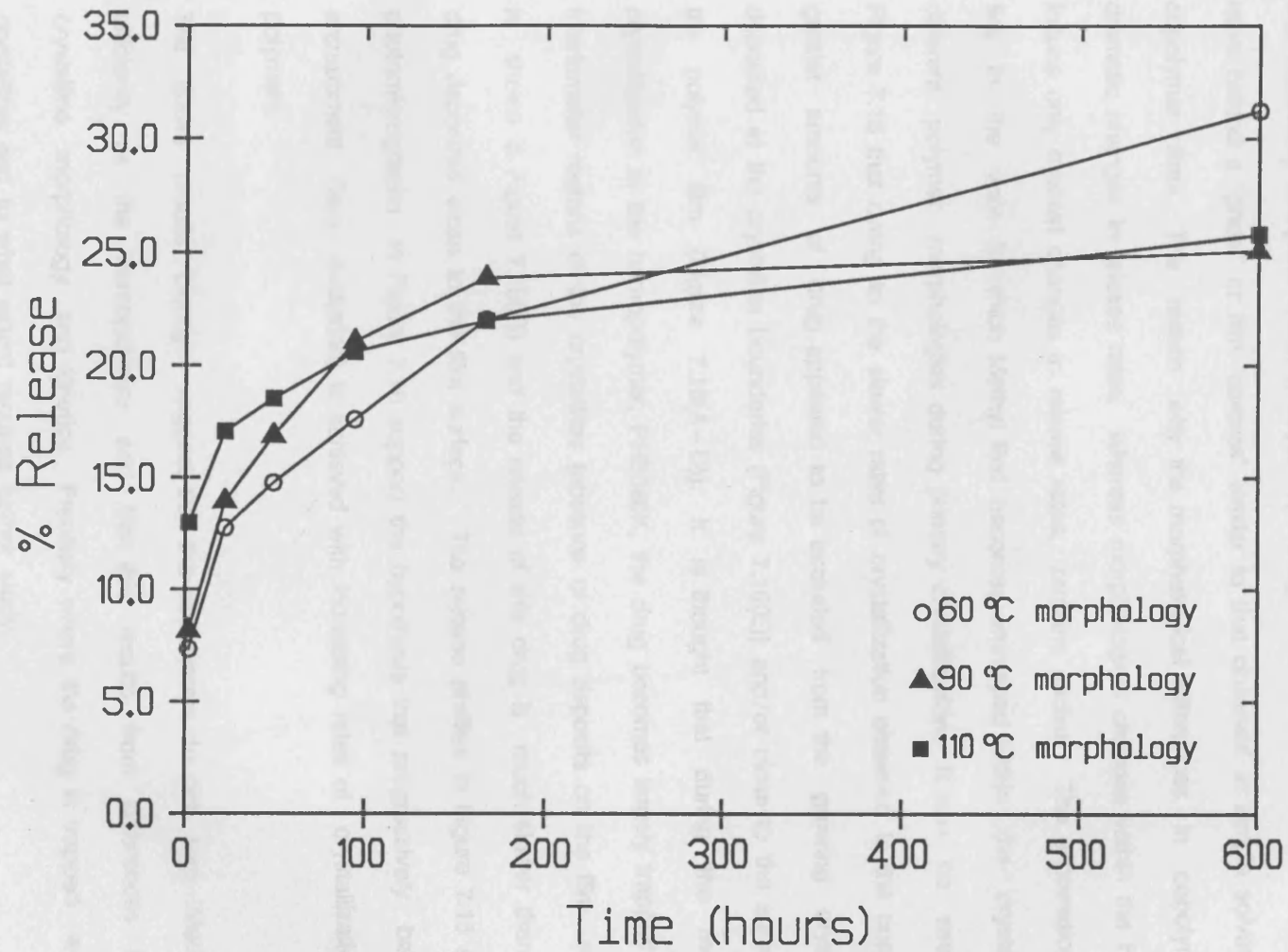
Figure 7.14. Drug release profiles of PHB380K films containing 4%w/w Methyl Red isothermally crystallized at 60°C, 90°C and 110°C. Standard deviations have been omitted for clarity. (Mean; n=2).

Methyl Red is shown in Figure 7.15. The P(HB–HV) copolymer films having characteristically different crystalline morphologies (Figure 7.16) clearly released drug at a more rapid rate than the homopolymer. Release of Methyl red from PHV12 films was essentially complete within 2 days. The drug leached out of the copolymer films to leave behind a "ghost" or film "carcass" similar to that observed in simple solvent cast copolymer films. The reason why the morphological differences in copolymers cause dramatic changes in release rates, whereas morphological changes within the homopolymer induce only modest changes in release rates, remains unclear. The explanation clearly lies in the way in which Methyl Red becomes entrapped within the crystals of the different polymer morphologies during primary crystallization. It can be seen from Figure 7.16 that owing to the slower rates of crystallization observed in the copolymers greater amounts of drug appeared to be excluded from the growing crystallites and deposited at the crystallite boundaries (Figure 7.16(E)) and/or close to the surface of the polymer film (Figure 7.16(A–D)). It is thought that during the more rapid crystallization in the homopolymer, PHB380K, the drug becomes largely trapped within the interlamellar regions of the crystallites (absence of drug deposits on the film surface is shown in Figure 7.16(F)) and the release of this drug is much slower than that of drug deposited close to the film surface. The release profiles in Figure 7.15 and the photomicrographs in Figure 7.16 support the hypothesis that progressively better drug entrappment (less exclusion) is achieved with increasing rates of crystallization in polymers.

The above results clearly suggest that the copolymers do not trap Methyl Red as efficiently as the homopolymer and that this results from differences in their crystalline morphology and kinetics. Precisely where the drug is trapped within the crystallites and to what extent requires further study.

7.4.4 Melt processed films

Methyl Red was also chosen as the model drug to investigate release behaviour from melt–processed films. To avoid confusion between melt pressed and solvent cast films the
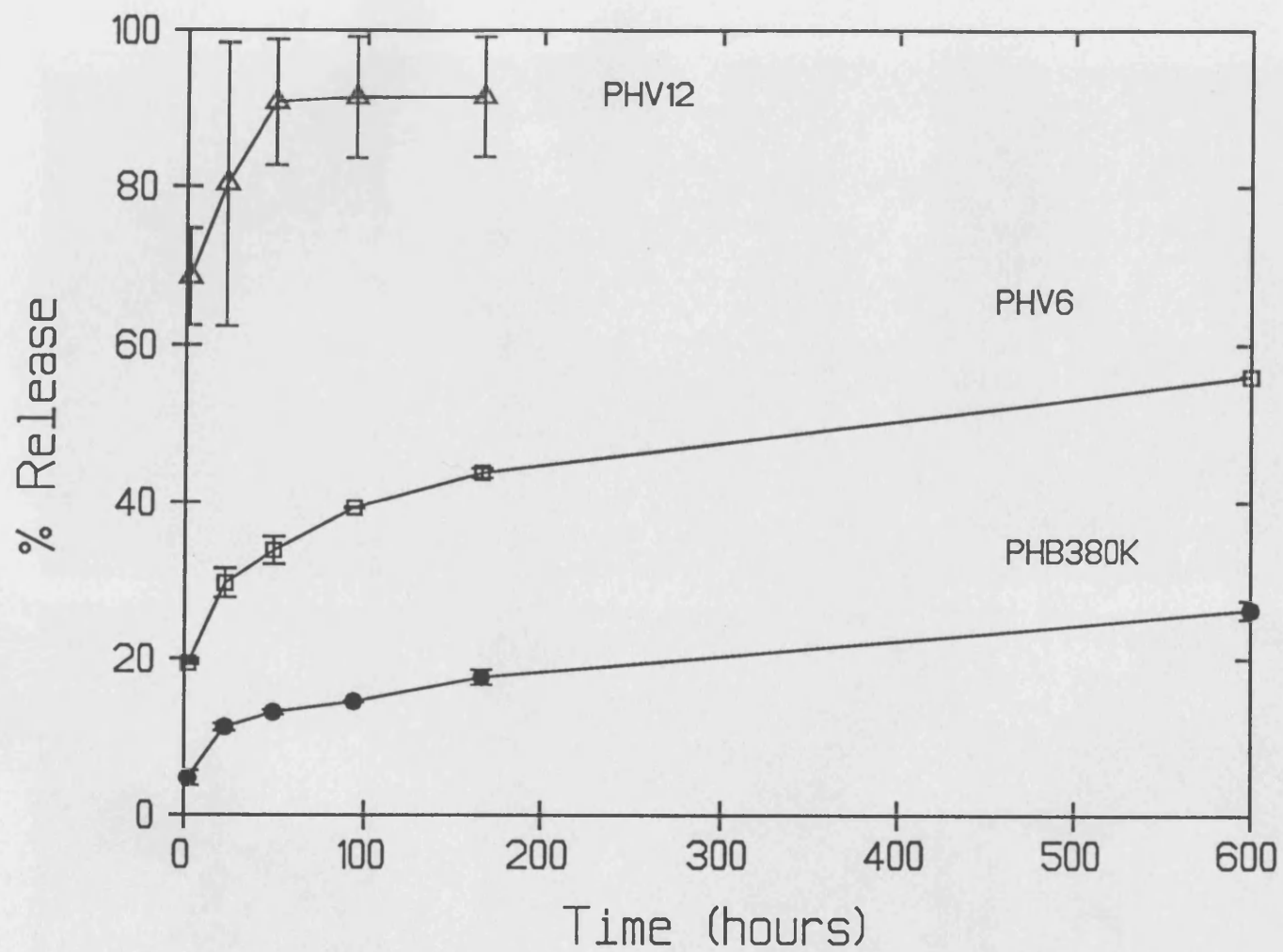
Figure 7.15. Drug release profiles of P(HB – HV) films containing 4%w/w Methyl Red isothermally crystallized at 90°C (Mean ± S.D., n = 2)

Figure 7.16. A series of optical micrographs showing morphology of isothermally crystallized (90°C) spherulites of P(HB – HV) polyester films containing 4%w/w Methyl Red.

A – B = PHV6; C – E = PHV12 and F = PHB380K.

Scale bar (A – D,F) = 500um

Scale bar (E) = 500um
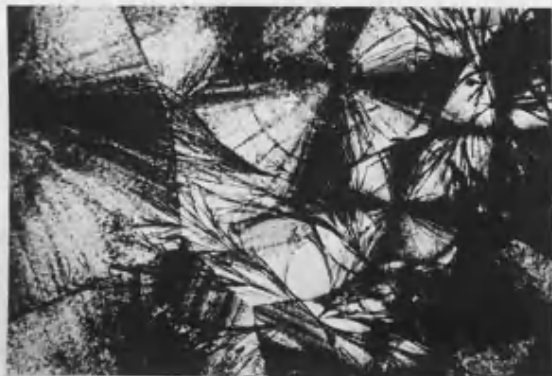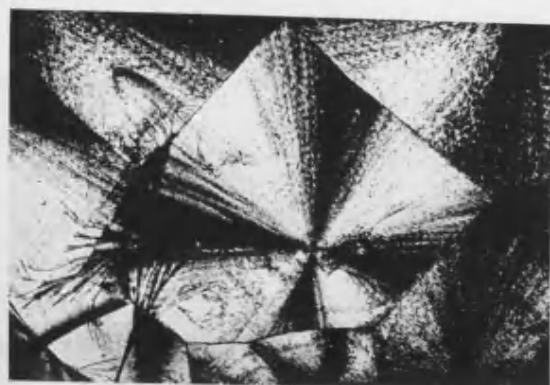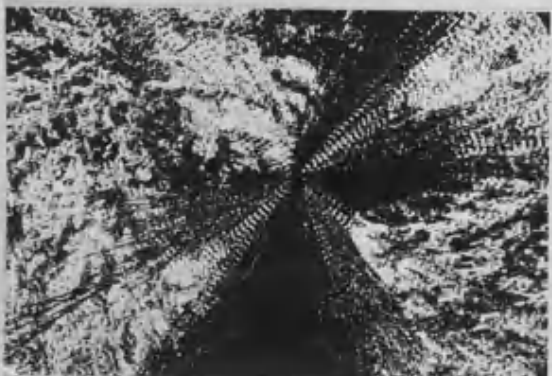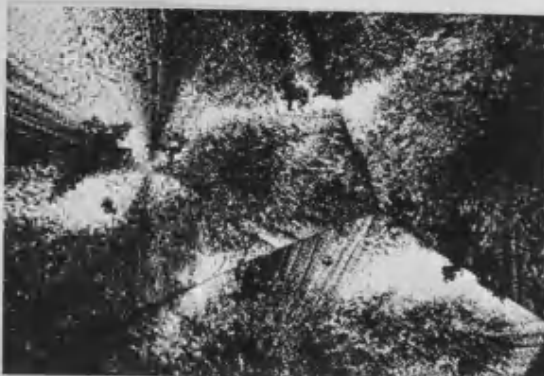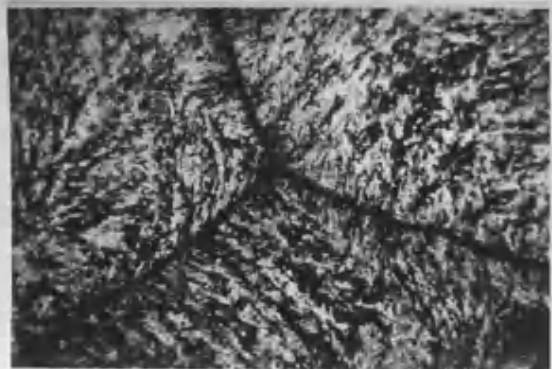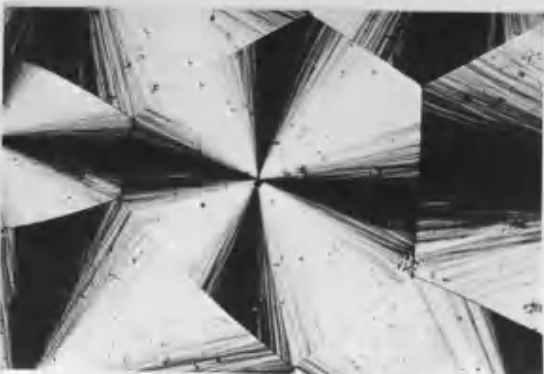
former will be referred to as discs. This refers to the shape of the specimens used for release studies.

7.4.4.1 Stability of drug following melt pressing.

The main concern following melt pressing was to ascertain whether any degradation of Methyl Red had taken place such as to modify its assay. The fact that Methyl Red could still be assayed in the same way was confirmed by comparing the UV – absorption spectra of Methyl Red – loaded melt pressed disks with those obtained from Methyl Red – loaded solvent cast films and pure Methyl Red. The uv – vis absorption spectra were qualitatively identical and are shown in Figure 7.17.

7.4.4.2 Release of Methyl Red from melt pressed discs of P(HB – HV) polymers.

Figure 7.18 shows release of Methyl Red from melt pressed discs. It can be seen that release of Methyl Red was retarded to a greater extent in melt pressed discs than in solvent cast films. Although the copolymers again released drug more rapidly than the homopolymer, this was not as rapid as that observed in solvent cast films (Figure 7.19). The reason for the greater sustained release seen in melt – pressed films was partly related to the greater thickness of films (300 – 400um) compared to solvent cast films (30 – 50um) and partly due to the absence of pores on the surface of the disks before release (Figure 7.20(A)). There was no evidence of pores in the melt pressed discs even in freeze – fractured cross – sections (Figure 7.20(B)). This reduced porosity of the matrix (due to fabrication under pressure and no evaporation of solvent) was thought to be responsible for delaying aqueous channel formation during release. The melt pressed discs were, by definition, more compact than solvent cast films and therefore the other factor that may have contributed in the greater sustained release is the expected slower erosion of compacts. This was not confirmed, however, and requires further study.

The dependence of release rates on the method of fabrication is not peculiar to the systems employed in this study. For example similar results have been reported for drug
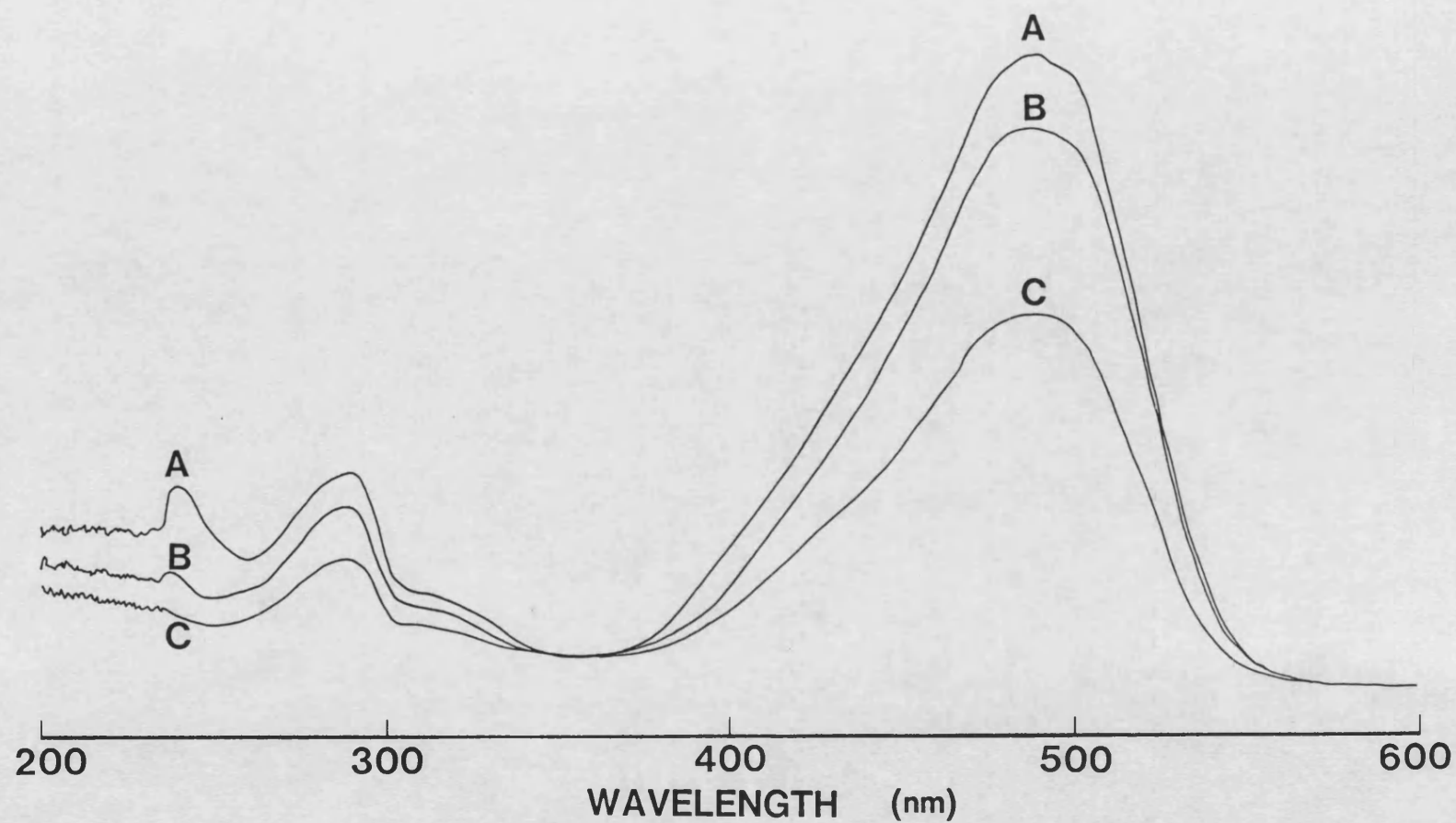
Figure 7.17. Absorption spectra in the uv–vis region for chloroform solutions of (A) pure Methyl Red, (B) solvent cast film of PHB380K containing Methyl Red and (C) melt pressed discs of PHB380K containing Methyl Red.
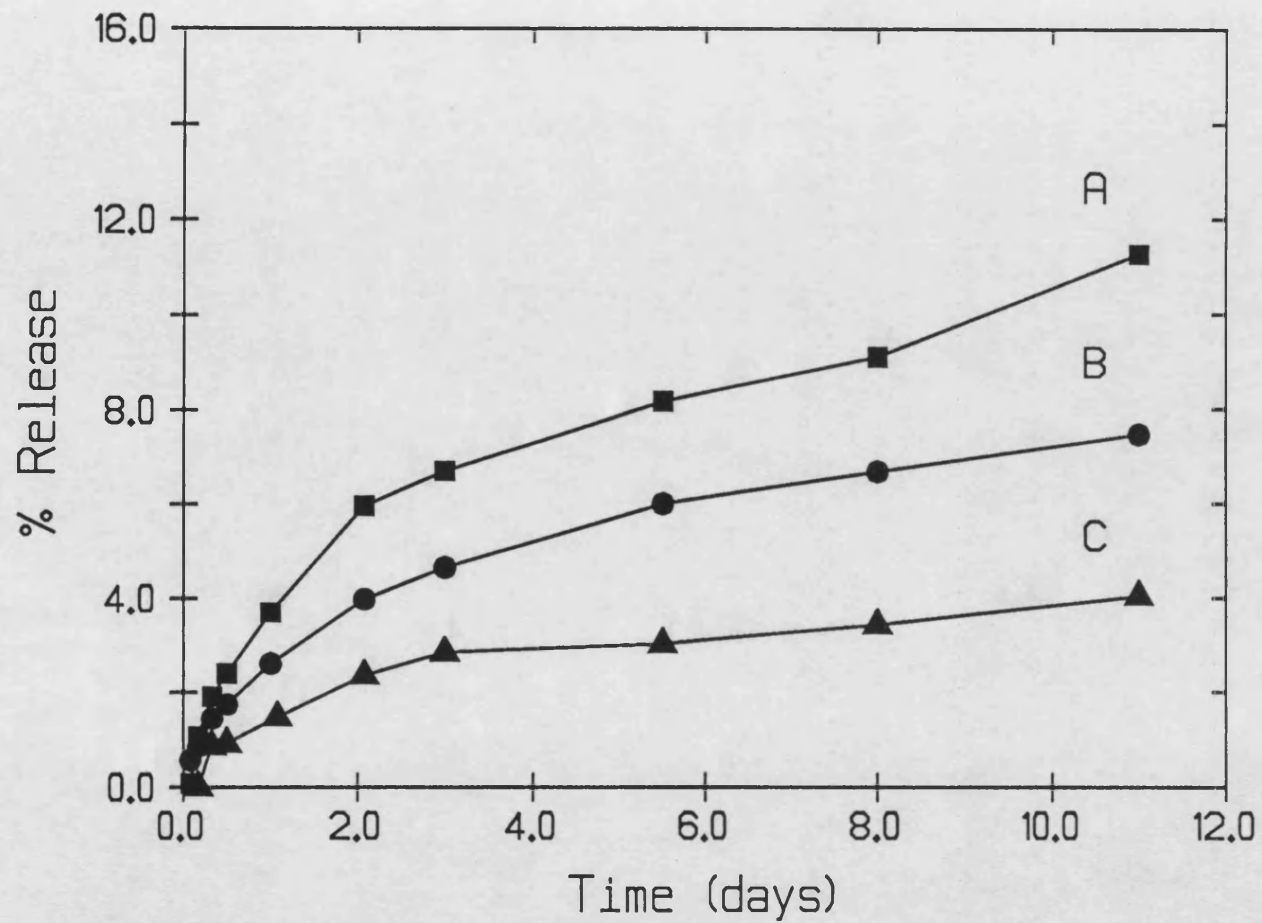
Figure 7.18. The influence of drug loading on release profiles of melt pressed discs of PHB380K containing Methyl Red; A = 8%w/w, B = 4% w/w and C = 2%w/w. (Mean; n=2).

(S.D = less than 12% of Mean)
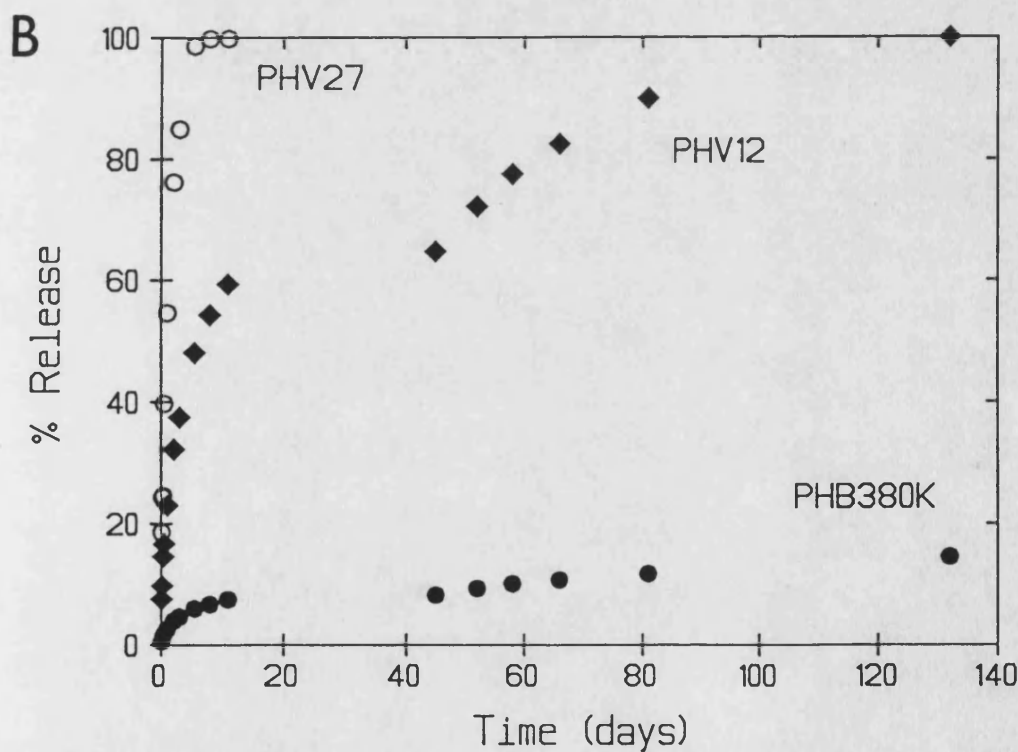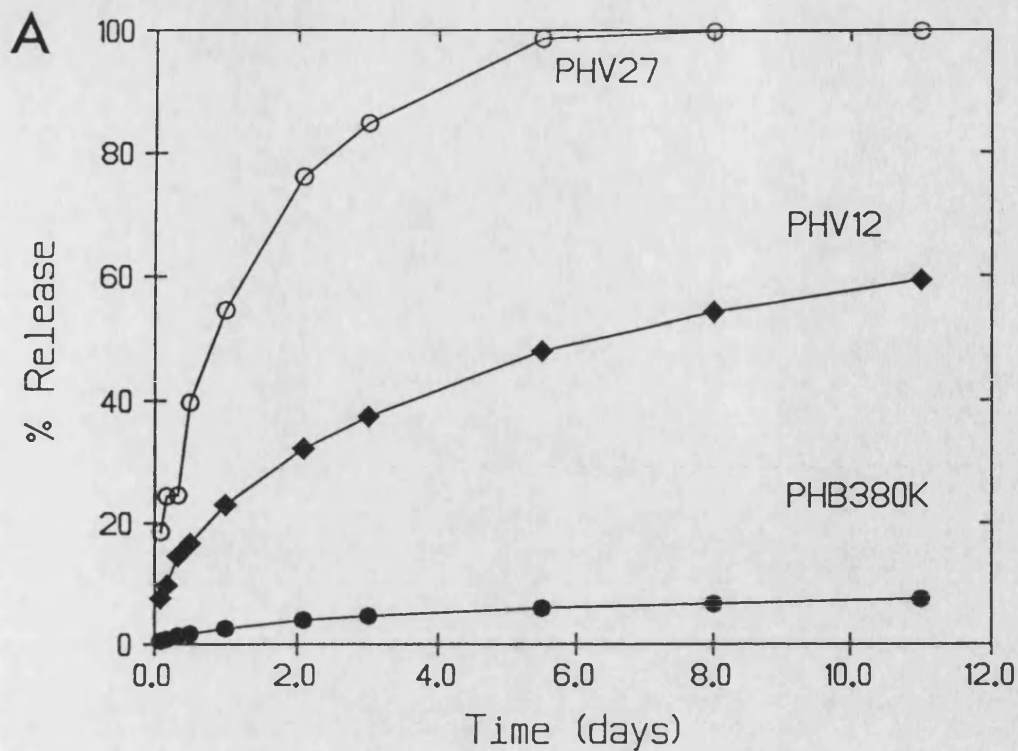
Figure 7.19. The influence of copolymer composition on drug release profiles of Methyl Red loaded melt-pressed discs of P(HB-HV) copolyesters A) release over the first 11 days and B) release over the full study period of 132 days (Mean; n=2). (S.D = less than 10% of Mean)

295

Figure 7.20. Scanning electron micrographs showing absence of pores in melt pressed discs of PHB380K:

A) surface view and

B) view of a freeze – fractured cross section.
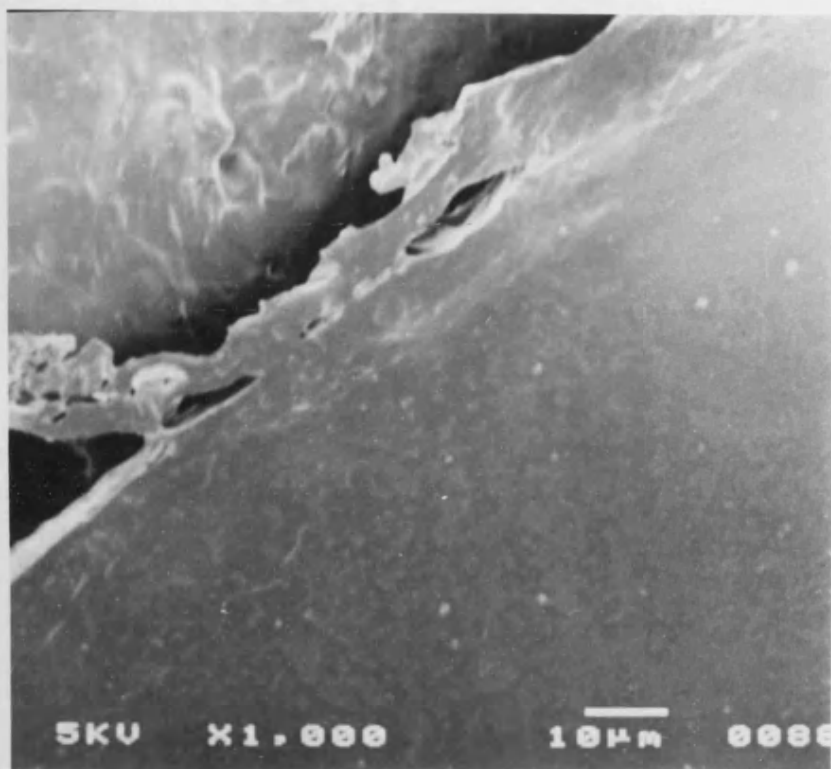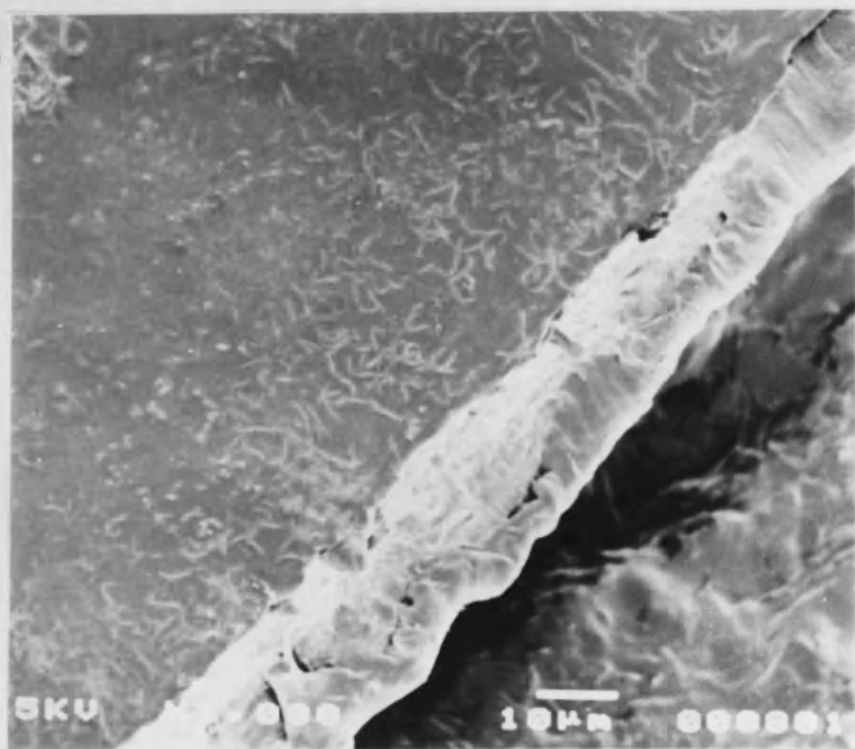
release from polyanhydrides [130]. The results showed that using the same polyanhydride release of p – nitroaniline could be sustained for only a few weeks when fabricated by compression moulding but when fabricated by injection moulding release was sustained for up to several months [130].

It is clear that the method of manufacture and variation of processing conditions affects drug release. By controlling the fabrication procedure it was possible to produce different rates of Methyl Red release from P(HB – HV) polymers. This is in addition to the controls possible by varying drug loading, molecular weight (chapter 6) and copolymer composition.

7.4.5 Solvent cast films containing Azocasein

Azocasein was insoluble in P(HB – HV) polymers and unlike Methyl Red could not be simply dissolved in chloroform solutions of polymer to achieve adequate drug distribution. However using ethanol as a cosolvent, aqueous solutions of azocasein could be mixed with polymer in chloroform as a single phase. The release of azocasein from polymer films cast from such solutions is shown in Figure 7.21.

If macromolecules such as azocasein can be effectively trapped within a biodegradable polymer matrix then because of the low diffusion coefficients of such molecules in polymers release may be controlled by erosion of polymer. However the results of Figure 7.21 show that release of azocasein from solvent cast P(HB – HV) and PLA polymer films occurred relatively quickly and was not primarily controlled by polymer erosion.

Release of azocasein was most rapid from PHB380K (over 80% release after 8 days) and most retarded, at least over the early stages, from PLA films. Release of the macromolecule from the P(HB – HV) copolymers lay between the two extremes given above. These results can be explained in terms of azocasein distribution in the respective polymers. Although the use of a cosolvent enabled a good distribution of drug in polymer solutions, subsequent drying of the solvent cast films resulted in segregation of the drug. In the case of drug loaded PHB380K films, the azocasein appeared to be largely
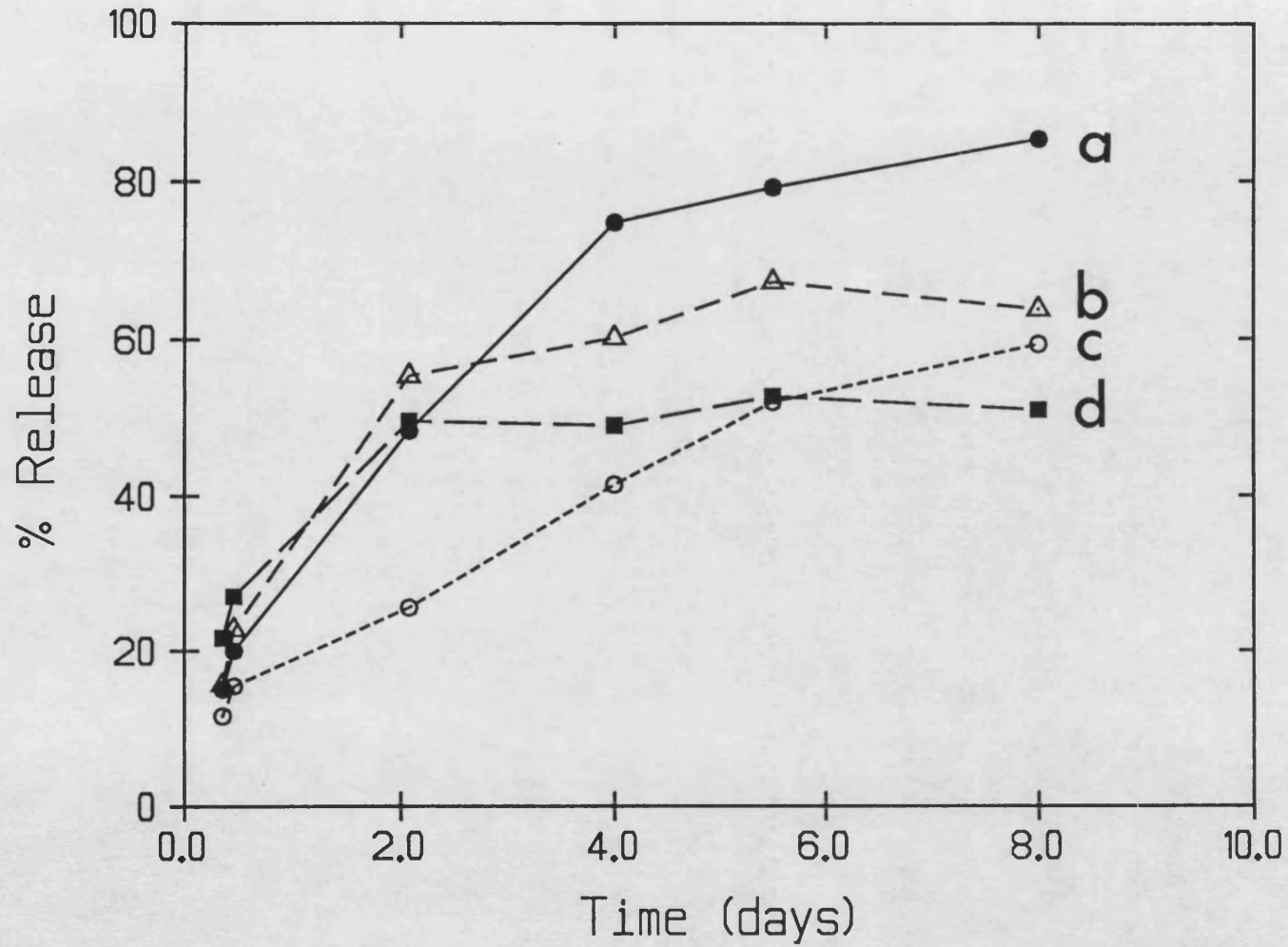
Figure 7.21. Release profiles of biodegradable polyester films containing 2%w/w Azocasein; a= PHB380K, b= PHV6, c= PLA and d= PHV12 (Mean, n=2). (S.D = less than 10% of Mean)

deposited on the air exposed surface of the films when cast on glass. Consequently over

70% of drug was released from such films over the first 4 days. The P(HB – HV) copolymers

had a patchy distribution of drug and the best distribution of azocasein was found in

PLA. The macromolecule appeared to be homogeneously distributed but as discrete solid

particles embedded within the polymer matrix. However the thinness of polymer films (30 –

50um) coupled with the large size of the azocasein molecules suggests that aqueous

channels formed easily to effect rapid release of drug from all the polymers studied.

The results of Figure 7.21 suggested that some drug was trapped within the polymers

which appeared to be released slowly but in all cases 40% or more of the drug was

released over the first 4 days.

Evidently the effective delivery of peptides and macromolecules will depend on suitable

entrappment within polymer matrices. Deviations from homogeneous distribution clearly

lead to rapid drug release even of large molecules. It is thought that more efficient

drug distribution of azocasein within polymer films may be possible by controlling the

rate of drying in films. Insulin has been suitably incorporated into polyorthoester

devices prepared by slow controlled solvent evaporation [500]. Furthermore, the use of

cryogenic techniques to slow down solvent evaporation in ethylene – vinyl – acetate devices

resulted in homgeneous drug distribution of peptides [64 – 65,69 – 70]. Clearly the

incorporation of macromolecules in polymeric devices requires further investigation.

However attention need not be focused on achieving zero – order release profiles as

optimal delivery of endogenous peptides may only be achieved if release is controlled to

mirror their normal physiological secretion [501]. This may often be of a pulsatile

nature and will require temporal considerations as influenced by the chronopharmacology

of the relevant peptide.

7.5 CONCLUSIONS

The method of fabrication was an important determinant of drug release rate. Release of

Methyl Red from P(HB – HV) polymer films was retarded to greater extent in melt – pressed

discs than in solvent cast films.

Drug release was dependent on drug loading and copolymer composition. Release of Methyl Red from the P(HB – HV) copolymers was more rapid than from the homopolymer, PHB, from both solvent cast and melt – pressed films. The more rapid release of drug from copolymers was thought to be due to differences in their crystalline morphology and kinetics leading to altered drug distributions.

CHAPTER 8

CONCLUDING REMARKS

The aim of this research was to study the physicomechanical properties of bacterial

P(HB – HV) polyesters and to evaluate their potential for controlled drug delivery.

Physicomechanical and drug release properties of P(HB – HV) polymers were generally

dependent on both polymer molecular weight and copolymer composition.

A study of the mechanical properties showed that a minimum molecular weight of

approximately 190K – 200K was necessary to form a mechanically intact film of PHB by

solvent casting. The properties of the homopolymer changed rapidly beyond this minimum

molecular weight to reach a plateau at a molecular weight of approximately 300K.

PHB was relatively hard and brittle exhibiting a relatively high elastic modulus and low

%elongation. On increasing HV content, P(HB – HV) copolymers were progressively tougher,

less brittle and more pliable. The copolymers were easier to handle and their superior

mechanical properties were thought to make them preferable for manufacturing purposes.

The inclusion of drugs may adversely affect polymer properties. The magnitude of the

effect was found to be influenced by the nature and concentration of the drug. Sodium

Fluorescein, a particulate water – soluble, drug progressively lowered both the tensile

strength and % elongation of PHV20 films. The effect was marked even at low (<2%w/w)

drug concentrations. However at concentrations up to 10%w/w, the mechanical properties

of PHV20 films were little affected on incorporation of the chloroform soluble drug,

Methyl Red.

On the basis of polymer melting points, steam sterilization was thought to be acceptable

for the virgin homopolymer but sterilization by gamma – irradiation may be preferable for

P(HB – HV) copolymers. The sterilization method chosen will also be influenced by the

nature and stability of the incorporated drug.

Thermoplastic P(HB – HV) polymers were found to have a wide range of melting

temperatures. The peak melting temperature was progressively lowered from a value of

174°C for PHB380K to 83°C for PHV27. Thermal degradation of all P(HB – HV) polymers

occurred over a narrow range (approximately 50°C) from around 300°C. The data on the thermal properties suggested that the window for safe thermal processing increased with increasing HV content of the copolymers and that the copolymers may be thermally more stable. It is, therefore, suggested that incorporation of thermally labile drugs (such as peptides) by melt processing may be more readily achieved by using copolymers with high HV contents which have lower melting temperatures and larger processing windows.

The glass transition temperatures of P(HB–HV) copolymers containing up to 28mole% were in the range -5 to 20°C and thus, below body temperature. At physiological temperatures the polymers will be in a rubbery state.

In a study of the ageing properties of P(HB–HV) polymers, it was found that mechanical and crystalline properties changed with time following fabrication. Surface properties of solvent cast films stabilized relatively rapidly (within 1 day) whereas bulk properties (mechanical properties, bulk crystallinity and shape of DSC thermograms) continued to change for up to 31 days following manufacture and were a function of HV content.

The obvious dependence of polymer properties on P(HB–HV) copolymer composition could not easily be explained by differences in their degrees of crystallinity. Although there had been conflicting reports on the relative crystallinity observed in the copolymers [149,246,247,210,211], the view held at the time of carrying out this research, was that the degree of crystallinity was independent of copolymer composition (at around 60–80%) [210–211]. It was originally proposed that this was due to isodimorphism in P(HB–HV) copolymers. However, the extent to which HV is incorporated into a common crystal lattice is now thought to be variable and requires further study.

In an attempt to further explain the dependence of physicomechanical properties of P(HB–HV) polymers on HV content, the crystallization morphology and kinetics of these polymers were investigated.

Rate of polymer crystallization from the melt was dependent on crystallization temperature (and undercooling), presence and concentration of drug and on copolymer composition. At a given undercooling, increasing HV content progressively retarded the growth rate of polymer spherulites.

The crystalline morphology of copolymers, as evidenced by changes in the internal fine structure of polymer spherulites when observed through a polarized light microscope, was found to be different for each copolymer. Working on the assumption that the degree of crystallinity is independent of HV content, it is suggested that differences in the physicomechanical and other properties of P(HB-HV) polyesters may be better explained by differences in their crystalline morphology.

To examine this hypothesis further, the influence of crystalline morphology of polymers on drug release was investigated. Thin films of PHB380K containing similar loadings of Methyl Red were melt-crystallized at different temperatures to yield different crystalline morphologies and drug release from each polymer morphology was determined. Drug release profiles were found to be a function of polymer morphology and hence, crystallization rate.

Using thin films of P(HB-HV) polymers crystallized at the same temperature, it was found that drug release (at similar loadings) was progressively more rapid in the copolymers and increased with increasing HV content. This phenomenon could be explained by reference to altered drug distribution resulting from the combined effects of crystallization rate and polymer morphology.

The progressively slower rates of crystallization in copolymers on increasing HV content resulted in progressively greater exclusion of drug from intra-spherulitic regions and hence, poorer drug distribution. At the relatively faster crystallization rates observed in the homopolymer, better drug entrappment was achieved and drug release was slower. Drug molecules were thought to be present within inter-lamellar regions and also at inter-spherulite boundaries within the P(HB-HV) polymer films. However, this requires

further study. It would also be interesting to investigate the distribution of peptide drugs within crystalline polymer systems and their influence on crystalline morphology. This may be best carried out using modern polymer etching techniques in combination with electron microscopy to reveal a more detailed picture of polymer morphology.

The influence of copolymer composition on drug release profiles was qualitatively similar for films prepared by solvent casting and melt-pressing suggesting that the same explanation holds true in both cases. However, exact rates of drug release were dependent on fabrication technique. Release of Methyl Red was sustained to a greater extent when P(HB-HV) devices were prepared by melt-pressing rather than by solvent casting. In most cases, drug release was not predominantly controlled by polymer erosion.

Drug release from spray-dried microparticles was more rapid than from both solvent cast and melt-pressed films. Release of Methyl Red was a function of drug loading and polymer molecular weight. Increasing molecular weight or drug loading in PHB resulted in more rapid release of drug.

The use of spray drying to produce injectable microparticles was limited to molecular weights of 140K and below for the homopolymer. The microparticles produced, even for low molecular weights, were not discrete individuals but aggregates. The morphology of the product produced was little affected by adjusting the processing parameters on the Buchi minispray dryer. Drug release from spray-dried microparticles was influenced by processing parameters such as polymer feed concentration and inlet temperature. However, these effects may have been complicated by the observed batch-to-batch variation in release profiles of microparticles produced with the bench model spray dryer. If such variation was to persist in particles prepared on a large industrial scale then batch-to-variation may preclude the use of spray drying as a method of producing injectable microparticulates. This requires further study.

In conclusion P(HB-HV) systems appear to be promising candidates for drug delivery and

have obvious advantages over existing materials. The current literature suggests that these polymers are biocompatible [148,293,297 – 300], biodegradable [286 – 289] and can be extracted in a very pure form from bacteria [214,262]. There are also reports [286 – 287] suggesting that these polymers degrade by surface hydrolysis (heterogeneous degradation) offering the potential for reproducible drug release kinetics and that rate of erosion can be controlled by copolymer composition.

This study showed that although release of low molecular weight drugs was not predominantly erosion controlled, time scales over which release was possible with P(HB – HV) polymer systems could be varied from several hours to several months. Release could be controlled by controlling polymer molecular weight, copolymer composition, drug loading, fabrication technique and form of the drug delivery device employed.

The use of P(HB – HV) polymers for delivering peptide drugs will be influenced by drug distribution. If the peptide can be trapped effectively such that release is determined by polymer erosion then drug release could be further controlled. In addition, appropriate choice of the controls listed above will enable release to be tailored to specific requirements within the long time frames of polymer degradation. However, in order for P(HB – HV) polymers to realize their full potential in drug delivery it is important to overcome the important technological challenge of how hydrophilic peptide drugs can be trapped homogeneously within these hydrophobic polymers such that release is indeed controlled by polymer erosion.

APPENDIX A

XPS AND SSIMS ANALYSIS OF P(HB – HV) POLYMERS.

A1.1 INTRODUCTION

X-Ray Photoelectron Spectroscopy (XPS) and Static Secondary Ion Mass spectroscopy (SSIMS) are complimentary techniques for the surface chemical characterization of polymeric interfaces [503-504].

A1.1.1 X-Ray Photoeletron Spectroscopy (XPS).

XPS, which is also known as ESCA (Electron Spectroscopy for Chemical Analysis) provides quantitative elemental (except for H and He) and functional group analysis of polymer surfaces to a sampling depth of approximately 1-10nm [496,503]. The technique has been reviewed in many books [505-506] and articles [496,503,507.511] and only a brief outline of its principles is given here.

When a photon source (e.g. X-rays) is directed at a sample, the photons interact with the electrons present in the sample material. If the photon has sufficient energy, it causes an electron to be emitted from an orbital. The theoretical relationship that describes this process is given by [503]:

$$K_E = h\nu - B_E - a$$

where K_E is the kinetic energy of the emitted photoelectron, $h\nu$ is the energy of the photon, B_E is the binding energy of the photon, and a is an instrument specific work function. K_E is determined in the XPS experiment, $h\nu$ and 'a' are known, and B_E can be calculated, yielding the energy with which the emitted electron was held in its atomic or molecular environment.

A schematic diagram of an XPS apparatus is shown in Figure A1.1. The sample for analysis is placed in an ultra high vacuum, typically less than 10^{-8} Torr and exposed to a low energy monochromatic X-ray source which causes the emission of photoelectrons from atomic shells of elements present in the surface. These electrons possess an energy characteristic of the element and molecular orbital from which they are emitted. The electrons are detected and counted according to the energy they possess and by counting
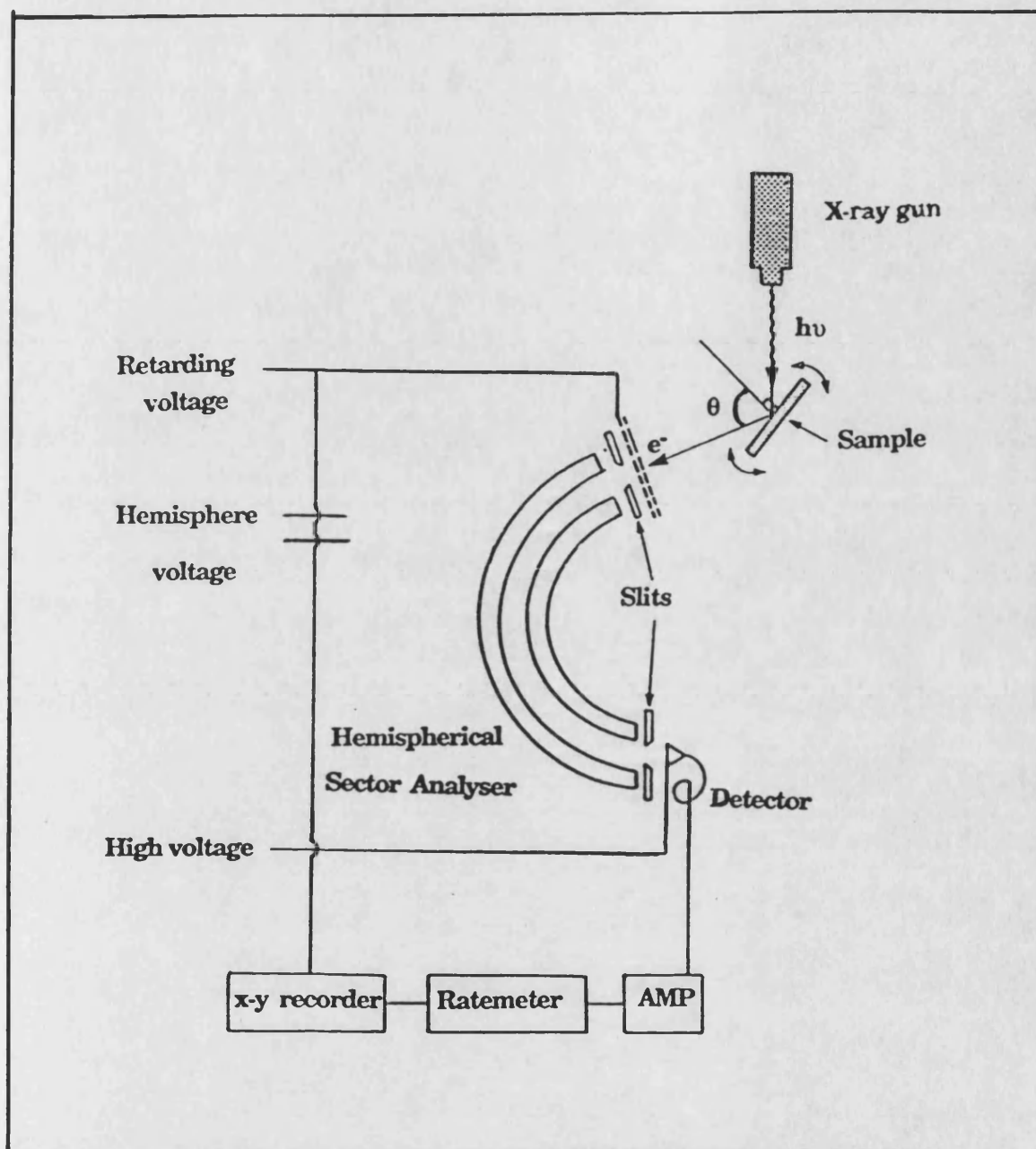
Figure A1.1. A schematic diagram of a XPS apparatus (after ref. 502).

the number of electrons at each energy value, a spectrum of peaks corresponding to the elements on the surface is generated. The area under each peak is a measure of the relative amount of each element present, while the shape and position of the peak reflects the chemical state of each element.

XPS is restricted to the surface (< 10nm) because electrons from much below the surface are not detected. They either suffer energy loss through collisions and are unable to make it out of the surface, or escape the surface with considerable energy loss. A summary of the information available from XPS is given in Table A1.1.

Table A1.1. Information derived from XPS Experiments on Polymers (After ref. 502)

- All elements except H and He.

- Surface concentrations of elements.

- Molecular environments (bonding state) and/or oxidation levels of most elements.

- Information on unsaturated or aromatic structures from shake up transitions.

- Positive identification of functional groups using derivatisation reactions.

A1.1.2 Static Secondary Ion Mass Spectroscopy (SSIMS).

SSIMS provides information on the molecular species present at the polymer surface [504] and is thought to be more surface sensitive than XPS in that it provides molecular information from a sampling depth of only 1 – 1.5nm [496 – 497,509,512].

In the SSIMS process a sample under ultra high vacuum (10^{-7} to 10^{-9} Torr) is bombarded with inert atoms or ions resulting in the sputtering of neutral species, electrons and ions from the surface region. The mass to charge ratio (m/e) of cationic or anionic species can be measured and a spectrum plotted of signal intensity as a function of m/e.

This spectrum or fragmentation pattern can be analysed using conventional mass spectrometry rules.

A1.2 MATERIALS AND METHODS

All materials used were identical to those given in chapters 2 and 3.

Thin films were prepared by spin casting from 0.1% chloroform solutions onto acetone/chloroform washed aluminium foils which were mounted directly onto analysis stubs ($1cm^3$). Samples were analysed within 24 hours of preparation.

XPS spectra were obtained using a VG Scientific ESCALAB Mk II electron spectrometer employing Mg K-alpha X-rays (hv = 1253.6 eV). A scan spectrum (1000 eV) and Narrow scans in the C1s and O1s regions were recorded for all the samples. The analyser was operated in Fixed Analyser Transmission mode and a pass energy of 50 eV (for survey scans) and 20 eV (for C1s and O1s envelopes). Data acquisition and analysis was performed by a VGS 5000 datasystem based on a DEC PDP 11/73 computer. Spectra were corrected for sample charging (referenced to C-H/C-C at 285 eV in the C1s envelope).

SSIMS spectra were acquired using a modified VG Scientific SIMSLAB which has been described in detail elsewhere [510]. Samples were bombarded with 2 eV argon atoms of flux density $3x10^9$ particles $cm^{-2}s^{-1}$ in UHV. Sample charging was neutralized using an electron flood gun in a manner described by Brown and Vikerman [511] for both positive and negative ion spectra. The total dose for setting up and acquisition of both positive and negative ion spectra was of the order of $2x10^{12}$ particles cm^{-2} per sample and lies within the limits established by Briggs and Hearn [508] for SSIMS spectra of "undamaged" surfaces.

A1.3 RESULTS AND DISCUSSION

The C1s and O1s core level spectra for the thin films of PHB and PHV20 from XPS are shown in Figure A1.2. There was good agreement between the experimental area ratios within the C1s envelope and those derived from the stoichiochemistry of the polyesters
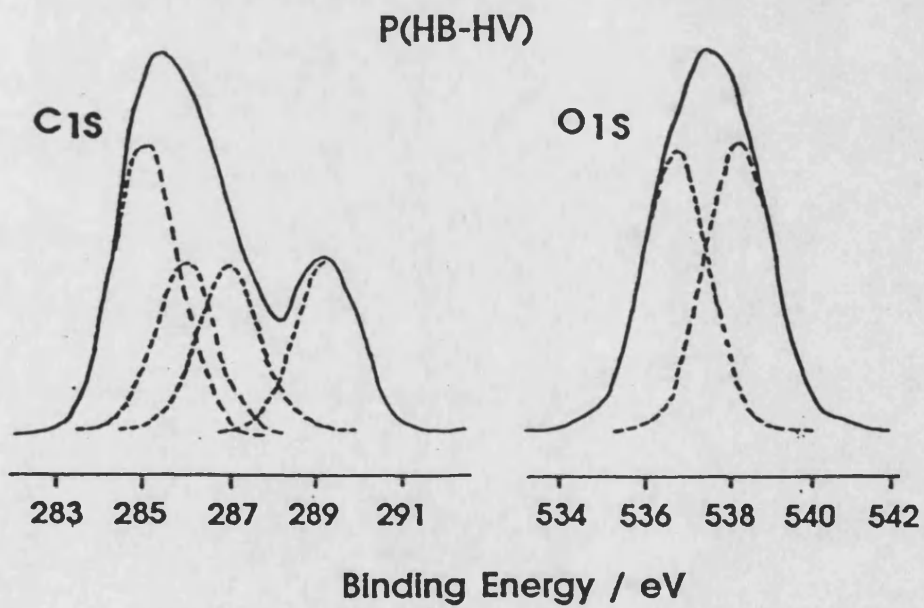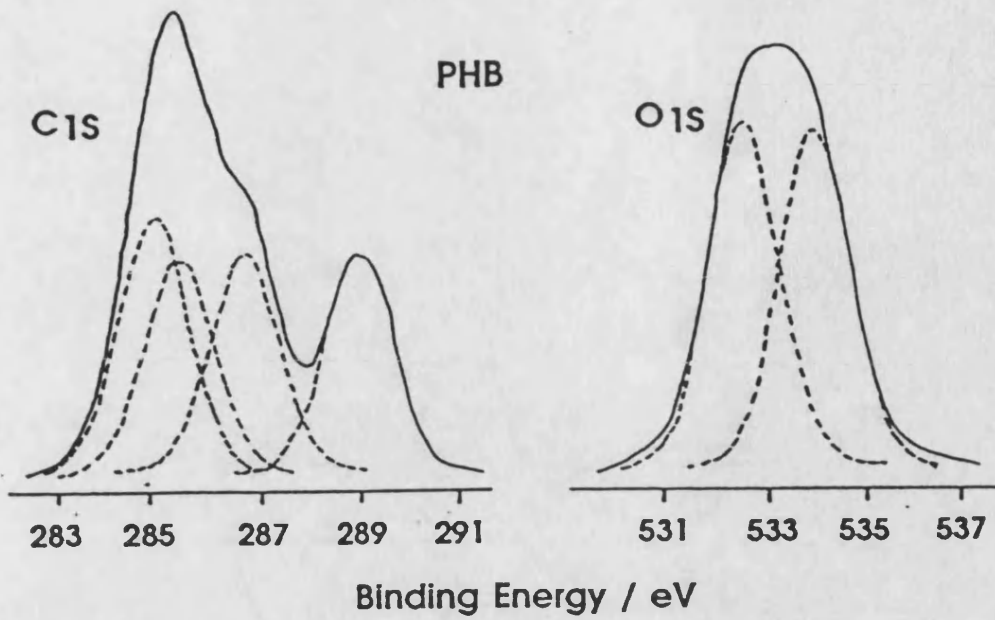
Figure A1.2. The C1s and O1s core level spectra for thin films of PHB380K and PHV20 from XPS analysis.

In terms of the $-\underline{C}-H$, $-\underline{C}-O$, $O-\underline{C}-O$, and $-\underline{C}-COOR$ environments. Similarly the C:O ratio of PHB and PHV20 determined from XPS correlated well with the stoichiochemistry (see Table A1.2).

Table A1.2. Experimental and Theoretical C:O Stoichiochemistry of PHB and PHV20.

Polymer	C:O Experimental	Theoretical
PHB	2.03:1	2.00:1
PHV20	2.15:1	2.09:1

The above results from XPS suggested the absence of C and O containing impurities at the surface of the polymers. No evidence was found for other elemental impurities. The absence of peak signals from the underlying aluminium substrate, i.e. the Al 2p core level, suggested that the spin cast films were at least 8-10nm thick.

Positive and negative ion SSIMS spectra for PHB are given in Figures A1.3 and A1.4 respectively. Both spectra were dominated by diagnostic fragments of the PHB monomer repeat units. In the positive ion spectrum (Figure A1.3), nM ±H and nM ±H were prominent for n=1-4 where M is the molecular weight of the PHB monomer. The nM ±H ions were observed at 85/87, 171/173, 257/259 and 343/345 Daltons (D) for n=1-4 respectively. Similarly, the nM-O ±H ions were present at 69, 155/157, 241/243 and 325/327 D for n=1-4 respectively. General structures for these ions are given in scheme 1 of Figure A1.5.

In the negative ion spectrum of PHB (Figure A1.4), the dominant ions were again diagnostic of the PHB monomer unit i.e. nM ±H at 85/87 and 171/173 and nM +O ±H at 101/103 and 187/189 D for n=1-2. The general structures for these negative ions are shown in scheme 2 of Figure A1.5.

The positive ion SSIMS spectrum of PHV20 (Figure A1.6) contained many fragments seen for the homopolymer, PHB. The PHB cations corresponding to nM ±H at 85/87, 171/173, and
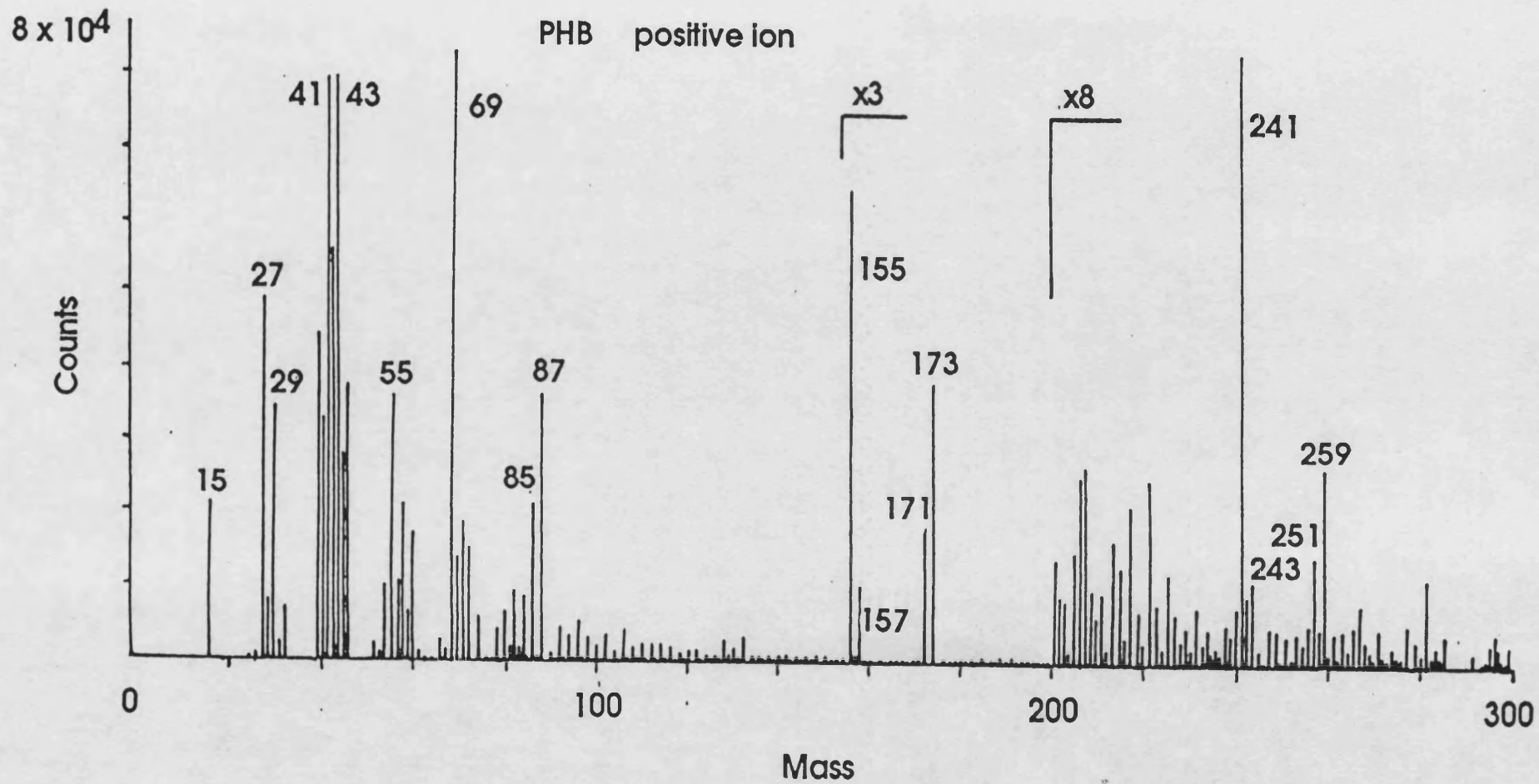
Figure A1.3. Positive ion SSIMS spectrum for PHB380K.
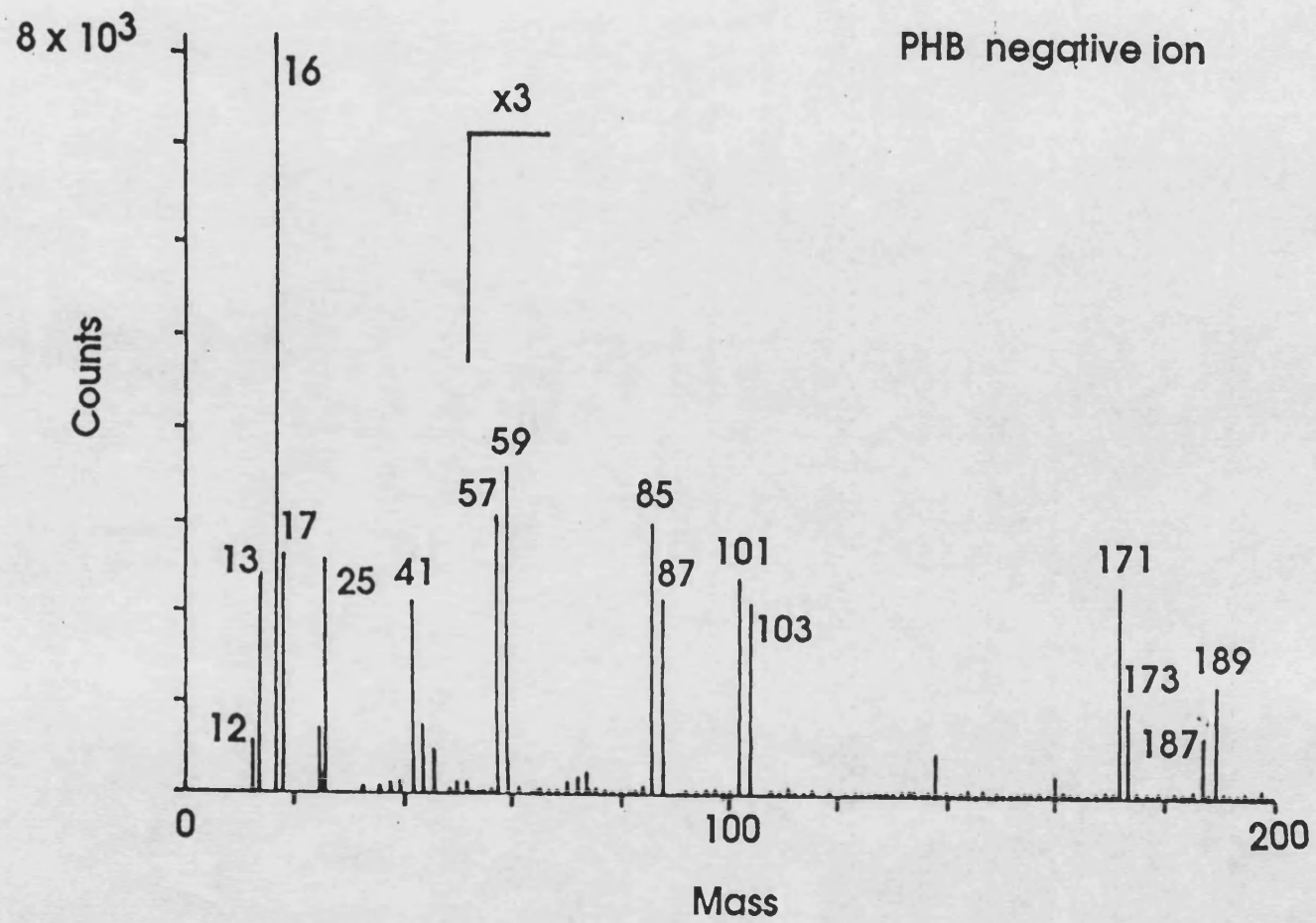
Figure A1.4. Negative ion SSIMS spectrum for PHB380K.
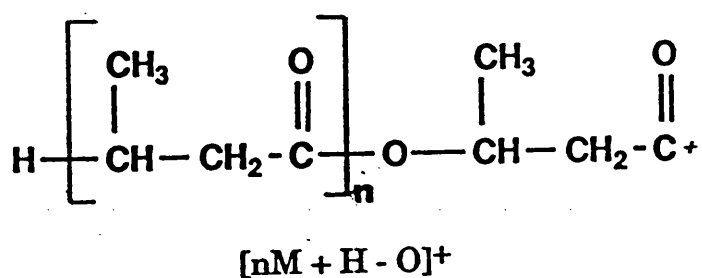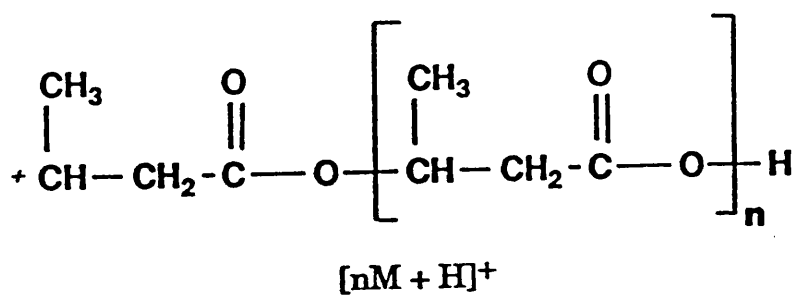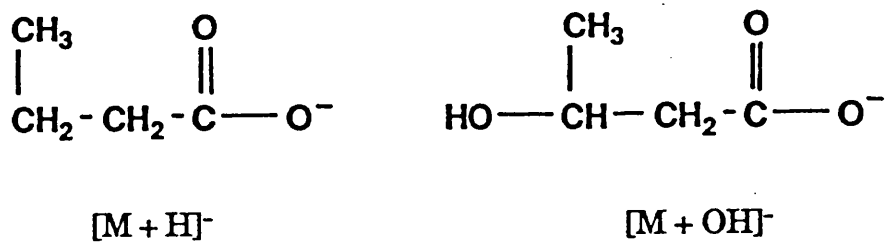
Figure A1.5. Chemical structures for schemes 1 and 2 in the fragmentation of PHB380K during SSIMS.
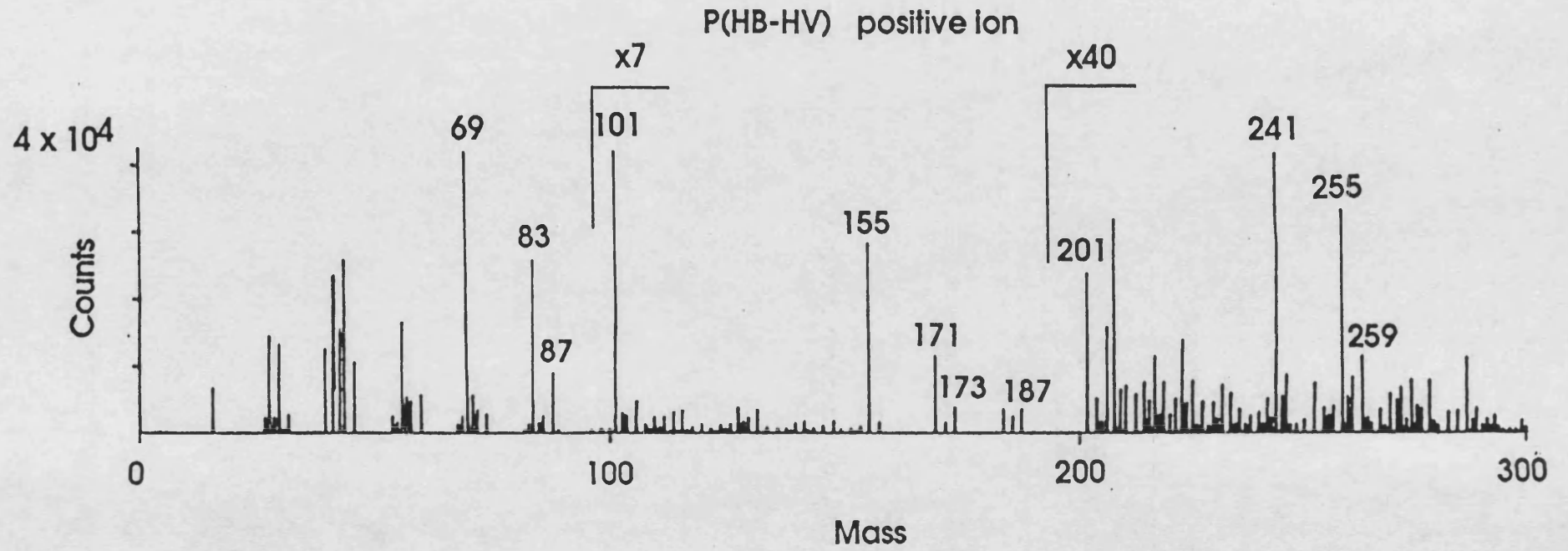
Figure A1.6. Positive ion SSIMS spectrum for PHV20.

257/259 D and nM$-$O $\pm$H at 69/71, 155/157, and 241/243 for n=1$-$3 respectively, were also prominent in the SSIMS spectrum of PHV20 in Figure A1.6. However, a number of significant ions were observed in the PHV20 spectrum which were not detected within the positive ion spectrum of PHB and can be attributed to the PHV monomer fragments. Namely, the 99/101 and the 199/201 D ions can be assigned to those of the PHV monomer unit, nM $\pm$H, and 83/85 and 185/187 D cations are diagnostic of nM$-$O $\pm$H, for n=1$-$2 respectively. The structures of these ions are given in scheme 3 of Figure A1.8.

In the positive ion spectrum of PHV20, there is also evidence of P(HB$-$HV) fragments. Namely cations corresponding to 187, 169/171 and 255 D are assigned to $(M_{PHB} + M_{PHV})$ +H, $(M_{PHB} + M_{PHV})$ $\pm$H and $(2M_{PHB} + M_{PHV})$ $\pm$H respectively. The structures of these ions are shown in scheme 4 of Figure A1.8. Clearly the positive ion SSIMS spectrum not only allows differentiation of PHB and PHV monomer units but also enables detection of fragments containing both monomer units.

The negative ion SSIMS spectrum of PHV20 (Figure A1.7) also provides a number of diagnostic ions for PHB at nM $\pm$H and nM+O $\pm$H i.e 85/87 and 171/173 D and 101/103 and 187/189 D respectively for n=1$-$2. Again a number of dominant ions were, however, detected for PHV20 which were absent in the negative ion SSIMS spectrum of the homopolymer, PHB. In this respect, 99/101 and 115/117 D ions may be assigned to M $\pm$H and M+O $\pm$H arising from the PHV portion of the copolymer. Similar to the findings in the positive ion spectrum of PHV20, the negative ion spectrum also provides evidence for the anions containing both monomers i.e the $(M_{PHB} + M_{PHV})$ $\pm$H ion at 185/187 D.

It is evident that many of the fragmentation patterns obtained previously from the SSIMS analysis of other polymers, such as PLA and PGA [504], extends to the higher molecular weight monomers of PHB and P(HB$-$HV) copolymers. The formation of the M $\pm$H ions in both positive and negative ion spectra of the polymers allows differentiation between the different monomer units.

317
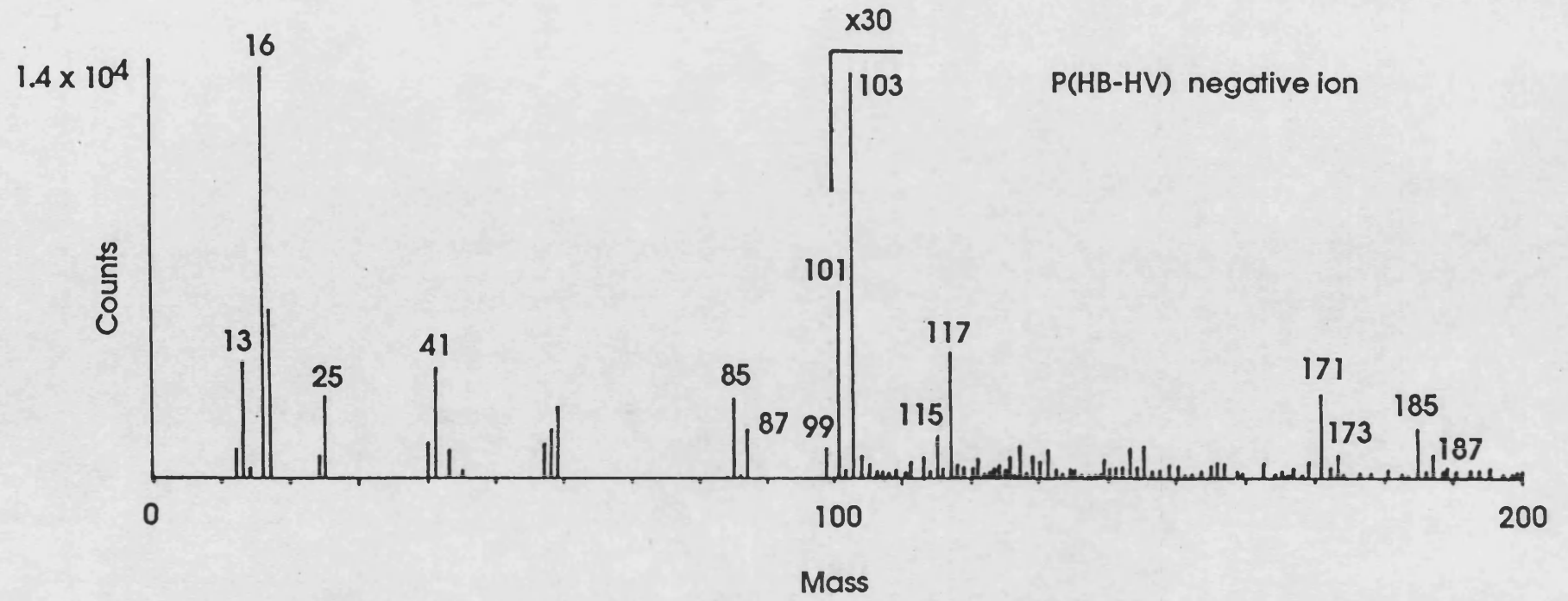
Figure A1.7. Negative ion SSIMS spectrum for PHV20.

Scheme 3 structures:

CH₂CH₃ ... O
⁺CH—CH₂-C—OH

[M + H]⁺

CH₂CH₃ ... O
HO—CH—CH₂-C—O⁻

[M + OH]⁻

CH₂CH₃ ... O
CH₂-CH₂-C⁺

[M - O + H]⁺

Scheme 3

Scheme 4 structures:

CH₃ ... O ... CH₂CH₃ ... O
CH₂-CH₂-C—O—CH—CH₂-C—O⁻

[M_PHB M_PHV + H]⁻

CH₃ ... O ... CH₂CH₃ ... O
HO—CH—CH₂-C—O—CH—CH₂-C—O⁻

[M_PHB M_PHV + OH]⁻

CH₃ ... O ... CH₂CH₃ ... O
⁺CH—CH₂-C—O—CH—CH₂-C—OH

[M_PHB M_PHV + H]⁺
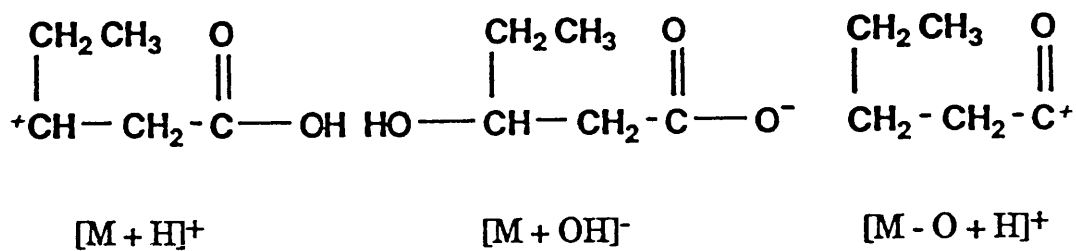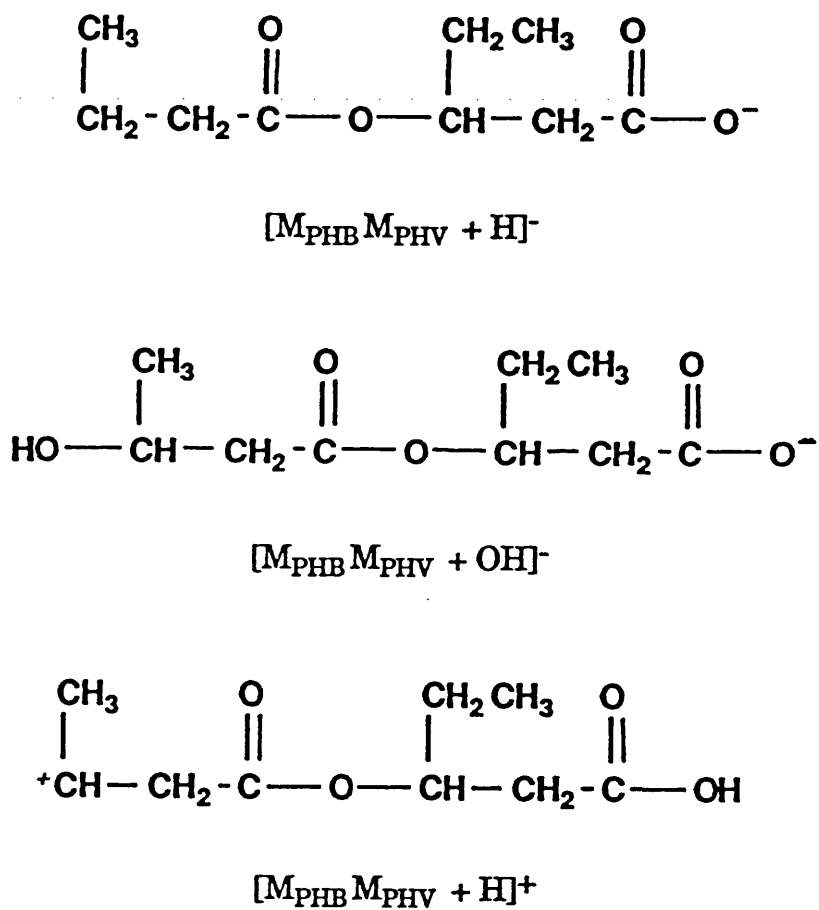
Scheme 4

Figure A1.8. Chemical structures for schemes 3 and 4 in the fragmentation of PHV20 during SSIMS.

319

A1.4 CONCLUSIONS

It has been shown that the quantitative elemental information from the XPS data coupled with the detailed molecular analysis provided by SSIMS spectra allow some insight into the surface chemical structure of P(HB-HV) polymers. The XPS data provides confirmatory evidence for the purity of these biopolymers extracted from a bacterial source. There was good correlation between the experimental and elemental ratios. Similarly the functional analysis is consistent with the expected stoichiochemistry of the polymers. The SSIMS data also showed no evidence of any extraneous inorganic or organic contamination of bacterial polyesters.

APPENDIX B

THE SESSILE DROP METHOD FOR DETERMINING CONTACT ANGLES

A2.1 METHOD

Solvent cast films were prepared as in chapter 2. Equilibrium aged films (for at least 3 months at 25°C)) were used in contact angle determinations. Water contact angles were measured for both the rough and smooth surface of P(HB–HV) films.

Triple distilled water used for contact angle measurements was prepared in an all glass still. All vessels used for transporting water were of glass which had previously been cleaned using chromic acid.

A 3 ul sessile drop of triple distilled water was placed onto the surface of the polymer film using a micropipette. The film had previously been placed onto the flat stage of a contact angle gonio – telemicroscope (Figure A2.1) specially constructed from commercially available parts (Table A2.1). The formed drop was illuminated via a cold light source and the required angle measured with a protractor eye piece following alignment of the eye piece cross–hair at both sides of the liquid drop. Contact angle measurements were performed on both sides of at least 5 drops for each sample surface.

Table A2.1. Parts used to construct the contact angle gonio – telescope (after ref. 502).

Part description	Catalogue No.
Viewing microscope	22 – 9153
Rack and pinion draw tube	11 – 8166
50mm objective lens	11 – 8232
mounting pin	22 – 7868
x10 eyepiece with cross line	24 – 4780
Protractor eyepiece	11 – 5188
Triangular optical bench	44 – 4315
Leveling cross feet	22 – 7108
Circular table	22 – 7900
Tranverse and vertical slide mount, 90mm base	22 – 5110
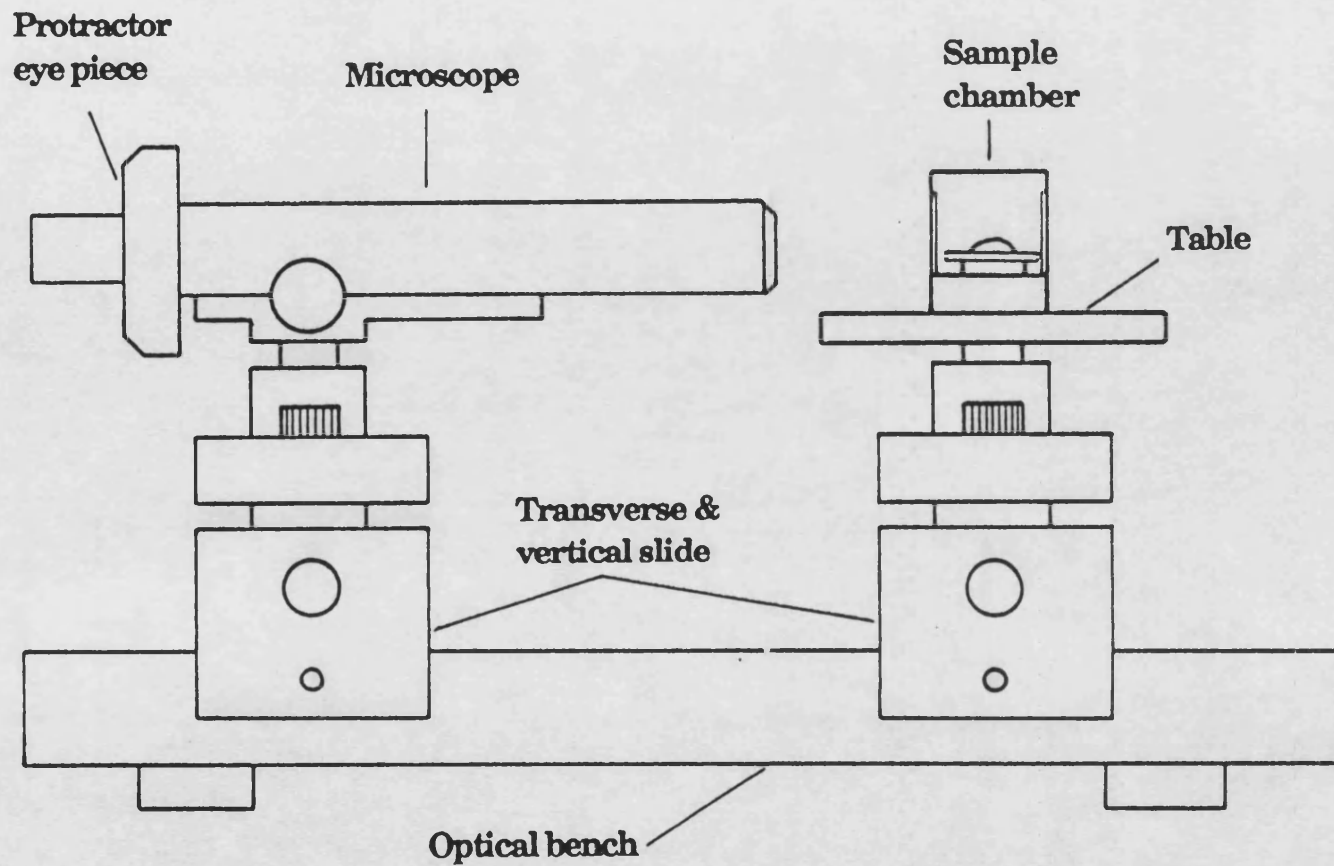
Figure A2.1. A schematic diagram of a contact angle gonio–
telemicroscope (after ref. 502).

A2.2 RESULTS

Table A2.2 Summary of water contact angles for P(HB – HV) polyester films cast from chloroform (Mean ± S.D; n = 10).

Polymer	Smooth surface of film		Rough surface of film	
	Contact angle (degrees)	Work of adhesion (mJm^{-2})	Contact angle (degrees)	Work of adhesion (mJm^{-2})
PHB380K	84.9 ±2.5	79.3 ±2.6	82.7 ±2.7	82.1 ±3.5
PHV6	80.2 ±3.4	85.2 ±4.3	82.6 ±1.2	82.2 ±1.5
PHV12	67.1 ±2.1	101.1 ±2.5	74.2 ±2.0	92.6 ±2.4
PHV20	69.6 ±0.7	98.2 ±0.9	74.2 ±2.9	92.6 ±3.5
PHV27	67.3 ±2.6	100.9 ±3.1	69.8 ±2.3	97.9 ±2.7

where Work of adhesion = $W_{slv} = \beta_{1v} (1 + \cos \theta)$

β_{1v} = surface tension of water = 72.8 mJm^{-2} (from ref. 502).

θ = contact angle

APPENDIX C

FORMULA FOR PHOSPHATE BUFFER.

Phosphate buffer pH 7.4 at 37°C.

Potassium dihydrogen orthophosphate..... 13.625g
Disodium hydrogen orthophosphate........ 24.200g
Sodium chloride................................ 9.350g
Distilled Water to................................ 5000cm^3

All salts were purchased from BDH Chemicals, Poole, Dorset.

APPENDIX D

STATISTICAL METHODS

All student 't' tests presented in this thesis were evaluated using the BBC INSTAT statistical package (Reading University, UK).

REFERENCES

1   Juliano R.L.,   ed.   *Drug Delivery Systems: Physicochemical and Biomedical Applications*,   Oxford University Press, New York, (1980).

2   Robinson J.R.,   ed. *Sustained and Controlled Release Drug Delivery Systems*, Marcel Dekker, New York, (1978).

3   Mills S.N, and Davis S.S., In: *Polymers in controlled drug delivery*, (Illum L., and Davis S.S., eds.) IOP Publishing Ltd, Bristol, (1987) p1.

4   Langer R.S., and Peppas N.A., *Biomaterials*, 2, 201, (1981)

5   Bruck S.D. ed. *Controlled Drug Delivery vol.1 Basic Concepts.* CRC Press, Inc., Boca Raton, Florida, (1983).

6   Rubinstein M.H., In: *Pharmaceutics: The Science of Dosage Form Design.* (Aulton M.E., ed.) Churchill Livingstone, Edinburgh, (1988) p304.

7   Proudfoot S.G., In: *Pharmaceutics: The Science of Dosage Form Design.* (Aulton M.E., ed.) Churchill Livingstone, Edinburgh, (1988) p174.

8   Lloyd J.B. In: *Drug Delivery systems, Fundamentals and Techniques.* Johnson P and Lloyd–Jones J.G., eds.   Ellis Horwood Ltd, Chichester, England, (1987) pp95–105.

9   Lloyd J.B.,   Duncan R., and Kopecek J., *Pure and Appl. Chem.* 56, 1301–1304, (1984)

10   Pouton C.W. *J. Clinical and Hospital Pharmacy*, 10, 45–58, (1985).

11   Rowland G.F., In: *Drug Delivery systems, Fundamentals and Techniques.* Johnson P and Lloyd–Jones J.G., eds.   Ellis Horwood Ltd, Chichester, England, (1987) pp81–94.

12   Brodsky F.M., *Pharm. Res.* 5, 1, (1988)

13   O'Neil G.J., In: *Drug Carriers in Biology and Medicine,* (Gregoriadis G., ed.), Academic Press, London, (1979), pp23–42.

14   Tomlinson E. *Advanced Drug Delivery Reviews* 1, 87–198, (1987)

15   Tomlinson E., and Davis S.S, eds. *Site–specific Drug Delivery*, John Wiley and Sons, Chichester, UK, (1986).

16   Illum L. *Microspheres and Site Specific Delivery*, Carson Offsett Ltd., Nottingham, (1987).

17   Illum L and Davis S.S., *Life Sciences* 40, 1553–1560, (1987).

18   Illum L, Davis S.S, Muller R.H, Mak E, and West P. *Life Sciences* 40, 367–374, (1987).

19   Illum L, Davis S.S., *FEBS Letters* 167, 79–82, (1984).

20   Douglas S.J.,   Davis S.S,   and Illum L., *Crit. Rev. Ther. Drug. Drug. Carrier Syst.* 3, 233–261, (1987).

21   Davis S.S, Washington C.W, West P, Illum L, Liversidge G, Sternson L, and Kirsh R. In: *Biological Approaches to the Controlled Delivery of Drugs* (Annals of the New York Academy of Sciences vol. 507),   Juliano R.L ed. (1987) pp75–88.

22   Juliano R.L, In: *Controlled Drug delivery: Fundamentals and Applications,* 2nd Ed. (Robinson J.R, and Lee V.H., eds.) Marcel Dekker, New York, (1987), pp555-580.

23   Juliano R.L, Daoud S. Krause H.J, and Grant C.W.M. In: *Biological Approaches to the Controlled Delivery of Drugs* (Annals of the New York Academy of Sciences vol. 507), Juliano R.L ed. (1987), pp89-103.

24   Lopez-Berestein G, Hopfer R L, Mehta R, Mehta K, Hersh E M, and Juliano R L., *J. Infect. Dis.* 150, 278-284, (1984).

25   Juliano R.L in: *Drug carrier sysytems* (Roerdink F.H.D and Kroon A M. eds), John Wiley and Sons, (1989) pp249-279

26   Ostro M., ed., *Liposomes, From Biophysics to Theraputics,* Marcel Dekker, New York, (1987).

27   Papahadjopoulos D. and Gabizon A., in: *Biological Approaches to the Controlled Delivery of Drugs* (Annals of the New York Academy of Sciences vol. 507), Juliano R.L ed. (1987) pp75-88.

28   Gregoriadis G., In: *Drug Carriers in Biology and Medicine,* (Gregoriadis G., ed.), Academic Press, London, (1979), pp286-341.

29   Roerdink F.H, Daemen T, Bakker-woudenberg I.A.J.M., Storm G., Crommelin D.J.A and Scherpof G.L In: *Drug Delivery systems, Fundamentals and Techniques.* Johnson P and Lloyd-Jones J.G., eds. Ellis Horwood Ltd, Chichester, England, (1987) pp66-80.

30   Kirsh R, Bugelski P.J and Poste G., in: *Biological Approaches to the Controlled Delivery of Drugs* (Annals of the New York Academy of Sciences vol. 507), Juliano R.L ed. (1987), pp 141-154.

31   Poznansky M.J., and Juliano R.L. *Pharmacological Reviews* 36, 277-336, (1984).

32   Juliano R.L *Advanced Drug Delivery Reviews* 2, 31-54, (1988)

33   Fidler I.J. *Advanced Drug Delivery Reviews* 2, 69-106, (1988)

34   Alving C.R. *Advanced Drug Delivery Reviews* 2, 107-128,(1988)

35   Davis S.S., Illum L. and Tomlinson E., eds. *Delivery Systems for Peptide Drugs* , Plennum Press, New York, (1986).

36   Liu D.T, Goldman N, Gates F., In: *Delivery Systems for Peptide Drugs,* Davis S.S., Illum L and Tomlinson E., eds. Plennum Press, New York, (1986), pp341-350.

37   Tomlison E, and Livingstone C., *Pharm. J.* 243, 646-648, (1989)

38   Banga A.K, and Chien Y.W., *Int. J. Pharm.* 48, 15-50, (1988).

39   Lee V.H.L *CRC Critical Reviews in Therapeutic Drug Carrier Syststems* 5, 69-98, 1988)

40   Hutchinson F.G and Furr B.J.A., in: *Delivery Systems for Peptide Drugs,* Davis S.S., Illum L and Tomlinson E., eds. Plennum Press, New York, (1986), pp115-124.

41   Hutchinson F.G and Furr B.J.A, In: *Drug Delivery systems, Fundamentals and Techniques.* Johnson P and Lloyd-Jones J.G., eds. Ellis Horwood Ltd, Chichester, England, (1987) pp106-119.

42   Langer R.S and Peppas N.A., *Biomaterials* 2, 201 – 213, (1981).

43   Wise D.L, Trantolo D.J, Marino R.T and Kitchell J.P. *Advanced Drug Delivery Reviews* 1, 19 – 39, (1987).

44   Heller J. In: *Recent Advances in Drug Delivery* Stystems (Anderson   J.M, and Kim S.W. eds)   Plennum Press, New York, (1984) pp101 – 122.

45   Siegel R.A and Langer R. *Pharm. Res.* 1, 2 – 10, (1984).

46   McIntosh R.P. *Trends in Pharmacological Sciences* 5, 429 – 431, (1984)

47   Leyendecker G., Struve T.,   and Plotz E.J., *Arch. Gynecol.* 229, 177 – 190, (1980)

48   Crowley W.F and McArthur J.W., *J. Clin. Endocrinol. Metab.* 52, 173 – 175, (1980)

49   Reinberg A.,   Smolensky,   M.   and Labrecque G.,   eds.   *Annual   Reviews   of Chronopharmacology*, Vol.2, Pergamon Press, Oxford, (1986)

50   Pauly J.E, *Am. J. Anat.,* 168, 365, (1983).

51   Bruck S.D., In: *Controlled Drug Delivery vol.1 Basic Concepts.* CRC Press, Inc., Boca Raton, Florida, (1983), pp2 – 13.

52   Holland S.J, Tighe B.J, and Gould P.L. *J.Controlled Release* 4, 155 – 180, (1986).

53   Williams D.F. *J.Mater. Sci.* 17, 1233 – 1246, (1982).

54   Gilding D.K. *Clin. Implant. Mater.,* 2, 209 – 232, (1981).

55   Heller J. *CRC Critical Rev.Ther. Drug Carrier Systems,* 1, 39 – 90 (1984).

56   Heller J. *Biomaterials* 1, 51 – 57, (1980).

57   Heller J., In: *Controlled Drug delivery: Fundamentals and Applications,* 2nd Ed. (Robinson J.R, and Lee V.H., eds.) Marcel Dekker, New York, (1987),pp179 – 212.

58   Desai S.J., Simonelli A.P., and Higuchi W.I., *J. Pharm. Sci.* 54, 1459, (1965).

59   Folkman J. and Long D.M., *J. Surg. Res.* 4, 139, (1964).

60   Waitz, J.A, Olszewski B.J, and Thompson P.E., *Science* 141, 723, (1963).

61   Davis B.K., *Experientia,* 28, 348, (1972)

62   Davis B.K., *Proc. Natl. Acad. Sci.* 71, 3120 – 3123, (1974).

63   Langer R. and Folkman J. *Nature (Lond.)* 263, 797 – 800, (1976).

64   Rhine W.D, Hsieh D.S.T and Langer R. *J. Pharm. Sci.* 69, 265 – 270, (1980)

65   Hsieh D.S.T, Rhine W.D, and Langer R. *J.Pharm.Sci.* 72, 17, (1983)

66   Hoffman A.R. and Crowley W.F., *N. Engl. J. Med.* 307, 1237 – 1241, (1982).

67   Skarin G.,   Nillius S.J.,   Wibell L.,   and Wida L., *J. Clin. Endocrin. Metabol.* 55, 723 – 726,   (1982).

68   Cutler G.B., Hoffman A.R, Swerdloff R.S, Santen R.J, Meldrum D.R and Comiti F. *Ann. Int. Med.* 102, 643 – 657, (1985)

69   Cohen J.M, Siegel R.A, and Langer R., *J. Pharm. Sci.* 73, 1034 – 1037, (1984).

70   Siegel R.A., Cohen J.M, Brown L, and Langer R. in: *Recent Advances in Drug Delivery systems,* (Anderson J.M, and Kim S.W., eds.), Plennum Press, New York, (1984) pp 315 – 320.

71   Langer R, Hsieh D.S.T, Rhine W, and Folkman J., *J.Membrane Sci.* 7, 333, (1980)

72   Langer R, Brown L, and Edelman E., in: *Recent Advances in Drug Delivery systems,* (Anderson J.M, and Kim S.W., eds.), Plennum Press, New York, (1984) pp 315 – 320.

73   Bawa R, Siegel R.A, Marasca K, and Langer R., *J. Controlled Release* 1, 259 – 267, (1985)

74   Edelman E R, Brown L, Taylor J, and Langer R. *J. Biomed. Mater. Res.* 21, 339, (1987).

75   Brown L, Siemer L, Munoz C, and Langer R., *Diabetes* 35, 684, (1986).

76   Hsu T.T.P, and Langer R., *J. Biomed. Mater. Res.* 19, 445, (1985)

77   Edelman E.R, Kost J.,Bobeck H., and Langer R., *J. Biomed. Mater. Res.* 19, 67, (1985)

78   Kost J., Nonecker R., Kunica E, and Langer R., *J. Biomed. Mater. Res.* 19, 935, (1985)

79   Langer R, Siegel R, Brown L, Leong K, Kost J, and Edelman E., *Chem. Tech.* 16, 108, (1986).

80   Brown L, Munoz C, Siemer L, Edelman E, and Langer R., *Diabetes,* 35, 692, (1986).

81   Pitt C.G., and Schindler A., in: *Controlled Drug Delivery vol.1 Basic Concepts.* CRC Press, Inc., Boca Raton, Florida, (1983), pp53 – 80.

82   Tatum H.J. *Contraception* 1, 253, (1970).

83   Frazza E.J. and Schmitt E.E. *J. Biomed.Mater. Res.* 1, 43 – 58, (1971)

84   Pitt C.G, Marks A, and Schindler A., in: *Controlled Release of Bioactive Materials,* (Baker R. ed.), Academic Press, New York, (1980).

85   Schindler A, Jeffcoat R, Kimmel G, and Pitt C.G., in: *Contemporary Topics in Polymer Science,* Vol.2, (Pearce E.M, and Schaefgen J.R. eds.) Plennum Press, New York, (1977).

86   Sidman K.R, Schwope S.D, Steber W.D, Rudolph S.E, and Poulin S.B., *J.Membrane. Sci.* 7, 227 – 291, (1980)

87   Maser B, Cefelin P, Lipatova T.E, Bakalo L.A, and Lugovskaya G.G., *J. Polym. Sci. Polym. Symp.* 66, 259 – 262, (1979).

88   Wood D.A, Whateley T.L, and Florence A.T., *Int. J. Pharm.* 8, 35 – 43, (1981).

89   Vezin W.R and Florence A.T., *J. Biomed. Mater. Res.* 14, 93 – 106, (1980).

90 De Visser A.C, Grulleman C.W.J, Van der Goot H, Timmerman H. *Proceed. Int. Symp. Contr. Rel. Bioact. Mater.* 10,46 – 49, (1983).

91 Eppstein D.A, and Longenecker J.P., *CRC Crit. Rev. Ther. Drug Carrier Systems.* 5, 99 – 139, (1988).

92 Feijen J. *NATO ASI Series Ser. E. (Appl.Sci),* 106, 62 – 78, (1986).

93 Wise D.L, Fellman T.D, Sanderson J.E and Wentworth R.L. in: *Drug carriers in Biology and Medicine* (Gregoriadis G., ed.), Academic Press, (1979), pp237 – 270.

94 Juni K and Nakano M., In: *Polymers in Controlled Drug Delivery* (Illum L and Davis S.S., eds,), Wright Publishers, Bristol, UK, (1987), pp49 – 59.

95 Brady J.M, Cutright D.E, Miller R.A, Battistone G.C, and Hunsack E.E., *J.Biomed. Mater. Res.* 7, 155 – 166, (1973).

96 Miller R.A, Brady J.M, and Cutright D.E., *J. Biomed. Mater. Res.* 11, 711, (1977).

97 Gilding D.K. and Reed A.M, *Polymer* 20, 1459 – 1464, (1979).

98 Wakiyama N, Juni K, and Nakano M., *Chem. Pharm. Bull.* 29, 3363 – 3368, (1981).

99 Wakiyama N, Juni K, and Nakano M., *Chem. Pharm. Bull.* 30, 3719 – 3727, (1981).

100 Spenlehauer G, Veillard M, Benoit J.P., *J. Pharm. Sci.* 8, 750 – 755, (1986)

101 Beck L.R, Cowsar D.R, Lewis D.H, Gibson J.W, and Flowers C.E., *Am. J. Obstet. Gynecol.* 135, 491 – 426, (1979).

102 Schwope A.D, Wise D.L, and Howes J.F, *Life Sci.* 17, 1877, (1975).

103 Mason W.S, Thies C, and Cicero T.J., *J. Pharm. Sci.* 65, 847 – 850, (1976).

104 Tice T.R, Pledger K.L, and Gilley R.M., *European Patent* Number 0248531, (1987).

105 Marcotte N, and Goosen M.F.A., *J. Controlled Release,* 9, 75 – 85, (1989)

106 Maulding H.V. *J. Controlled Release* 6, 167 – 176, (1987).

107 Tabata Y, and Ikada Y., *J.Controlled Release* 6, 189 – 204, (1987)

108 Redding T.W, Schally A.V, Tice T.R, and Meyers W.E., *Proc. Natl. Acad. Sci. (USA),* 81, 5845 – 5848, (1984).

109 Sanders L.M, Kent J.S, McRae G.I, Vickery B.H, Tice T.R, and Lewis D.H., *J. Pharm. Sci.* 73, 1294 – 1297, (1984).

110 Sanders L.M, Kell B.A, McRae G.I, and Whitehead G.W., *J. Pharm. Sci.* 75, 356 – 360, (1986).

111 Sanders L.M, Vitale K.M, McRae g.I, and Mishky P.B., In: *Delivery Systems for Peptide Drugs,* Davis S.S., Illum L. and Tomlinson E., eds., Plennum Press, New York, (1986), pp125 – 138.

112 ABPI Data Sheet Compendium 1988 – 89; Datapharm Publications Ltd, London, (1988).

113   Beck L.R, Pope V.Z, Flowers C.E, Cowsar D.R, Tice T.R, Lewis D.H, Dunn R.L, Moore A.B, and Gilley R.M., *Biol. Reprod.*, 28, 186–195, (1984).

114   Heller J. *Pharm, Int.* 7(12), 316–318, (1986).

115   Wise D.L, Gregory J.B, Newberne P.M,Batholow L.C, and Stanbury J.B., in: *Polymeric Delivery Systems*, (Kostelnick R.J, ed.) Gordon and Breech Science Publishes, New York, (1978) pp 121–138.

116   Cappozza R.C, Schmitt E.E, and Sendelback L.R., in: *Narcotic Antagonist*, NIDA Research Monograph Series No.4, Willete R.E.,ed., DHEW Publication No. ADM–76–296, (1976).

117   Heller J. and Himmelstein K.J. *Methods in Enzymology* 112, 422–436, (1985)

118   Sparer R.V, Shih C, Ringirsen C.D, and Himmelstein K.J. *J.Controlled Release* 1, 23–32, (1984).

119   Heller J, Penhale D.W.H, Fritzinger B.K, Rose J.E and Helwing R.F. *Contracept. Deliv. Syst.* 4, 43–53, (1983)

120   Heller J. *CRC Critical Reviews in Therapeutic Drug Carrier Syststems* 1, 39–90, (1984)

121   Heller J, Penhale D.W.H, and Helwing R. *Polym. Lett.* 18, 619–624, (1980)

122   Heller J, Fritzinger B.K, Ng S.Y, and Penhale D.W.H, *J. Controlled Release* 1, 225–232, (1985)

122   Heller J, Fritzinger B.K, Ng S.Y, and Penhale D.W.H, *J. Controlled Release* 1, 233–238, (1985)

124   Heller J, Penhale D.W.H, Fritzinger B.K, and Ng S.Y. *J. Controlled Release* 5, 173–177, (1987)

125   Heller J, Ng S.Y, Penhale D.W, Fritzinger B.K, Sanders L.M, Burns R.A, Gaynon M.G, and Bhosale S.S., *J. Controlled Release* 6, 217–224, (1987)

126   Chow A.W, Hamlin R.D, and Heller J. *J. Controlled Release* 9, 123–131, (1989)

127   Hill J., *J.A.C.S.* 52, 4110–4114, (1930), as cited in ref.130.

128   Hill J., and Carothers W.H., *J.A.C.S.* 54, 1569–1579, (1932) as cited in ref. 130.

129   Rosen H.B, Chang J, Wnek G.E, Linhardt R.J. and Langer R. *Biomaterials* 4, 131–133, (1983)

130   Leong K.W, Brott B.C, and Langer R., *J.Biomed. Mater, Res.* 19, 941–955, (1985)

131   Leong K.W, Amore P.D, Marletta M, Langer R., *J. Biomed. Mater. Res.* 20, 51–64, (1986)

132   Mathiowitz E., and Langer R., *J. Controlled Release* 5, 13–22, (1987).

133   Mathiowitz E, Saltzman W.M, Domb A, Dor Ph. and Langer R. *J. Appl. Polym. Sci.* 35, 755–774, (1988)

134 Chasin M, Lewis D, and Langer R. *BioParm.* 1(2), 33 – 35,38 – 40,46, (1988).

35   Lemoigne M., *Ann. Inst. Pasteur* 39, 144 – 173, (1925).

136 Lemiogne M., *C. r. hebd. Seanc. Soc. Biol.* 94, 1291 – 1292, (1926); as cited in ref.137.

137 Dawes E.A and Senior P.J., *Advances in Microbial Physiology* 10, 203 – 267, (1973).

138 Herron J.S., King J.D, and White D.C., *Appl. Environ. Microbiol.* 35, 251 – 257, (1978).

139 Carr N.G., *Biochem. Biophys. Acta.* 120, 308 – 310, (1966).

140 Ward A.C, Rowley B.I, and Dawes E.A., *J. Gen. Microbiol.* 102, 61 – 68, (1977).

141 Stanler R.Y, Palleroni N.J, and Doudoroff M., *J. Gen. Microbiol.* 43, 159 – 271, (1966).

142 Lundgren D.G., and Bott K.F., *J.Bacteriol.* 156, 778 – 788, (1963).

143 Stevenson L.H, and Socolofsky M.D., *J. Microbiol. Serol.* 39, 341 – 350, (1973).

144 Reusch R.N, and Sadoff H.L, *J. Bacteriol.* 156, 778 – 788, (1978).

145 Williamson D.H, and Wilkinson J.F., *J. Gen. Microbiol.* 19, 198 – 209, (1958)

146 Merrick J.M, and Doudoroff M., *Nature (London)* 189, 890 – 892, (1961).

147 Lundgren D.G, Alper R, Schnaltman C. and Marchessault R.H. *Journal of Bacteriology* 89, 245 – 251, (1965).

148 Laffferty R.M, Korsatko B, and Korsatko W., In: *Biotechnology* (Rehm H.J. and Reed G., eds.) Volume 6b *Special Microbial Processes,* (Rehm H.J ed.), VCH Verlagsgesellschaft, Weinhhelm, FRG., (1988) pp135 – 176.

149 Holmes P.A, *Phys. Technol.* 16, 32 – 36, (1985).

150 King P.P, *J. Chem. Tech. Biotechnol.* 32, 2 – 8, (1982).

151 Collins S.H, *Spec. Publ. Soc. Gen. Microbiol.* 21, 161 – 168, (1987).

152 Byrom D., *Tib – Tech* 5, 246 – 25, (1987).

153 Howells E.R, *Chemistry and Industry* 7, 508 – 511, (1982).

154 Senior P.J., and Dawes E.A., *Biochem. J.* 134, 225 – 238, (1973).

155 Oeding V., and Schlegel H.G., *Biochem J.* 134, 239, (1973).

156 Dawes E.A., *Bioscience Reports* 8, 537 – 547, (1988).

157 Griebel R., and Merrick J.M., *J. Bacteriol.* 108, 782, (1971).

158 Haywood G.W, Anderson A.J, and Dawes E.A., *FEMS Microbiol. Lett.* 57, 1 – 6, (1989).

159 Ballard D.G.H., Holmes P.A, and Senior P.J., *NATO ASI Ser* C. 215, 293 – 314, (1987).

160 Suzuki T, Yamane T, and Shimizu S., *Appl. Microbiol. Biotechnol.* 23, 322-329, (1986).

161 Leak D.J, and Dalton H., *J. Gen. Microbiol.* 129, 3487-3498, (1983).

162 Doi Y., *European Patent* No: 0 288 908. (1988)

163 Doi Y, Tamaki A, Kunioka M and Soga K., *J. Chem. Soc. Chem. Commun.* 21, 1635-13, (1987)

164 Doi Y, Kunioka M, Nakamura Y, and Soga Y., *J. Chem. Soc. Chem. Commun.* 23, 1696-1697, (1986)

165 Doi Y, Kunioka M, Nakamura Y, and Soga Y., *Macromolecules* 19, 1274-1276, (1986).

166 Doi Y, Kunioka M, Nakamura Y, and Soga Y., *Macromolecules* 20, 2988-2991, (1987).

167 Kunioka M, Nakamura Y, and Doi Y., *Polymer Commun.* 29, 174-176, (1988)

168 Doi Y, Tamaki A, Kunioka M and Soga K. *Appl. Microbiol. Biotechnol.* 28, 330-334 (1988).

169 Doi Y, Kunioka M, Nakamura Y, and Soga Y., *Macromolecules* 21, 2722-2727, (1988).

170 Doi Y, Kunioka M, Nakamura Y, and Soga Y., *Makromol. Chem. Rapid. Commun.* 7, 661-664, (1986).

171 Doi Y, Kunioka M, Tamaki A, Nakamura Y, and Soga Y., *Makromol. Chem.* 189, 1077-1086, (1988).

172 Doi Y., Segawa A, and Kunioka M., *Polymer Commun.* 30, 169-171, (1989).

173 Kamiya N, Yamamoto Y, Inoue Y, Chujo R, and Doi Y., *Macromolecules* 22, 1676-1682, (1989).

174 Ballisteri A., Garazzo D, Giuffrida M, Impallomeni G, Montaudo G., *Macromolecules* 22, 2107-2111, (1989).

175 Helleur R., *Polym. Prepr. (Am. Chem. Soc. Div. Polym. Chem.)* 29, 609-610, (1988).

176 Doi Y, Kunioka M, Nakamura Y, and Soga Y., *Macromolecules* 19, 2860-2864, (1986).

177 Bluhm T.L, Hamer G.K, Marchessault R.H., Fyfe C.A, and Veregin R.P., *Macromolecules* 19, 2871-2876, (1986).

178 Wallen L.L, and Rohwedder W.K., *Environ. Sci. Technol.* 8, 576-579, (1974).

179 Findlay R.H, and White D.C, *Appl. Environ. Microbiol.* 45, 71-78, (1983).

180 De Smet M, Eggink G, Witholt B, Kingma J, and Wynberg H., *J. Bacteriol.* 154, 870, (1983).

181 Brandl H, Gross R.A, Lenz R.W, and Fuller C.W., *Appl. Environ. Microbiol.* 54, 1977-1982, (1988).

182 Gross R.A, DeMello C, Lenz R.W, Brandl H, and Fuller C.W., *Macromolecules* 22, 1106-1115, (1989).

183 Peoples O.P, and Sinskey A.J., *Prog. Biotechnol. Ind. Polysaccharides* 3, 51 – 56, (1987).

184 Peoples O.P, and Sinskey A.J., *Proceedings of 193rd. Annual meeting of ACS, April,* (1987) No.70., ISBN 8412 – 1013 – 6.

185 Masamune S, Walsh C.T, Sinskey A.J., and Peoples O.P., *Pure and Applied Chem.* 61, 303 – 312, (1989).

186 Page W.J., and Knosp O., *Appl. Environ. Microbiol.* 55, 1334 – 1339, (1989).

187 Fries K., and Lafferty R.M., *J. Biotechnol.* 10, 285 – 292, (1989).

188 Slater S.C, Voige W.H, and Dennis D.E., *J. Bacteriol.* 170, 4431 – 4436, (1988).

189 Schubert P., Steinbuchel A., and Schlegel H.G., *J. Bacteriol.* 170, 5837 – 5847, (1988).

190 Pool R., *Science* 245, 1187 – 1189, (1989).

191 Ellar D, Lundgren D.G, Okamura K, and Marchessault R.H., *J. Mol. Biol.* 35, 489, (1968)

192 Jensonand T.E, and Sicko L.M, *J. Bacteriol.* 106, 683, (1971)

193 Barnard G.N, and Sanders J.K.M., *FEBS Lett.* 231, 16 – 18, (1988).

194 Barnard G.N, and Sanders J.K.M., *J. Biol. Chem.* 264, 3286 – 3291, (1989).

195 Sillerud L.O, and Schulman R.G., *Biochemistry* 22, 1087 – 1094, (1983).

196 Kung F.E. US patent 2 361 036, (1950).

197 Gresham T.L, Jansen J.E, and Shaver F.W., *J. Am. Chem. Soc.* 102, 61, (1948).

198 Inoue S, Tomoi Y, Tsuruta T, and Furukawa J., *Makromol. Chem.* 48, 229, (1961).

199 Shiota T, Goto Y, and Hayaski K., *J. Appl. Polym. Sci.* 11, 753, (1967).

200 Agostini D.E, Lando J.B, and Shelton J.R. *J. Polym. Sci.* A – 1, 9, 2775 – 2787, (1971).

201 Shelton J.R. Agostini D.E, and Lando J.B. *J.Polym. Sci.* A – 1, 9, 2789 – 2799, (1971)

202 Shelton J.R. Lando J.B, and Agostini D.E, *J. Polym. Sci. Polym. Lett.* B 9, 173 – 178, (1971).

203 Tani H, Yamashita S, and Teranishi K., *Polym. J.* 3, 417, (1972)

204 Teranishi K, Iida M, Araki T, Yamshita S, and Tani H. *Macromolecules* 7, 421, (1974).

205 Yokouchi M, Chatani Y, Tadokora H, and Tani H. *Polymer J.* 6, 248 – 255, (1974).

206 Bloembergen S, Holden D.A, Bluhm T.L, Hamer G.K, and Marchessault R.H., *Macromolecules* 22, 1656 – 1663, (1989).

207 Bloembergen S, Holden D.A, Bluhm T.L, Hamer G.K, and Marchessault R.H., *Macromolecules* <u>20</u>, 3086 – 3089, (1987).

208 Bloembergen S, Holden D.A, Bluhm T.L, Hamer G.K, and Marchessault R.H., *Macromolecules* <u>22</u>, 1663 – 1669, (1989).

209 Yokouchi M, Chatani Y, Tadokora H, Teranishi K, and Tani H. *Polymer* <u>14</u>, 267, (1973).

210 Bluhm T.L, Hamer G.K, Marchessault R.H, Fyfe C.A, and Veregin R.P., *Macromolecules* <u>19</u>, 2871 – 2876, (1986)

211 Bloembergen S, Holden D.A, Hamer G.K, Bluhm T.L, and Marchessault R.H., *Macromolecules* <u>19</u>, 2865 – 2871, (1986).

212 Roe R.J. in: *Enclyclopedia of Polymer Science,* (Mark H.F., Bikales N.M., Overberger C.G., and Menges G., Eds.) vol 17, Wiley – Interscience, New York, (1989) p961.

213 Chu C.C., *Adv. Biomaterials* <u>3</u>, 781 – 786, (1982).

214 Barham P.J, Keller A, Otun E.L and Holmes P.A *J. Mater. Sci.* <u>19</u>, 2781 – 2794, 1984.

215 Barham P.J, *J. Mater. Sci.* <u>19</u> 3826 – 3834, 1984

216 Barham P.J and Keller A., *J.Polym.Sci.Polym.Phys.Ed.* <u>24</u>, 69 – 77, (1986)

217 Avella M and Martuscelli E. *Polymer* <u>29</u>, 1731, (1989).

218 Greco P and Martuscelli E., *Polymer* <u>30</u>, 1475 – 1483, (1989).

219 Khoury F and Passaglia E, in: *Treatise on solid state chemistry,* ed. Hanney N.B, Plennum Press, New York, vol.3 p335, 1976

220 Hoffman J.D, Davies G.T and Lauritzen J.I in:*Treatise on solid chemistry,* ed. Hanney N.B, Plennum Press, New York, vol.3 p497, 1976

221 Gerngoss O, Herrman K, and Abitz W., *Z. Physik. Chem. B* <u>10</u>, 371, (1930)

222 Bunn C.W In: *Fibres from Synthetic Polymers,* Hill R. ed. Elsevier, New York, (1953) pp240 – 300.

223 Bunn C.W and Alcock T.C, *Trans. Faraday Soc.* <u>41</u> 317 – 325, (1945).

224 Keller A., *Phil.Mag.* <u>2</u>, 1171 – 1175, (1957)

225 Fischer E.W, *Naturforsch.* <u>12a</u> 753 – 754, (1957)

226 Till P.H., *J. Polym. Sci.* <u>24</u>, 301, (1957).

227 Bassett D.C., *CRC Critical Reviews in solid State and Materials Sciences* <u>12</u>(2),97 – 163, (1984).

228 Bunn C.W. *Trans. Faraday. Soc.* <u>35</u>, 482 – 491, (1939).

229 Vaughan A.S and Bassett D.C, in: *Comprehensive Polymer Science,* (Allen G and Bevington J.C, eds.) vol.2, Booth C and Price C, eds., Pergamon Press, (1989) p415.

230 Clark E.S., In: *Polymeric Materials: Relationship between Structure and Mechanical Behaviour,* (American Society for Metals), ASM press, Ohio, USA., (1975).pp1 – 54.

231 G Giannoni, Padden F.J., and Keith H.D. *Proc. Nat. Acad. Sci.* (US) 62, 964 – 971, (1969).

232 Keith H.D., G Giannoni, and Padden F.J. *Biopolymers* 7, 775 – 792, (1969).

233 North A.C.T. and Rich A., *Nature* 191, 1242 – 1245, (1961).

234 Alper R, Lundgren D.G, Marchessault R.H. and Cote W.A. *Biopolymers* 1, 545 – 556, (1963).

235 Okamura K. and Marchessault R.H. In: *Conformation of Biopolymers,* (Ramachandran G.N., ed.) vol 2, p709 – 720, Academic press, London. (1967).

236 Okamura K. PhD thesis, Syracuse University, USA, (1967).

237 Cornibert J. and Marchessault R.H. *J. Mol. Biol.* 71, 735 – 756, (1972)

238 Marchessault R.H, Coulombe S, Morikawa H, Okamura K, and Revol J.F. *Can. J. Chem.* 59, 38 – 44, (1981)

239 Brisse F. and Marcessault R.H. *Am. Chem. Soc. Symp. Series. (fiber diffraction methods)* 141, 267 – 277, (1980)

240 Bruckner S, Meille S.V, Malpezzi L, Cesaro A, Navarini L, and Tombolini R. *Macromolecules* 21, 967 – 972, (1988).

241 Pundsack A.L. and Bluhm T.L. *J. Mater. Sci.* 16, 545 – 547, (1981)

242 Marchessault R.H, Morikawa H, Revol J.F and Bluhm T.L, *Macromolecules* 17, 1882 – 1884, (1984)

243 Mitomo H., Barham P.J, and Keller A., *Sen – i – Gakkaishi* 42, T – 589 – T – 596, (1986).

244 Mitomo H., Barham P.J, and Keller A., *Polymer Journal* 19, 1241 – 1253, (1987).

245 Barham P.J. Private Communication (1988).

246 Imperial Chemical Industries Literature on Biopols, (1985).

247 Billingham N.C, Henman T.J, and Holmes P.A. *Dev. Polym. Degrad.* 7, 81 – 121, (1987).

248 Owen A.J. *Colloid Polym. Sci.* 263, 799 – 803, (1985).

249 Barker P.A, Mason F, and Barham P.J. *J. Mater. Sci.* in press.

250 Organ S, Barker P.A and Barham P.J. Private Communication (1989)

251 Akhtar S., Pouton C.W, and Notarianni L.J., *Pharm. Res.* 6, S – 103, (1989).

252 Ritchie G.A.F. PhD Thesis, Univeristy of Hull, 1969.

253 Lafferty R.M., Korsatko B., and Korsatko W. in: *Biotechnology* Vol 6b, (Rehm H.J, and Reed G., eds.), VCH, Weinheim, FRG, (1988), pp135 – 176.

254 Marchessault R.H, Okamura K, Su C.J., *Macromolecules* 3, 735 – 740, (1970).

255 Cornibert J., Marchessault R.H, Benoit H, and Weill G., *Macromolecules* 3, 741 – 746, (1970).

256 Akita S, Einaga Y, Miyaki Y, and Fujita H., *Macromolecules* 9, 774 – 780, (1976)

257 Miyaki Y, Einaga Y, Hirosye T and Fujita H. *Macromolecules* 10, 1356 – 1364, (1977)

258 Miyaki Y, Einaga Y, and Fujita H. *Macromolecules* 11, 1180, (1978).

259 Hiroyse T, Einaga Y, and Fujiata H., *Polymer Journal* 11, 819 – 826, (1979).

260 Baptist J.N, and Werber F.X., *SPE Transactions*, October, 245 – 250, (1964).

261 Scandola M, Pizzolli M, Cerrocorulli G, Cesaro A, Paoletti S. and Navarini L., *Int. J. Macromol.* 10, 373 – 377, (1989).

262 Marchessault R.H, Bluhm T.L, Deslandes Y, Hamer G.K, Orts W.J, Sundarajan P.R, and Taylor M.G., *Makromol. Chem. Macromol. Symp.* 19, 235 – 254, (1988).

263 Akhtar S., and Pouton C.W., *Drug News and Perspectives* 2, 89 – 93, (1989).

264 Akhtar S, Pouton C.W, Notarianni L.J and Gould P.L. *J. Pharm. Pharmacol.* 39, 43P (1987)

265 Knowles J.C and Hastings G.W., Abstracts of the 8th European Conference on Biomaterials, 7 – 9th Sept., Heidelberg, FRG., B4 – 4, p87, (1989).

266 Tanner K.E, Doyle C, Bonfield W., Abstracts of the 8th European Conference on Biomaterials, 7 – 9th Sept., Heidelberg, FRG., D5 – 5, p163, (1989).

267 Doyle C, Luklinska Z.B, Tanner K.E, and Bonfield W., Abstracts of the 8th European Conference on Biomaterials, 7 – 9th Sept., Heidelberg, FRG., D6 – 5, p169, (1989).

268 Doyle C and Bonfield W in 'Engineering applications of New Composites' Paipetis S A, and Papanicolaou G C. eds. Omega Scientific, Wallingford, UK, (1988) p114 – 118.

269 Scandola M., Ceccorulli G, and Pizzoli M. *Makromol. Chem. Rapid Commun.* 10, 47 – 50, (1989)

270 Webb A., ICI (Marlborough Biopolymers Ltd)., Private communication (1989).

271 McRae R.M. and Wilkinson J. F., *J. Gen. Microbiol.* 19, 210, (1958)

272 Grassie N, Murray E.J and Holmes P.A *Polymer degradation and stability*, 6 47 – 61, (1984)

273 Grassie N, Murray E.J and Holmes P.A *Polymer degradation and Stability*, 6 127 – 134, (1984)

274 Fukada E., *Ferroelectrics* 60, 285 – 296, (1984).

275 Ando Y., and Fukada E., *J.Polym. Sci. Polym, Phys.* 22, 1821 – 1834, (1984)

276 Fukada E., and Ando Y., *Int. J. Biol. Macromol.* 8, 361 – 366, (1986)

277 Fukada E, and Ando Y., *Biorheology* 25, 297 – 302, (1988).

278 Black J., *Electrical Stimulation. Its role in Growth, Repair, and Remodeling of the Musculoskeletal System.* Praeger Publishers, New York, (1987).

279 Chowdhury A.A., *Arch. MiKrobiol.* 47, 167 – 200, (1963).

280 Merrick J.M, Delafield F.P, and Doudoroff M., *Federation Proc.* 21, 228, (1962)

281 Delafield F.P, Doudoroff M, Palleroni N.J, Lusty C.J and Contropoulos R. *J. Bacteriol.* 90, 1455 – 1466, (1965).

282 Lusty C.J., and Doudoroff M. *Biochemistry* 56, 960 – 965, (1966)

283 Tanio T, Fukui T, Shirakura Y, Saito T, Tomita K, Kaiho T, and Masamune K., *Eur. J. Biochem.* 124, 71 – 77, (1982).

284 Shirakura Y, Fukui T, saito T, Okamoto Y, Narikawa T, Koide K, Tomita K, Takemasa T, and Masamune S., *Biochem. Biophys. Acta.* 880, 46 – 53, (1986).

285 Fukui T, Narikawa T, Miwa K, Shirakura Y, saito T, and Tomita K., *Biochem. Biophys. Acta.* 952, 164 – 171, (1988).

286 Majid M.I.A PhD. Thesis, University of Bath, UK. (1988).

287 Pouton C.W., Majid M.I.A, and Notarianni L.J. *Proceed. Int. Symp. Control. Rel. Bioact. Mater.* 15, 181 – 183, (1988)

288 Holland S.J, Jolly A.M, Yasin M, and Tighe B.J. *Biomaterials* 8, 289 – 295, (1987).

289 Yasin M, Holland S.J, Jolly A.M, and Tighe B.J. *Biomaterials* 10, 400 – 412, (1989).

290 Akhtar S., Pouton C.W., and Notarianni L.J., *Unpublished Results.*

291 Miller N.D, and Williams D.F. *Biomaterials* 8, 129 – 137, (1987).

292 Williams D.F and Miller N.D. *Advances in Biomaterials* 7, 471 – 476, (1987).

293 Gerlach K.L and Pesch H.J. Abstracts of the 8th European Conference on Biomaterials, 7 – 9th Sept., Heidelberg, FRG., B3 – 1, p79, (1989).

294 Kronenthal R.L., In: *Polymers in Medicine and Surgery*, Kronenthal R.L, User Z., and Martin E., eds., Plennum Press, New York, (1974) p126.

295 Williams D.F., In: Techniques of Biocompatibility Testing, Vol.2, Williams D.F ed., CRC Press, Boca Raton, (1986)

296 Korsatko W, Wabnegg B, Tillian H.M, Egger G, Pfragner R, and Walser V., *Pharm. Ind.* 46, 952 – 954, (1984).

297 Kennedy J.E, Notarianni L.J, and Pouton C.W., *J. Pharm. Pharmacol.* 39, 58P, (1987).

298 Pouton C.W, Kennedy J.E, Notarianni L.J, and Gould P.L., *Proceed. Int. Symp. Control Rel. Bioact. Mater.* 15, 179 – 180, (1988).

299 Kennedy J.E, Notarianni L.J, and Pouton C.W., *J. Pharm. Pharmacol.* 40, 33P, (1988).

300 Juni K., and Nakano M., *CRC Crit. Rev. Ther. Drug Carrier Systems.*, 3, 209 – 232,

(1987).

301   Doyle C. Private Communication (1989).

302   Schmitt E, (W.R. Grace & Co.), *United States Patent* 3 297 033 (1963)

303   Korasatko W., Wabnegg B., Braunegg G, Lafferty R.M, and Strempfl F., *Pharm. Ind.* 45, 525 – 527, (1983).

304   Korasatko W., Wabnegg B., Braunegg G, and Lafferty R.M, *Pharm. Ind.* 45, 1004 – 1007, (1983).

305   Gould P.L, Holland S.J., and Tighe B.J., *Int. J. Pharm.* 38, 231 – 237, 1987),

306   Brophy M.R, and Deasy P.B., *Int. J. Pharm.* 29, 223 – 231, (1986).

307   Bissery M.C, Valeriote F, and Thies C., in: *Microspheres and Drug Therapy. Pharmaceutical, Immuniological and Medical Aspects,* (Davis S.S, Illum L, McVie J.G, and Tomlinson E., eds.) Elsevier Science Publishers, Amsterdam, (1984) pp217 – 227.

308   Bissery M.C, Valeriote F, and Thies C., *Proceed. Int. Symp. Control Rel. Bioact. Mater.* 11, 25 – 26, (1984).

309   Bissery M.C, Valeriote F, and Thies C., *Proceedings of AACR,* 26, 335, (1985)

310   Juni K, Nakano M, and Kubota M., *J. Controlled Release,* 4, 25 – 32, (1986).

311   Kubota M, Nakano M, and Juni K., *Chem. Pharm. Bull.* 36, 333 – 337, (1988).

312   Koosha F, Muller R.H, and Washington C.W., *J. Pharm. Pharmacol* 39, 136P, (1987).

313   Koosha F, Muller R.H, and Davis S.S., *J. Pharm. Pharmacol.* 40, 131P, (1988).

314   Akhtar S, Pouton C.W. Notarianni L.J. and Gould P.L., *J. Pharm. Pharmacol.* 41, 5P, (1989).

316   Collins A.E.M,, Deasy P.B, MacCarthy D.J, and Shanley D.B., *Int. J. Pharm.* 51, 103 – 114, (1989).

317   Deasy P.B, Collins A.E.M. MacCarthy D.J, and Russell R.J., *J. Pharm. Pharmacol.* 41, 694 – 699, (1989).

318   Konig W, Seidel H.R, and Sandow J.K., *European Patent* Number 0 133 988. (1984).

319   Sandow J, Seidel H.R., *German Patent* A 61K 9/52 (1986).

320   McLeod B.J, Haresign W., Peters A.R, Humke R, and Lamming G.E., *Animal Reproduction Science* 17, 33 – 50, (1988).

321   Morikawa H, and Marchessault R.H., *Can. J. Chem.* 59, 306 – 2313, (1981)

322   Seebach D, and Zueger M., *Helv. Chim. Acta.* 65, 495, (1982).

323   Seebach D, and Zueger M., *Tetrahedron Letters* 25, 2747, (1985).

324   Seebach D, Roggo S, and Zimmerman J., in: *Stereochemistry of Organic and Bioorganic Transformations,* (Bartman W, and Sharpless K.B, eds.), VCH:Weinheim, FRG, (1987) Vol.17, pp87 – 502.

325 Webb A, and Adsetts J.R, *U.K. Patent Appl.* GB 2 166 354 A (1986).

326 Holmes P.A., *U.K Patent Appl.* GB 2 160 208 A (1985).

327 Franesco M, Luigi P, and Paolo V., *European Patent* Number 0 226 439 (1987).

328 Japan Kokal Tokyo Koho Japanese Patent 63/302845 A2 (1988).

329 Bonfield W In: *'Engineering applications of New Composites'* Paipetis S A, and Papanicolaou G C. eds. Omega Scientific, Wallingfod, UK, (1988) pp17 – 21.

330 Hastings G.W., *Polymer* 26, 1331 – 1335, (1985).

331 Book of ASTM Standards, American Society for Testing and Materials, 1916 Race St., Philadelphia, Pa, USA.

332 Book of British Standards, British Standards Institute, UK.

333 Aulton M.E., *Int. J. Pharm. Tech. Prod. Mfr.* 3, 9 – 16, (1982).

334 Lever A.E, and Rhys J.A., *The Properties and Testing* of *Plastic Materials,* Temple Press Books, UK, 3rd Ed. (1968).

335 Kambour R.P, and Robertson R.E., in: *Polymer Science,* (Jenkins A.D., ed.), North – Holland Publishing Co.,Vol.1., Chapter 11. (1972)

336 Nielsen L.E., *Mechanical Properties of Polmers and Composites,* Vol.2, Marcel Dekker Inc., New York, (1974).

337 Aulton M.E, and Abdul – Razzak M.H., *Drug Dev. Ind. Pharm.* 7, 649 – 668, (1981).

338 Aulton M.E, and Abdul – Razzak M.H., *Drug Dev. Ind. Pharm.* 10, 541, (1984).

339 Porter S., *Pharm. Tech.* 4, 67, (1980).

340 Rowe R.C., *Pharm. Acta. Helv.* 57, 221, (1982).

341 Ononokpono O.E, and Spring M.S., *J. Pharm. Pharmacol.* 40, 313 – 319, (1988).

342 Chu C.C and Welch L., *J. Biomed. Mater. Res.* 19, 903 – 916, (1985).

343 Okazaki M, and Ohmae H., *Biomaterials* 9 345 – 348, (1988).

344 Hertweck S.P, von Fraunhofer J.A, Masterson B.J., *Biomaterials* 9, 457 – 459, (1988)

345 von Fraunhofer J.A., Storey R.J, and Masterson B.J., *Biomaterials* 9, 324 – 327, (1988).

346 Briston J.H., *Plastics Films,* Iliffe Books, London, (1974) p85.

347 Barker P.A, and Barham P.J., *J. Mater. Sci. Lett.* 8, 1049 – 1051, (1989).

348 Marchessault R.H, and Nedea M.E., *Polymer Commun.* 30, 261 – 263, (1989).

349 Majid M.I.A, Pouton C.W, and Notarianni L.J.N., *J. Pharm. Pharmacol.* 40, 34P, (1988).

350 Gent A.N, *J. Polym. Sci. A2*, <u>10</u>, 571, (1972).

351 Peterlin A.J., *J. Mater. Sci.* <u>6</u>, 490, (1971)

352 Vincent P.I *Polymer* <u>1</u>, 425, (1960).

353 Merz E.H, Nielsen L.E, and Buchdahl R. *Ind. Eng. Chem.,* <u>43</u>, 1396 – 1401, (1951).

354 McCormick H.W, Brower F.M, and Kin L., *J. Polym. Sci.* <u>39</u>, 87 – 100, (1959).

355 Snooke A.M, and Harris M., *Ind. Eng. Chem.,* <u>37</u>, 478 – 482, (1945).

356 Flory P.J., *Ind. Eng. Chem.,* <u>38</u>, 417 – 436, (1946).

357 Snooke A.M, and Harris M., *J. Res. Nat. Bur. Stds.* <u>34</u>, 467 – 476, (1945).

358 Griffiths A.A., *Philosphical Transactions of the Royal Society of London, series A,* <u>221</u>, 163 – 198, (1920).

359 Nielsen L.E., *J. Appl. Polym. Sci.* <u>10</u>, 97, (1966).

360 Smith T.L, *Trans. Soc. Rheol.* <u>3</u>, 113, (1959).

361 Nicolais L, and Narkis M., *Polym. Eng. Sci.* <u>11</u>, 194, (1971).

362 Okhamafe A.O, and York P., *Pharm. Res.* <u>1</u>, 19 – 23, (1985).

363 Okhamafe A.O, and York P., *J. Pharm. Pharmacol.* <u>37</u>, 385 – 390, (1985).

364 Okhamafe A.O, and York P., *Int. J. Pharm.* <u>39</u>, 1 – 21, (1987).

365 Pittman C.U, Iqbal M, and Chen C.Y., *J. Polym. Sci. Polym. Chem. Ed.* <u>16</u>, 2721 – 2724, (1978)

366 Bruck S.D, and Mueller E.P., *J. Biomed. Mater. Res. Appl. Biomater.* <u>A2</u>, 133 – 144, (1988).

367 Keller A., in: *Developments in Crystalline Polymers,* Vol.1 (Bassett D.C., ed.), Applied Science Publishers, (1981) pp37 – 113.

368 Jellinek H.H.J., in: *Polymer Year Book 1st Ed,* (Elias H.G, and Pethrick RA, ed.), Harwood Academic Publishers, London, (1984), pp227 – 247.

369 Mackenzie R.C., *Thermochim Acta* <u>28</u> 1 (1979).

370 Mackenzie R.C., *Anal. Proc.* <u>17</u> (6) 217 – 220 (1980)

371 Smothers W.J, and Chiang Y., *'Handbook of Differential Thermal Analysis',* Chemical publishing Co.,New York, (1966).

372 Mackenzie R.C, Editor *'Differential thermal Analysis',* Academic, New York, vol. 1, (1970); vol. 2, (1972).

373 Murphy CB 'Treatise on Analytical Chemistry, part 1, Wiley (Interscience), New York, (1968), p5243.

374 Wunderlich B, in: *Physical Methods of Chemistry,* part 5, (Weissberger A, Rossiter BW, eds.), Wiley (Interscience), New York, (1971).

375 Shultze D, *Differential – thermoanalyse*, 2nd ed.,Verlag Chemie, Weinham, (1971).

376 Turi E.A., *Thermal Characterization of Polymeric Materials* Academic Press, London , (1981), p235.

377 Chiu J, Editor *'Polymer characterization by Thermal Analysis'*, Marcel Dekker, New York, (1974).

378 Smith D.A, *Rubber* 150(4),21, (1968).

379 Barrel EM and Johnson JF, *Crit. Rev. Anal. Chem.* 2(1), 105, (1971).

380 Chiu J in: *'Polymer characterization by Thermal Analysis'*, (Chiu J., ed.) Marcel Dekker, New York, (1974)., p3 – 23.

381 MacCullum J.R., in: *Comprehensive Polymer Science*, (Allen G and Bevington J.C, eds.) vol.1, Booth C and Price C, eds., Pergamon Press, (1989) pp903 – 909.

382 Thompson E., in: *Encyclopedia of Polymer Science and Engineering*, vol.16, (Mark H.F, Bikales N.M, Overberger C.G., Menges G, and Kroschiwitz J.I., eds.), John Wiley and Sons, New York, (1989) pp711 – 746.

383 Zitomer F, *Anal Chem.* 40, 1091 (1968)

384 Wilson D.E and Hamaker F.M In:*Thermal Analysis*, Academic Press, New York, (1969), 2 vols. p517

385 Chiu J, *Anal. Chem.*, 40 1516, (1968)

386 Chang T.L and Mead T.E *Anal. Chem.* 43 534 (1971)

387 Mandelkern L, *Chem. Revs.*56 903 (1956)

388 Hay J.N, Trainor A and Haward R.N *J Polymer Sci. Phys. Ed.* 15 1077, (1977)

389 Hay J.N *The British Polymer Journal* 11 137 – 145 (1979).

390 Daniels T, In: *'Thermal Analysis'*, Kogan Page, London (1973).

391 Flory P.J *J. Chem. Phys.* 17 223 (1949)

392 R.J Young, *Introduction to polymers*, Chapman and Hall Ltd, London, (1981), p203.

393 Shalaby S.W In: *Thermal Characterization of Polymeric Materials*, Turi E.A ed. Academic Press, London, (1981), p235.

394 Allcock H.R and Lampe F.W, *Contemporary Polymer Chemistry* Prentice – Hall, New Jersey, (1981), p428

395 Van Krevelan D.W and Hoftijzer P.J *Properties of Polymers. Their estimation and correlation with chemical structure*, 2nd ed. Elsevier, Amsterdam, (1976).

396 Geil P.H., in: *Polymeric Materials: Relationship between Structure and Mechanical Behaviour*, (American Society for Metals), ASM press, Ohio, USA., (1975).pp 119 – 174

397 Boyer R.F *Rubber Chem Tech*, 36, 1303, (1963)

398   Askadskii, A.A Viskomolek. soedin., ser.A,9,N2,418, 1967 as cited in ref. 399.

399   Askadskii, A.A, In: Polymer Year Book 4, Pethrick RA, ed., Harwood Academic Publishers, London, (1987), p93

400   Akhtar S, Pouton C.W, Notarianni L.J.N and Gould P.L., J. Pharm. Pharmacol., 40, 118P, (1988).

401   Grassie N, Murray EJ and Holmes PA Polymer degradation and stability, 6 95 – 103, (1984)

402   Gupta M.C and Deshmukh V.G Colloid & Polymer Science 260, 514 – 517, (1982).

403   Cohn D., Younes H, and Marom G., Polymer 28, 2018 – 2022, (1987).

404   Struik L.C.E., 'Physical Aging of Amorphous Polymers and other Materials' Elsevier, Amsterdam, (1978).

405   Struik L.C.E., Polymer 28, 1521 – 1533, (1987)

406   Struik L.C.E. Polymer 21, 962, (1980)

407   Kandil S.H, Kamar A.A, Shaaban S.A, Taymour N.M and Morsi S.E., Biomaterials 10, 540 – 544, (1989).

408   Young R.J Introduction to Polymers, Chapman and Hall, London, (1981)

409   Cebe H and Hong S.D Polymer 27, 1183, (1986)

410   Cheng S.Z.D, Cayo M.Y and Wunderlich B Macromolecules 19 1868, (1986)

411   Blundel D.J Polymer 28 2248 – 2251, 1987

412   Blundel D.J and Osbourn B.N., Polymer 24 953,1983

413   Bassett D.C, Olley R.H, and Al Raheil A.M., Polymer 29, 1745 – 1754, (1988).

414   Chang S.S., Polymer Commun. 29, 138 – 141, (1988)

415   Lee Y, Porter R.S and Lin J.S Maromolecules 22 1756 – 1760, (1989)

416   Bell J.P and Dumbleton J.H J polym. Sci., Polym. Phys. Ed. 7 1033, (1969) and ibid 7, 1950, (1969)

417   Bell J.P, Slade P.E and Dumbleton J.H J polym. Sci., Polym. Phys. Ed. 6 1773, (1968)

418   Nealy DL, Davies TG and Kibler CJ J polym. Sci., Polym. Phys. Ed. 8 2141, (1970)

419   Wunderlich B Macromolecualr Physics, Academic Press, New York, (1980), vol. 3. p190

420   Ruddy M and Hutchinson J.M., Polymer Commun. 29, 132 – 134, (1988)

421   Statton W.O Journal Appl. Polym. Sci. 7 803, 1963.

422   Spuriell J.E and Clark E.S in: Methods of Experimental Physics (Marton L and Marton C, eds) vol.16, Polymers: Part B. Crystal Structure and Morphology, Fava R.F, ed., Academic Press, London, (1980), p1.

423 Bassett D.C., In: *Principles of polymer morphology*, Cambridge University Press, Cambridge, UK; (1981), p1.

424 Bassett D.C; *Principles of polymer morphology*, Cambridge University Press, Cambridge, UK; 1981, p24.

425 Geil P.H In: *Polymer Single Crystals*, Wiley, New York, (1963)

426 Sanchez *J. Polym. Sci. Polym. Symp.* 59, 109–120, (1977).

427 Ross G.S and Frolen L.J In: *Methods of experimental physics*, (Marton L and Marton C, eds.) vol 16 part B, *Polymers: Crystal structure and morphology*, (Fava R.A, ed.), Academic Press, New York, 1980 p339.

428 Keith H.D and Padden F.J, *J Appl. Phys.* 35 1270, (1964).

429 Keith H.D and Padden F.J, *J Appl. Phys.* 35 1286, (1964).

430 Cross W., *Bull. Phil. Soc. Washington*, 11, 411–443,(1891) (as cited in reference 219).

431 Point J.J, *Bull. Acad. Roy. Belg.* 41 982–990, 1955.

432 Keller A., *J.Polym.Sci.* 17, 351–364, (1955).

433 Binsbergen F.L and De Lang B.G.M., *Polymer* 9, 23–40, (1968)

434 Palmer R.P and Cobbold A.J, *Makromol. Chemie.* 74 174–189, (1964)

435 Keller A and Sawada S, *Makromol. Chemie* 74 190–221, 1964

436 Welland E.L, Stejny J, Halter, A and Keller A., *Polymer Communications* 30 (Oct), 302–304, (1989).

437 Organ S and Barham P.J., *J. Mater. Sci. Letters,* 8, 621–623, (1989)

438 Hemsley D, In: Comprehensive Polymer Science, (Allen G and Bevington J.C, eds.) vol.2, Booth C and Price C, eds., Pergamon Press, 1989 p765.

439 Bunn C.W and Daubeny R.P *Trans. Faraday. Soc.* 50 1173–1177, (1954)

440 Keedy D.A, Powers J and Stein R.S *J Appl. Phys.* 31 1911–1915, (1960).

441 Keller A, *Nature* 169 913–1914, 1952

442 Wallerant F., *Bull. Soc. Fr. Mineral.* 30,43–60, (1907) as cited in ref. 219.

443 Keith H.D and Padden F.J, *J Polym. Sci.* 39 101–122, 1959.

444 Keith H.D and Padden F.J, *J Polym. Sci.* 39 122–138, 1959.

445 Price F.P, *J Polym. Sci.* 39 139–150, 1959.

446 Keller A, *J Polym. Sci.* 39 151–173, 1959.

447 Hoffman J.D. and Lauritzen J.I, *J. Res. Nat. Bur. Std. (U.S)* 65A, 297–336, (1961).

448 Bassett D.C., Keller A. and Mitsuhashi S., *J.Polym.Sci.* A $\underline{1}$,763 – 788, (1963).

449 Koury F., and Barnes J.D., *Bull.Am.Phys.Soc.* $\underline{11}$, 248 (FA 11), (1966).

450 Keith H.D., and Padden F.J. *J.Appl. Phys.* $\underline{34}$,2409 – 2421, (1963)

451 Keith H.D *J.Polym.Sci.* A$\underline{2}$,4339 – 4360, (1964)

452 Young R.J. *Introduction to polymers*, Chapman and Hall, London, (1981), p188.

453 Avrami M. *J. Chem. Phys.* $\underline{7}$ 1103, (1939)

454 Avrami M. *J. Chem. Phys.* $\underline{8}$ 212, (1940).

455 Hoffman J.D. SPE Trans $\underline{4}$(4), 315 (1964)

456 Richardson M.J In: *Comprehensive Polymer Science*, (Allen G and Bevington J.C, eds.) vol.1, Booth C and Price C, eds., Pergamon Press, (1989) p867

457 Grenier D and Prud'Homme R.E *J. Polym. Sci. Polym. Phys. Ed.* $\underline{18}$, 1655 – 1657, (1980).

458 Point J.J. *Macromolecules* $\underline{12}$, 770 – 775, (1979)

459 Turnbull D and Fisher J.C. *J. Chem. Phys.* $\underline{17}$, 71, (1949).

460 Hoffman J.D. *Polymer* $\underline{24}$, 3, (1983)

461 Hoffman J.D., *Macromolecules*, $\underline{18}$, 772 – 786, (1985)

462 Hoffman J.D., and Miller R.L., *Macromolecules* $\underline{21}$, 3038 – 3051, (1988)

463 Lauritzen J.J and Hoffman J.D, *J. Res. Natl. Bur. Stds.* $\underline{64A}$, 73, (1960).

464 Point J.J. *Macromolecules* $\underline{19}$, 929 – 930, (1986)

465 Point J.J., and Dosiere M., *Polymer* $\underline{30}$,(Dec) 2292 – 2296, (1989)

466 Sadler D.M., *Polymer* $\underline{24}$, 1401 – 1409, (1983).

467 Mandelkern L In: *Comprehensive Polymer Science*, (Allen G and Bevington J.C, eds.) vol.1, Booth C and Price C, eds., Pergamon Press, (1989) p363

468 Hoffman J.D and Weeks J.J *J. Res. Natl. Bur. Stand. sect.* A $\underline{66}$, 13 (1962)

469 Bair H.E, Huseby W and Salovey R, *J.Appl.Phys,* $\underline{39}$, 4969, (1968)

470 Bassett D.C; *Principles of polymer morphology*, Cambridge University Press, Cambridge, UK; 1981, p160

471 Msuya W.F, and Yue C.Y. *J. Mater. Sci. Lett.* $\underline{8}$, 1266 – 1268, (1989)

472 Keller A., *J.Macromol. Sci.* $\underline{8}$, 105 (1973).

473 Moyer, J.D. and Ochs, R.J., *Science* $\underline{142}$, 1316, (1963)

474 Revol J.F, Chanzy H.D, Deslandes Y. and Marchessault R.H. *Polymer* $\underline{30}$, 1973 – 1976, (1989).

475   Barham P.J and Keller A., *J.Polym.Sci.Polym.Phys.Ed.* 24, 69-77, (1986)

476   Barham P.J and Keller A., *J. Mater. Sci.* 12, 2141, (1977).

477   Martinez-Salazar J, Sanchez-Cuesta M, Barham P.J, and Keller A., *J. Mater. Sci. Lett.* 8, 490-492, (1989).

478   Lindenmeyer P.H and Holland V.F, *J Appl. Phys.* 35 55-58, (1964).

479   Luzzi LA   *J. Pharm. Sci.* 59 1367, (1970).

480   Maulding H.V In: *'Advances in drug delivery systems,3'* (Eds Anderson J.M, Kim S.W), Elsevier Science Publishers, Amsterdam, (1987) pp 167-176.

481   Tice T.R, and Gilley R.M., *J Controlled Release* 2, 343-52 (1985).

482   Benoit J.P, Benita S, Puisieux F, and Thies C., in: *Microspheres and Drug Therapy. Pharmaceutical, Immuniological and Medical Aspects,* (Davis S.S, Illum L, McVie J.G, and Tomlinson E., eds.) Elsevier Science Publishers, Amsterdam, (1984), pp91-102.

483   Deasy P.B *'Microencapsulation and related drug processes'* (Drugs and the pharmaceutical sciences, Ed. Swarbrick J., Vol 20) Marcel Dekker, New York, (1984) p 181.

484   Masters K. *'Spray Drying Handbook'* George Godwin Ltd, London, (1979) p1

485   Deasy P.B *'Microencapsulation and related drug processes'* (Drugs and the pharmaceutical sciences, Ed. Swarbrick J., Vol 20) Marcel Dekker, New York, (1984) p182.

486   Masters K. *'Spray Drying Handbook'* George Godwin Ltd, London, (1979) p35.

487   Masters K. *'Spray Drying Handbook'* George Godwin Ltd, London, (1979) pp3 and 24.

488   Masters K. *'Spray Drying Handbook'* George Godwin Ltd, London, (1979) p21-53.

489   Higuchi T., *J. Pharm. Sci.* 50, 874, (1961).

490   Brophy M.R, and Deasy P.B., *Int. J. Pharm.* 37, 41-47, (1987).

491   Cardinal JR In: *Recent Advances in Drug Delivery Systems,* Anderson JM and Kim SW, eds., Plenum Press, New York,1984, p229

492   Roseman TJ and Higuchi WI, *J. Pharm. Sci* 59 353, 1970

493   Donbrow M, Hoffman A and Benita S, *J Pharm. Pharmacol.* 40: 93-96, 1987

494   Siegel R.A., Kost J, and Langer R., *J. Controlled Release* 8, 223-236, (1989).

495   Tice T.R, Mason D.W, and Gilley R.M., in: *Novel Drug Delivery and its Therapeutic Application,* (Prescott L.F., and Nimmo W.S., eds), John Wiley and Sons, Chichester, UK, (1989) pp223-235.

496   Ratner B.D, Yoon S.C., and Maeto N.B., in: *Polymer Surfaces and Interfaces,* (Feast W.J., and Munro H.S., eds.), Wiley and Sons, U.K, (1987) pp231-251.

497   Davies M.C, Khan M.A, Short R.D, Akhtar S, Pouton C.W and Watts J.F. *Biomaterials* in press.

498 Koosha F, Muller R.H, Davis S.S and Davies M.C. *J. Controlled Release* 9, 149 – 157, (1989).

499 Davies M.C, Pouton C.W and Akhtar S. *Unpublished results*, (1989).

500 Heller J. *Private communication*, (1989)

501 Theeuwes F., in: *Novel Drug Delivery and its Therapeutic Application,* (Prescott L.F., and Nimmo W.S., eds), John Wiley and Sons, Chichester, UK, (1989) pp323 – 340.

502 Khan M.A. *PhD Thesis*, University of Nottingham, (1988).

503 Briggs D., *Surf. Interface Anal.,* 9, 391 – 404, (1986).

504 Davies M.C, Short R.D, Khan M.A, Watts J.F, Brown A, Eccles A.J, Humphries P., and Vikerman J.C., *Surf. Interface Anal.,* 14, 115 – 120, (1989).

505 Briggs D., and Seah M.P, (Eds.), *Practical Surface Analysis by Auger and PS,* Wiley and Sons, NY, (1983), pp 359 – 396.

506 Gosh P.K, *Introduction to Photoelectron Spectroscopy,* Wiley and Sons, NY, (1983).

507 Briggs D., *Polymer* 25, 1379 – 1391, (1984)

508 Briggs D., In: *Comprehensive Polymer   Science,* (Allen G and Bevington J.C, eds.) vol.2, Booth C and Price C, eds., Pergamon Press, (1989) pp543 – 559.

509 Andrade J., In: *Surface and Interfacial Aspects of Biomedical Aspects of Biomedical Polymers,* (Andrade J, ed.), Plennum Press, NY, (1985).

510 Brown A, and Vikerman J.C., *Analyst,* 109, 851 – 857, (1984).

511 Brown A, and Vikerman J.C., *Surf. Interface Anal.* 8, 75 – 81, (1986).

512 Ratner B.D, Johnston A.B, and Lenk T.J., *J. Biomed. Mater. Res.* 21, 59 – 90, (1987).